Development of Novel Iridium(III) Complexes for Light-Emitting Devices

By Joshua Adams

A Thesis Submitted in Partial Fulfilment of the Requirements for the Degree of Doctor of Philosophy

School of Applied Sciences

Department of Chemistry

The University of Huddersfield

June 2023

Copyright Statement

Acknowledgements

First and foremost, I would like to thank Prof. Paul Elliott for giving me the opportunity to be a part of his research group to carry out this work, and for all his kindness, support and help throughout the project. I would also like to give a special thank you to Dr Paul Scattergood for all his assistance, help and generosity in and outside of the laboratory. I really would like to extend my appreciation to the entirety of the Elliott Group, who have provided me with so much support and assistance. I would like to specifically mention Dr Rayhaan Boota who is a great friend and person, who has helped and encouraged me from the day I started. I would like to thank the EPSRC and the University of Huddersfield for funding this doctorate.

I would also like to pay thanks to the following people within the Department of Chemistry for their help and support; Dr Neil McLay for support with NMR. Sean Ward and IPOS for the Dr Fiona Ordway, Jim Rooney and Ibrahim George for help in running the department and assisting me whenever I needed them. I am also grateful for all the other colleagues I have worked with. I am also grateful to Dr Samantha Hardman at the University of Manchester who assisted with the transient absorption spectroscopy.

Finally, I am ever-so grateful to my family, friends and my amazing girlfriend who have been incredibly supportive over the years.

Abstract

Photochemistry and photophysics are omnipresent in the natural world, making them of great scientific interest. The reproduction and application of their processes in chemical, physical, biological, and medical technologies have emerged as areas of great interest. The forefront of current research lies in the development of highly efficient light-emitting devices, where increased efficiency translates to reduced energy consumption. This pursuit holds paramount importance in mitigating the climate crisis by curbing carbon emissions. Recent advancements in OLEDs and LEECs have demonstrated significantly more efficiency compared to traditional lighting methods.

Amongst transition metal complexes, Ir(III) complexes emerge as the most promising candidates for photo- and electroluminescence. Tunability across the colour spectrum can be achieved by modifying their ligands. These complexes exhibit a remarkable array of photophysical properties, including the ability to modify emission characteristics via ligand manipulation, good kinetic and thermodynamic stability, and exceedingly high quantum yields.

The primary objective of this thesis revolves around the advancement and exploration of light-emitting complexes through the synthesis of novel Ir(III) complexes, aiming to modulate the highest occupied molecular orbital (HOMO) and lowest unoccupied molecular orbital (LUMO). This research work seeks to contribute to the development and progress of light-emitting devices, enriching our understanding of their properties, and open up new possibilities for a multitude of applications.

This thesis presents the findings of my research in the development of Ir(III) complexes for light-emitting devices:

Chapter 2 consists of the synthesis of heterodinuclear Ir(III)-Ru(II) complexes where the bridging ligand between the two metal centres is based on aryl-1,2,3-triazole ligands. The mononuclear counterparts were also synthesised. The photophysical properties of these complexes were investigated. It was revealed that two of the fluorinated multinuclear complexes were white light emitting. The reported complexes were tested for their photostability and were found to be photolabile. The photochemical properties were investigated for the heterodinuclear Ir(III)-Ru(II) complexes. The metal centres separated through photolysis resulting in a turning of the Ir(III) emission.

Chapter 3 consists of the synthesis of a series of cyclometalated Ir(III) complexes designed to explore the high energy T_1 states for Ir(III) complexes. The cyclometalating C^N ligand was selected to be 3, 5-Dimethylpyrazole phenyl whilst the N^N ancillary ligand was a series from 2,2'-bipyridyl (bpy)→ 2-(1-benzyl-1H-1,2,3-triazol-4-yl)pyridine (pytz) → 4,4-bi-1,2,3-triazol-4-y (btz) and 2-(1-benzyl-1H-1,2,3-triazol-4-yl)-6-methylpyridine (m-pytz). The photophysical properties were investigated for these complexes. It was found that the btz and m-pytz complexes were readily accessing the ^{3}MC states upon excitation. Computational studies confirm that the btz complex accesses the ^{3}MC states, this was

achieved through manipulation of the electronic properties of the complex. Whilst the m-pytz complex also accesses the ^{3}MC states, this was performed through the ligand architecture, designed to increase bond lengths through steric hindrance.

Chapter 4 consists of the synthesis of novel Ir 3+2+1 triazoles complexes based on the $[Ir(N^\wedge N^\wedge N)(C^\wedge N)Cl]^+$ structure. The synthesis entails aryl-1,2,3-traizole ligands and archetypal pyridine-based ligands. The complexes were designed to explore new chemical space thus their photophysical properties were assessed. The C^N triazole based complex showed respectable photophysical properties, with a relative photoluminescent quantum yield (ϕ) of 9.1 % and lifetime (τ) of 1.7 μs. The N^N^N triazole based complexes had less impressive relative quantum yields (ϕ = <0.1 to 1.8 %) but some complexes had long lifetimes, τ = 3.5 to 4.0 μs.

Table of Contents

Copyright Statement 2

Acknowledgements 3

Abstract 4

List of Figures 12

List of Schemes 19

List of Tables 20

List of Abbreviations 21

1. Introduction 24

  1. 1 Photochemistry and Photophysics 24

  1. 2 Molecular Photophysics – Absorption of Light 25

    1. 2. 1. Characteristics of Light 25

    1. 2. 2. Beer-Lambert Law 26

    1. 2. 3 Time-dependent Perturbation Theory 26

    1. 2. 4 Symmetry Selection Rules 29

    1. 2. 5 Spin Selection Rules 29

    1. 2. 6 Franck-Condon Principle 30

    1. 2. 6 The Jablonski Diagram 30

  1. 3. Molecular Photophysics - The Excited States 31

  1. 4. Photophysics of d^6 Metal Complexes 36

    1. 4. 1. Photophysics of Ru(bpy)$_3$ 36

    1. 4. 2. Luminescence in Cyclometalated Ir Complexes 39

  1. 5. Ir(III) Complexes 41

    1. 5. 1. Ir(III) Cyclometalated Complexes 41

    1. 5. 2. Triazole Ligands 44

    1. 5. 3. Ir(III) Triazole Complexes 46

  1. 6. Applications of Ir(III) Complexes 50

    1. 6. 1. Biological Imaging 50

    1. 6. 2. Photodynamic Therapy (PDT) 52

1. 6. 3. Light Emitting Devices 54

1. 7. Aims and Objectives 57

2. Development of Heterodinuclear Ir(III)-Ru(II) Complexes for White Light Emission 59

2. 1. Introduction 59

2. 1. 1. Aims and Objectives 63

2. 2. Synthesis of Ligands and Complexes 66

2. 2. 1. Synthesis of Ligands 66

2. 2. 2. Synthesis and Characterisation of Complexes 66

2. 3. Electrochemistry 70

2. 4. Photophysical Properties 75

2. 4. 1. Electronic UV-Vis Absorption Spectroscopy 75

2. 4. 2. Emission Spectroscopy 80

2. 4. 2. 1. Excitation Dependent Emission 87

2. 4. 2. 2. Oxygen Dependant Emission 88

2. 4. 2. 3. CIE Coordinate Plot 92

2. 5. Photostability of Complexes 94

2. 5. 1. ^{1}H NMR Spectroscopic Monitoring of Photolysis 95

2. 5. 2. UV-Vis Spectroscopic Monitoring of Photolysis 95

2. 5. 3. Emission Spectroscopic Monitoring of Photolysis 97

2. 6. Conclusion 100

3. Development of Ir(III) Complexes to Investigate the High Energy T_1 States 102

3. 1. Introduction 102

3.1.1 Aims and Objectives 108

3. 2. Synthesis of Ligands 109

3. 2. 2. General procedure for synthesis of triazole based ligands 110

3. 3. Synthesis and Characterisation of Iridium Complexes 110

3. 3. 1. General procedure for synthesis of complexes **JA4-7** 110

3. 4. Electrochemistry 112

3. 5. Photophysical Properties 115

    3. 5. 1. Electronic UV-Vis Absorption Spectroscopy 115
    3. 5. 2. Emission Spectroscopy 117
    3. 5. 2. 1. Oxygen Dependent Emission 119
    3. 5. 2. 2. Low Temperature Emission 121
    3. 5. 3. Transient Absorption Spectroscopy 123
  3. 5. DFT and TD-DFT Characterisation 128
  3. 6. Conclusion 133
4. Development of Novel Ir(III) 3+2+1 Cyclometalated Complexes, $[Ir(N^{\wedge}N^{\wedge}N)(C^{\wedge}N)Cl)]^+$ 134
  4. 1. Introduction 134
    4. 1. 1. Aim and Objectives 137
  4. 2. Synthesis of Ligands 137
    4. 2. 1 Synthesis of ptz-bn 137
    4. 2. 2. Synthesis of tz-py-tz and tz-pyz-tz 138
  4. 3. Synthesis and Characterisation of Iridium Complexes 138
  4. 4. Electrochemistry 140
  4. 5. Photophysical Properties 143
    4. 3. 1. Electronic UV-Vis Absorption Spectroscopy 143
    4. 3. 2. Emission Spectroscopy 145
  4. 5. DFT Characterisation 149
  4. 6. Conclusion 152
5. General Conclusions and Future Work 153
  5.1 General Conclusions 153
  5.2 Future Work 154
6. Experimental 157
  6.1 General Characterisation Methods 157
  6.2 Electrochemistry 158
  6.3 Transient Absorption Spectroscopy 159
  6.4 Density Functional Theory Calculations 160
  6.5 Ligand Release Photochemistry 161

6.6 General Synthesis of pytz-*o/m/p*-xyl-pytz[160] 162

6.5.1 1,4-bis((4-(pyridin-2-yl)-1*H*-1,2,3-triazol-1-yl)methyl)benzene 162

6.5.2 1,3-bis((4-(pyridin-2-yl)-1*H*-1,2,3-triazol-1-yl)methyl)benzene 162

6.5.3 1,2-bis((4-(pyridin-2-yl)-1*H*-1,2,3-triazol-1-yl)methyl)benzene 162

6.7 Synthesis of 2-(1-benzyl-1*H*-1,2,3-triazol-4-yl)pyridine (pytz)[227] 163

6.8 Synthesis of 2-methyl-6-((trimethyl-silylidyne)methyl)pyridine[228] 164

6.9 Synthesis of 2-(1-benzyl-1*H*-1,2,3-triazol-4-yl)-6-methylpyridine (m-pytz)[227] 165

6.10 Synthesis of 1-benzyl-4-phenyl-1*H*-1,2,3-triazole (ptz)[227] 166

6.11 Synthesis of 1,1'-dibenzyl-1*H*,1'*H*-4,4'-bi(1,2,3-triazole) (btz)[227] 167

6.12 Synthesis of 3,5-dimethyl-1-phenyl-1*H*-pyrazole (dmppz) 168

6.13 Synthesis of 2,6-bis((trimethyl-silylidyne)methyl)pyridine[228] 169

6.14 Synthesis of 2,6-bis((trimethyl-silylidyne)methyl)pyrazine[228] 170

6.15 Synthesis of 2,6-bis(1-benzyl-1*H*-1,2,3-triazol-4-yl)pyridine (tz-py-tz)[227] 171

6.16 Synthesis of 2,6-bis(1-benzyl-1*H*-1,2,3-triazol-4-yl)pyrazine (tz-pyz-tz) 172

6.17 General synthesis of [Ru(bpy)$_2$(pytz-*o/m/p*-xyl-pytz)]2PF$_6$, JA1-3.Ru 173

6.17.1 [Ru(2,2'-bipyridine)$_2$(1,4-bis((4-(pyridin-2-yl)-1*H*-1,2,3-triazol-1-yl)methyl)benzene)]2PF$_6$ 173

6.17.2 [Ru(2,2'-bipyridine)$_2$(1,3-bis((4-(pyridin-2-yl)-1*H*-1,2,3-triazol-1-yl)methyl)benzene)]2PF$_6$ 174

6.17.3 [Ru(2,2'-bipyridine)$_2$(1,2-bis((4-(pyridin-2-yl)-1*H*-1,2,3-triazol-1-yl)methyl)benzene)]2PF$_6$ 174

6.18 General synthesis of [Ir(ppy)$_2$(pytz-*o/m/p*-xyl-pytz)]PF$_6$, JA1-3.Ir 175

6.18.1 [Ir(2-phenylpyridine)$_2$(1,4-bis((4-(pyridin-2-yl)-1*H*-1,2,3-triazol-1-yl)methyl)benzene)]PF$_6$ 175

6.18.2 [Ir(2-phenylpyridine)$_2$(1,3-bis((4-(pyridin-2-yl)-1*H*-1,2,3-triazol-1-yl)methyl)benzene)]PF$_6$ 176

6.18.3 [Ir(2-phenylpyridine)$_2$(1,2-bis((4-(pyridin-2-yl)-1*H*-1,2,3-triazol-1-yl)methyl)benzene)]PF$_6$ 176

6.19 General synthesis of [Ir(dfppy)$_2$(pytz-*o/m/p*-xyl-pytz)]PF$_6$, JA1-3.IrF 177

6.19.1 [Ir(2-(4,6-difluorophenyl)pyridine)$_2$(1,4-bis((4-(pyridin-2-yl)-1*H*-1,2,3-triazol-1-yl)methyl)benzene)]PF$_6$ 177

6.19.2 [Ir(2-(4,6-difluorophenyl)pyridine)$_2$(1,3-bis((4-(pyridin-2-yl)-1*H*-1,2,3-triazol-1-yl)methyl)benzene)]PF$_6$ 178

6.19.3 [Ir(2-(4,6-difluorophenyl)pyridine)$_2$(1,2-bis((4-(pyridin-2-yl)-1*H*-1,2,3-triazol-1-yl)methyl)benzene)]PF$_6$ 178

6.20 General synthesis of [Ru(bpy)$_2$(pytz-*o/m/p*-xyl-pytz)Ir(ppy)$_2$]3PF$_6$, JA1a-JA3a 179

6.20.1 [Ru(2,2'-bipyridine)$_2$(1,4-bis((4-(pyridin-2-yl)-1*H*-1,2,3-triazol-1-yl)methyl)benzene)Ir(2-phenylpyridine)$_2$]3PF$_6$ 179

6.20.2 [Ru(2,2'-bipyridine)$_2$(1,3-bis((4-(pyridin-2-yl)-1*H*-1,2,3-triazol-1-yl)methyl)benzene)Ir(2-phenylpyridine)$_2$]3PF$_6$ 180

6.20.3 [Ru(2,2'-bipyridine)$_2$(1,2-bis((4-(pyridin-2-yl)-1*H*-1,2,3-triazol-1-yl)methyl)benzene)Ir(2-phenylpyridine)$_2$]3PF$_6$ 180

6.21 General synthesis of [Ru(bpy)$_2$(pytz-o/m/p-xyl-pytz)Ir(dfppy)$_2$]3PF$_6$, JA1b-JA3b 181

6.21.1 [Ru(2,2'-bipyridine)$_2$(1,4-bis((4-(pyridin-2-yl)-1*H*-1,2,3-triazol-1-yl)methyl)benzene)Ir(2-(4,6-difluorophenyl)pyridine)$_2$]3PF$_6$ 181

6.21.2 [Ru(2,2'-bipyridine)$_2$(1,3-bis((4-(pyridin-2-yl)-1*H*-1,2,3-triazol-1-yl)methyl)benzene)Ir(2-(4,6-difluorophenyl)pyridine)$_2$]3PF$_6$ 182

6.21.3 [Ru(2,2'-bipyridine)$_2$(1,2-bis((4-(pyridin-2-yl)-1*H*-1,2,3-triazol-1-yl)methyl)benzene)Ir(2-(4,6-difluorophenyl)pyridine)$_2$]3PF$_6$ 182

6.22 Synthesis of [Ir(3,5-dimethyl-1-phenyl-1*H*-pyrazole)$_2$(1,1'-dibenzyl-1*H*,1'*H*-4,4'-bi(1,2,3-triazole)]PF$_6$, JA4 183

6.23 Synthesis of [Ir(3,5-dimethyl-1-phenyl-1*H*-pyrazole)$_2$(2,2'-bipyridine)]PF$_6$, JA5 184

6.24 Synthesis of [Ir(3,5-dimethyl-1-phenyl-1*H*-pyrazole)$_2$(2-(1-benzyl-1*H*-1,2,3-triazol-4-yl)pyridine)]PF$_6$, JA6 185

6.25 Synthesis of [Ir(3,5-dimethyl-1-phenyl-1*H*-pyrazole)$_2$(2-(1-benzyl-1*H*-1,2,3-triazol-4-yl)-6-methylpyridine)]PF$_6$, JA7 186

6.26 Synthesis of [Ir(4'-(*p*-tolyl)-2,2':6',2''-terpyridine)(1-benzyl-4-phenyl-1*H*-1,2,3-triazole)Cl]PF$_6$, JA8 187

6.27 Synthesis of [Ir(2,6-bis(1-benzyl-1*H*-1,2,3-triazol-4-yl)pyridine)(2-phenylpyridine)]PF$_6$, JA9 188

6.28 Synthesis of [Ir(2,6-bis(1-benzyl-1*H*-1,2,3-triazol-4-yl)pyrazine)(2-phenylpyridine)]PF$_6$, JA10 189

6.29 Synthesis of [Ir(2,6-bis(1-benzyl-1*H*-1,2,3-triazol-4-yl)pyridine)(2-(4-fluorophenyl)pyridine)]PF_6, JA11 190

6.30 Synthesis of [Ir(2,6-bis(1-benzyl-1*H*-1,2,3-triazol-4-yl)pyrazine)(2-(4-fluorophenyl)pyridine)]PF_6, JA12 191

7. References 192

8. Appendix 200

- 8. 1. ^{1}H NMR Spectroscopic Monitoring of Photolysis 200
  - 8. 1. 1. [Ir(ppy_2)(pytz-*p*-xyl-pytz)Ru(bpy)]$^+$, **JA1a** 200
  - 8. 1. 2. [Ir(ppy_2)(pytz-*m*-xyl-pytz)Ru(bpy)]$^+$, **JA2a** 200
  - 8. 1. 3. [Ir($dfppy_2$)(pytz-*m*-xyl-pytz)Ru(bpy)]$^+$, **JA2b** 201
  - 8. 1. 4. [Ir(ppy_2)(pytz-*o*-xyl-pytz)Ru(bpy)]$^+$, **JA3a** 201
  - 8. 1. 5. [Ir($dfppy_2$)(pytz-*o*-xyl-pytz)Ru(bpy)]$^+$, **JA3b** 202
- 8. 2 Emission Spectroscopic Monitoring of Photolysis 202
  - 8. 2. 1 [Ir(ppy_2)(pytz-*m*-xyl-pytz)Ru(bpy)]$^+$, **JA2a** 202
  - 8. 2. 2 [Ir($dfppy_2$)(pytz-*m*-xyl-pytz)Ru(bpy)]$^+$, **JA2b** 203
  - 8. 2. 3 [Ir(ppy_2)(pytz-*o*-xyl-pytz)Ru(bpy)]$^+$, **JA3a** 203
  - 8. 2. 4 [Ir($dfppy_2$)(pytz-*o*-xyl-pytz)Ru(bpy)]$^+$, **JA3b** 204

List of Figures

Figure 1.1 Jablonski diagram, showing ground state and excited state transitions. Spins are shown for a pair of electrons in each state. Redrawn from reference.[52] 30
Figure 1.2 Primary processes of the light-matter interaction. Redrawn from reference.[54] 31
Figure 1.3 Primary and secondary processes of the light-matter interaction. When an excited state (A*) has been populated by another excited state (A**) through a non-radiative process. Redrawn from reference.[54] 35
Figure 1.4 Simplified molecular orbital diagram of $[Ru(bpy)_3]^{2+}$, structure shown of complex in top left. Redrawn from referemce.[61] 37
Figure 1.5 Potential energy surface diagram of $[Ru(bpy)_3]^{2+}$ describing key photophysical processes. r.c. = reaction coordinate. Redrawn from reference.[61] 38
Figure 1.6 Series of Ru(II) complexes reported by Elliott and co-workers.[63] Shows the variation in the number of btz moieties on the complexes. 39
Figure 1.7 Simplified molecular orbital diagram of $[Ir(ppy)_2(bpy)]^+$ and structure of complex (top-left).[69] 40
Figure 1.8 Diagram demonstrating the effects, on the energy levels, of the frontier orbitals when modified with EWG and EDG using $[Ir(ppy)_2(bpy)]^+$. 41
Figure 1.9 $Ir(R\text{-}ppy)_3$ complexes reported by Sweigart and co-workers,[70] modulation of the aryl moiety with EWG and EDG groups. 42
Figure 1.10 Series of complexes developed by Thompson and co-workers based on $[Ir(ppz\text{-}R)_2(bpy\text{-}R)]^+$ structure.[71] A variety of EWG and EDG used to modulate the HOMO and LUMO. 43
Figure 1.11 Phenylpyridine (ppy) and highly investigated ppy based complexes. 44
Figure 1.12 Catalytic cycle for the Cu(I) catalysed Huisgen-Sharpless 1,4-triazole route. Redrawn from reference.[76] Different molecules of the same Cu complexes identified as a and b. 45
Figure 1.13 Structures of common triazole based ligands and their ascribed shorthand names. 46
Figure 1.14 Ir triazole complexes reported by De Cola (left),[85-87] Donnelly (centre),[88] and Elliott (right).[83, 84] 47
Figure 1.15 Cylcometalated triazole Ir complexes reported by Schubert and co-workers.[87] 48
Figure 1.16 Cylcometalated triazole Ir complexes reported by De Cola and co-workers.[93] 48
Figure 1.17 Cylcometalated triazole Ir complexes reported by De Cola and co-workers (left),[94] and Zysman-Colman and co-workers (right).[95] 49
Figure 1.18 Cyclometalated triazole Ir complexes with btz ancillary ligands reported by Zysman-Colman and co-workers.[84] 49
Figure 1.19 Complexes reported for use as cytoplasm staining reported by Li and co-workers. a) Initial complexes reported as stain.[104] b) Complexes further developed for staining.[105] 50

Figure 1.20 Nucleus imaging probe reported by Li and co-workers.[110] 51

Figure 1.21 Near infra-red mitochondria imaging probe developed by Chao and co-workers.[115] 52

Figure 1.22 Structure of complexes developed by Zhou and co-workers for use in PDT,[121] using the "ping-pong" effect. 53

Figure 1.23 Ir complexes developed by the Sun and McFarland groups,[122] utilising the pyrene moiety to increase their capabilities as PDT agent. 53

Figure 1.24 Simplified diagrams showing structure of the devices for OLEDs (left) and LEECs (right).[125] 54

Figure 1.25 Neutral Ir complexes that have potential to be used in OLEDs, $Ir(ppy)_3$ (left) is a green emitter,[75] $Ir(piq)_3$ (centre) is a red emitter,[73] and $Ir(dfppy)_2(pic)$ (right) is a blue emitter.[126]................ 55

Figure 1.26 Structure of the most prominent cationic Ir complexes used in LEEC's. The orange emitting complex by Wong and co-workers (top left),[130] the sky-blue emitting complex reported by Thompson and co-workers (top right),[71] the most efficient green emitter developed by Baranoff and co-workers (bottom left),[132] and the effective red emitter reported by Bryce and co-workers (bottom right).[133].... 56

Figure 2. 1 Efficient Ir(III) triazole complexes reported by De Cola and co-workers.[89] The H substituted complex was a sky-blue /green emitter and the F substituted complex was a blue/sky-blue emitter... 59

Figure 2. 2 Reported heteromultinuclear Ir(III)-Eu(III) complexes that utilise partial energy transfer to induce white light emission. De Cola and co-workers 1,2,4-triazole based ligand architecture (top),[155] Sambri and co-workers exploring the substituents on the cyclometalated ligands (centre),[156] and the heterodinuclear complex developed by Ward and co-workers (bottom).[157] 62

Figure 2. 3 Reported emissive Ru triazole complex by Schubert and co-workers (top left).[159] Novel heterodinuclear complexes **JA1-3** designed for white light emission and potential use in WLEECs (bottom). Mononuclear analogues of the dinuclear complexes separating the Ir(III) (centre) and Ru(II) (top right) metal centre for comparison. 65

Figure 2. 4 ^{1}HNMR spectrum of pytz-p-xyl-pytz bridging ligand and ESI-MS (top right). There are 7 unique hydrogen environments, a) aromatic, b) benzyl CH_2, c) triazole, and the pyridine resonances (d,e,f,g)... 66

Scheme 2. 1 a) Preparation of bridging ligands pytz-o/m/p-xyl-pytz via "click" CuAAC reaction. b) Preparation of $[Ru(bpy)_2(pytz\text{-}o/m/p\text{-}xyl\text{-}pytz)]^{2+}$. c) Preparation of mononuclear Ir complexes $[Ir(R\text{-}ppy)_2(pytz\text{-}o/m/p\text{-}xyl\text{-}pytz)]^+$. d) Preparation of heterodinuclear target complexes $[Ir(R\text{-}ppy)_2(pytz\text{-}o/m/p\text{-}xyl\text{-}pytz)Ru(bpy)_2]^{2+}$.. 68

Figure 2. 5 ^{1}H NMR spectrum of JA1a in CD_3CN with zoom in on the region between 5.0-9.0ppm.. 69

Figure 2. 6 Cyclic Voltammograms of **JA1** (para) heterodinuclear and mononuclear complexes. Recorded in MeCN using Fc+/Fc as an internal standard, NBu_4PF_6 was used as the supporting electrolyte with a solution concentration of 0.2 moldm^{-3}. Measurements were performed under an atmosphere of N_2 at a scan rate of 100mV s^{-1}. 70

Figure 2. 7 Cyclic Voltammograms of **JA2** (meta) heterodinuclear and mononuclear complexes. Recorded in MeCN using Fc+/Fc as an internal standard, NBu_4PF_6 was used as the supporting electrolyte with a solution concentration of 0.2 $moldm^{-3}$. Measurements were performed under an atmosphere of N_2 at a scan rate of 100mV s^{-1}. 71

Figure 2. 8 Cyclic Voltammograms of **JA3**(ortho) heterodinuclear and mononuclear complexes. Recorded in MeCN using Fc+/Fc as an internal standard, NBu_4PF_6 was used as the supporting electrolyte with a solution concentration of 0.2 $moldm^{-3}$. Measurements were performed under an atmosphere of N_2 at a scan rate of 100mV s^{-1}. 72

Figure 2. 9 UV-visible electronic absorption spectra recorded for **JA1** (para) heterodinuclear and mononuclear complexes. Recorded in MeCN at 298K. 75

Figure 2. 10 UV-visible electronic absorption spectra recorded for **JA2** (meta) heterodinuclear and mononuclear complexes. Recorded in MeCN at 298K. 76

Figure 2. 11 UV-visible electronic absorption spectra recorded for **JA3** (ortho) heterodinuclear and mononuclear complexes. Recorded in MeCN at 298K. 77

Figure 2. 12 Emission spectra of **JA1** (para) heterodinuclear and mononuclear complexes. Recorded in MeCN aerated solution at 298K.Excitation wavelength for emission spectroscopy was 380 nm for JA1a+b, JA1.Ir and JA1.IrF. The excitation wavelength for JA1.Ru was 445 nm. 80

Figure 2. 13 Emission spectra of **JA2** (meta) heterodinuclear and mononuclear complexes. Recorded in MeCN aerated solution at 298K. Excitation wavelength for emission spectroscopy was 380 nm for JA2a+b, JA2.Ir and JA2.IrF. The excitation wavelength for JA2.Ru was 445 nm. 81

Figure 2. 14 Emission spectra of **JA3** (ortho) heterodinuclear and mononuclear complexes. Recorded in MeCN aerated solution at 298K. Excitation wavelength for emission spectroscopy was 380 nm for JA3a+b, JA3.Ir and JA3.IrF. The excitation wavelength for JA3.Ru was 445 nm. 82

Figure 2. 15 Low temperature emission spectra of **JA1** (para) heterodinuclear and mononuclear complexes. Recorded in EtOH:MeOH (4:1) glass at 77K. Excitation wavelength for emission spectroscopy was 380 nm for JA1a+b, JA1.Ir and JA1.IrF. The excitation wavelength for JA1.Ru was 445 nm. 85

Figure 2. 16 Low temperature emission spectra of **JA2** (meta) heterodinuclear and mononuclear complexes. Recorded in EtOH:MeOH (4:1) glass at 77K. Excitation wavelength for emission spectroscopy was 380 nm for JA2a+b, JA2.Ir and JA2.IrF. The excitation wavelength for JA2.Ru was 445 nm. 86

Figure 2. 17 Low temperature emission spectra of **JA3** (ortho) heterodinuclear and mononuclear complexes. Recorded in EtOH:MeOH (4:1) glass at 77K. Excitation wavelength for emission spectroscopy was 380 nm for JA3a+b, JA3.Ir and JA3.IrF. The excitation wavelength for JA3.Ru was 445 nm. 87

Figure 2. 18 Emission spectra of complexes **JA1-3** whilst being excited at different wavelengths between the Ir absorption band. Recorded in aerated MeCN at room temperature. 88

Figure 2. 19 Emission spectra of heteronuclear and mononuclear complexes **JA1-3** in MeCN solutions with varying levels of oxygen presence. Excitation wavelength for emission spectroscopy was 380 nm for JA1-3a, JA1-3b, JA1-3.Ir and JA1-3.IrF. The excitation wavelength for JA1-3.Ru was 445 nm. Air is for aerated solution, Nitrogen is a deaerated solution that has been freeze pump thawed and filled with nitrogen, Oxygen is for an 100% oxygen saturated solution. Recorded at room temperature...... 89

Figure 2. 20 CIE coordinate plot for heterodinuclear and mononuclear complexes JA1-3. Deaearted complexes are filled icons, aerated complexes are just the border, and oxygen saturated complexes are dashed border. JA1 (para) complexes are black, JA2 (meta) icons are grey and JA3 (ortho) icons are white. JA1-3.Ru = squares, JA1-3.Ir = diamonds, JA1-3.IrF = crosses, JA1a-3a = circles, and JA1b-3b = triangles. 92

Scheme 2. 2 Photolysis of heterodinuclear complexes **JA1-3** in a solution of MeCN, resulting in mononuclear Ir complexes (**JA1-3.Ir/F**) and [Ru(bpy)$_2$(NCMe)$_2$]$^{2+}$ as the photoproducts. 94

Figure 2. 21 ^{1}H NMR Spectra taken of the Complex **JA1b** in MeCN at 298K at different times of exposure to white light. Stars = Chelated CH$_2$, Triangle = Non-chelated CH$_2$, Square = Triazole, Circle = [Ru(bpy)$_2$(NCMe)$_2$]$^{2+}$ 95

Figure 2. 22 Photolysis process monitored by UV-vis for heterodinuclear complexes **JA1-3** in MeCN. The light source is mercury emission lines from a 23 W fluorescent light bulb.................................. 96

Figure 2. 23 Emission spectra recorded whilst monitoring the photolysis process for heterodinuclear complexes JA1-3. Excitation wavelength for emission spectroscopy was 380 nm for JA1-3a, JA1-3b, JA1-3.Ir and JA1-3.IrF. The excitation wavelength for JA1-3.Ru was 445 nm. Complex JA1a emission profile over 60mins (top left), complex JA1b emission profile over 60 mins (bottom left) and JA1.Ru emission profile recorded undergoing photolysis over 60mins (top right). The Ir(III) emission intensity for each of the complexes was plotted over time to observe it across the series (bottom right). 98

Figure 2. 24 CIE Coordinate plot of heterodinuclear complexes **JA1-3** throughout the photolysis process. JA1 = black, JA2 = purple and JA3 = blue. Non-fluorinated = block colour and fluorinated = stripes. 99

Scheme 2. 3 Jablonski diagram showing the photophysical processes and partial energy transfer in the excited states for heterodinuclear complexes **JA1-3**. 101

Figure 3. 1 Highly efficient neutral Ir(III) emitting complexes, Thompson and co-workers (green emitter), [75] Tsuboyama and co-workers (red emitter),[73] and Liu and co-workers (red emitter).[170]..... 103

Figure 3. 2 Highly efficient sky-blue emitters reported by Wang and co-workers,[174] and Yersin and co-workers. [175] 103

Figure 3. 3 Neutral cyclometalated Ir(III) triazole complexes reported by Fernandez-Hernandez and co-workers. [89] 104

Figure 3. 4 Deep blue emitting carbene Ir(III) complexes developed by Holmes and co-workers. [179] 105

Figure 3. 5 Archetypal cationic Ir(III) complexes reported by Guedl and co-workers, [180] and Zysman-Colman co-workers complex that has been thoroughly investigated. [181] 106

Figure 3. 6 Sky-blue emitting complexes reported by Su and co-workers, [187] and Zysman-Colman and co-workers.. 107

Figure 3. 7 Blue emitting triazole based Ir(III) complexes reported by De Cola and co-workers, [85, 86] and Elliott and co-workers. [78] 108

Figure 3. 8 Target Ir(III) complexes to explore the high energy triplet excited states....................... 109

Figure 3. 9 ^{1}H NMR spectrum of the dmppz ligand in $CDCl_3$... 110

Scheme 3. 1 a) Preparation of cyclometalated ligand dmppz. b) Preparation of $[Ir(dmppz)_2(\mu\text{-}Cl)]_2$, c) Preparation of target complexes **JA4-7**. N^N diimine ligands for each complex (bottom)................ 111

Figure 3. 10 ^{1}H NMR spectrum of complex JA4, in CD_3CN, showing the different resonances....... 112

Figure 3. 11 ^{1}H NMR spectrum of JA6, in CD_3CN, showing the difference in the asymmetric pytz complex.. 112

Figure 3. 12 Cyclic Voltammograms of complexes **JA4-7**. Recorded in MeCN using Fc+/Fc as an internal standard, NBu_4PF_6 was used as the supporting electrolyte with a solution concentration of 0.2 moldm^{-3}. Measurements were performed under an atmosphere of N_2 at a scan rate of 100mV s^{-1}. .. 113

Figure 3. 13 UV-visible absorption spectra recorded for **JA4-7** complexes. Recorded in MeCN at 298K. 116

Figure 3. 14 Emission recorded for **JA4-7** complexes. Recorded in de-aerated MeCN at 298K. Wavelength of excitation for JA4= 310 nm, JA6 and JA7 = 340 nm, and for JA5 = 350 nm........... 118

Figure 3. 15 Emission spectra of complexes **JA4-7** in MeCN solutions with varying levels of oxygen presence Aerated (green), deaerated solution (blue) was free-pump thawed with all gases removed, solution was saturated with O_2 (red). Recorded at 298K. Wavelength of excitation for JA4= 310 nm, JA6 and JA7 = 340 nm, and for JA5 = 350 nm. 120

Figure 3. 16 Low temperature emission spectra of **JA4-7** complexes. Recorded in EtOH:MeOH (4:1) glass at 77K. Wavelength of excitation for JA4= 310 nm, JA6 and JA7 = 340 nm, and for JA5 = 350 nm. 122

Figure 3. 17 UV-visible transient absorption spectra for complex **JA4** in MeCN at 298K (λ_{ex} = 285 nm). Two excited state absorption maxima at 380 nm and 460 nm that broaden rapidly followed by excited state absorption decay.. 124

Figure 3. 18 Time profile and kinetic fit from global analysis for associated transient absorption spectra for complex **JA4**. 125

Figure 3. 19 UV-visible transient absorption spectra for complex **JA5** in MeCN at 298K (λ_{ex} = 285 nm). Two excited state absorption maxima at 380 nm and 505 nm that are still present at the end of time window. 125

Figure 3. 20 UV-visible transient absorption spectra for complex **JA6** in MeCN at 298K (λ_{ex} = 285 nm). Two excited state absorption maxima at 340 nm and 410 nm that are still present at the end of time window.. 126
Figure 3. 21 UV-visible transient absorption spectra for complex **JA7** in MeCN at 298K (λ_{ex} = 285 nm). Excited state absorption maximum at 345 nm which decays within the time window. 127
Figure 3. 22 Time profile and kinetic fit from global analysis for associated transient absorption spectra for complex **JA7**. 127
Figure 3. 23 Ground state molecular orbital energy level diagram for complexes **JA4-7**, displaying the frontier orbitals on the isosurfaces. 129
Figure 3. 24 Molecular orbital energy level diagram for complexes **JA4-7**. 130
Figure 3. 25 TDDFT calculated absorption spectra for complexes **JA4-7** with transition intensities. 131
Figure 4. 1 Ir terdentate complexes reported by Bernhard and co-workers.[199] 134
Figure 4. 2 Ir 3+2+1 complexes designed by Bernhard and co-workers. [203] 135
Figure 4. 3 Ir complex reported by Sadler and co-workers for utilisation as a PDT agent. [204] 136
Figure 4. 4 Ir 3+2+1 complexes developed by Bernhard and co-workers. [206] 136
Figure 4. 5 Ir complexes designed to investigate novel chemical spaces with triazoles, **JA8-12**. 137
Scheme 4. 1 Synthetic procedure for tz-py/z-tz ligands, a) Sonogashira coupling that afford the pyridine/pyrazine compound with protected acetylenes. b) A “click” CuAAC reaction using the acetylenes and the benzyl azide to produce the target ligand. 138
Scheme 4. 2 Synthetic process for these [Ir(N^N^N)(C^N)Cl]$^{+}$ complexes, initial trichlorides are prepared, then the desired complexes are afforded. 139
Figure 4. 6 Cyclic Voltammograms of complexes **JA8-12**. Recorded in MeCN using Fc+/Fc as an internal standard, NBu_4PF_6 was used as the supporting electrolyte with a solution concentration of 0.2 moldm^{-3}. Measurements were performed under an atmosphere of N_2 at a scan rate of 100mV s^{-1}. .. 140
Figure 4. 7 UV-visible absorption spectra recorded for **JA8-12** complexes. Recorded in MeCN at 298K 144
Figure 4. 8 Emission recorded for **JA8-12** complexes. Recorded in aerated MeCN at 298K. Wavelengths of excitation; λ_{ex} = 350 nm for **JA9** and **JA10**, λ_{ex} = 355 nm for **JA11** and **JA12**, and λ_{ex} = 400 nm for **JA8**. 146
Figure 4. 9 Low temperature emission spectra of **JA8-12** complexes. Recorded in EtOH:MeOH (4:1) glass at 77K. Wavelengths of excitation; λ_{ex} = 350 nm for **JA9** and **JA10**, λ_{ex} = 355 nm for **JA11** and **JA12**, and λ_{ex} = 400 nm for **JA8**. 148
Figure 4. 10 Ground state molecular orbital energy level diagram for complexes **JA8-12**, displaying the frontier orbitals on the isosurfaces. 150
Figure 4. 11 Molecular orbital energy level diagram for complexes **JA8-12** 151

Figure 5. 1 Concepts for developing an efficient white light emitter, developing on JA1b and JA2b. 155
Figure 5. 2 Modified Ir(III) 3+2+1 complex JA8 with a series of R groups........ 155

List of Schemes

Scheme 2. 1 a) Preparation of bridging ligands pytz-o/m/p-xyl-pytz via "click" CuAAC reaction. b) Preparation of $[Ru(bpy)_2(pytz\text{-}o/m/p\text{-}xyl\text{-}pytz)]^{2+}$. c) Preparation of mononuclear Ir complexes $[Ir(R\text{-}ppy)_2(pytz\text{-}o/m/p\text{-}xyl\text{-}pytz)]^{+}$. d) Preparation of heterodinuclear target complexes $[Ir(R\text{-}ppy)_2(pytz\text{-}o/m/p\text{-}xyl\text{-}pytz)Ru(bpy)_2]^{2+}$..68

Scheme 2. 2 Photolysis of heterodinuclear complexes **JA1-3** in a solution of MeCN, resulting in mononuclear Ir complexes (**JA1-3.Ir/F**) and $[Ru(bpy)_2(NCMe)_2]^{2+}$ as the photoproducts........94

Scheme 2. 3 Jablonski diagram showing the photophysical processes and partial energy transfer in the excited states for heterodinuclear complexes **JA1-3**. 101

Scheme 3. 1 a) Preparation of cyclometalated ligand dmppz. b) Preparation of $[Ir(dmppz)_2(\mu\text{-}Cl)]_2$, c) Preparation of target complexes **JA4-7**. N^N diimine ligands for each complex (bottom)......111

Scheme 4. 1 Synthetic procedure for tz-py/z-tz ligands, a) Sonogashira coupling that afford the pyridine/pyrazine compound with protected acetylenes. b) A "click" CuAAC reaction using the acetylenes and the benzyl azide to produce the target ligand. 138

Scheme 4. 2 Synthetic process for these $[Ir(N\text{^}N\text{^}N)(C\text{^}N)Cl]^{+}$ complexes, initial trichlorides are prepared, then the desired complexes are afforded..139

List of Tables

Table 1.1 Summarised Electrochemical Properties and Emission Maxima of Thompson and co-workers Complexes in MeCN (Figure 1.10)[71] 44

Table 2.1 Summarised Electrochemical Data for 1.5mmol dm^{-3} MeCN Solutions of JA1-3 Measured at r.t.at 100mV s^{-1}.[*a,b*] 74

Table 2.2 Summarised Photophysical Data for MeCN Solutions of JA1-3 and Mononuclear Counterparts Measured at r.t. 79

Table 2.3 Summarised Photophysical Data of JA1-3 at Low Temperature (77K) in EtOH:MeOH glass and in Aerated, Deaerated and Oxygenated MeCN Solutions Measured at r.t. 91

Table 2.4 CIE Coordinates for MeCN Solutions of JA1-3 and their Mononuclear Counterparts Measured at r.t. 93

Table 2.5 Quantum Yields for Photochemical Release of [Ir(R-ppy)$_2$(pytz-*o/m/p*-xyl-pytz)]$^+$ from [Ir(R-ppy)$_2$(pytz- *o/m/p*-xyl -pytz)Ru(bpy)$_2$]$^{3+}$ in MeCN 97

Table 2.6 CIE Chromaticity Coordinates and Quantum Yields of Photoluminescence as Complexes JA1-3 are Monitored by Emission Spectroscopy[a] 100

Table 3.1 Summarised Electrochemical Data for 1.5mmol dm^{-3} MeCN Solutions of JA 4-7 Measured at r.t.at 100mV s^{-1}.[*a,b*] 114

Table 3.2 Summarised Photophysical Data for MeCN Solutions of JA4-7 at 298 K. 115

Table 3.3 Summarised Photophysical Data of JA4-7 at Low Temperature (77K) in EtOH:MeOH glass and in Aerated, Deaerated and Oxygen Saturated MeCN Solutions Measured at r.t. 121

Table 3.4 Summary of Excited State Lifetimes for JA4-7 123

Table 3.5 Summarised HOMO and LUMO Energy Values from DFT Calculations for Complexes JA4-7 131

Table 3.6 Selected Energies (eV), Oscillator Strength (*f*), Wavelength (nm) and Compositions of Vertical Excitations from TDDFT Calculations. 132

Table 4.1 Summarised Electrochemical Data for 1.5mmol dm^{-3} MeCN Solutions of JA8-12 Measured at r.t.at 100mV s^{-1}.[*a,b*] 142

Table 4.2 Summarised Photophysical Data for MeCN Solutions of JA8-12 at 298 K 143

Table 4.3 Summarised HOMO and LUMO Energy Values from DFT Calculations for Complexes JA8-12 152

List of Abbreviations

^{13}C NMR	Carbon-13 nuclear magnetic resonace
^{1}H NMR	Proton nuclear magnetic resonace
^{3}ILCT	Triplet intra-ligand charge transfer
^{3}LLCT	Triplet ligand-to-ligand charge transfer
^{3}MLCT	Triplet metal-to-ligand charge transfer
A	Absorbance
aq.	Aqueous
bpy	2,2'-bipyridyl
btz	4,4-bi-1,2,3-triazol-4-yl
$CDCl_3$	Deuterated chloroform
cm^{-1}	Wavenumber
CuAAC	Copper catalysed azide/alkyne cycloaddition
DCM	Dichloromethane
dfppy	2-(2,4-diflouro)pyridine
DFT	Density-functional theory
DMF	Dimethylformamide
dmppz	3,5-dimethyl-1-phenyl-1H-pyrazole
DMSO	Dimethylsulfoxide
EDG	Electron donating group
EQE	External quantum efficency
Et_2O	Diethyl ether
EtOH	Ethanol
EWG	Electron withdrwaing group
Fc+/Fc	Ferrocenium/Ferrocene
g	Grams
HOMO	Highest occupied molecular orbital
Hz	Hertz
ISC	Intersystem crossing
K	Kelvin
k_{nr}	Non-radiative decay constant
k_r	Radiative decay constant
LC	Ligand centred
LED	Light-emitting diode

LEEC	Light-emitting electrochemical cell
LUMO	Lowest unoccupied molecular orbital
M	Molarity/Molar
m/z	mass-to-charge
MC	Metal centred
MeCN	Acetonitrile
MeOH	Methanol
mg	Milligrams
ml	Millilitre
m-pytz	2-(1-benzyl-1H-1,2,3-triazol-4-yl)-6-methylpyridine
mV	Millivolts
nm	Nanometers
ns	Nanosecond
º	Degrees
ºC	Degrees Celsius
OLED	Organic light emitting device
-OMe	Methoxy-
org.	Organic
PACT	Photoactivated chemotherapy
PDT	Photodynamic therapy
PLQY	Photoluminescent quantum yield
ppy	2-phenylpyridine
ppz	1-phenylpyrazole
ptz	1-benzyl-4-phenyl-1H-1,2,3-triazole
pytz	2-(1-benzyl-1H-1,2,3-triazol-4-yl)pyridine
pytz-*o/m/p*-xyl-pytz	*orhto/meta/para*-bis((4-(pyridin-2-yl)-1H-1,2,3-triazol-1-yl)methyl)benzene
r.t.	Room temperature
RBF	Round bottomed flask
S_0	Singlet ground state
S_1	Lowest singlet excited state
T_1	Lowest tripet excited state
TA	Transient absorption
-*t*Bu	tert-Butyl-
TCSPC	Time-correlated single photon counting
TDDFT	Time-dependent density function theory

THF	Tetrahydrofuran
TMS	Trimethylsilyl
TMS	Trimethylsilyl
tol-terpy	4'-(p-tolyl)-2,2':6',2''-terpyridine
tpy	2,2':6',2''-terpyridine
tz-py-tz	2,6-bis(1-benzyl-1H-1,2,3-triazol-4-yl)pyridine
tz-pyz-tz	2,6-bis(1-benzyl-1H-1,2,3-triazol-4-yl)pyrazine
UV-Vis	Ultraviolet-visible
V	Volts
WLEEC	White light-emitting electrochemical cell
λ	Wavelength
μs	Microsecond
τ	Excited state lifetime
ϕ	Quantum yield

1. Introduction

1. 1 Photochemistry and Photophysics

Photochemistry and photophysics have had significant influence on the world, the light from the Sun has created life as we know it. Small organic molecules were generated from photochemical reactions with the Earth's fundamental atmosphere, instigated by the Sun's rays. Photosynthesis, a complex series of photochemical and photophysical processes, ensured that simple cells would become autotrophs, endow us with the necessities for life, stored solar energy as fossil fuels and is still the main source of the vast majority of our food.[1,2]

Photochemistry is more than just utilising the energy of light, it also is used by living things for vision, an indicator of time,[3] a source of cellular damage,[4] and also can be used to in mechanisms to repair cellular damage.[5] Not only is photochemistry involved in living matter it is also employed in processes that are used to determine composition of matter in interstellar space.[6] Photophysical processes happen in nature all the time, as sunlight is not entirely absorbed or reflected, and thus we have colour. Bioluminescence occurs in a number of natural applications such as in animals and bacteria;[7,8] fireflies, glow worms and a whole variety of sea creatures. Photochemistry and photophysics are omniscient in nature, making them inherently scientifically interesting, their processes are of interest in being artificially reproduced and utilised in chemical, physical, biological, and medical technologies. Transition metal complexes have been developed effectively in this field for a wide variety of applications; artificial photosynthesis (e.g. Ru(II) complexes),[9-11] photocatalysis (e.g. Fe(III), Co(II/III), Ni(II), Pd(II), Mo(IV), W(IV) and Pt(II) complexes),[12-14] molecular switches (e.g. Ru(II), Os(II), Re(I), Fe(II), Co(II) and Zn(II) complexes),[15-17] photovoltaics (e.g Ti(IV) and Cd(II) complexes)[18-20] light emitting devices (e.g. Ir(III), Pt(II) and Re(I) complexes),[21-23] biological imaging probes (e.g. Ir(III), Rh(III), Re(I), Pt(II) and Au(I) complexes),[24-26] sensors (e.g. Ir(III), Os(II), Re(I), Cu(I), Ag(I) and Au(I) complexes),[27-29] photodynamic therapy (PDT) and photoactive chemotherapy (PACT) agents (e.g Ru(II), Fe(II), Re(I), Pt(II) and Ir(III) complexes).[30-33]

1. 2 Molecular Photophysics – Absorption of Light

1. 2. 1. Characteristics of Light

Light, therefore electromagnetic radiation in the UV-visible spectrum, is modelled in two methods: the wave model and the quantum model.[34, 35] The wave model is defined by the following equation:

$$\lambda \nu = c$$

Eq 1.1

Where λ is the wavelength, which characterises the electromagnetic radiation, ν is the frequency and c is the velocity. The λ and ν have units as m and Hz and can cover a wide span of values but c is constant, the speed of light (2.998×10^{8} m s^{-1}). Wavenumber $\bar{\nu}$, the number of waves per cm, can correspondingly be used to characterise electromagnetic radiation. Differing types of radiation are discerned by their wavelengths on the electromagnetic spectrum, when looking at photochemistry and photophysics the main area of interest is light region from the near UV to near IR region, from 200 to 1000 nm. This region can also be defined in frequency, ν, between 1.5×10^{15} to 3×10^{14} Hz and by wavenumber, $\bar{\nu}$, between 5×10^{4} to 1×10^{4} cm^{-1}.

The other model used, the quantum model, considers radiation to be a stream of photons.[36] A photon is a packet of energy, E, corresponding to the frequency of the radiation, ν. This is defined by the following equation, where h is Planck's constant (6.63×10^{-34} J s):

$$E = h\nu$$

Eq 1.2

Photons, thereby light, are both information bits and energy quanta, this can be seen in scenarios for two key natural photochemical processes, photosynthesis and vision.

When light interacts with a molecule it is generally an interaction described as being between one molecule and one photon, this is written in the following equation:

$$\mathrm{A} + h\nu \rightarrow {}^{*}\mathrm{A}$$

Eq1.3

In this equation A is the molecule in the ground state and $h\nu$ is the photon that is absorbed, *A is the molecule which is in the excited state. Moles are used to calculate the number of molecules of a compound, this can be extended to photons. As one photon is absorbed by one molecule, a mole of photons can be used as a quantity of photons, this is defined as an einstein. Therefore, one mole of molecules absorbs one einstein of photons. The energy absorbed from photons in the shorter wavelength section of the UV-visible light region is comparative to the amount of energy required to break chemical bonds. Due to the availability of such an excess amount of energy the molecule when in the excited state is considered a new chemical species with its own individual chemical and physical properties.[37]

1. 2. 2. Beer-Lambert Law

As stated by Theodor von Grotthuss in 1817 and reiterated by John W. Draper in 1841; ‘only the light absorbed is effective in producing photochemical change’, now known as the Grotthuss-Draper law.[38] This shows the importance the measurement of light being absorbed by a system is for investigating its photophysical and photochemical properties. The Beer-Lambert law defines the absorption of a monochromatic beam of light by a substance in a transparent solution.[39] It is defined in the following equations, where I is intensity of the transmitted light, I_0 is the intensity of the incident light, ε is the extinction coefficient (M^{-1} cm^{-1}) or can be referred to as the molar absorption coefficient, b is the optical path (cm) and c is the concentration of the solution (M):

$$I = I_0 \times 10^{-\varepsilon bc}$$

Eq 1.4

$$\mathrm{A} = \log(I_0/I) = \varepsilon bc$$

Eq 1.5

Decadic logarithms are often used, Eq 1.5, as most spectrophotometers use absorbance, A. The ability for a substance to absorbs is shown by the extinction coefficient, ε, and is dependent on the wavelength of the incident light.

1. 2. 3 Time-dependent Perturbation Theory

As discussed previously the absorption of one photon by one molecule results in the molecule being excited from the ground state to the electronically excited state. This is dependent on the Bohr equation,[40] where the energy change and frequency of light are related. Where E_i and E_f is the energy for the ground state and excited state wave functions[i] , Ψ_i and Ψ_f :

$$h\nu = E_\mathrm{f} - E_\mathrm{i}$$

Eq 1.6

$$\hat{H}_0\Psi_\mathrm{i} = E\Psi_\mathrm{i}$$

Eq 1.7

The Schrödinger equation is applied to a wave function Ψ_i, where the molecule in an initial stationary state (Eq 1.7).[41, 42] E for this equation is defined as the electric vector of the electromagnetic wave and

---

[i] A wave function is the single valued solution to a standing wave with a finite amplitude that is a continuous function of coordinates in the stationary states of a system.

electric dipole. However, when the system is perturbed by the exposure to light, oscillating forces are induced on the charged particles of the molecule by the sinusoidal electric vector of the light and the static Hamiltonian operator $\hat{H}_0$ is no longer a valid descriptor of the systems energy. $\hat{H}_0$ is substituted with $(\hat{H}_0 + \hat{H}')$, where $\hat{H}'$ is the perturbation operator and thusly accounts for the radiation fields effect.[43] The newly substituted functions will behave differently than the initial wave and will also be functions of time, the following equation is used:

$$\left(\hat{H}_0 + \hat{H}'\right)\Psi(x,t) = E\Psi(x,t)$$

Eq 1.8

The new wave functions are able to be expanded in regard to the terms of the wave functions of the unperturbed system, in the following equation:

$$\Psi(x,t) = \Sigma a_k(t)\Psi_k$$

Eq 1.9

The coeffecients $a_k(t)$ introduce the requisite time dependence as they are functions of time. Perturbation can be represented as a time-dependent combination of the initial wave function for the system with all the further possible wave functions, effectively the initial state evolves with time into different states.[44] If the radiation, and therefore perturbation, is removed at a certain time t, there is a finite probability that the system will be in a different final state than the initial state. The probability, from $[a_f(t)]^2$ is proportional to transition moment (TM) $\langle\Psi_\mathrm{i}|\hat{\mu}|\Psi_\mathrm{f}\rangle^2$, which is more commonly written as the integral $\int \Psi_\mathrm{i}\hat{\mu}\Psi_\mathrm{f}\mathrm{d}\tau$. The character $\hat{\mu}$ refers to the dipole-moment operator $e\Sigma r_j$, e for the electronic charge, and r_j for the vector distance between the kth electron and the centre of the positive charge of the molecule. The proportional relationship is shown in the following equation:

$$[a_\mathrm{f}(t)]^2 = \frac{8\pi^3}{3h^2}\langle\Psi_\mathrm{i}|\hat{\mu}|\Psi_\mathrm{f}\rangle^2\rho(\nu_\mathrm{if})t$$

Eq 1.10

In Eq 1.10, The radiation density (energy per unit volume) was shown in the equation as $\rho(\nu_\mathrm{if})$ at the specific frequency ν_if correlating to the transition and t is the time the system was irradiated. Consequently, the probability of any given transition is proportional to the square of the transition moment and therefore can be attained from absorption spectra via its relation to the oscillator strength f, and is a measure of integrated intensity of absorption over the whole band. Displayed in the formula, where m_e is the electronic mass:

$$f = 4.315 \times 10^9 \int \varepsilon d\nu = \frac{8\pi^2\nu_\mathrm{if}m_\mathrm{e}}{3h\mathrm{e}^2}\langle\Psi_\mathrm{i}|\hat{\mu}|\Psi_\mathrm{f}\rangle^2\rho(\nu_\mathrm{if})t$$

Eq 1.11

Therefore, we can deduce that if the final state has a higher energy than the initial state the difference in energy must have come from the radiation field, and Eq 1.10 provides the probability of absorption of a photon.

$$\Psi = \psi\theta$$

Eq 1.12

In comparison to the time scale of nuclear (vibrational) movements, light absorption takes place in a very short time frame.[45] Meaning that it is possible to divide the total wave function Ψ into the electronic wave function, ψ, and the nuclear wave function, θ, (Eq 1.12) giving the transition moment (TM) as:

$$\mathrm{TM} = \int \psi_\mathrm{f}\theta_f\hat{\mu}\psi_i\theta_i \,\mathrm{d}\tau$$

Eq 1.13

The dipole moment operator only operates on the electronic wave functions as it is independent from the nuclear coordinates.[46] Therefore, the equation can be rewritten as the following:

$$\mathrm{TM} = \int \psi_\mathrm{i}\hat{\mu}\psi_\mathrm{f} \,\mathrm{d}\tau_e \int \theta_\mathrm{i}\theta_\mathrm{f}\mathrm{d}\tau_\mathrm{N}$$

Eq 1.14

The electronic wave function can be further divided into orbitals ϕ_i (one electron wave functions) and their spin functions S_i. Due to these approximations the orbitals are assumed to be the same in the ground and excited state and only one electron transitions can be considered. However, the transition moment (TM) can now be broken down into three different terms Eq 1.15, where ϕ_i and ϕ_f are the initial and final orbitals of the excited electron and S_i and S_f are their relating spin functions.

$$\mathrm{TM} = \int \phi_\mathrm{i}\hat{\mu}\phi_\mathrm{f} \,\mathrm{d}\tau_e \int S_\mathrm{i}S_\mathrm{f}\mathrm{d}\tau_\mathrm{s} \int \theta_\mathrm{i}\theta_\mathrm{f}\mathrm{d}\tau_\mathrm{N}$$

Eq 1.15

The first terms value relates to the symmetry and spatial overlap of the initial and final orbitals and is called the electronic transition moment. The second terms value relates to the initial and final spin states of the promoted electron, defined as the spin overlap integral. The third terms are the quantum mechanical foundation of the Franck-Condon principle and is defined as the overlap integral of the initial and final wave functions for nuclear vibrations.[47, 48]

1. 2. 4 Symmetry Selection Rules

On the basis of the terms appearing in Eq 1.15 the intensity of electronic transitions can be predicted; these are called selection rules. There are three integrals in the equation, if any of these integrals have a value of zero the TM will be zero. When this occurs, this is formally a forbidden transition, if the TM value is not zero than the transitions are formally allowed. As the TM is used as an approximation, forbidden transitions do occur in practice.[49]

It is possible to tell whether a particular transition has a value of zero or not from the symmetry properties of their wave functions. This is because it has been mathematically demonstrated that an integral over all the space of symmetric function does not vanish, whilst the integral over all the space of antisymmetric function does vanish.[50]

The symmetry of orbitals is related to the electronic transition moment $\int \phi_{\mathrm{i}}\hat{\mu}\phi_{\mathrm{f}}\,\mathrm{d}\tau_e$ and as the dipole moment operator $\hat{\mu}$ is a vector it can be resolved along the Cartesian axes, resulting in three separate components, Eq 1.16. However, all the components of the vector operator are antisymmetric functions.

$$\int \phi_{\mathrm{i}}\hat{\mu}_{Total}\phi_{\mathrm{f}}\,\mathrm{d}\tau_e = \int \phi_{\mathrm{i}}\hat{\mu}_x\phi_{\mathrm{f}}\,\mathrm{d}\tau_e + \int \phi_{\mathrm{i}}\hat{\mu}_y\phi_{\mathrm{f}}\,\mathrm{d}\tau_e + \int \phi_{\mathrm{i}}\hat{\mu}_z\phi_{\mathrm{f}}\,\mathrm{d}\tau_e$$

Eq 1.16

A significant specific instance of the symmetry selection rule is when it applies to molecules with a centre of symmetry, such as transition metals. All wave functions are either symmetric or antisymmetric in regard to the centre of symmetry. They are either *gerade* (even), *g*, or *ugerade* (odd), *u*, and as per Eq 1.16 all components of the $\hat{\mu}$ vector are ungerade, *u*. If the point groups of these molecules have totally symmetric representation then they are gerarde, *g*. The result of two functions can only be gerarde if the initial wave function ϕ_{i} and final wave function ϕ_{f} have unequal gerarde/ungerarde nature. Thus *g*→*u* and *u*→*g* transitions are symmetry allowed and *g*→*g* and *u*→*u* are symmetry forbidden. The symmetry rule applies for + and – charges as well, + → + and - → - are allowed but + → - and - → + are not allowed.

1. 2. 5 Spin Selection Rules

The term $\int S_{\mathrm{i}}S_{\mathrm{f}}\mathrm{d}\tau_{\mathrm{s}}$ from the transition moment expression (Eq 1.15) shows the effect the electron spin will have on the transition intensities. Singlet → singlet and triplet → triplet transitions are spin allowed, there is no change in multiplicity therefore $\int S_{\mathrm{i}}S_{\mathrm{f}}\mathrm{d}\tau_{\mathrm{s}} = 1$. Due to the orthogonality of spin wave functions, when the initial and final states have different multiplicities the $\int S_{\mathrm{i}}S_{\mathrm{f}}\mathrm{d}\tau_{\mathrm{s}} = 0$ and is spin forbidden, hence singlet → triplet transitions are spin forbidden.

When the spin and orbital functions are separated rigorously the spin selection rule is valid, however there are departures from the approximation and this is due to spin orbit coupling, where states of different spin multiplicity can be mixed. Organic molecules have low intensity spin forbidden transitions where almost all are unobservable. Conversely, spin forbidden transitions for metal complexes can be intense this is due to the heavy metals strong charge on the nucleus inverts the spin of the electron.[51]

1. 2. 6 Franck-Condon Principle

The summation of the third term of the transition moment (Eq 1.15) will always be 1 therefore the intensity of the absorption band only depends on the first two terms. Nonetheless, the third term still plays a significant factor, as it determines the shape of the absorption band.[47, 48]

This relates to the distortion of the excited state, so when the excited is identical in equilibrium geometry and force constant, the transitions occurring in a sharp lined band, in this case the ground and excited state nuclear wave functions are solutions of the same vibrational problem. When the excited state is highly distorted, there is a different equilibrium geometry and force constant. The excited state transitions are to different vibrational states that are higher in energy this results in broader Gaussian-shaped bands. There is also the possibility that some of the transitions are higher than their dissociation energy, there would be no band for these.

Often in solvents there is a superposition of the differing vibrational progressions and interactions with the solvent molecules which often results in complete loss of vibrational structure. However, if the molecules were in rigid glasses at low temperature these vibronic structures can be seen.

1. 2. 6 The Jablonski Diagram

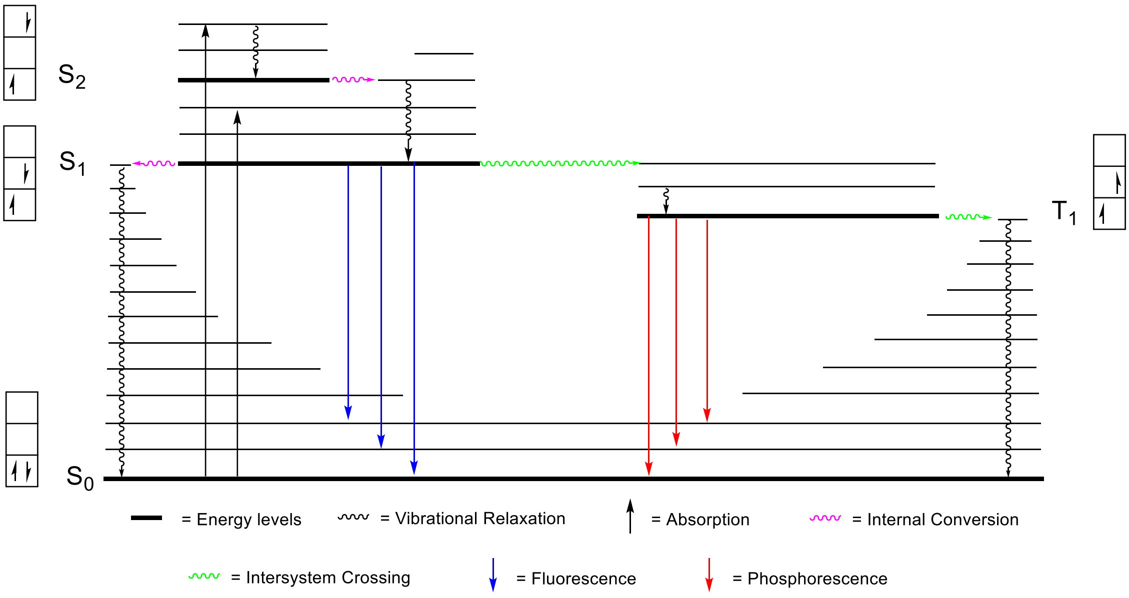

Figure 1.1 Jablonski diagram, showing ground state and excited state transitions. Spins are shown for a pair of electrons in each state. Redrawn from reference.[52]

Due to the high energy content of the excited states, they must be deactivated relatively fast. Deactivation occurs through photophysical processes back to the original molecule in the ground state or through photochemical processes where there is formation of a new species.

The photophysical processes, including light absorption are displayed on the Jablonski diagram (Figure 1.1).[53] The electronic states are represented by the thick horizontal lines that are in a vertical order to reflect the energy level of each state. The ground state S_o is a singlet state, as it generally always is, the multiplicity of the excited states is differentiated horizontally, as you can see the singlet excited states S_1 and S_2 are on the left hand side whilst the triplet excited state T_1 is on the right. The thin black lines represent the vibrational levels with the lowest one being designated to the $\nu = 0$ level. Radiative transitions such as the absorption or emission of a photon are represented by straight arrows, whereas the non-radiative transitions such as internal conversion and intersystem crossing are represented by wavy arrows. The $S_0 \rightarrow T_n$ transitions are spin forbidden following the selection rules, however this can occur in certain species.

It is important to consider that the difference in energy between the ground state and lowest excited states is significantly larger than the energy gap with any subsequent excited states. Due to the Franck-Condon principle and excited state distortion the light absorption is into a higher vibrational energy in the excited state. This applies conversely, where emission generates in a higher vibrational level of the ground state.

1. 3. Molecular Photophysics - The Excited States

In molecules that are in the ground state the only way to measure the reactivity of a certain reaction is the rate of reaction or known as the rate constant. This is similar for excited state molecules except there are several processes that are in competition with each other, where the rate constants can only be measured indirectly. The excited state deactivates through three competing processes, chemical (rate constant k_p), radiative (k_r) and non-radiative (k_{nr}). The chemical process is where the energy absorbed from light causes chemical reactions (photochemistry), the radiative and non-radiative processes fall under photophysics, all three processes are interlinked and competitive.

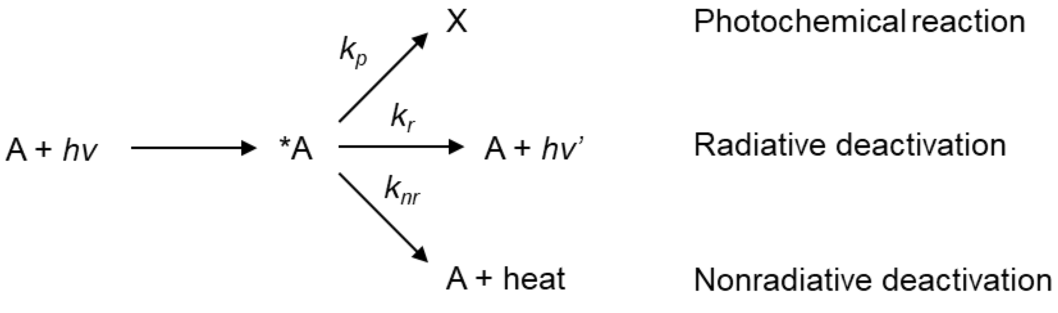

Figure 1.2 Primary processes of the light-matter interaction. Redrawn from reference.[54]

To quantify these processes the quantum yield (ϕ_i) can be calculated for each primary process:

$$\phi_i = \frac{\text{Number of molecules undergoing the process}}{\text{Number of photons absorbed}}$$

Eq. 1.17

As mentioned previously light absorption is generally to a higher vibrational level in the excited state. The species then has excess vibrational energy, which will then dissipate either thermally or via interactions with surrounding molecules. This process is defined as vibrational relaxation (V.R.), this can be seen on the aforementioned Jablonksi diagram (Figure 1.1), and in solution this process occurs very fast, in approximately the picosecond timeframe. When in a situation where a high number of collisions a cannot occur, gas phase at a low pressure, molecules can undergo intramolecular vibrational redistribution.[55] This is where the energy that has been localised to a mode, when populated by light absorption, rapidly redistributes it to all the other vibrational modes. The fastest process in the excited state are the vibrational relaxation and vibrational redistribution, therefore any subsequent processes occur from a thermally equilibrated excited states and compete with each other.

Non-radiative transitions occur between different levels of the excited state, as the overall energy of the system does not change, no photon is emitted. Non-radiative transitions are effectively irreversible processes as there is an increase in entropy and the vibrational relaxation is very fast.[56] Non-radiative transitions occur between states of the same multiplicity, known as internal conversion (I.C.), or different a multiplicity, intersystem crossing (I.S.C.).

Only states of the same symmetry can go through internal conversion, thus $S_0 \rightarrow S_1$ internal conversion forbidden, as S_0 and S_1 have different symmetries. When molecules have many different types of vibrations, the symmetry restraints are relaxed by vibronic coupling. Internal conversion is exceedingly fast (in the picosecond region). Intersystem crossing occurs between the lowest excited states of any multiplicity, this happens relatively fast to moderate on the sub nanosecond to nanosecond timescale. In the absence of heavy metal atoms, intersystem crossing may be forbidden as there is no/weak spin orbit coupling. However, in the presence of a heavy metal atom the strong charge on the nucleus inverts the spin of the electron,[51] in this scenario intersystem crossing is allowed. Intersystem crossing occurs within some organic systems featuring heavier halides such as iodine. The conversion rate within organic systems is less efficient, ~25 %, than that of heavy transition metals, ~99 %. Non-radiative deactivations from the excited state to the ground states are slower than ISC, $S_1 \rightarrow S_0$ is on a nanosecond timescale, and $T_1 \rightarrow S_0$ is even slower on the microsecond to second timescale.

Luminescence is the description of the process which leads to the radiation of light; which is the excitation and subsequent relaxation of electrons from the ground state to the excited state and back down to the ground state. The relaxation back to the ground state emits photons which usually occur in the UV or visible region of the spectrum, as for the absorption the same spin and symmetry selection rules apply. There are two different types of luminescence, fluorescence, and phosphorescence.[57]

Fluorescence happens when an excited state molecule emits a photon through a spin-allowed transition to relax to the ground state ($S_1 \rightarrow S_0$), this process occurs rapidly. Phosphorescence occurs when the excited state molecule emits through a spin-forbidden transition, the molecule is excited to the singlet state (S_1) and then undergoes intersystem crossing (i.s.c) to the triplet state (T_1), due to spin-orbit coupling, and finally undergoes spin forbidden relaxation to the ground state ($T_1 \rightarrow S_0$).[51] Both processes are shown on the Jablonski diagram in (Figure 1.1), phosphorescence usually occurs at lower energies than fluorescence and with significantly longer lifetimes.

Emission can only be observed from the lowest energy excited state of any multiplicity, Kasha's rule).[58] Similarly, to the absorption the Franck-Condon factor determines the band shape of radiative deactivation, dependant on the distortion of the excited state relative to the ground state. The absorption and emission maxima are at different energies, this is due to the distortion between the two states, the absorption maxima is higher in energy than the emission for the same transition. The shift between the two maxima is called the Stokes shift and indicated the degree of distortion between the excited and ground states.[2]

Excited states, *A, decay corresponding to overall first-order kinetics, and the lifetime τ(*A) is given by the following equation:

$$\tau({}^{*}\mathrm{A}) = \frac{1}{k_p + k_r + k_{nr}} = \frac{1}{\sum_j k_j}$$

Eq. 1.18

A primary process is defined as process starting with the absorption of a photon and resulting in the deactivation to the ground state or the molecule disappearing.[59] The probability of each of these processes is related to its relative rate, therefore an efficiency of each process can be defined as:

$$\eta_i({}^{*}\mathrm{A}) = \frac{k_i}{\sum_j k_j} = k_i \tau({}^{*}\mathrm{A})$$

Eq. 1.19

When the molecules are continuously irradiated, the concentration of excited states is assumed to have reached a steady value, the following equation is true:

$$\frac{\mathrm{d}[^*\mathrm{A}]}{\mathrm{d}t} = I_m - k_p[^*\mathrm{A}] - k_r[^*\mathrm{A}] - k_{nr}[^*\mathrm{A}] = 0$$

Eq. 1.20

I_m, is defined as the average number of einsteins absorbed by the reactant in a unit of volume and time.

$$I_m = \left(k_p + k_r + k_{nr}\right)[^*\mathrm{A}]$$

Eq. 1.21

When the excited state is directly irradiated some or all the primary processes occur, the quantum yield ϕ of a specific process (i) can be worked out as a ratio between the rate constant (k_i) of one of the processes and the sum of the rate constants of the processes that are involved in the deactivation of the excited states.

$$\phi_p = \frac{k_p[^*\mathrm{A}]}{I_m} = \frac{k_p}{k_p + k_r + k_{nr}}$$

Eq. 1.22

$$\phi_i = \frac{k_i}{\sum_j k_j}$$

Eq. 1.23

Following on from the previous equations (1.19, 1.22 and 1.23), it can be drawn that the quantum yield ϕ_i and the efficiency η_i(*A) are equivalent numerically.

$$\phi_i = k_i\tau(^*\mathrm{A}) = \eta_i(^*\mathrm{A})$$

Eq. 1.24

The rate constant for the processes can be gathered through experimental data, as the following equation shows the quantum yield ϕ_i of a process and the lifetime τ(*A) of the excited state can be used to calculate k_i:

$$k_i = \frac{\phi_i}{\tau(^*\mathrm{A})}$$

Eq. 1.25

The rate constant for the radiative constant and the photochemical constant can be calculated via quantitative methods. However, the non-radiative decay constant cannot be characterised directly from quantitative methods therefore this equation is required:

$$k_{nr} = \frac{1}{\tau} - (k_r + k_p)$$

Eq. 1.26

When the excited state *A is populated from another excited state (Figure 1.3) through one or more non-radiative steps, for example $S_1 \rightarrow T_1$, then the quantum yield ϕ_i and the rate constant k_i of the deactivation processes are defined as equation 1.27 and 1.28 respectively, η_n is the efficiency of the steps prior to the population of *A.

$$\phi_i({}^*\mathrm{A}) = \eta_i({}^*\mathrm{A}) \prod_n \eta_n$$

Eq. 1.27

$$k_i = \frac{\phi_\mathrm{i}({}^*\mathrm{A})}{\tau({}^*\mathrm{A}) \prod_n \eta_n}$$

Eq. 1.28

Due to the remarkably high rate of internal conversion the decay from the upper excited states to the lowest state with the same multiplicity happens extremely fast and combined with Kasha rule that the emission comes from the lowest excited state of that multiplicity, the competing and consecutive processes that occur in an excited state molecule can be considerably simplified.[51, 57, 58] For heavy metal complexes, as seen in this thesis, intersystem crossing has a near total efficiency, due to the spin orbit coupling induced by the heavy metal centre, therefore the deactivation process can be simplified to the primary and secondary processes in Figure 1.3.

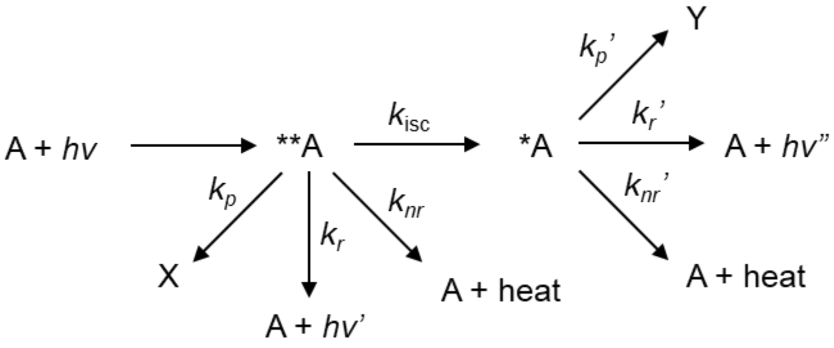

Figure 1.3 Primary and secondary processes of the light-matter interaction. When an excited state (A) has been populated by another excited state (A**) through a non-radiative process. Redrawn from reference.[54]*

The lifetime τ is calculated as the time it takes for the molecules that populate the excited state to have reduced to 1/e of the starting number. It can be recorded experimentally by tracking the number of excited state molecules and the proportional number of decaying molecules.

The quantum yields can be calculated from two quantities, as per equation 1.17 and 1.27, for photochemical processes this can be change in concentration of the products/reactants and for photophysical processes this can be the number of photons emitted. The other quantity will be the number of photons absorbed by the molecules undergoing the processes. When calculating quantum yield the light used for excitation should be monochromatic as there can be significant change in properties depending on the wavelength of light that is absorbed.

1. 4. Photophysics of d^6 Metal Complexes

1. 4. 1. Photophysics of $Ru(bpy)_3$

Key electronic transitions that occur in the excited states can be shown on molecular orbital (MO) diagrams (Figure 1.4), molecular orbitals of metal complexes are ascribed metal and ligand based character. The main transition is when an electron from the highest occupied molecular (HOMO) is promoted to the lowest unoccupied molecular orbital (LUMO).[60] In general terms the HOMO is metal centred and the LUMO is localised on the ligands. When the ligand field is weak or the ligands are not easily reduced the LUMO can be localised on the metal centre. It should be noted that transitions can happen between lower and higher energy orbitals such as HOMO-1, HOMO-2, etc. and LUMO-1, LUMO-2 etc. Some key terms used to describe the processes that occur in the excited states:

- Metal Centred (MC), describes the process of a d–d* transition, in an octahedral complex this will be from a t_{2g} orbital to the e_g* orbital.
- Metal-to-Ligand Charge Transfer (MLCT), a process from the metal-based d orbital to the ligand based π* antibonding orbital.
- Ligand Centred (LC), describes the process that occurs on a ligand between the π – π* orbitals.

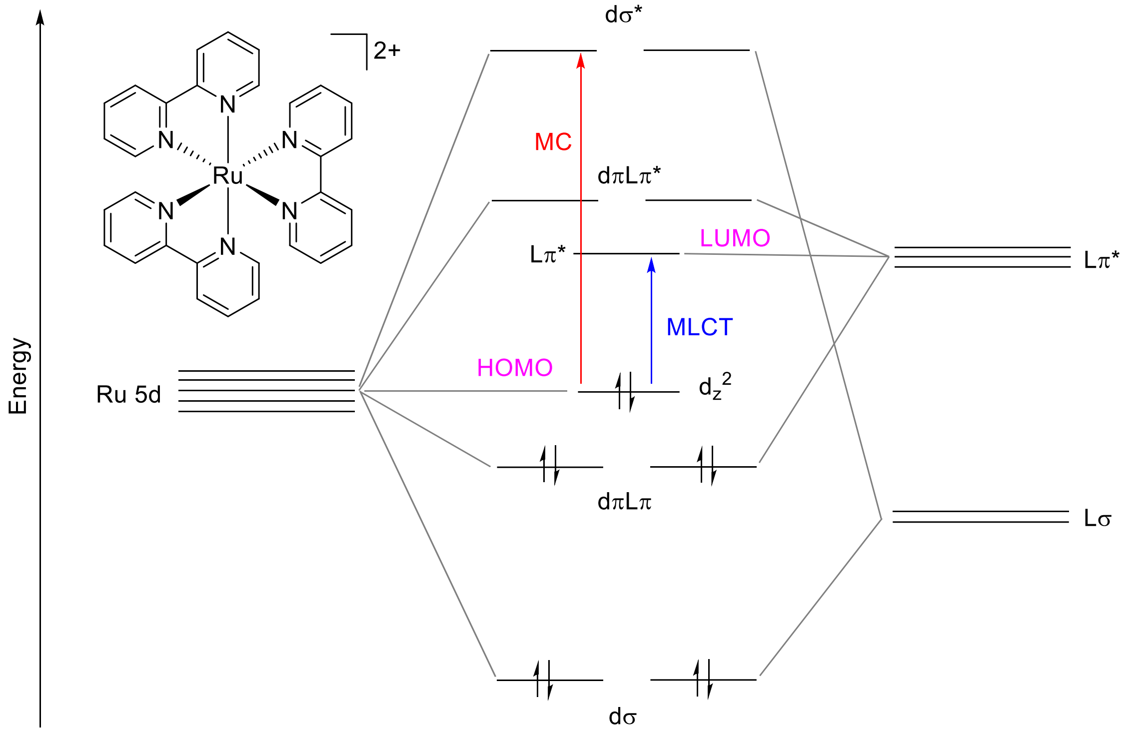

Figure 1.4 Simplified molecular orbital diagram of [Ru(bpy)$_3$]$^{2+}$, structure shown of complex in top left. Redrawn from referemce.[61]

Looking at the MO for Ru(bpy)$_3$ (Figure 1.4) can help to further explain these transitions, the HOMO → LUMO transition here occurs from the metal d_z^2 orbital to the ligand π* antibonding orbital, this is a singlet MLCT transition. MC $d_z^2 \rightarrow d\sigma^*$ transitions are also shown here from the HOMO → LUMO+2. Potential energy surface (PES) diagrams are used to portray the transitions that occur in the excited states (Figure 1.5). The aforementioned singlet MLCT absorption is shown through process *a* from the ground state (^{1}GS) to ^{1}MLCT, complex then undergoes ISC, process *b*, to the ^{3}MLCT. Phosphorescence derives from the spin-forbidden radiative relaxation from the ^{3}MLCT to the ^{1}GS, process *c*. When the ^{3}MC state is low enough in energy it can be thermally populated from the ^{3}MLCT as shown by process *d*, this results in non-radiative relaxation to the ground state and can photochemically alter the structure of the metal complexes, through decomposition or ligand ejection.[61,62]

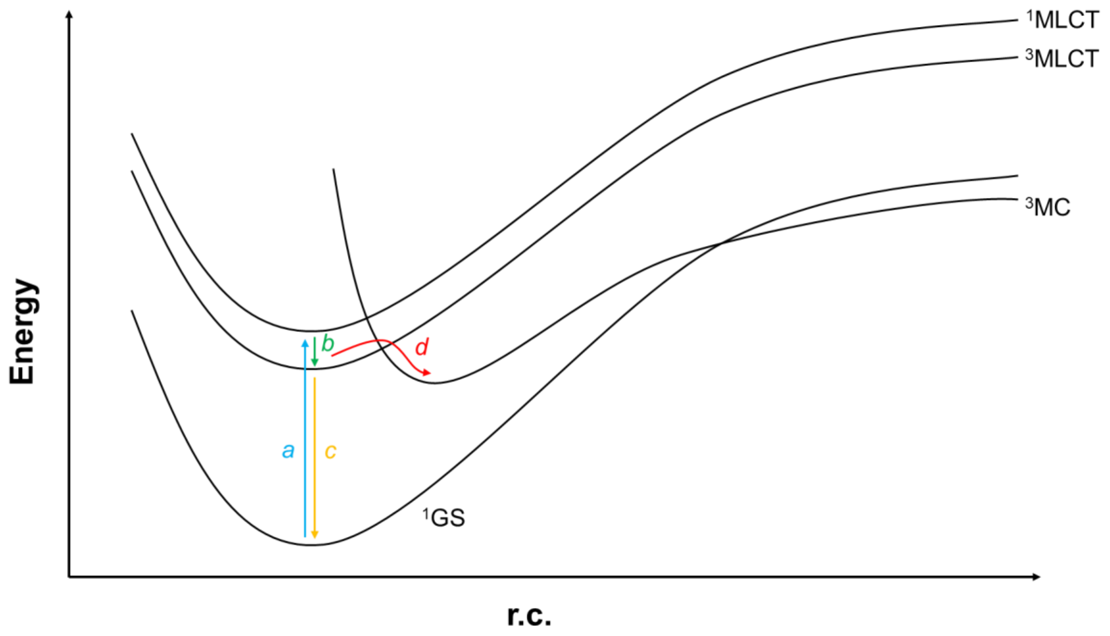

Figure 1.5 Potential energy surface diagram of $[Ru(bpy)_3]^{2+}$ describing key photophysical processes. r.c. = reaction coordinate. Redrawn from reference.[61]

Huge changes in the excited state energy can be performed by changing the ligands involved in the MLCT, allowing tuning of the photophysical properties. This is mainly done through stabilising/destabilising the HOMO or LUMO and therefore modifying the HOMO-LUMO energy gap. Stabilising the LUMO can be done by using ligands with π* molecular orbitals but are lower lying-in energy and destabilising the HOMO by using π-donor or π-acceptor ligands. More fine-tuning can be done by altering the substituents on the aromatic rings of the ligands where the LUMO/HOMO is situated. Adding electron withdrawing groups (EWG) to the ligand where the LUMO is localised will stabilise the LUMO, opposingly adding electron donating groups (EDG) will destabilise the LUMO. The HOMO is generally metal centred, as is the case with $[Ru(bpy)_3]^{2+}$, however it can be partially localised on a cyclometalated aryl groups and therefore can be tuned via substituents on that ligand. Adding EWGs will stabilise the HOMO whilst EDGs will destabilise it.

A great example of the tuning of the HOMO-LUMO gap and in turn the photophysical properties by changing the ligand was shown by Elliott and co-workers.[63] By increasingly substituting btz ligands for bpy ligands providing the series (Figure 1.6): $[Ru(bpy)_3]^{2+}$ - $[Ru(bpy)_2(btz)]^{2+}$ - $[Ru(bpy)(btz)_2]^{2+}$ - $[Ru(btz)_3]^{2+}$. The theoretical study of this series showed that the substitution of the bpy ligand for btz had a great effect on the LUMO energy, it had increased dramatically in correlation with the number of btz ligands. The destabilisation occurred as the btz ligand had no aromatic rings as opposed to the bpy, meaning there was no longer π-back bonding and thus the π* antibonding orbital increased significantly in energy. The experimental study saw the ^{1}MLCT absorption bands for the corresponding complexes had blue shifted in accordance with the increase in HOMO-LUMO gap. The emissive properties were also significantly affected as $[Ru(btz)_3]^{2+}$ ^{3}MLCT was destabilised to a higher energy where ^{3}MC was more readily thermally populated, consequently quenching emission and inducing photochemical ligand ejection.

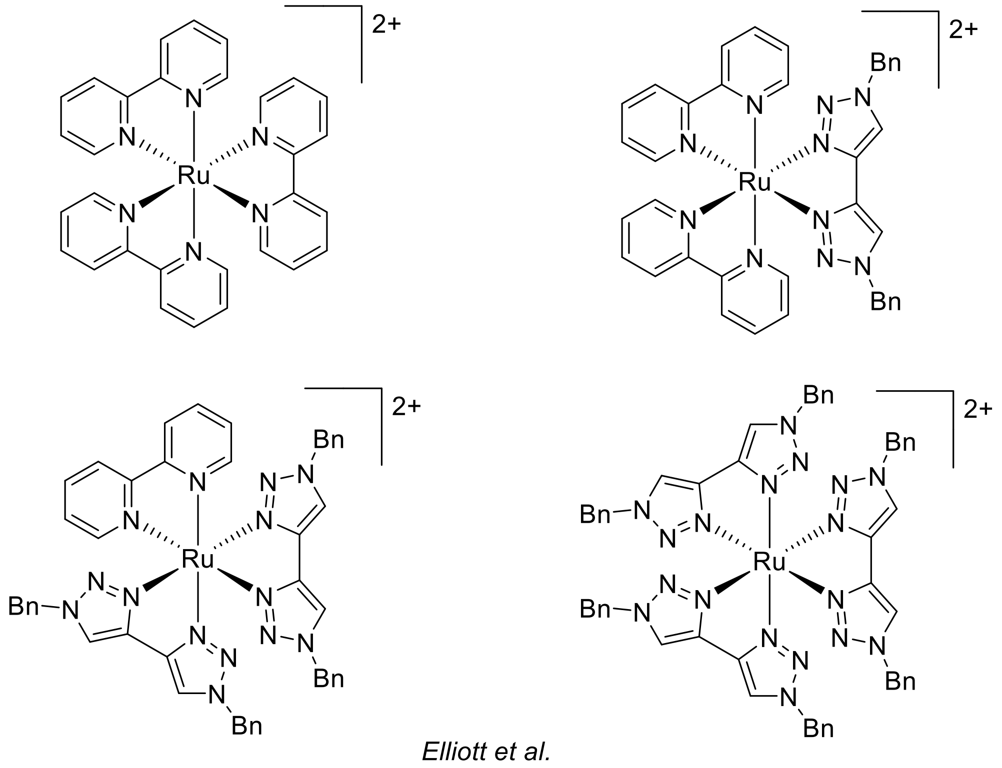

Figure 1.6 Series of Ru(II) complexes reported by Elliott and co-workers.[63] Shows the variation in the number of btz moieties on the complexes.

1. 4. 2. Luminescence in Cyclometalated Ir Complexes

Iridium complexes are the most promising set of compounds for photo- and electroluminescence. Ir(III) complexes can be tuned across the colour spectrum via modification of their ligands.[64, 65] They have a unique set of photophysical properties which makes them inherently interesting, ability to alter emission by modifying the ligands, good stability, and very high quantum yields.[66] Cyclometalated Ir(III) complexes are the most important set of compounds for high performance emitters as they have a strong Ir-C bonds.[67] More specifically, the metalation of the anionic aryl rings results in a good mixing of the Ir(III) d-orbital and the aryl π system, therefore the HOMO is the combination of π-donor aryl bonding and metal based. This allows for tuning of the HOMO by altering the cyclometalated ligand structure, by adding EWGs and EDGs, which allows for a varied spectrum of colours of emission. Adding electron withdrawing substituents will stabilise the HOMO blue shifting the emission, whilst electron donating substituents would destabilise the HOMO red shifting the emission. The Ir-C bond is accounted for the excellent photo and thermal stability of the complexes, as the MC states are destabilised, so they are not easily populated.[68] Triplet emission from these complexes can come from a combination of ^{3}LLCT, ^{3}MLCT, and ^{3}LC transitions (Figure 1.7):

- Ligand-to-Ligand Charge Transfer (LLCT), often a combination MLCT and LLCT, is the process occurring between two ligands on the same complexes where the HOMO is based on the cyclometalated ligand with a mixture of d and π character to a LUMO π* antibonding orbital on an ancillary ligand.
- MLCT/LC, a mixture of the two processes, used to denote the process that occurs on one cyclometalated ligand, such as phenylpyridine, where the HOMO is based on the d and π mixed orbital and the LUMO is the π* antibonding orbital on the N-coordinated pyridyl moiety.

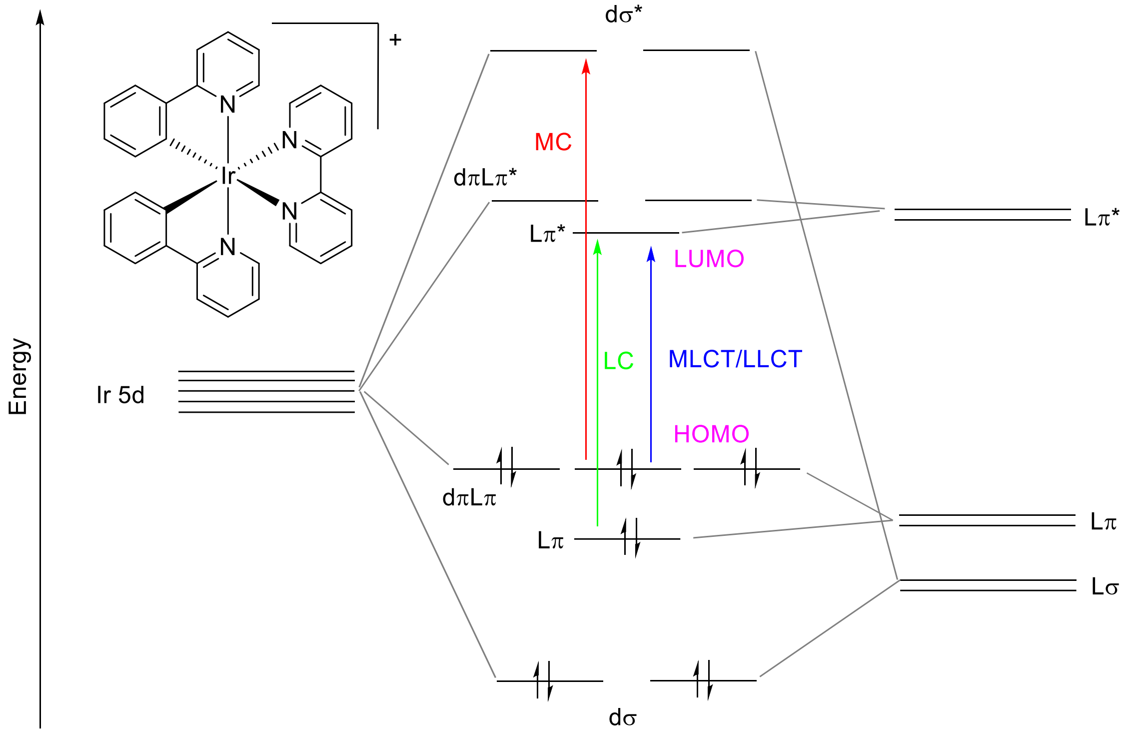

Figure 1.7 Simplified molecular orbital diagram of [Ir(ppy)$_2$(bpy)]$^+$ and structure of complex (top-left).[69]

As mentioned previously, the mixing of the Ir(III) d orbital and cyclometalated π aryl orbitals means the HOMO is localised over both allowing for much greater tuning than non-cyclometalated complexes. The stereochemical structure of heteroleptic Ir(C^N)$_2$(N^N) complexes are defined by the nitrogen atoms of N^C ligands being trans due to the *trans* effect and a greater *trans* influence, caused by the cyclometalated carbons. This allows for a predictable and well-defined orbital distribution, with the HOMO being a mixture of metal and aryl character and the LUMO being on the ancillary N^N ligand. This permits a great range of tuning as two different types of ligands can be functionalised allowing for fine tuning of the HOMO and LUMO, Figure 1.8 shows the effects of EWG and EDG on the frontier orbitals.

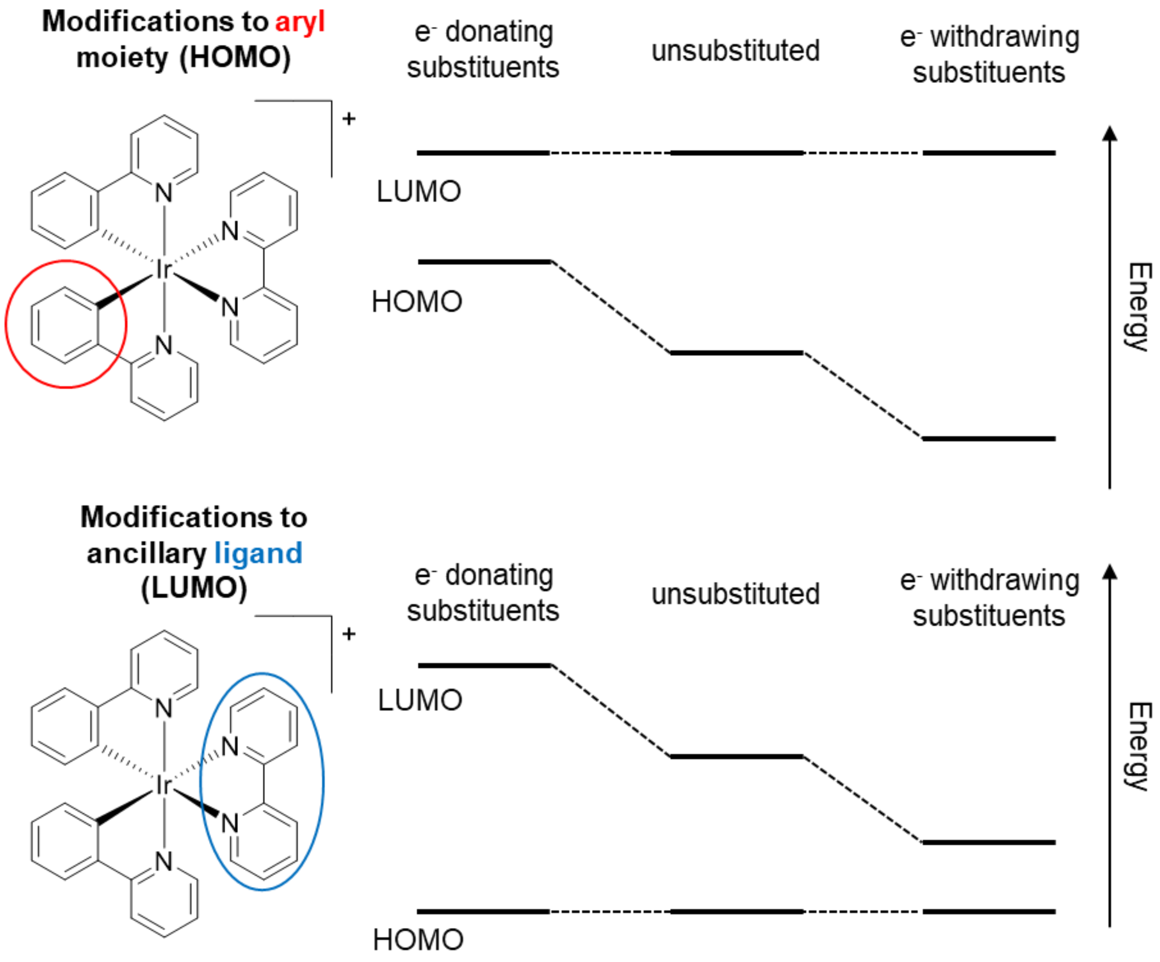

Figure 1.8 Diagram demonstrating the effects, on the energy levels, of the frontier orbitals when modified with EWG and EDG using [Ir(ppy)$_2$(bpy)]$^+$.

1. 5. Ir(III) Complexes

1. 5. 1. Ir(III) Cyclometalated Complexes

As previously mentioned in 1.4.2, cyclometalated Ir(III) complexes are a set of unique and interesting complexes due to their tunability via ligands and excellent photo/thermal stability.

In 1991, Sweigart and co-workers,[70] compared the homoleptic Ir(III) cyclometalated complex series of Ir(ppy)$_3$ against complexes with the phenyl rings being substituted, Ir(R-ppy)$_3$ where R = F or *t*Bu (Figure 1.9). They substituted the phenyl with a range of electron withdrawing and electron donating moieties, this affected the σ-donation of the cyclometalated carbon, which in turn modified the energy level of the HOMO and/or LUMO. Sweigart and co-workers observed the photophysical and electrochemical properties of these complexes, Ir(ppy)$_3$ had λ_{em} = 494 nm and the Ir(III)-(IV) oxidation potential was +0.77 V. When the phenyl ring was substituted with an EWG such as a fluorine, the emission blue shifted, λ_{em} = 468nm, and the oxidation potential increase to +0.97 V. When the substituent was an EDG, *t*-Bu, the emission only red shifted marginally, λ_{em} = 497nm, whilst the oxidation potential of Ir(III) decreased to +0.66 V. This change in oxidation potential was expected to affect the emitting energy levels, this can clearly be seen in the blue shifting of the emission for the F-ppy substituted complex.

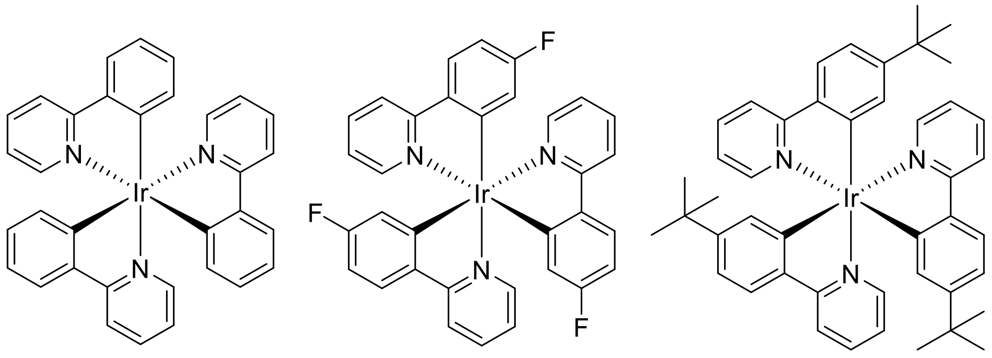

Figure 1.9 Ir(R-ppy)$_3$ complexes reported by Sweigart and co-workers,[70] modulation of the aryl moiety with EWG and EDG groups.

As per Sweigart's body of work, the focus on heteroleptic complexes was to investigate cationic complexes rather than neutral complexes as this allows for more flexibility with the tuning of the photophysical properties. Heteroleptic Ir(III) complexes are a very interesting species as they allow for even further tuning of the photophysical properties, the Ir-C bond and the ancillary ligand can be tuned. If a complex had ^{3}LLCT/MLCT character, the HOMO would be localised on the Ir-C bond and the LUMO would have been on the ancillary ligand, the HOMO and LUMO could have been modulated individually by adding EWGs or EDGs to the respective ligands.

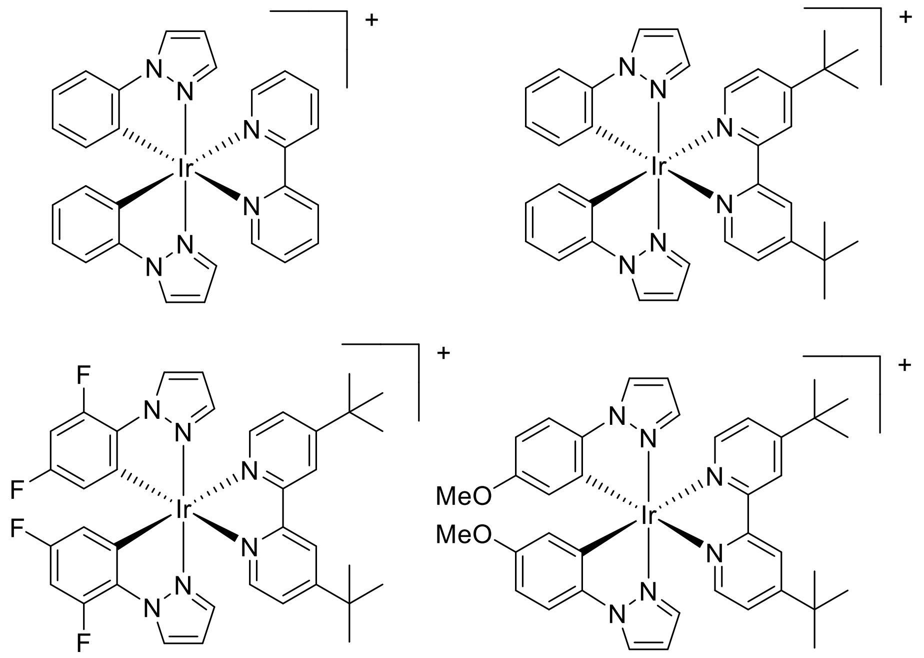

Thompson et al.

Figure 1.10 Series of complexes developed by Thompson and co-workers based on [Ir(ppz-R)$_2$(bpy-R)]$^+$ structure.[71] A variety of EWG and EDG used to modulate the HOMO and LUMO.

Thompson and co-workers looked at a series of complexes with a neutral N^N diimine ancillary ligand,[71] with the overall structure of [Ir(ppz-X)$_2$(N^N)]$^+$ (Figure 1.10). This series had ^{3}LLCT/MLCT character and thus a wider variation of emission wavelengths, 625-493 nm. A combination of EWGs on the cyclometalated ligand and EDGs on the ancillary ligand, [Ir(ppz-F$_2$)$_2$(bpy-*t*Bu)]$^+$, resulted in a significantly blue shifted emission, λ_{em} = 493 nm, compared to [Ir(ppz)$_2$(bpy)]$^+$ λ_{em} = 565 nm (Table 1.1). The electrochemical properties also concur with this as the HOMO-LUMO energy gap, between the oxidation and reduction potentials, were confirmed to be 3.08 V and 2.75 V, respectively. The addition of electron donating groups to the cyclometalated ligand, [Ir(ppz-OMe)$_2$(bpy-*t*Bu)]$^+$, red shifted the emission, λ_{em} = 615 nm, as the energy gap according to electrochemistry was reduced, 2.52 V. The oxidation potential for the methoxy substituted complex was significantly lower, +1.03 V, than the fluorinated complex, +1.66 V, or [Ir(ppz)$_2$(bpy-*t*Bu)]$^+$, +1.36 V, whilst the reduction potential remains similar for these complexes -1.42-49 V. Clearly demonstrating that substituents on the cyclometalated ligand have a significant effect on the energy level of the HOMO. The reduction potential for the unsubstituted complex, -1.39 V was higher than the electron donated substituted complexes, demonstrating that the LUMO can be perturbed by ligand modification.

Table 1.1 Summarised Electrochemical Properties and Emission Maxima of Thompson and co-workers Complexes in MeCN (Figure 1.10)[71]

Complex	$E_{ox}{}^{a}$ / V	$E_{red}{}^{a}$ / V	E_{ox}-E_{red} Gap^{a} / V	$\lambda_{em}{}^{b}$ / nm
$[Ir(ppz)_2(bpy)]^+$	0.95	-1.80	2.75	563
$[Ir(ppz)_2(bpy\text{-}t\text{Bu})]^+$	0.95	-1.89	2.84	555
$[Ir(ppz\text{-}F_2)_2(bpy\text{-}t\text{Bu})]^+$	1.25	-1.83	3.08	495
$[Ir(ppz\text{-}OMe)_2(bpy\text{-}t\text{Bu})]^+$	0.62	-1.90	2.52	618

a) Cyclic voltammograms were recorded in an anhydrous MeCN solution using Fc^+/Fc as an internal standard. *b)* Aerated solution at 298K

1. 5. 2. Triazole Ligands

Pyridine based ligands are ubiquitously used for photo- and electroluminescent complexes as they have excellent and interesting photophysical properties.[54, 72, 73] The complex $Ru(bpy)_3$ is arguably the most studied and well known mid-late transition metal complex.[74]

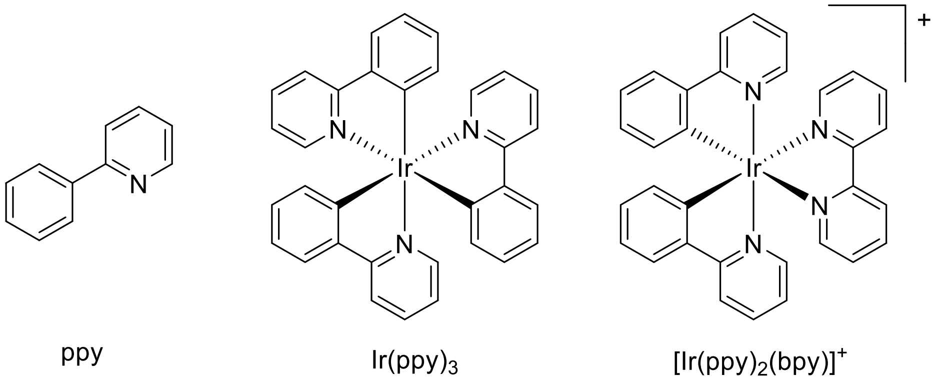

Figure 1.11 Phenylpyridine (ppy) and highly investigated ppy based complexes.

Phenylpyridine (ppy) based ligands are commonly used in Ir(III) complexes (Figure 1.11), such as $Ir(ppy)_3$ and $[Ir(ppy)_2(bpy)_2]^+$ which provides excellent quantum yields, $Ir(ppy)_3$ $\phi = 97$ %,[75] and good photo/thermal stability. They can also be readily functionalised allowing for a great range of photophysical tuning.

Triazoles have been popularised due to the development of the Huisgen-Sharpless copper catalysed azide/alkyne cycloaddition (CuAAC) synthesis route (Figure 1.12).[76] One of main benefits of the CuAAC is the wide availability of the starting materials, terminal alkynes and azides, and/or relatively straightforward methods to prepare them. The route provides high yields under moderate conditions with a facile work up and purification.

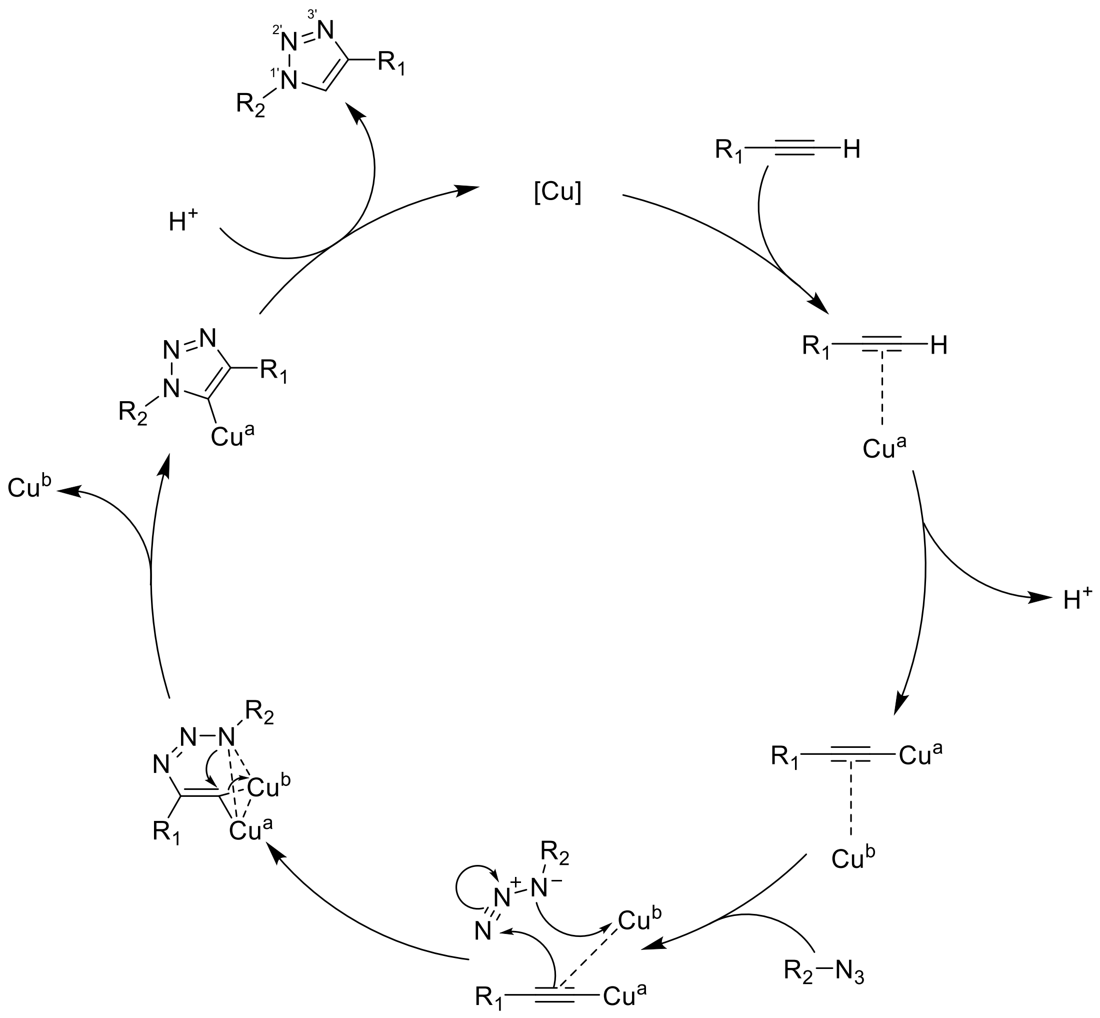

Figure 1.12 Catalytic cycle for the Cu(I) catalysed Huisgen-Sharpless 1,4-triazole route. Redrawn from reference.[76] Different molecules of the same Cu complexes identified as a and b.

Due to the availability of several different coordination sites the 1,2,3-triazole moiety has great potential to be used as a ligand due to its versatility. The most common coordination site is through the lone pair on the N(3) position (Figure 1.12), the N(2) position is also a primed position for metal coordination. However, the N(3) position is generally more favourable as it slightly more basic. Compared to pyridine donors triazole ligands are poor π-acceptors due to the much higher in energy π* orbitals, reducing metal-ligand orbital overlap.

As mentioned previously the pyridine-based ligands, bpy and 2,2':6',2''-terpyridine (tpy), have been the main focus of diimine based ligands, however 1,2,3-triazoles are garnering more and more interest, therefore analogous triazole ligands to these pyridine ligands have been designed to explore this chemical space (Figure 1.13).

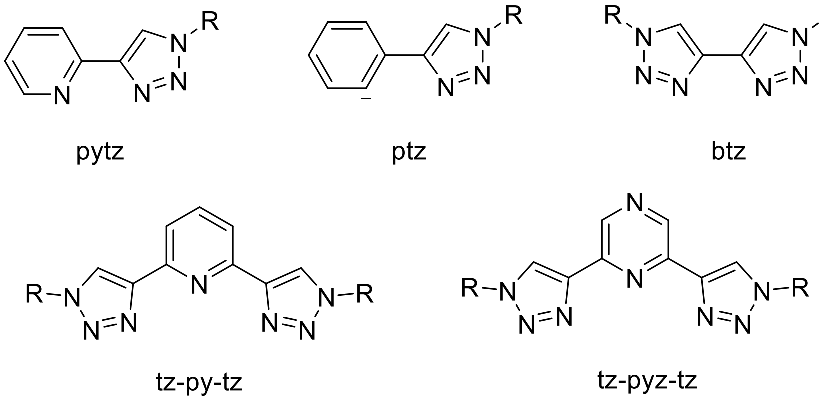

Figure 1.13 Structures of common triazole based ligands and their ascribed shorthand names.

The coordination of triazole based ligands has been probed with kinetically inert metals to explore the photophysical properties, such as Re(I),[77] Ru(II),[78-80] Os(II),[81, 82] and Ir(III).[61, 83, 84] Triazoles can displace the ubiquitous pyridyl moieties on ligands leading to different photophysical properties and different aspect on ligand architecture.

1. 5. 3. Ir(III) Triazole Complexes

Substitution of pytz from bpy on cationic Ir(III) complexes has very interesting effects on the photophysical properties and on the localisations of the emissive states. De Cola and co-workers,[85-87] reported the analogue triazole complexes, $[Ir(R\text{-}ppy)_2(pytz)]^+$ (Figure 1.14), of the archetypal complexes $[Ir(R\text{-}ppy)_2(bpy)]^+$. The bpy based complexes observed broad featureless emission bands that correspond to ^{3}MLCT/^{3}LLCT character and where the excited electron is on the bpy ancillary ligand. The pytz complexes have good and comparable quantum yields (ϕ = 21-22 %), their emission bands occur at higher energies (λ_{em} = 477, 507 nm for ppy and 452, 483 nm for dfppy) in a vibronic structure which is indicative of ^{3}MLCT/^{3}ILCT character. The LUMO is still found on the ancillary pytz ligand, where it is destabilised to the point where the unpaired electron undergoes relocalisation in the T_1 excited state to the cyclometalated R-ppy ligands.

Donnelly and co-workers reported similar effects with their analogous complexes,[88] where the pytz ligand has methylene spacer between the pyridine and triazole moieties (Figure 1.14). This ligand forces the coordination of the triazole to be through the N(2) position, the emission spectra (λ_{em} = 478, 506 nm for ppy and 455, 484 nm for dfppy) are similar to the De cola and co-workers counterparts,[89] with vibronic structure emission that correlates to ^{3}MLCT/^{3}ILCT character.[90-92]

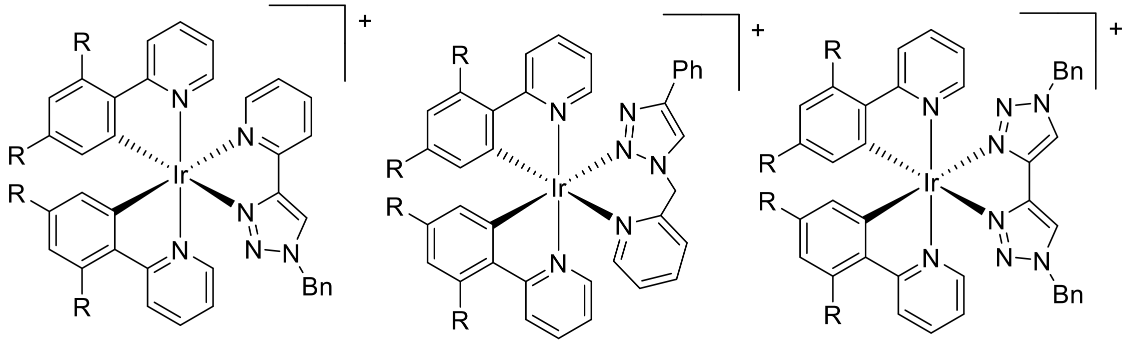

R = H or F

De Cola et al.

R = H or F

Donnely et al.

R = H or F

Elliott et al.

Figure 1.14 Ir triazole complexes reported by De Cola (left),[85-87] Donnelly (centre),[88] and Elliott (right).[83, 84]

When the bpy ligand is fully substituted with triazoles, btz, and coordinated to Ru(II), the LUMO is destabilised to high enough energies that the ^{3}MC states can be thermally populated and are therefore non-emissive. Elliott and co-workers developed [Ir(R-ppy)$_2$(btz)]$^+$ complexes,[83, 84] however due to the much higher energy of the ^{3}MC states of 5d metals these complexes were emissive (λ_{em} = 476, 506 nm for ppy and 454, 483 nm for dfppy) with quantum yields of ϕ = 0.82 % and 0.28 %, respectively. Again, the emission spectra are similar to the pytz complexes as the unpaired electron switches to the cyclometalated ligands in the excited state. The quantum efficiency of emission was reported to be significantly less for the btz complexes as the triazole moieties are weaker σ-donors and much weaker π-acceptors than the pyridine moieties.

The first cyclometalated phenyl-triazole (ptz) complexes were reported by Schubert and co-workers.[87] The complex design of [Ir(ptz)$_2$(L)]$^+$ was developed with different ancillary ligands (Figure 1.15). The bpy based complex had blue shifted in emission (λ_{em} = 560 nm) compared to the [Ir(ppy)$_2$(bpy)]$^+$ counterpart (λ_{em} = 580 nm). The reduced π-accepting nature of the triazole moieties on the ptz ligands, in comparison to the pyridine rings on the ppy analogues, means there is an increased electron density at the metal and thus more π-back bonding with the bpy ligand increasing the LUMO. The complexes showed excellent quantum yields for both the bpy and the pytz based complexes.

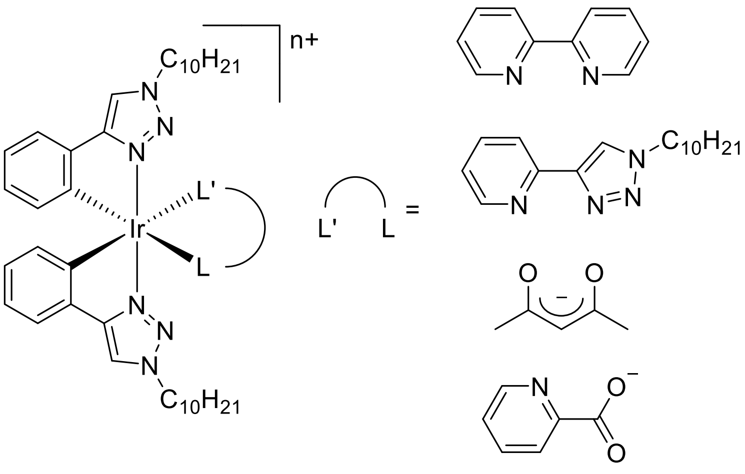

Schubert et al.

Figure 1.15 Cylcometalated triazole Ir complexes reported by Schubert and co-workers.[87]

Picolinate and 1,2,4-triazolate complexes based on dfptz as the cyclometalated ligand were reported by De Cola and co-workers (Figure 1.16).[93] The picolinate complex had blue shifted emission compared to its ptz counterpart reported by Schubert and co-workers (λ_{em} = 527nm, Figure 1.15), this is due to the fluorine substituents stabilising the HOMO. The picolinate complex showed emission character indicative of more ^{3}LLCT involvement and the triazolate complex emission exhibited much more ^{3}ILCT character.

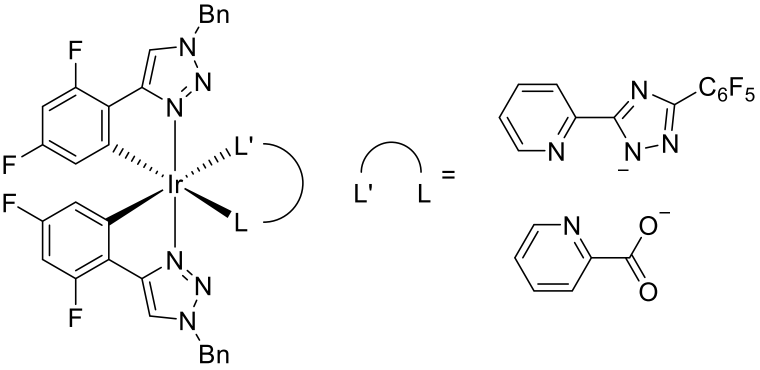

De Cola et al.

Figure 1.16 Cylcometalated triazole Ir complexes reported by De Cola and co-workers.[93]

Cationic biscyclometalated complexes containing ptz or dfptz, with a bpy ancillary ligand, have been investigated by Zysman-Colman and De Cola groups (Figure 1.17).[94, 95] Similarly to reported above, the fluorinated complexes displayed higher energy emission (λ_{em} = 497-514 nm) than those of the non-fluorinated analogues (λ_{em} = 575-580 nm). The complexes all displayed excellent quantum efficiency, fluorinated complexes between 73-81 % and between 25-35 % for the non-fluorinated complexes. Substituting π-donating moieties further shifts the emission towards the blue as this destabilises the LUMO.

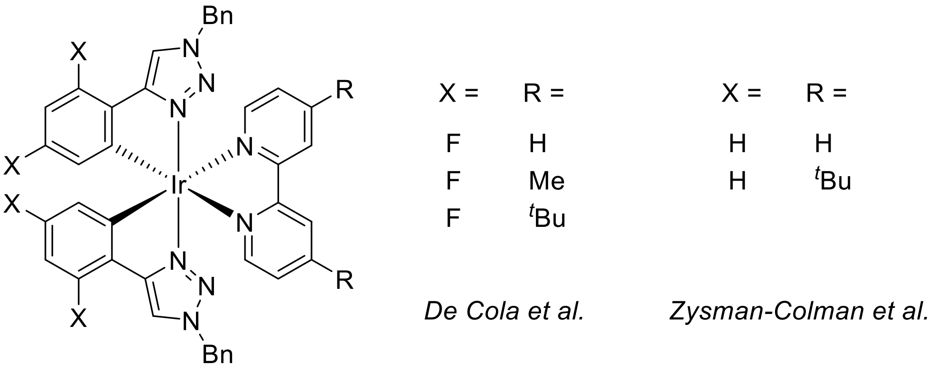

Figure 1.17 Cyclometalated triazole Ir complexes reported by De Cola and co-workers (left),[94] and Zysman-Colman and co-workers (right).[95]

The triazole moiety can be used in both the ancillary and cyclometalated ligands, [Ir(R-ptz)$_2$(pytz)]$^+$.[87] The emission of these complexes display broad band emission to that of ^{3}MLCT/^{3}LLCT character. The triazole moiety substitution on the cyclometalated ligands leads to a dramatic destabilisation of their unoccupied orbitals. Compared to the R-ppy analogues the localisation of the excited electron switches to the pyridine moiety on the pytz ancillary ligand.

Zysman-Colman and co-workers reported the btz complexes,[84] [Ir(R-ptz)$_2$(btz)]$^+$, which were either weakly emissive (λ_{em} = 495 nm, ϕ = 2.7 %) for the non-fluorinated complex or non-emissive for the fluorinated complex. As the ^{3}MLCT/^{3}LLCT states are localised on the ancillary btz ligand, the high energy of these states allows for deactivation through the ^{3}MC states.

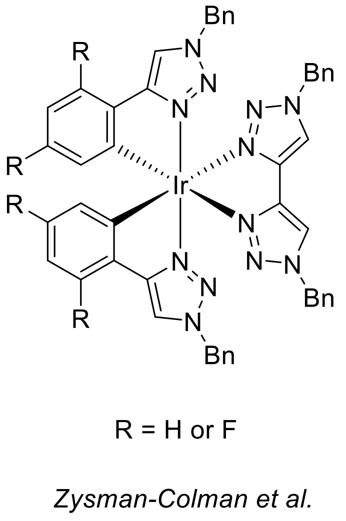

Figure 1.18 Cyclometalated triazole Ir(III) complexes with btz ancillary ligands reported by Zysman-Colman and co-workers.[84]

1. 6. Applications of Ir(III) Complexes

1. 6. 1. Biological Imaging

Cellular imaging is a very important aspect of life sciences, being able to directly visualize cells at a sub-cellular resolution allows for imaging of the whole cells and the subcompartments and organelles within the cell.[96-102]

The cytoplasm is the area between the cellular membrane and the nucleus, it hosts organelles and macromolecules. A multitude of metabolic performances also occur in this area, these interactions are highly regulated so imaging the cytoplasm space is an important aspect of life science.[103]

Cationic Ir(III) complexes are the most effective for cytoplasm staining as their positive charge made them more soluble in aqueous solutions, these probes also have low cytotoxicity. Li and co-workers,[104] reported the first cytoplasm staining Ir(III) probes (Figure 1.19a) . Both complexes had strong intracellular luminescence whilst also maintaining a high signal-to-noise ratio between the cytoplasm and the background, ensuring excellent viability as a cytoplasm probe. Li and co-workers developed on the previous complexes and reported a new series of complexes (Figure 1.19b) that have higher π conjugation on the ligands.[105] The biological properties remained similar however the photophysical behaviour varied, the emission colour red shifted significantly from blue to deep red (457-632 nm) and even to the near-infrared (732 nm) region.[106] Emission in the near-infrared is highly desirable in biological imaging as it allows for deeper tissue penetration and allows for signal discrimination from autofluorescence.[107, 108]

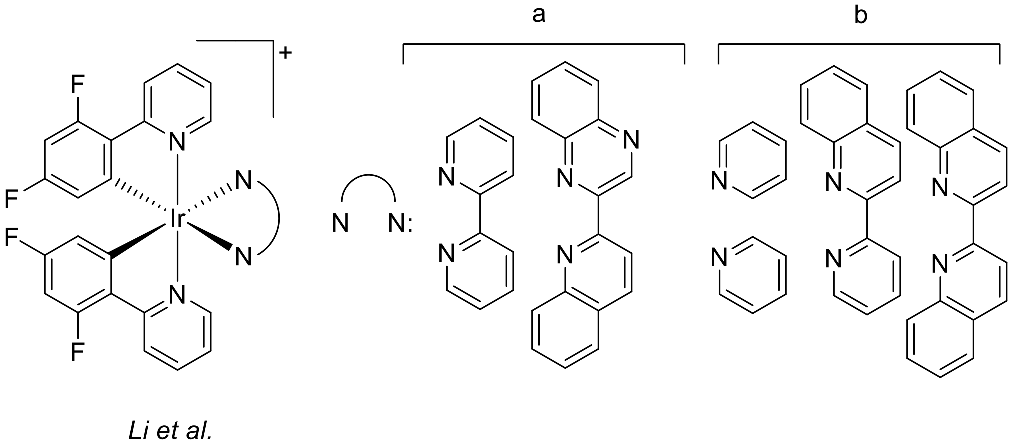

Figure 1.19 Complexes reported for use as cytoplasm staining reported by Li and co-workers. a) Initial complexes reported as stain.[104] b) Complexes further developed for staining.[105]

There are two main functions for the nucleus, storage of hereditary cellular information via DNA and management of many processes such as; growth, protein synthesis, intermediary metabolism and cell division.[109] Due to this, imaging the nucleus is of high interest, Ir(III) complexes have been developed to investigate, similar to the cytoplasm staining the majority of developed Ir(III) nucleus probes are cationic. The Li group developed non-emissive $[Ir(ppy)_2(DMSO)_2]^+$ (Figure 1.20) that reacted selectively with histidine and histidine rich proteins resulting in a dramatic 300-fold increase in emission.[110] When tested in HeLa cell lines it showed exclusive staining of the nuclei, also showed low toxicity and great viability in the cells. The cellular viabilities, the number of healthy cells in the sample, were thought to be greater than 94 % and 90 % after incubation for 24 h and 48 h. A standard live/dead staining procedure was used to observe cytotoxicity at imaging concentrations, the cells treated with the complex retained a 97 % viability suggesting low toxicity.[110]

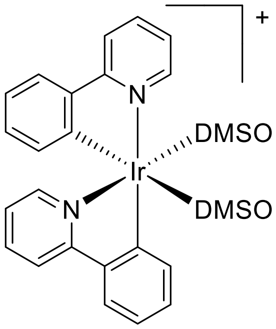

Li et al.

Figure 1.20 Nucleus imaging probe reported by Li and co-workers.[110]

Mitochondrial staining is of key interest due to the vast number of functions they are involved in: apoptosis, calcium modulation, redox signalling and energy production through oxidative phosphorylation.[111, 112] Mitochondria vary their number, shape, size and distribution within the cytoplasm depending on what environmental or metabolic stress is occurring.[113] Due to their vital application in several important processes, mitochondria are thought to have a key role in a number of diseases such as cancer, neurodegenerative diseases (Alzheimer's and Parkinson's) and metabolic disorders.[114] Therefore the development of imaging probes for the mitochondria is quintessential, the Ir(III) complexes that have been reported all generally have a positive charge as this allows for localisation in the mitochondria due to their membranes having an electrical potential. Chao and co-workers reported two near-infrared Ir(III) probes (Figure 1.21),[115] these complexes exhibited strong emission bands at ~750 nm and excellent photostability, low cytotoxicity and excellent viability in HeLa cells, cell viability as high as 95 % over 0-6 h. These probes were used to track the changes in mitochondrial behaviour in the beginning stages of apoptosis.

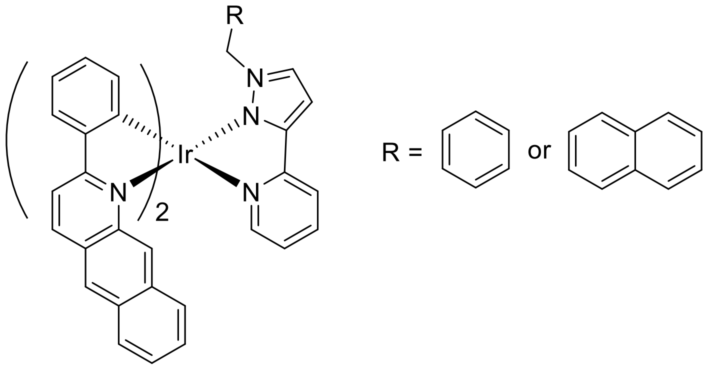

Chao et al.

Figure 1.21 Near infra-red mitochondria imaging probe developed by Chao and co-workers.[115]

1. 6. 2. Photodynamic Therapy (PDT)

There are two mechanisms for PDT, Type-I and Type-II.[116] Both mechanisms are dependent on the formation of the triple state (T_1) via ISC, hence phosphorescent metal complexes are ubiquitously used for PDT, the mechanisms differ with their interaction with ground state oxygen ($^3O_2$). In the Type-I mechanism the electron is transferred to the ground state oxygen resulting in the formation of reactive oxygen species which damage cancer cells,[117-119] such as superoxide ($O_2^{-\bullet}$) and hydroperoxyl radical ($HO_2^{\bullet}$). The Type-II mechanism transfers energy to the ground state oxygen to produce singlet oxygen ($^1O_2$), generation of singlet oxygen in live cells is considerably photocytotoxic and causes cell death within cancer cells. Metal complexes used in this process are non-cytotoxic when incubated in the dark and have a turn-on switching effect when exposed to light, allowing for extremely high selectivity.

Ir complexes have been investigated for application as a PDT photosensitiser,[120] due to their unique abilities being kinetically inert and highly tuneable. Octahedral Ir(III) complexes have been the focus of many investigations, as they can emit at a wide range of wavelengths. In addition, the tethering of chromophores will increase the excited state lifetime and thusly promote more Type-II PDT. Zhou and co-workers added a pyrene moiety to terpy to produce $[Ir(ppy)_2(terpy\text{-}pyrene)]^+$ (Figure 1.22),[121] the addition of the chromophore produced a back-and-forth energy transfer which increased the excited state lifetime (15 μs) by 230-fold compared to the non-substituted analogue (65 ns). The "ping-pong" effect is defined as the energy transfer from the singlet states of the terpy-pyrene ligand to the Ir(III) metal centre and then transferred to the triplet states of the terpy-pyrene ligand. The addition of the pyrene chromophore resulted in a dramatic increase in $^1O_2$ quantum yield from, 26 % for the unsubstituted complex to 98 % for the appended pyrene complex.

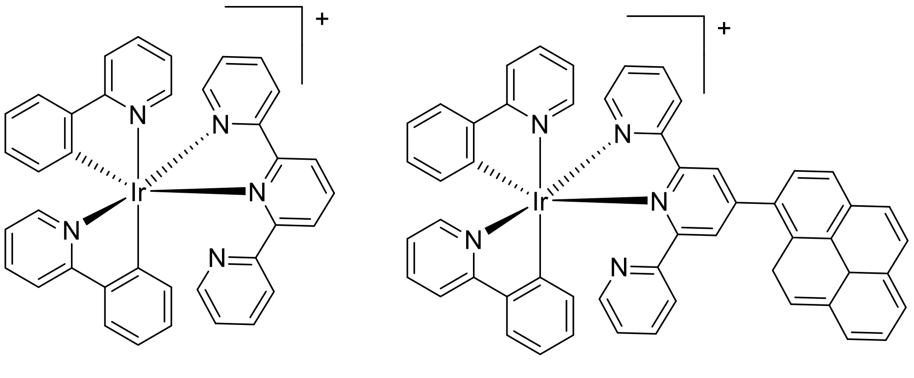

Zhou et al.

Figure 1.22 Structure of complexes developed by Zhou and co-workers for use in PDT,[121] using the "ping-pong" effect.

Ir(III)$^{3+}$ N_6 polypyridyl complexes were developed by the Sun and McFarland groups (Figure 1.23) to sensitise $^1O_2$.[122] The complexes, appended with pyrene moieties, were reported to have very long excited state lifetimes, τ = 31-33 μs and efficient singlet oxygen sensitivity with quantum yields of 66 % and 72 % respectively. These complexes have higher quantum efficiencies than known singlet oxygen sensitisers such as methylene blue and $[Ru(bpy)_3]^{2+}$.[123] One of the main issues with using Ir(III) complexes as photosensitisers for PDT is that their absorption bands tend to be in the ultraviolet spectrum rather than in the desired visible window, occasionally there is a very weak tail that stretches into the visible spectrum. Excitation via ultraviolet light is not used as it leads to photodamage of the biological architecture. Sun and McFarland's complexes have absorption bands reaching into the visible region, allowing for greater viability as PDT photosensitisers.

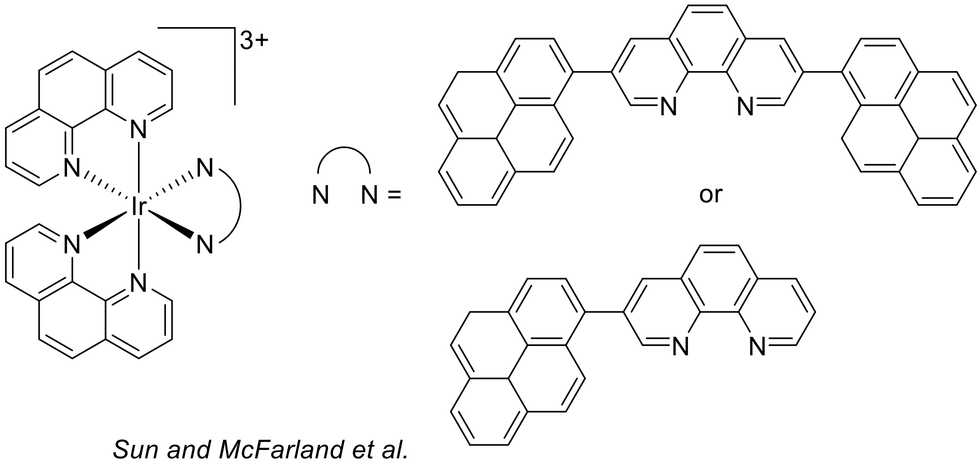

Sun and McFarland et al.

Figure 1.23 Ir complexes developed by the Sun and McFarland groups,[122] utilising the pyrene moiety to increase their capabilities as PDT agent.

1. 6. 3. Light Emitting Devices

OLEDs work by the injection of electrons, from the cathode, into the LUMO and holes, from the anode, into the HOMO so when they combine an excited state (exciton) is formed, when this decays radiatively a photon is produced.

In most OLEDs there is an anode electrode, typically indium tin oxide (ITO), and a cathode which is an evaporated metal, such as Ag.[124] Then organic compounds that can charge transport and emit light are layered on the transparent substrate (Figure 1.24). Electrons are injected via a low work function metal or by an *n*-doped electron injection layer, both are very unstable in air therefore the entire system sealed.

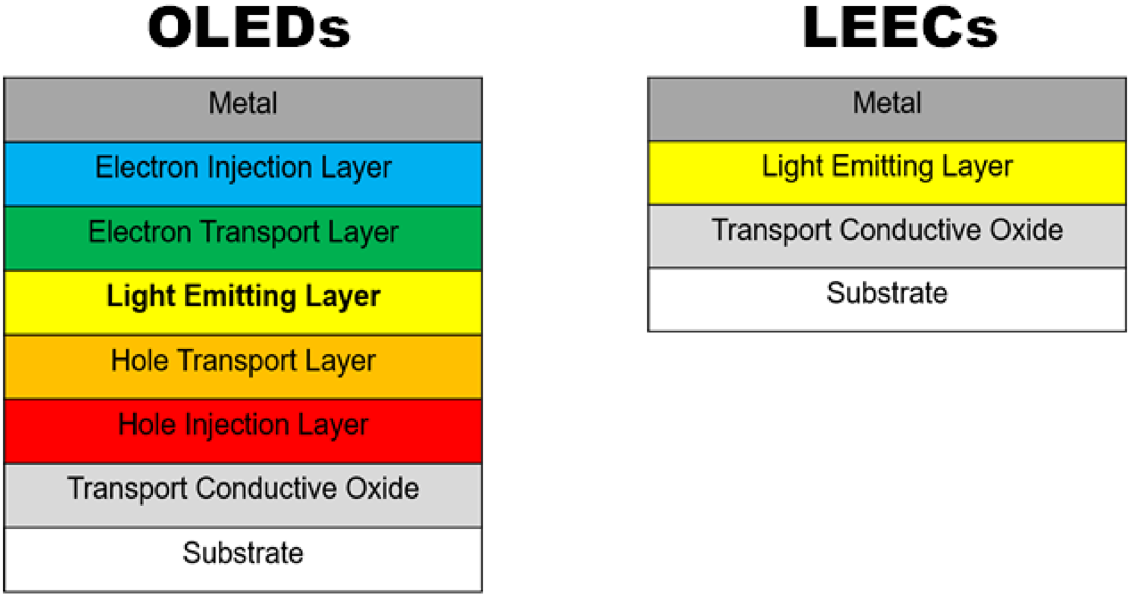

Figure 1.24 Simplified diagrams showing structure of the devices for OLEDs (left) and LEECs (right).[125]

Neutral cyclometalated Ir(III) complexes have gained significant attention in the field of organic light-emitting diodes (OLEDs) due to their remarkable electroluminescent properties. In particular, a pioneering contribution by Thompson and co-workers who introduced $Ir(ppy)_3$ (Figure 1.25) as part of an OLED,[75] the complex was reported to be an highly efficent, $\phi = 97$ %, green emitter. Red light-emitting Ir(III) complexes display comparatively lower quantum yields than their green and blue counterparts. This disparity arises from a reduced energy gap between the excited and ground states, resulting in an elevated non-radiative decay rate (k_{nr}) due to the the increase vibrational overlap between ground and excited states. Tsuboyama and co-workers reported $Ir(piq)_3$ (Figure 1.25) which is an efficent ($\phi = 26$ %) red emitter that has application in OLEDs.[73] When comparing red and green emitting Ir(III) complexes to their blue counterparts, it becomes apparent that blue light emitting complexes are less commonly employed in light emitting devices. This is primarily due to the challenges associated with achieving a deep pure blue color and ensuring long-term operational stability. Among the reported Ir(III) complexes, the majority of those capable of emitting blue light are efficient sky-blue complexes

(450-485 nm), while the number of deep-blue phosphorescent complexes remains limited. The most efficent sky-blue emitting complex that has potential to be used in OLEDs is Ir(dfppy)$_2$(pic) (Figure 1.25) as it is higly efficent (ϕ = >80 %).[126]

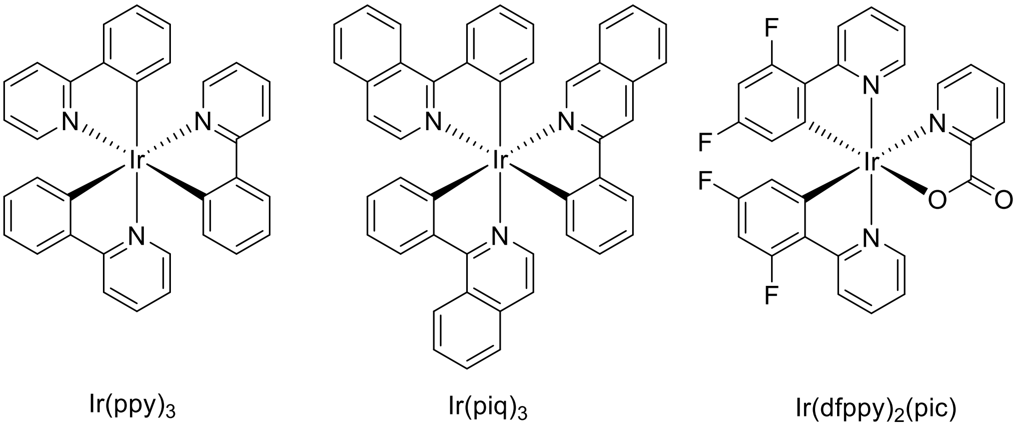

Figure 1.25 Neutral Ir complexes that have potential to be used in OLEDs, Ir(ppy)$_3$ (left) is a green emitter,[75] Ir(piq)$_3$ (centre) is a red emitter,[73] and Ir(dfppy)$_2$(pic) (right) is a blue emitter.[126]

Light emitting electrochemical cells (LEECs) are simple single layer devices, compared to state-of-the-art OLEDs which require multiple layers (Figure 1.23.). As the emitting layer is sandwiched between the two electrodes, ions are displaced when an external bias is applied which allows for efficient hole and electron injection.[127] Light emitting electrochemical cells are very attractive for industrial manufacturing as they allow for air-stable electrode materials, reduce the need for thick active layers making the systems more fault tolerant and they can be prepared by solution-based technologies.[125] The turn-on times for these systems range from milliseconds to hours therefore the applications for these devices are more likely for lighting and signage. The turn on times are dependent on the size of the counter ions, the smaller the faster, smaller counter ions are also less stable. Charged emitting dopants either polymers or transition metal complexes are used for the emitting layer, hence the specific interest in this thesis.[128]

Light emitting electrochemical cells work by having a bias applied to the system causing the counterions to move toward the anode lowering the barrier for hole injections in the HOMO and the metal complex ions for at the cathode enhancing electron injection. At the same time electrons and holes are being injected and migrate to the opposite electrodes. Then emission occurs when there is electron transfer from the electron rich ion to the electron deprived metal ion.[129]

Cationic Ir(III) complexes are the most used metal complexes in LEECs due to their stability and high tunability, some very efficient stable complexes have been developed for yellow/orange emitters. Wong and co-workers developed a complex (Figure 1.26) that is an efficient emitter ϕ = 23 % with an EQE of 9.16 % with good stability ($t_{1/2}$ = 100-1000s h), that has λ_{em} = 605 nm in the orange region.[130, 131]

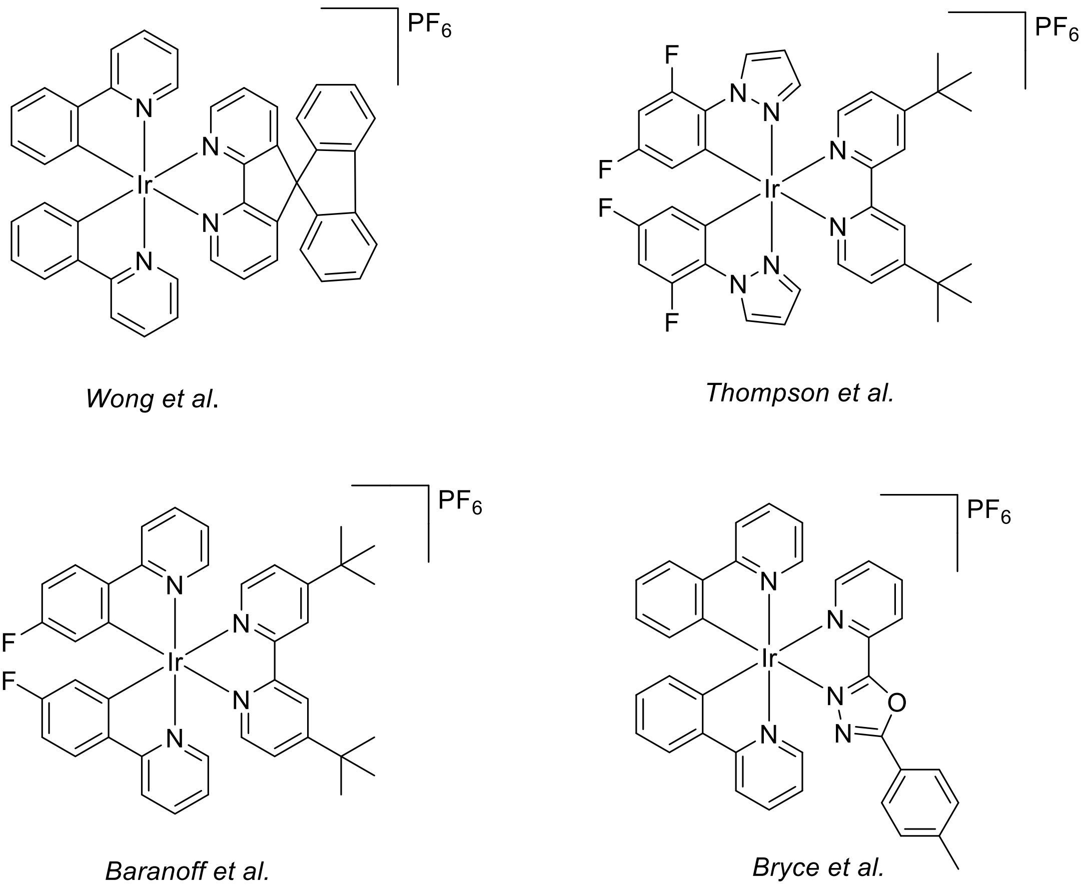

Wong et al.

Thompson et al.

Baranoff et al.

Bryce et al.

Figure 1.26 Structure of the most prominent cationic Ir complexes used in LEEC's. The orange emitting complex by Wong and co-workers (top left),[130] the sky-blue emitting complex reported by Thompson and co-workers (top right),[71] the most efficient green emitter developed by Baranoff and co-workers (bottom left),[132] and the effective red emitter reported by Bryce and co-workers (bottom right).[133]

Achieving blue emission for LEECs is very difficult due to producing efficient pure blue emitting Ir(III) complexes and the stability of their devices, however the best emitter for the sky blue region was developed by Thompson and co-workers (Figure 1.26).[71] The device has a very high efficiency (EQE = 14.4%) but a low device lifetime ($t_{1/2}$ = 2.17 h), the lack of stability is detrimental for blue light LEECs.[131, 134]

Green LEECs have similar issues with stability as blue light emitters, they are efficient but struggle with device lifetimes. The best green light Ir based LEEC has been developed by Baranoff and co-workers (Figure 1.26).[132] The complex itself had excellent efficiency (ϕ = 69%) but it also had remarkable device efficiency (EQE = 8.2%) and stability ($t_{1/2}$ = 98 h) as well as a relatively fast turn on time (t_{on} = 0.2 s).

Similar to the blue LEECs pure red devices struggle with stability compared to the orange/yellow devices. Bryce and co-workers,[133] developed a complex (Figure 1.26), that was emissive in the yellow region in solution (λ = 573 nm), however when in the device the emission is red shifted and emitted at 624 nm in the red region. This significant shift is attributed to excimer formation from strong π-π

stacking interactions. The device is very efficient (EQE = 9.51%) but does have poor stability with a short device lifetime ($t_{1/2}$ = 8.17 h).

1. 7. Aims and Objectives

Developing novel higly efficent light emitting devices is at the forefront of research, the greater the efficency the less energy is used. This is vital in reducing the amount of carbon emissions used that is affecting the climate crisis. Recent developments of OLEDs and LEECs have shown considerably more efficent light emitting devices than previous more conventional lighting methods.[135-138]

As discussed previously Ir(III) complexes are the superior complexes for light emitting devices due to their excellent efficency, stability, tunability and versatility.[64-66] The modification of their ligands can directly modulate the frontier orbitals allowing for tuning of colours across the visible spectrum. Ir(III) complexes have versatility and can be used in light emitting devices (OLEDs and LEECs), biological imaging and in photodynamic therapy.[26, 129, 139]

The primary objective of this thesis is to advance and explore the field of light-emitting complexes by synthesizing new Ir(III) complexes that modulate the HOMO and LUMO. The tuning strategies discussed in Chapter 1 have been thoroughly assessed and serve as a basis for the careful selection of ligands and complex architectures presented throughout. The photophysical and electrochemical properties of the newly synthesized light-emitting complexes will be extensively characterized and analyzed. These investigations will provide insights into their light-emitting capabilities and electronic behavior. This work aims to contribute to the development and advancement of light-emitting devices, expanding our understanding of their properties and opening up new possibilities for their utilization in a multitude of applications. This work successfully accomplishes the aforementioned objectives by pursuing the following specific aims:

- To build on our groups effective use of triazole based ligands to develop a bridging ligand that can facilitate heterodinuclear complexes for the purpose of producing white light emission. The application and design of Ir(III) triazole complexes in a multinuclear system that will have photoinduced energy transfer between the metal centres.
- Investigate the the higher energy T_1 excited states of Ir(III) complexes by careful ligand design. Thompson and co-workes developed Ir phenylpyrazine complexes that promote high energy emission. The De Cola and Zysman-Colman groups have reported a number of high energy emitters through the application of triazole moieties.[84-86, 95] Looking to manipulate the excited states so the high lying ^{3}MC states are thermally accesible via electronic and steric effects. Use computational methods to garner a full comprehensive understanding of these processes.
- Design ligand architectures to explore new chemical space in the form of Ir(III) 3+2+1 complexes (3 = terdentate, 2 = bidentate and 1= monodentate). To have an insight into the photophysical properties of this relativley unexplored complex structure. Assess the

photophysical properties against the computational calculations to have a full overview of the unique complex structure.

Comprehensive characterization of all complexes will be conducted using advanced analytical techniques, including ^{1}H and ^{13}C NMR spectroscopy, mass spectrometry, as well as UV-vis absorption and fluorescence spectroscopy to probe their photophysical properties. The photoluminescent quantum yields (ϕ_{rel}) were calculated from equation 1.29 using the relative standard $[Ru(bpy)_3]2(PF_6)$ which has an absolute quantum yield ϕ_{abs} = 1.8%. Moreover, the lifetimes of luminescent excited states exhibited by these complexes will be determined through the application of time-correlated single-photon counting luminescence spectroscopy. In addition to this, the electrochemical properties will be investigated by cyclic voltammetry.

$$\phi_u = (\frac{A_{ref} * I_u * \eta_u^2}{A_u * I_{ref} * \eta_{ref}^2}) * \phi_{ref}$$

Eq. 1.29 (A = abosrbance at wavelength of excitation, I = intergrated emission intensity, η = solvent refractive index, u = unkown, and ref = reference)

2. Development of Heterodinuclear Ir(III)-Ru(II) Complexes for White Light Emission

2. 1. Introduction

Ir(III) cyclometalated complexes have a multitude of applications due to their excellent photophysical properties, as shown in Chapter 1. These complexes are highly tuneable, have excellent phosphorescent quantum efficiency and long excited state lifetimes. This makes these complexes excellent candidates for a variety of applications; light emitting devices,[129, 139] biological imaging,[26] photocatalysis,[140] dye-sensitised solar cells and more.[65, 141]

In Chapter 1 a comprehensive review of efficiently emissive Ir(III) complexes, the structure that allowed for the greatest amount of tuning was found to be $[\mathrm{Ir(C^\wedge N)_2(N^\wedge N)}]^+$ initially based on archetypal $[\mathrm{Ir(ppy)_2(bpy)}]^+$ complex developed by Watts and co-workers.[142] As discussed in Chapter 1.5.3, Ir(III) triazole complexes based on this structure have been reported by De Cola and co-workers (Figure 2.1) with good quantum efficiency (ϕ = 21-22 %) and reasonable lifetimes.[85, 86]

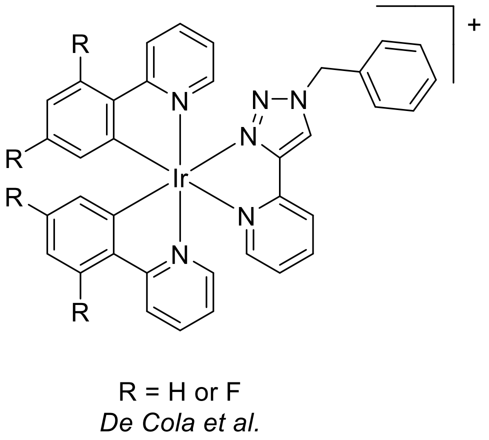

Figure 2. 1 Efficient Ir(III) triazole complexes reported by De Cola and co-workers.[89] The H substituted complex was a sky-blue /green emitter and the F substituted complex was a blue/sky-blue emitter.

White organic light-emitting devices, similar to OLEDs, achieve broadband white light electroluminescence via an emissive layer between the cathode and anode (Figure 1.24.). In WOLEDs the electroluminescent materials can either be singlet emitters or triplet emitters.[143] Fluorescent materials can only harvest singlet excitations, limiting their efficiencies to a maximum of 25% internal efficiency. However, phosphorescent materials can harvest both singlet and triplet excitations making them very efficient with up to 100% internal efficiency.[2, 139]

Light-emitting electrochemical cells represent a compelling alternative to the current state-of-the-art OLEDs due to their simplicity as single-layer devices (Figure 1.24).[64] This simplicity offers several advantages, particularly in terms of industrial manufacturing. LEECs facilitate the utilization of air-stable electrode materials and diminish the necessity for thick active layers, thereby increasing system resilience to failure.[128] Moreover, these devices can be prepared using solution-based technologies, further enhancing their suitability for large-scale production.

Light-emitting electrochemical cells find promising applications in the fields of lighting and signage due to their varied turn-on times, which can range from milliseconds to hours.[134] These turn-on times are closely correlated with the size of the counter ions; smaller counter ions result in faster turn-on times but exhibit reduced stability. The emitting layer of LEECs uses charged emitting dopants, such as polymers or transition metal complexes,[129] with the capability of producing white light. Consequently, single-molecule systems featuring intermolecular energy transfer (IET) can be employed in the emitting layer, facilitating white light emission in LEECs.[144]

To produce white light emission, either a combination of equal intensities of blue, green and red emission or of two corresponding colours such as blue and orange is require.[143, 145] For both methods there will be a combination of emitters which therefore requires control of potential energy transfer between them.[146] There must be a downward flow of energy from the higher energy emitters (blue) to the lowest energy emitters (red/orange). However, when complete energy transfer occurs only the lowest energy emitters emit.[147] The control over the energy transfer phenomena is quintessential to being able to produce white light, to ensure the correct ratio of emission of each component.[148] A blue light emitter is always used and blue emission has subsequently been explored thoroughly. An effective example of generating blue emission is fluorination, this has been shown in many different classes of luminescent materials.[149, 150]

There are two main approaches to obtain white light as the emissive layer; multiple emitters or single emitters. Multiple emitters can either be used in a multilayer architecture or combined in a single layer. Multilayer architecture prevents interlayer mixing and means that concentrations of dopants can be adjusted.[151] Some major drawbacks of these systems are that they are more complex to manufacture, there are greater operating voltages than in single layer devices due to the thickness of the device and there can be voltage dependent colour changes observed.[152] Multiple emitters in a single layer is an attractive approach as it is a low-cost method for large area manufacturing as the one layer can be processed from solution or from evaporation techniques. The concentration ratio of the dopants is less crucial in this system compared to the multi-layered system, unfortunately the efficiency and brightness are lower, and the different components degrade at different rates.[153]

There are two main types of single molecule emitter systems, single molecules that form aggregates and excimer emission, and single molecule emitters which incorporate more than one emitting chromophore between which there is only partial IET resulting in dual emission behaviour. These single molecule systems are highly desirable as they would simplify manufacturing, lower costs and they avoid problems that occur in multiple emitter systems such as changes in concentrations or aging of dopants whilst the devices are active.[145] Aggregate based single molecule systems are passed on the monomers emission (blue) combined with the aggregate induced excimer emission (orange/red). Whereas, IET single molecules have two separate moieties that are responsible for the blue and the orange/red emission. A key benefit of these systems is that these devices do not change colour of emission with age and deterioration, as seen in emitters with multiple molecules, it is a single molecule responsible for both blue and orange/red light emission. The main issues for these devices are that they require complex molecular design and current complexes have general low efficiencies.[154]

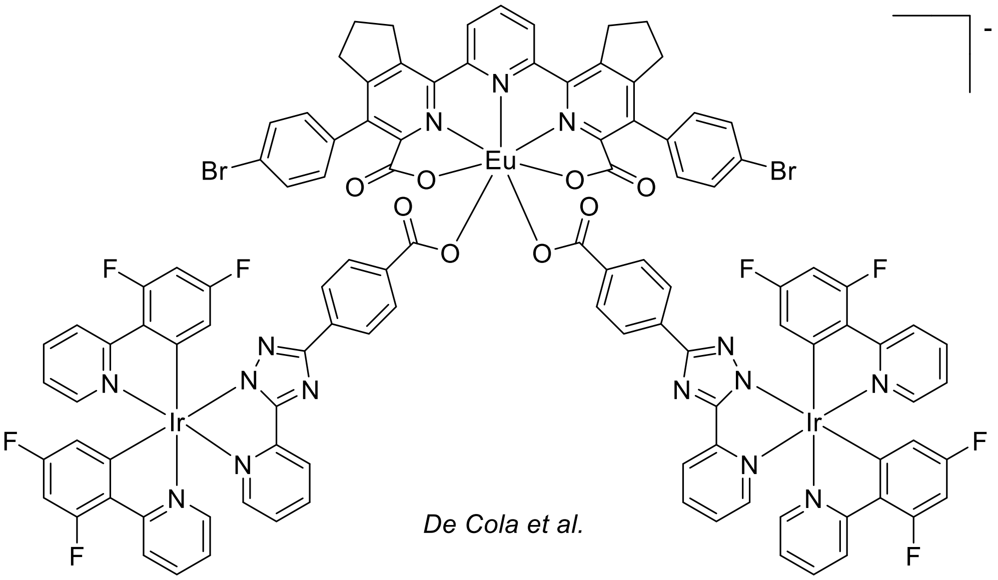

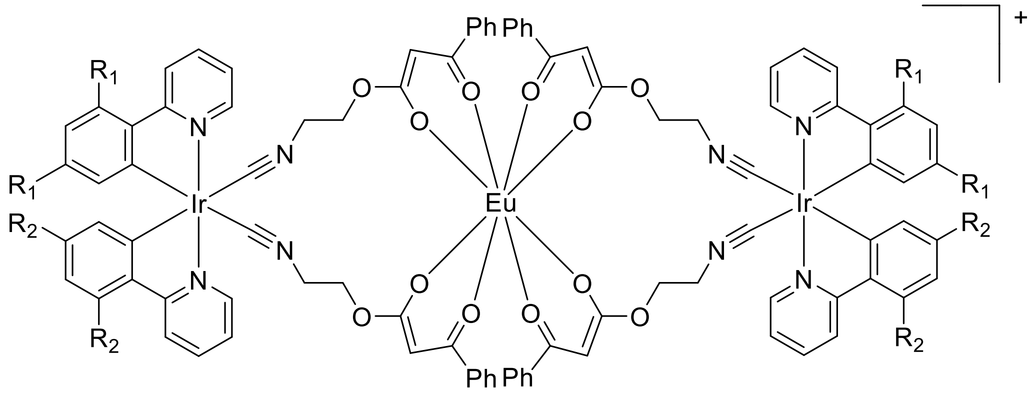

Sambri et al.
ppy $R_1 = R_2 = H$
fppy $R_1 = H, R_2 = F$
dfppy $R_1 = R_2 = F$

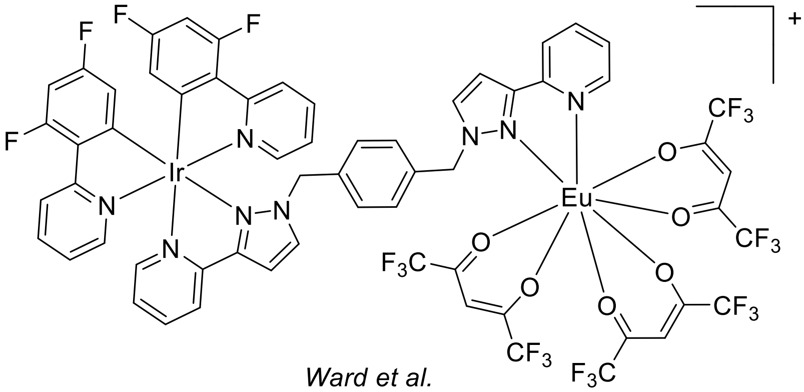

Figure 2. 2 Reported heteromultinuclear Ir(III)-Eu(III) complexes that utilise partial energy transfer to induce white light emission. De Cola and co-workers 1,2,4-triazole based ligand architecture (top),[155] Sambri and co-workers exploring the substituents on the cyclometalated ligands (centre),[156] and the heterodinuclear complex developed by Ward and co-workers (bottom).[157]

Molecules based on IET rely on the downward energy transfer from the higher energy blue emitter to the lower energy orange/red emitter. Part of the difficulties of molecular design is developing a molecule that has the right degree of partial energy transfer between the moieties so that the blue emitter is not completely quenched.[158] This can occur between different organometallic components and has been reported in a few cases using kinetically inert transition metals. De Cola and co-workers reported a Ir(III)$_2$-Eu(III) complex (Figure 2.2) exhibiting partial excited state energy transfer from the blue/green Ir(III) centres to the red Eu(III) centre which resulted in white light emission,[155] with commission internationale de l'éclairage (CIE) coordinates of x= 0.28 y= 0.30 and a quantum yield of 7%. Sambri and co-workers developed a series of Ir(III)$_2$-Eu(III) complexes, changing the R-ppy substituents.[156] The ppy based complex, showed no Ir(III) emission and only Eu(III) emission due to a complete energy transfer, but when electron withdrawing fluorine substituents were added (fppy and dfppy), there was only partial energy transfer due to the triplet energy of the Ir(III) centres being raised. The fppy complex showed near pure white light emission with CIE coordinates x= 0.33 y= 0.36. Ward and co-workers also reported a near pure white light emission for their Ir(III)-Eu(III) complex, with CIE coordinates of x= 0.34 y= 0.32.[157]

2. 1. 1. Aims and Objectives

Single molecule WOLED devices and LEECs are of high interest due to lower costs, simpler manufacturing and will be less affected by long term use. The current issue being the development of the necessary complex structure for efficient white emitting molecules. Multinuclear organometallic complexes have been reported by De Cola, Sambri and Ward all achieving white light emission through excited state partial energy transfer.

The aim was to develop a dinuclear complex combining a high energy (blue/green) emitter and a lower energy (orange/red emitter) to produce a white light, following these objectives:

- As discussed previously the combination of a green/blue emitter and orange/red emitter will yield white light emission in the right ratio. A specific amount of partial energy transfer will be required to observe this therefore a specific ligand architecture will be required to bridge the two metal centres. Inspiration was taken from Ward and co-workers Ir(III)-Eu(III) complexes bridging ligand, as it had the correct balance of partial energy transfer,[157] modified with triazole moieties instead of pyrazoles due to relative synthetic ease for potential industrial production. As the bridging ligand was centred around the phenyl moiety the *para-*, *meta-* and *ortho-* were also produced as we would expect this to have an effect on the partial energy transfer.
- For the blue/green emitting part of the complex, Ir(III) complexes were designed due to their excellent photophysical properties. The complexes reported by De Cola and co-workers (Figure 2.1) are ideal candidates for the high energy emitters as they have reported good quantum yields and reasonable excited state lifetimes.[85, 86] The complexes utilise the 1,2,3-triazole moiety

which was integrated onto our variation of Ward's ligand, ensuring synthetic capability. It was anticipated that that through the triazole design there would be limited effect on the emissive properties of the Ir(III) complexes due to the ^{3}MLCT/^{3}ILCT character of these complexes. However, there would be some partial energy transfer from the T_1 state of these Ir(III) complexes to the orange/red emitting complex.

- Ru triazole complexes have been reported to be emissive in the orange/red region of the visible spectrum by Schubert and co-workers.[159] To balance the intensity of emission, and provide white light, the orange/red emitter would need to be a weaker emitter as the downward energy transfer from the higher energy blue/green emitting metal centre will increase the emission intensity. An analogous Ru(II) complex to Schubert's (Figure 2.3) was developed for the orange/red light emitting metal centre as the complex is pytz based it has viability with the bridging ligand. It was expected the amount of partial energy transfer to the Ru metal centre would increase its emission intensity so white light emission would be achieved.
- Complexes **JA1-3** (Figure 2.3) were designed to produce efficient white light for potential use in WLEECs. The mononuclear analogues (Figure 2.3, **JA1-3.Ir**, **JA1-3.IrF and JA1-3.Ru**) of complexes **JA1-3** were designed to be used as a comparison of photophysical properties.

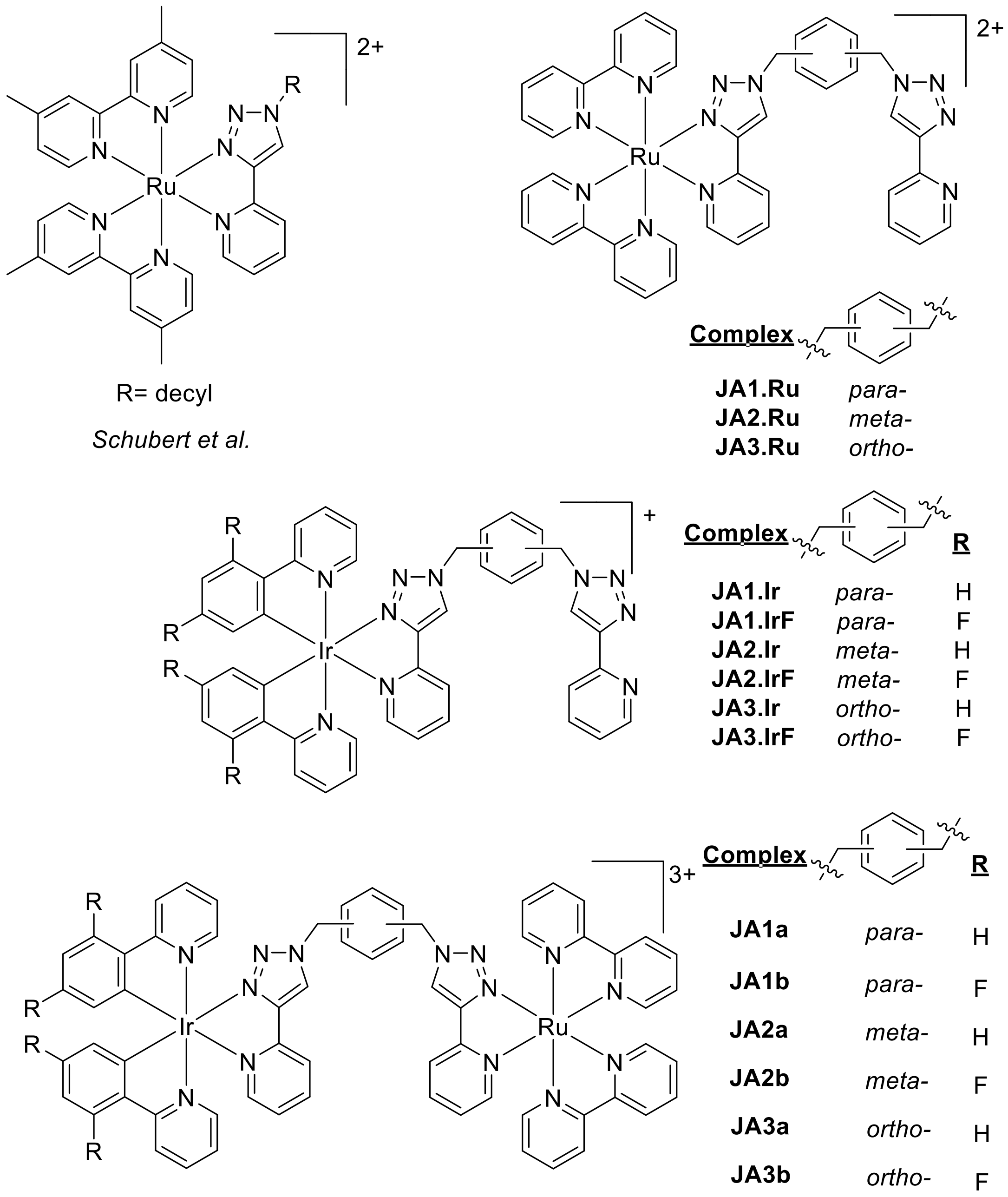

Complex	
JA1.Ru	*para-*
JA2.Ru	*meta-*
JA3.Ru	*ortho-*

Complex		R
JA1.Ir	*para-*	H
JA1.IrF	*para-*	F
JA2.Ir	*meta-*	H
JA2.IrF	*meta-*	F
JA3.Ir	*ortho-*	H
JA3.IrF	*ortho-*	F

Complex		R
JA1a	*para-*	H
JA1b	*para-*	F
JA2a	*meta-*	H
JA2b	*meta-*	F
JA3a	*ortho-*	H
JA3b	*ortho-*	F

Figure 2. 3 Reported emissive Ru triazole complex by Schubert and co-workers (top left).[159] *Novel heterodinuclear complexes* ***JA1-3*** *designed for white light emission and potential use in WLEECs (bottom). Mononuclear analogues of the dinuclear complexes separating the Ir(III) (centre) and Ru(II) (top right) metal centre for comparison.*

2. 2. Synthesis of Ligands and Complexes

2. 2. 1. Synthesis of Ligands

Bridging ligands, pytz-*o/m/p*-xyl-pytz (*o* = *ortho*, *m* = *meta*, *p* = *para*), were prepared via a copper(I)-catalysed alkyne-azide cycloaddition following a reported procedure by Crowley and co-workers (Scheme 2.1a).[160] Starting materials *o/m/p*-xylene dibromide, 2-ethynlpyridine and sodium azide were combined with sodium ascorbate, copper sulphate, sodium carbonate and DMF/H_2O (4:1) as the solvent, left to stir at room temperature for 20 h. After work-up this afforded the target ligands in good yields, 71-78%. The bridging ligands were characterised by ^1H NMR spectroscopy, ^{13}C NMR spectroscopy, and electrospray ionisation mass spectrometry (ESI-MS). Representative spectra of the *para* isomer are shown in Figure 2.4. The ^1H NMR spectrum shows singlets for the aromatic (a), the benzyl CH_2 (b), and the triazole (c); the pyridine rings show four H environments (d,e, f, g).

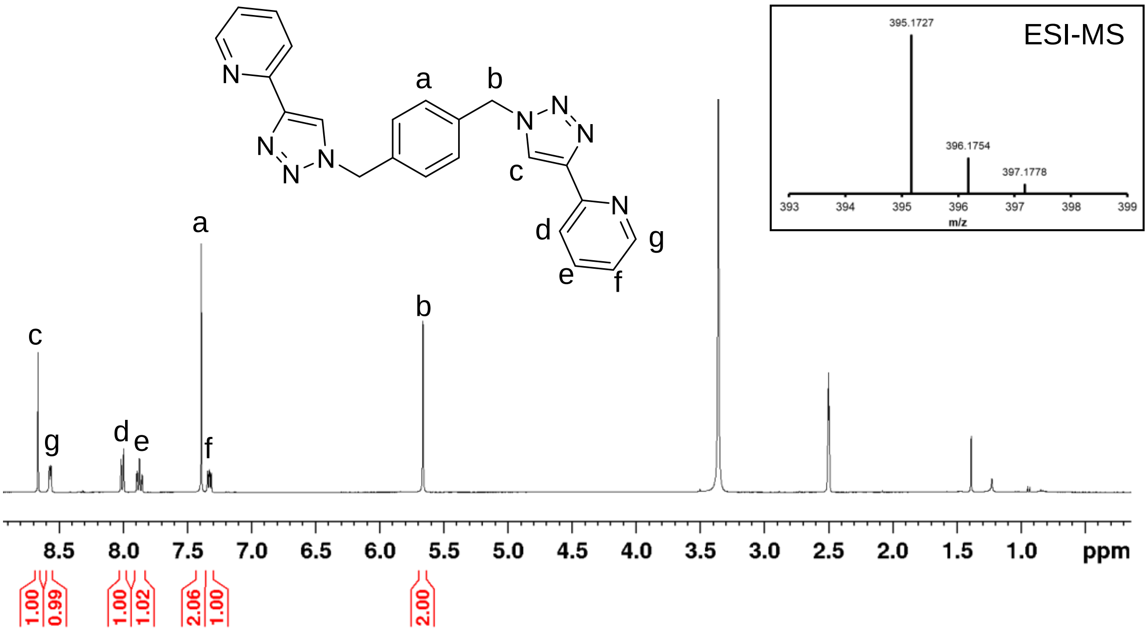

Figure 2. 4 ^{1}HNMR spectrum of pytz-p-xyl-pytz bridging ligand and ESI-MS (top right). There are 7 unique hydrogen environments, a) aromatic, b) benzyl CH_2, c) triazole, and the pyridine resonances (d,e,f,g).

2. 2. 2. Synthesis and Characterisation of Complexes

Mononuclear Ru(II) complexes, **JA1-3.Ru**, were prepared from $Ru(bpy)_2Cl_2$ and pytz-*o/m/p*-xyl-pytz was heated to reflux for 20 h (Scheme 2.1b) where, $Ru(bpy)_2Cl_2$ was prepared following literature procedures.[161] This afforded a combination of the desired mononuclear complexes and their dinuclear analogues, $[Ru(bpy)_2($pytz-*o/m/p*-xyl-pytz$)Ru(bpy)_2]^{4+}$, the desired complexes were separated and purified by column chromatography and recrystallisation. For the Ir(III) mononuclear complexes, **JA1-3.Ir** and **JA1-3.IrF**, were prepared from starting materials $[Ir(R\text{-}ppy)_2(\mu\text{-}Cl)]_2$, where R = H or F, and pytz-*o/m/p*-xyl-pytz refluxed for 20 h (Scheme 2.1c) where, starting materials [Ir(R-ppy)$_2$(μ-Cl)]$_2$ were prepared from literature procedures.[162] Similarly to the mononuclear Ru complexes, the desired complexes were produced in combination with their dinuclear analogues, [Ir(R-ppy)$_2$(pytz-*o/m/p*-xyl-pytz)Ir(R-ppy)$_2$]$^{2+}$, they were separated and purified via column chromatography and recrystallisation.

Heterodinuclear complexes **JA1-3** were prepared from **JA1-3.Ru** and [Ir(R-ppy)$_2$(μ-Cl)]$_2$ refluxed for 20 h which afforded the desired complexes (Scheme 2.1d). They were subsequently purified by column chromatography and recrystallisation. Both the mononuclear and heterodinuclear complexes were confirmed by ^{1}H NMR spectroscopy, ^{13}C NMR spectroscopy and electrospray ionization mass spectrometry (ESI-MS). ^{1}H NMR spectra of the heterodinuclear complexes contain a large number of resonances (Figure 2.5). Due to formation of a mixture of Δ(Ir)Δ(Ru), Λ(Ir)Λ(Ru), Δ(Ir)Λ(Ru) and Λ(Ir)Δ(Ru) isomers there will be two overlaid NMR spectra for these diastereomers which makes full assignment challenging. However, resonances for the chelated CH$_2$ are observed at 5.62 ppm for the Ir(III) fragment and the Ru(II) fragments chelated CH$_2$ is observed at 5.52. The triazole resonances match both the mononuclear Ir(III) and Ru(II) complexes, this was observed for complex **JA1a**. As some of the spectra are not clear and a number of the peaks are not resolved, formation of desired heterodinuclear complexes is confirmed by ESI-MS data.

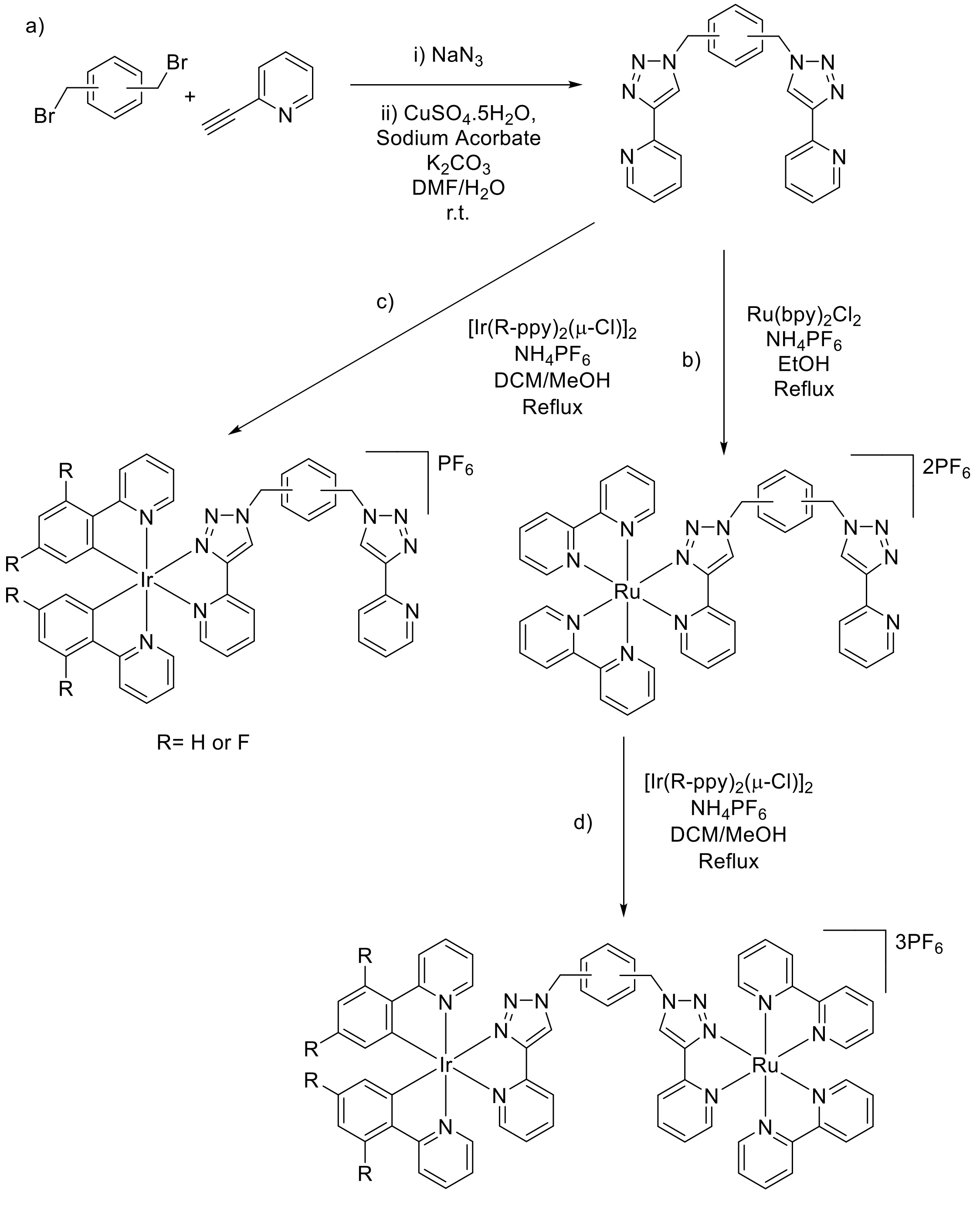

Scheme 2. 1 a) Preparation of bridging ligands pytz-o/m/p-xyl-pytz via "click" CuAAC reaction. b) Preparation of $[Ru(bpy)_2(pytz\text{-}o/m/p\text{-}xyl\text{-}pytz)]^{2+}$. c) Preparation of mononuclear Ir complexes $[Ir(R\text{-}ppy)_2(pytz\text{-}o/m/p\text{-}xyl\text{-}pytz)]^{+}$. d) Preparation of heterodinuclear target complexes $[Ir(R\text{-}ppy)_2(pytz\text{-}o/m/p\text{-}xyl\text{-}pytz)Ru(bpy)_2]^{2+}$.

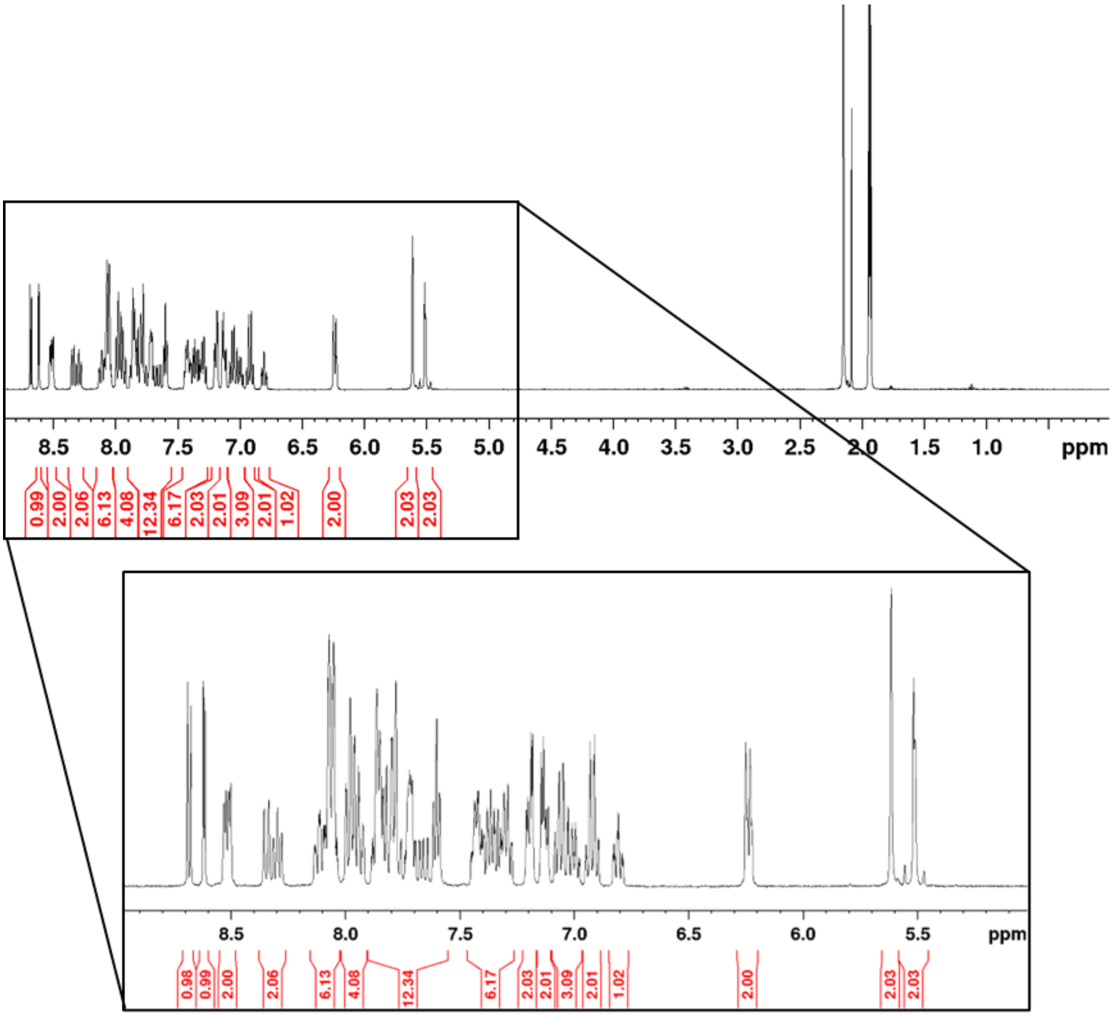

Figure 2. 5 ^{1}H NMR spectrum of JA1a in CD$_3$CN with zoom in on the region between 5.0-9.0ppm.

2. 3. Electrochemistry

Cyclic voltammograms were recorded for this series of complexes, **JA1-3**, in MeCN (Figure 2.6-2.8 and Table 2.1) as well as for the mononuclear complexes for comparison, to investigate their electrochemical properties.

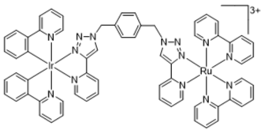

JA1a

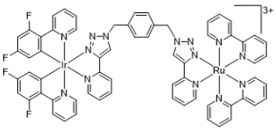

JA1b

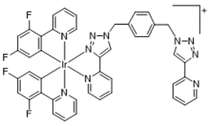

JA1.IrF

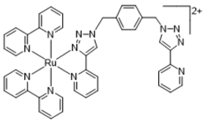

JA1.Ir

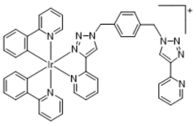

JA1.Ru

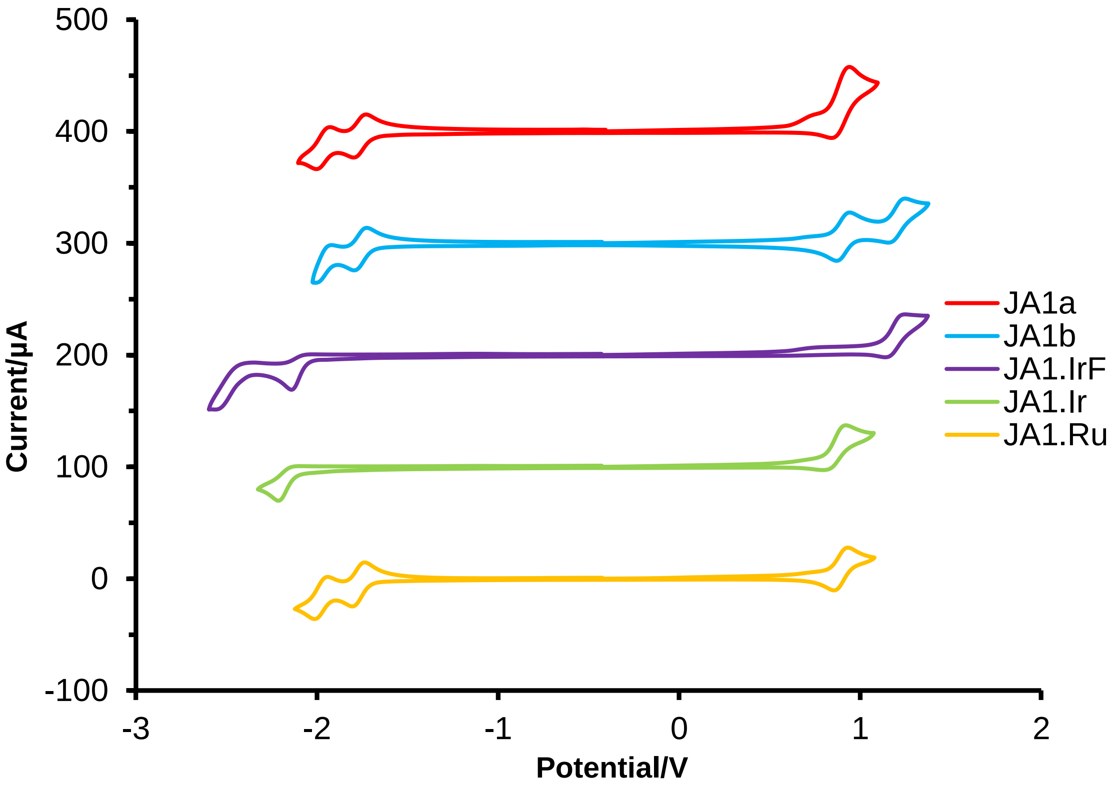

*Figure 2. 6 Cyclic Voltammograms of **JA1** (para) heterodinuclear and mononuclear complexes. Recorded in MeCN using Fc+/Fc as an internal standard, NBu$_4$PF$_6$ was used as the supporting electrolyte with a solution concentration of 0.2 moldm^{-3}. Measurements were performed under an atmosphere of N$_2$ at a scan rate of 100mV s^{-1}.*

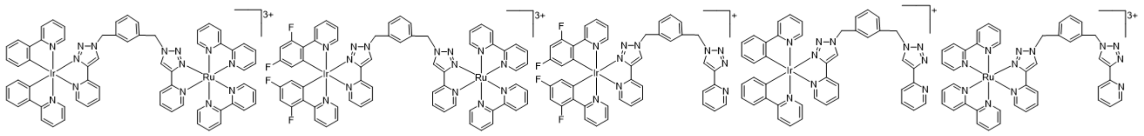

JA2a JA2b JA2.IrF JA2.Ir JA2.Ru

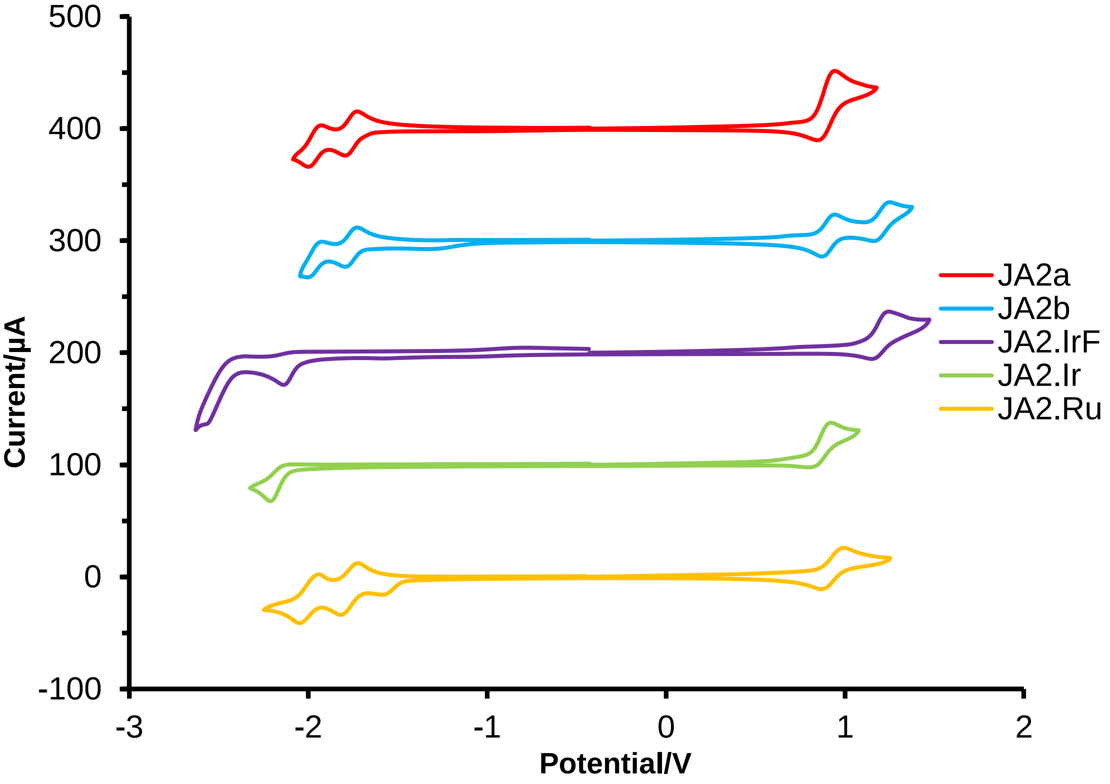

Figure 2. 7 Cyclic Voltammograms of ***JA2*** *(meta) heterodinuclear and mononuclear complexes. Recorded in MeCN using Fc+/Fc as an internal standard, NBu_4PF_6 was used as the supporting electrolyte with a solution concentration of 0.2 moldm^{-3}. Measurements were performed under an atmosphere of N_2 at a scan rate of 100mV s^{-1}.*

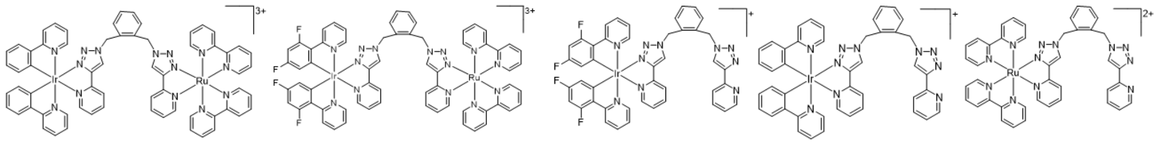

JA3a JA3b JA3.IrF JA3.Ir JA3.Ru

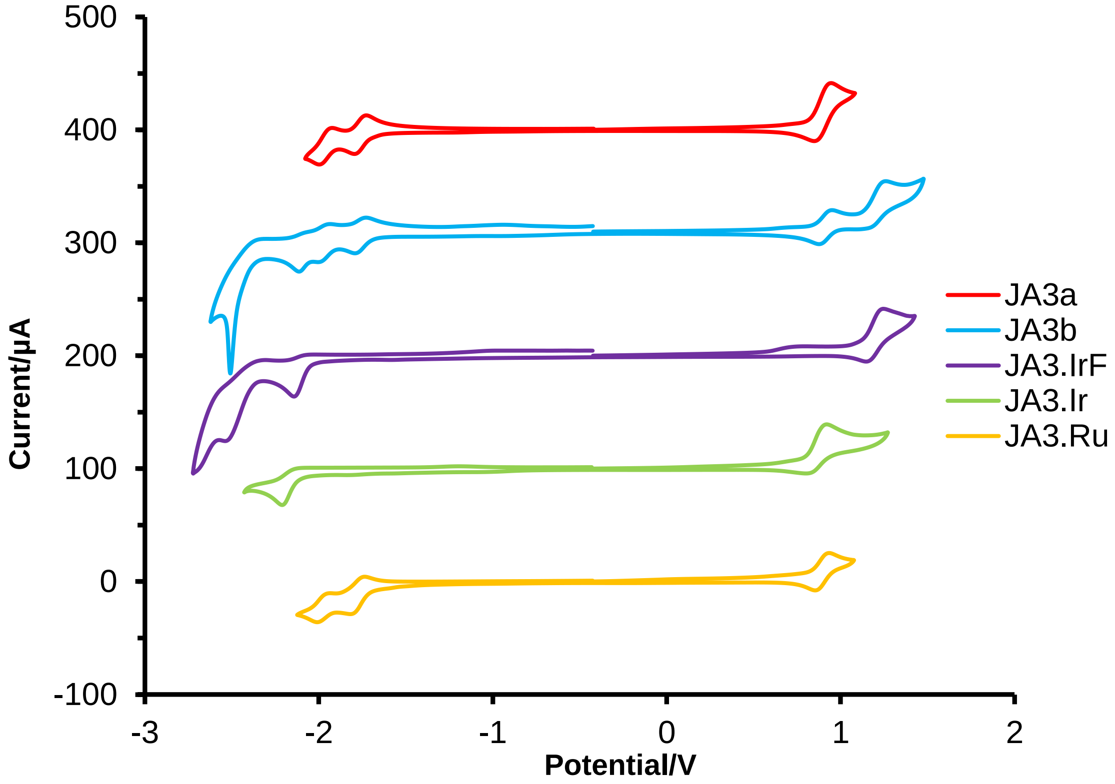

*Figure 2. 8 Cyclic Voltammograms of **JA3**(ortho) heterodinuclear and mononuclear complexes. Recorded in MeCN using Fc+/Fc as an internal standard, NBu_4PF_6 was used as the supporting electrolyte with a solution concentration of 0.2 moldm^{-3}. Measurements were performed under an atmosphere of N_2 at a scan rate of 100mV s^{-1}.*

Mononuclear Ir-ppy complexes **JA1-3.Ir** showed a partially reversible oxidation potential at ~ +0.92 V which correlates to reported Ir(III) ppy containing complexes and is assigned to the Ir(III)→Ir(IV) oxidation.[163] This was further confirmed by the anodic shift of the oxidation potential for the fluorinated counterparts, **JA1-3.IrF**, to +1.25 V. The shift was due to the electron withdrawing effects of the aryl fluorine substituents stabilising the HOMO. For **JA1-3.Ir** and **JA1-3.IrF**, the irreversible reduction potential of -2.21 V and -2.14 V is assigned to the pyridine moiety on the pytz ligand, as reported for $[Ir(R\text{-}ppy)_2(pytz)]^+$ complexes.[85, 86, 163] Reduction potentials for the cyclometalated R-ppy ligands and the triazole moiety were outside the solvent window so could not be detected. The mononuclear Ru(II) complexes **JA1-3.Ru**, showed a reversible oxidation potential at ~ +0.93 V assigned to the Ru(II)→Ru(III) oxidation and two reversible reductions at ~ -1.75 V and -2.01 V are assigned to the bpy ligands.

The E_{ox}-E_{red} energy gap for **JA1-3.IrF**, 3.39 V, was larger than that of **JA1-3.Ir**, 3.14 V, this can be used to estimate the HOMO-LUMO energy gap. The E_{ox}-E_{red} energy gap of 2.73 V, of the mononuclear Ru(II) complexes (**JA1-3.Ru**), are lower than the Ir(III) complexes, as this can be used to predict the HOMO-LUMO energy gap. This is expected as Ru(II) bpy complexes are reported to have lower energy and red shifted photophysical properties compared to Ir(III) triazole complexes.[159]

Heterodinuclear complexes **JA1-3** had accordant oxidation and reduction potentials with their ppy or dfppy counterparts, seen in Table 2.1. For complexes **JA1-3**, the E_{ox}-E_{red} energy gap can only be observed for the Ru(II) metal centre and bpy ligands, as the redox potentials for the triazole moiety and R-ppy ligands are outside of the solvent window. The pyridine moiety on the pytz ligand cannot be observed for most of the heterodinuclear complexes, unlike the mononuclear complexes, as the irreversible processes caused build-up of oxidised/reduced material on the electrode, resulting in an unusable cyclic voltammogram. However, for complex **JA3b**, the reduction for the pyrdine moiety, on the pytz ligand, can be observed at -2.11 V. Cyclic voltammetry traces for the heterodicnulear complexes are essentially the sum of those for the mononuclear Ru(II) and mononuclear Ir(III) components. For the dfppy containing heterodinuclear complexes, two distinct oxidation process are observed for independent Ru(II)/Ru(III) and Ir(III)/Ir(IV) processes. For the ppy containing heterodinuclear complexes, these processes are coincident.

For complexes **JA1a-3a** the height of the oxidation peak, +0.94 V, is approximately twice the height of the reduction process peaks in its C.V. trace thus corresponds to a two one-electron processes occurring at the same potential. This is in agreement with the coincident positions of the oxidation of the mononuclear Ir(III) and Ru(II) complexes. It also shows that there is no electronic coupling between the Ir(III) and Ru(II) centres and they behaved as independent redox centres.

Table 2.1 Summarised Electrochemical Data for 1.5mmol dm^{-3} MeCN Solutions of JA1-3 Measured at r.t.at 100mV s^{-1}.^{a,b}

Complex	E_{ox} / V	E_{red} / V	E_{ox}-E_{red} Gap^{c} / V
JA1a	+0.94	-1.80 (70), -2.00 (70)	2.74
JA1b	+0.94 (70), +1.25	-1.80 (80), -2.01(90)	2.74
JA1.Ru	+0.93 (70)	-1.80 (60), -2.01 (70)	2.73
JA1.Ir	+0.92	-2.21	3.13
JA1.IrF	+1.25	-2.14, -2.56	3.39
JA2a	+0.94	-1.79 (80), -2.00 (70)	2.73
JA2b	+0.94 (70), +1.25	-1.79 (70), -2.00 (80)	2.73
JA2.Ru	+0.97 (100)	-1.81 (90), -2.05 (110)	2.78
JA2.Ir	+0.92	-2.21	3.13
JA2.IrF	+1.25	-2.14, -2.56	3.39
JA3a	+0.95 (100)	-1.79 (70), -2.00 (80)	2.74
JA3b	+0.95 (80), +1.26	-1.79 (70), -2.01 (80), -2.11, -2.51	2.74, 3.37
JA3.Ru	+0.93 (80)	-1.82 (70), -2.01 (110)	2.75
JA3.Ir	+0.92	-2.21	3.13
JA3.IrF	+1.25	-2.14, -2.54	3.39

a) Potentials are shown in V vs Fc+/Fc. Reversible couples E1/2 is quoted with anodic-cathodic peak separation shown in mV in brackets. b) NBu_4PF_6 was used as the supporting electrolyte with a solution concentration of 0.2 moldm^{-3}. c) Difference in potential of the first oxidation and the first reduction.

From this cyclic voltammetry data we can anticipate that mononuclear complexes **JA1-3.IrF** should have high energy blue shifted absorption and emission due to the stabilisation of the HOMO, compared to **JA1-3.Ir**. By contrast, Ru(II) mononuclear complexes, **JA1-3.Ru,** will have lower energy red shifted absorption and emission due to the lower E_{ox}-E_{red} gap, and therefore lower HOMO-LUMO energy gap. As the two metal centres on the heterodinuclear complexes act as independent redox centres, we also expect a similar blue shift from the fluorinated Ir(III) metal centre, compare to the non-fluorinated, whilst not effecting the Ru(II) base absorption and emission.

2. 4. Photophysical Properties

2. 4. 1. Electronic UV-Vis Absorption Spectroscopy

The absorption spectra of all heterodinuclear and mononuclear complexes were recorded, in MeCN at RT (Figure 2.9-2.11, Table 2.2), The absorption bands <320nm on all complexes are assigned to ligand centred ($\pi\rightarrow\pi^*$) transitions.[62, 83] All complexes have a lower energy absorption band between 360-450nm assigned as a ^{1}MLCT transition, these bands are $S_0\rightarrow S_1$ involving mainly the Ir(III)/Ru(II) d orbitals.

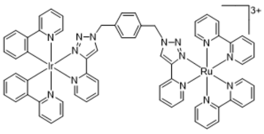
JA1a

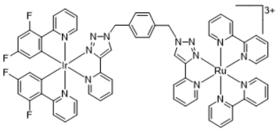
JA1b

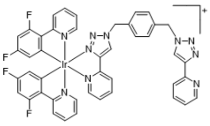
JA1.IrF

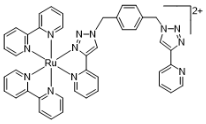
JA1.Ir

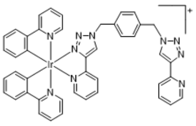
JA1.Ru

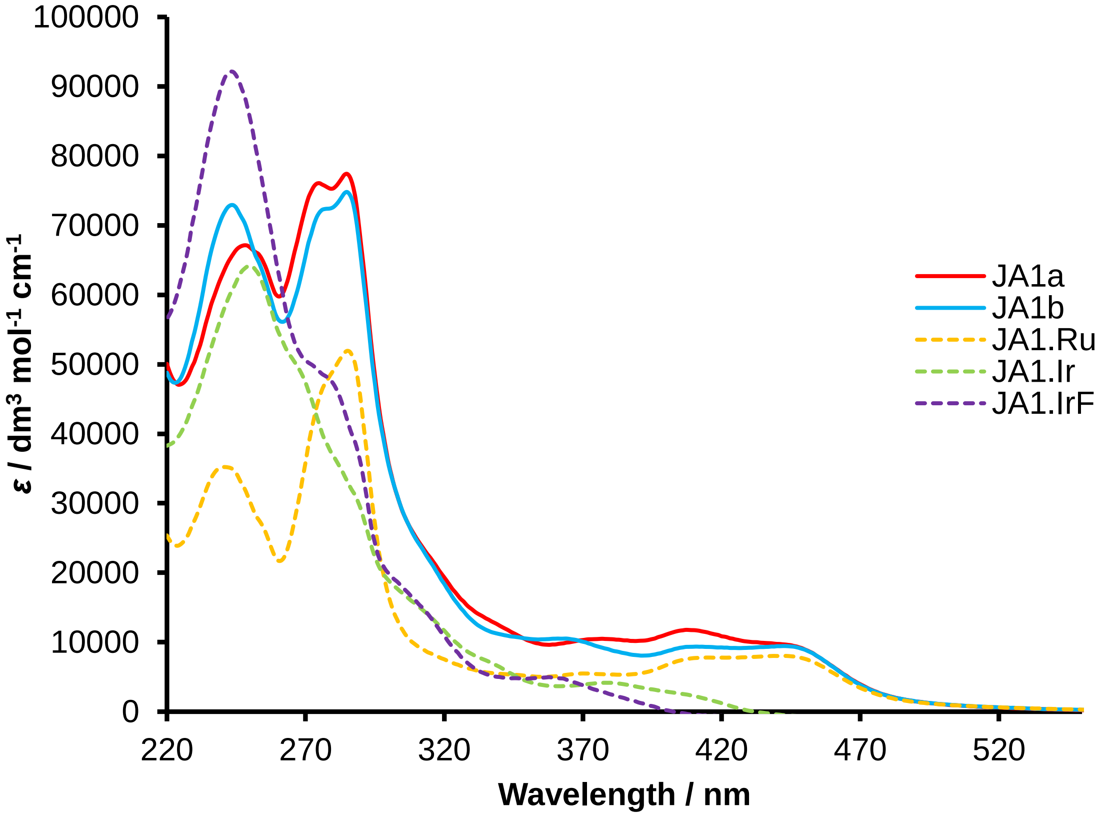

*Figure 2. 9 UV-visible electronic absorption spectra recorded for **JA1** (para) heterodinuclear and mononuclear complexes. Recorded in MeCN at 298K.*

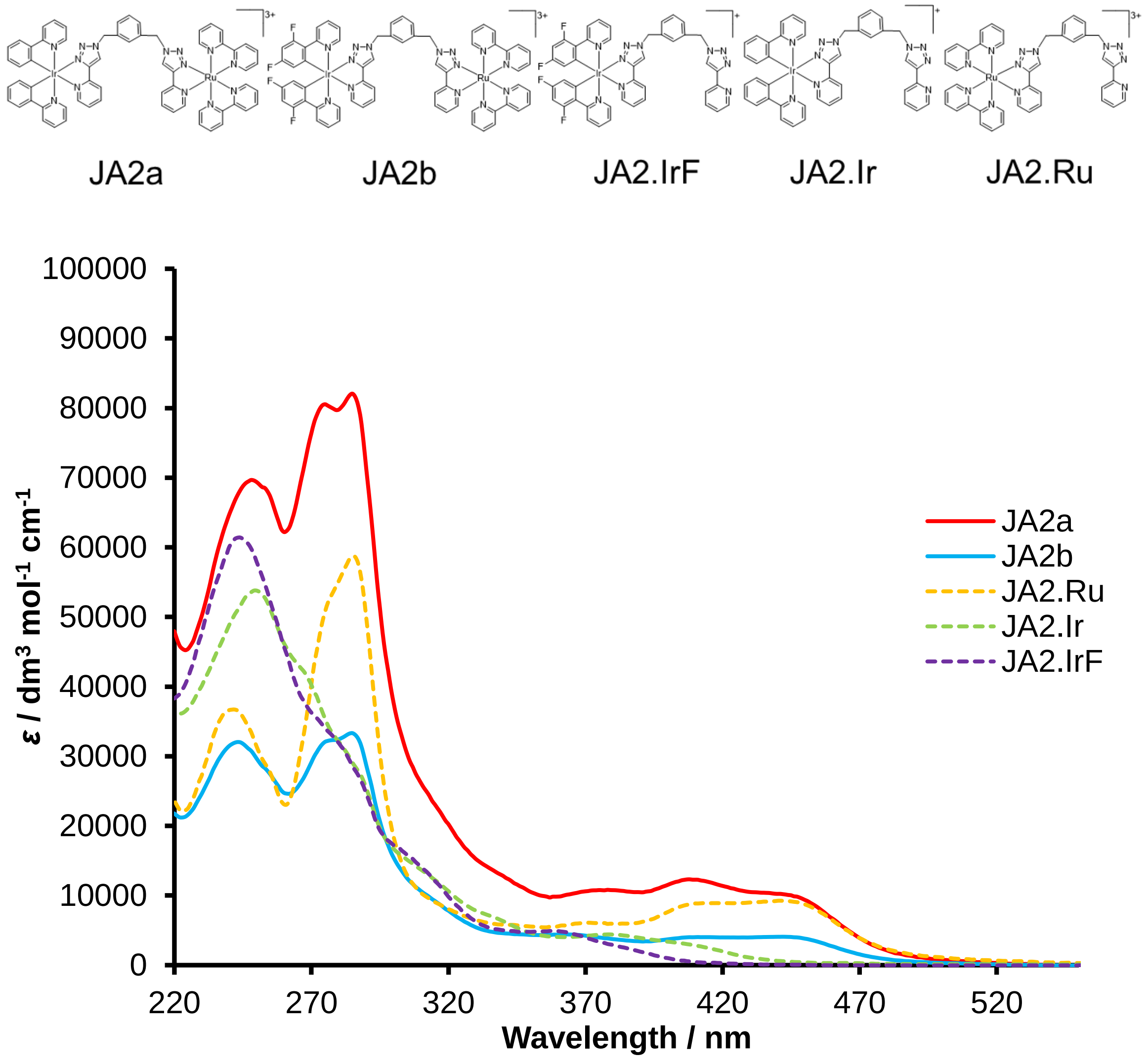

Figure 2. 10 UV-visible electronic absorption spectra recorded for ***JA2*** *(meta) heterodinuclear and mononuclear complexes. Recorded in MeCN at 298K.*

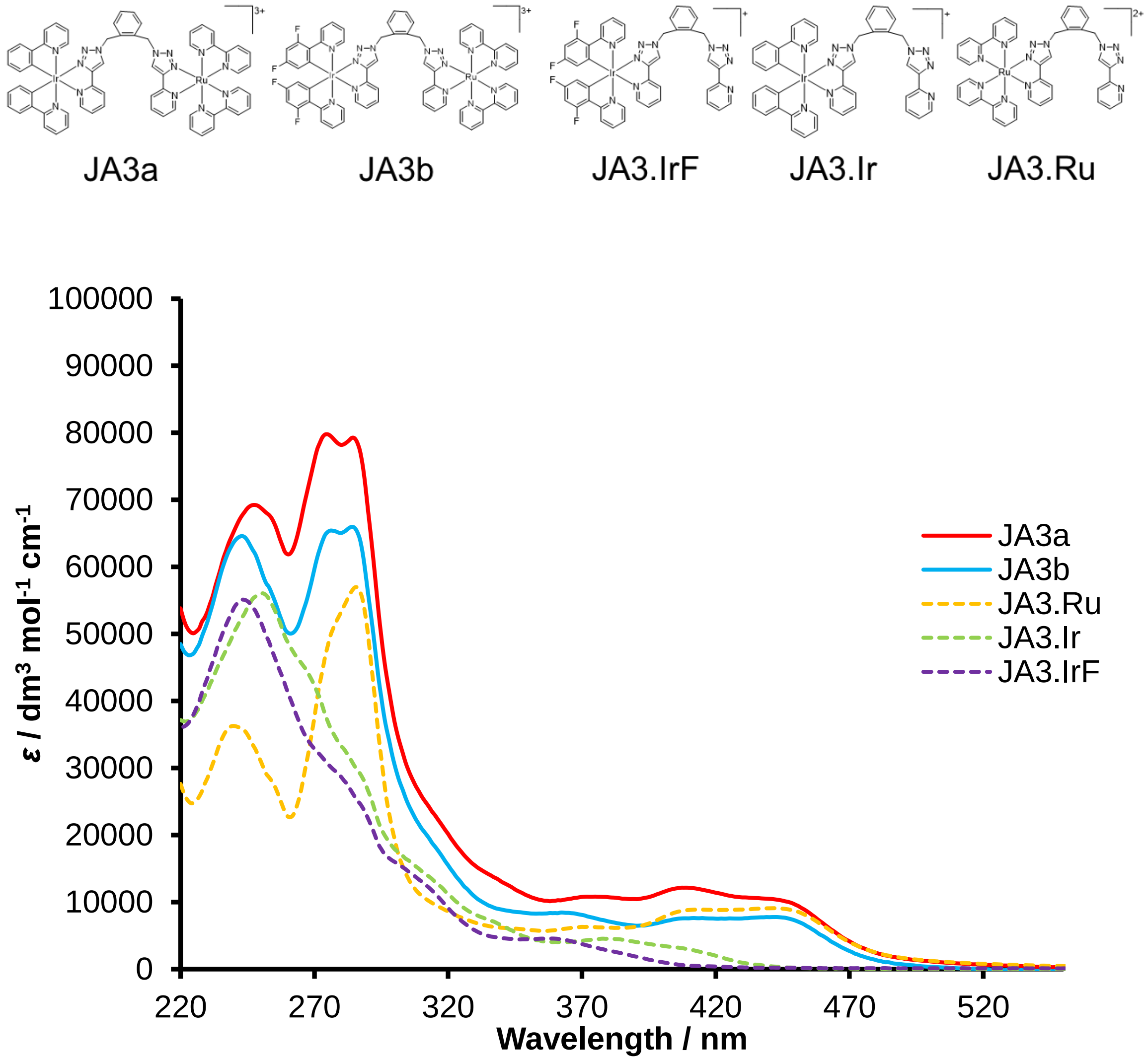

Figure 2. 11 UV-visible electronic absorption spectra recorded for ***JA3*** *(ortho) heterodinuclear and mononuclear complexes. Recorded in MeCN at 298K.*

Ru(II) mononuclear complexes (**JA1-3.Ru**) had high energy absorptions at 242 nm and 286 nm, the absorption bands <300 nm are ^{1}LC transitions, and a lower energy absorption in the visible region, 400-470 nm, that corresponds to ^{1}MLCT transitions, agreeing with the reported [Ru(bpy)$_2$(pytz)]$^{2+}$.[159] Complex reported by Schubert and co-workers, [Ru(dmbpy)$_2$(pytz-decyl)]$^{2+}$, observed an absorption of 446 nm, this is comparative to the mononuclear Ru(II) complexes, **JA1-3.Ru**, and the Ru(II) fragment of the heterodinuclear complexes.

The Ir-ppy mononuclear complexes (**JA1-3.Ir**) have a high energy band at 248 nm and one in the UV/Vis region at ~380 nm. Ir-dfppy mononuclear complexes (**JA1-3.IrF**) also have a high energy band at 243nm and an energy band at ~361 nm. For both ppy and dfppy Ir(III) complexes the high energy absorption bands <300 nm are ^{1}LC transitions, whereas the lower absorption bands between 300-400 nm are ^{1}MLCT transitions. Both Ir(III) mononuclear complexes correspond to the ^{1}MLCT character as reported for the analogue complexes reported.[163] The absorption spectra for the heterodinucelar complexes **JA1-3** were essentially the addition of the Ir(III) and Ru(II) mononuclear complexes. There was no significant difference in the absorption spectra between the *ortho*-, *meta*- and *para*- isomers of the complexes in terms of features. However, **JA2b** had a lower molar absorptivity than **JA1b** and **JA3b**. It is unclear why this is the case; it would be expected that any similar effects would be observed in another complex of the series. Complex **JA3b** does also have slight lower molar absorptivity compared to **JA3a** and **JA1b**. Very tentatively there could be a link in the relation to the fluorination on the Ir(III) fragment and potentially in relation to the different stereoisomers. Further investigations could be done by modulating the number of fluorine's and there positions on the cyclometalating ligand, whilst investigating alternative bridging ligands that control the distance between the Ir(III) and Ru(II) metal centres.

As expected from the electrochemistry, the fluorinated complexes are higher in energy due their electron withdrawing effect stabilising the HOMO, localised over the Ir(III) metal centre and cyclometalated phenyl rings, increasing the HOMO-LUMO energy gap. De Cola and co-workers reported the $[Ir(ppy)_2(pytz)]^+$ and $[Ir(dfppy)_2(pytz)]^+$ analogous complexes to have absorption at ~380 nm and 363 nm respectively,[85, 86] these correspond to the absorptions seen for the Ir(III) mononuclear complexes and therefore for the Ir(III) fragment of the heterodinuclear complexes.

Table 2.2 Summarised Photophysical Data for MeCN Solutions of JA1-3 and Mononuclear Counterparts Measured at r.t.

Complex	λ^{abs}/nm^a	λ^{em}/nm^a	ϕ/%^{b,c}	τ/ns^b		10^5 kr/s$^{-1\ b}$	10^6 k_{nr}/s$^{-1\ b}$
				Ir^d	Ru^e		
JA1a	249, 275sh, 285, 377, 407, 449	476, 505, 607	0.30	895	856	0.0335	1.11
JA1b	243, 276sh, 285, 362, 407, 450	452, 479	0.13	1628	1701	0.0145	1.12
JA1.Ru	241, 285, 408, 450	613	0.10	-	-	-	-
JA1.Ir	250, 268sh, 289sh, 315sh, 340sh, 380	475, 506, 538sh	24.2	813	-	2.97	0.932
JA1.IrF	243, 279sh, 315sh, 361	451, 480, 509sh	17.8	973	-	1.83	0.845
JA2a	248, 275sh, 285, 378, 408, 450	477, 506, 610	0.23	1996	1858	0.0257	1.11
JA2b	243, 276sh, 285, 361, 408, 450	453, 480, 607	0.12	1693	1392	0.0134	1.12
JA2.Ru	242, 285, 408, 450	609	<0.1	-	-	-	-
JA2.Ir	250, 268sh, 289sh, 315sh, 339sh, 381	475, 505, 539sh	23.7	716	-	3.31	1.07
JA2.IrF	244, 280sh, 314sh, 362	451, 480, 510sh	16.7	873	-	1.91	0.954
JA3a	248, 275, 284, 375, 409, 451	475, 505, 608	0.27	1895	1837	0.0302	1.11
JA3b	243, 276, 284, 361, 409, 449	452, 481, 607	0.18	1726	2096	0.0201	1.12
JA3.Ru	240, 286, 408, 450	608	<0.1	-	-	-	-
JA3.Ir	250, 269sh, 289sh, 314sh, 339sh, 380	476, 505, 538sh	35.0	1247	-	2.81	0.521
JA3.IrF	243, 280sh, 314sh, 360	451, 480, 509sh	15.8	1087	-	1.45	0.775

a) MeCN, aerated at 298 K *b*) MeCN deaerated at 298 K *c*) PLQY, $[Ru(bpy)_3](PF_6)_2$ in MeCN was used as relative standard. *d)* Filter applied to beam before detector for TCSPC between 450-500 nm. *e)* Filter applied to beam before detector for TCSPC between 600-650 nm.

2. 4. 2. Emission Spectroscopy

The room temperature emission spectra were recorded in the same solvent as the absorption, MeCN. The emission spectra for the heterodinuclear and mononuclear complexes for each isomer were compared against each other (Figures 2.12-2.14 and Table 2.2). The photoluminescent quantum yields and lifetimes were recorded in a deaerated solution of MeCN, as this represents the conditions of the light-emitting devices.[164] The photoluminescent quantum yields were calculated from the relative standard (ϕ_{rel}), [Ru(bpy)$_3$][PF$_6$]$_2$ which has an absolute quantum yield of 1.8%. The calculations used the emission spectra that were excited at the following wavelengths of excitation; λ_{ex} = 380 nm for **JA1-3** and **JA1-3.Ir/F** , and λ_{ex} = 445 nm for **JA1-3.Ru**.

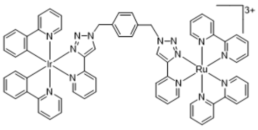
JA1a

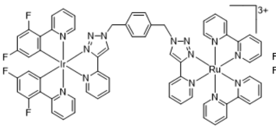
JA1b

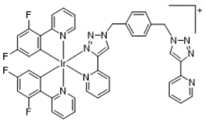
JA1.IrF

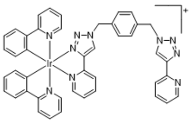
JA1.Ir

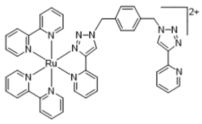
JA1.Ru

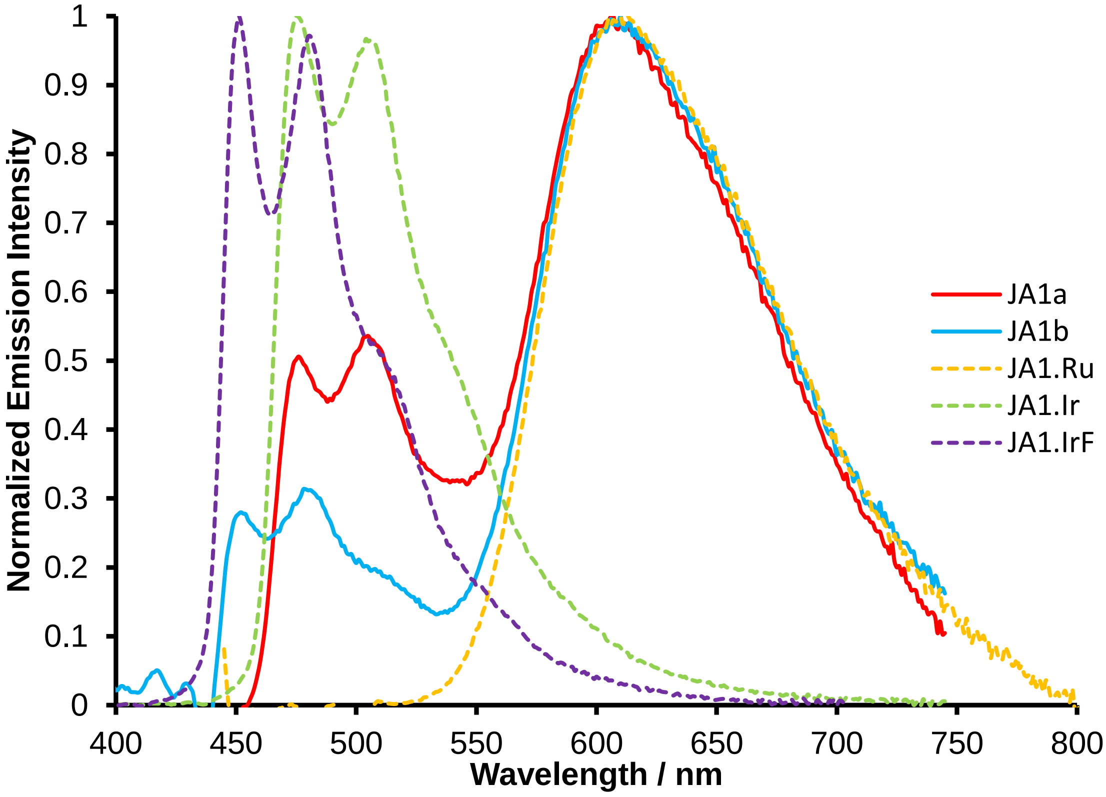

*Figure 2. 12 Emission spectra of **JA1** (para) heterodinuclear and mononuclear complexes. Recorded in MeCN aerated solution at 298K.Excitation wavelength for emission spectroscopy was 380 nm for JA1a+b, JA1.Ir and JA1.IrF. The excitation wavelength for JA1.Ru was 445 nm.*

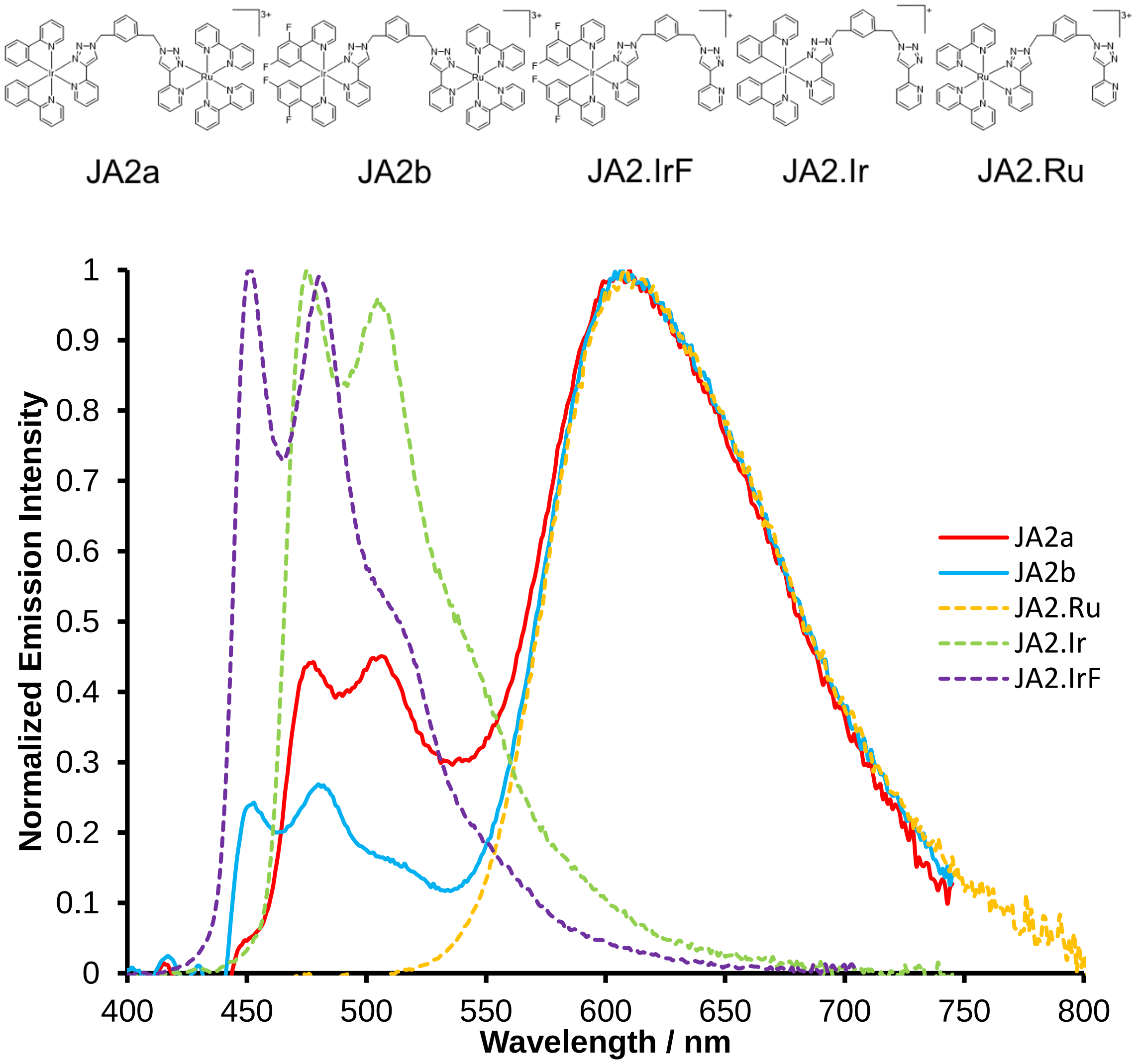

*Figure 2. 13 Emission spectra of **JA2** (meta) heterodinuclear and mononuclear complexes. Recorded in MeCN aerated solution at 298K. Excitation wavelength for emission spectroscopy was 380 nm for JA2a+b, JA2.Ir and JA2.IrF. The excitation wavelength for JA2.Ru was 445 nm.*

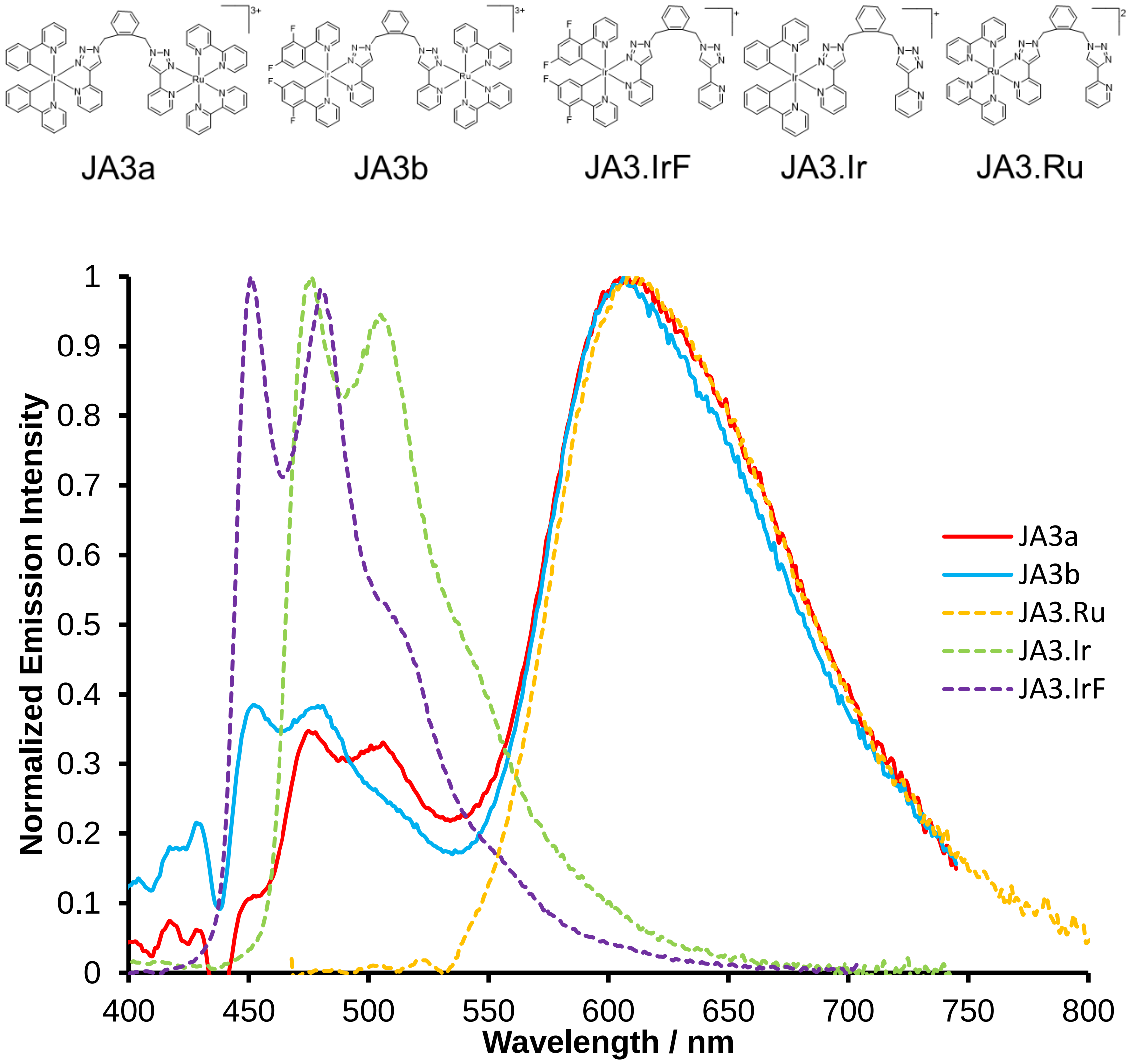

Figure 2. 14 Emission spectra of ***JA3*** *(ortho) heterodinuclear and mononuclear complexes. Recorded in MeCN aerated solution at 298K. Excitation wavelength for emission spectroscopy was 380 nm for JA3a+b, JA3.Ir and JA3.IrF. The excitation wavelength for JA3.Ru was 445 nm.*

The broad emission band λ_{max} = ~610 nm corresponds to a weak red emission of the Ru(II) mononuclear complex and the Ru(II) fragment of the heterodinculear complexes, corroborating with reported similar Ru(II) bipyridine based complexes.[62, 159] The broad featureless band is likely to be ^{3}LLCT/^{3}MLCT in character. Complexes **JA1-3.Ru** observed low quantum efficiency in deaerated solutions, ϕ_{rel} = ~0.1%, which was anticipated as the non-radiative ^{3}MC states are thermally accessible. This was similarly seen in the Ru(II) fragment of the heterodinuclear complexes, even though the complexes showed respectable efficiencies (ϕ_{rel} = 0.12-0.30%), the Ru(II) fragment was accountable for <0.1% of the quantum yields. The excited state lifetimes were not able to be recorded through TCSPC.

The Ir(III) mononuclear complexes (**JA1-3.Ir** and **JA1-3.IrF**) have structured emission bands at λ_{max} = 475 and 505 nm for the **JA1-3.Ir** complexes and at λ_{max} = 451 and 480 nm for the **JA1-3.IrF** complexes, emitting in the green/blue visible region. The structure emission bands displayed inform us of ^{3}ILCT/^{3}MLCT character. The moderate quantum efficiencies of the mononuclear complexes **JA1-**

3.Ir and **JA1-3.IrF**, in deaerated solutions, were ϕ_{rel} = 23.7-35.0 % and 15.8-17.8 % respectively. The mononuclear Ir(III) complexes all had respectable lifetimes in deaerated solutions, τ = 0.7-1.2 μs. The emission profiles match the reported analogues of these complexes $[Ir(ppy)_2(pytz)]^+$ = 477 and 507 nm, $[Ir(dfppy)_2(pytz)]^+$ = 452 and 483 nm and also reported comparative quantum yields, 21 % and 22 %.[85, 86]

For the heterodinuclear complexes, **JA1-3**, the emission profiles are the addition of the mononuclear complexes. Complexes were excited at 380nm and had respectable relative quantum yields (ϕ_{rel} = 0.12-0.30 %). The quantum efficiency was mainly made up of the more intense Ir(III) emission, compared to the Ru(II) emission. **JA1a-3a**, had higher quantum yields than their fluorinated counterparts, **JA1b-3b**. All complexes had respectable lifetimes in the low microsecond region, 0.7-2 μs.

The Ir(III) emission in the heterodinuclear complexes has matching emission profiles compared to the mononuclear complexes and have corresponding emission bands for the fluorinated and non-fluorinated complexes (Table 2.2). The fluorinated complexes (λ_{em} = 451-453, 479-481 nm) show a significant blue shift compared to the non-fluorinated (λ_{em} = 475-477, 505-506 nm). This is due to the electron withdrawing effects of the fluorine, stabilising the HOMO and increasing the HOMO-LUMO energy gap. The blue shifted emission further confirms the larger HOMO-LUMO energy gap as was hypothesised from the electrochemistry and absorption data. Similar shifts have been reported in many other Ir complexes.[26, 85, 86, 139] The non-fluorinated complexes and fragments have higher quantum efficiencies than their fluorinated counterparts, this could be due to the bridging ligand on the pytz moiety, similar effects were recorded when the adamantly moiety was substituted on the pytz ligand by De Cola and co-workers,[90] $[Ir(ppy)_2(pytz\text{-}ada)]^+$ ϕ_{rel} = 35 % and $[Ir(dfppy)_2(pytz\text{-}ada)]^+$ ϕ_{rel} = 16 %. Even though the emission maxima remain the same, suggesting the involvement of the ancillary ligand has not changed between complexes, the quantum efficiencies vary. From these two examples it could be speculated that the Ir(III) centre is being protected from deactivating solvent interactions. However, this is just speculation and further investigations would need to take place by designing ligand architecture to probe this area of chemical space and compare photophysical properties.

The heterodinucelear complexes **JA1-3** have a considerably lower quantum efficiency (ϕ_{rel} = 0.12-0.30 %) than the mononuclear Ir(III) complexes, **JA1-3.Ir** and **JA1-3.IrF**, (ϕ_{rel} = 23.7-35.0 % and 15.8-17.8 %). They have similar quantum yields to the mononuclear Ru(II) complexes **JA1-3.Ru** (ϕ_{rel} = ~0.1 %). Due to the Ir(III) emission being significantly less efficient it is reasonable to presume there is an alternate deactivation pathway from the Ir(III) triplet excited states, this strongly suggested that partial energy transfer had occurred from Ir(III) to the Ru(II). The lifetimes recorded for the Ir(III) and Ru(II) metal centres on **JA1-3** further support the partial energy transfer as the lifetimes are similar for both metal centres. Where the ^{3}MC states are readily populated from the ^{3}MLCT, resulting in non-radiative relaxation to the ground state.[62] A wide range of Ru(II) triazole complexes have been reported to undergo thermal population of the ^{3}MC states resulting in them being weakly/non-emissive.[61, 62, 78]

When the different structural isomers, based around the phenyl ring on the bridging ligand (*para*-, *meta* - and *ortho*-), of the heterodinuclear complexes emission profiles were compared, the intensity of the Ir(III) emission varied. The intensity of the *para*-bridging ligand complexes was greater than the intensity for *meta*- and *ortho*-bridging ligand complexes. The lower emission intensities indicated there was more energy transfer. The *meta*- and *ortho*- complexes metal centres are likely closer together than the *para*- complexes, meaning that Förster energy transfer had occurred in complexes **JA2-3** but to a lesser extent in complexes **JA1**.

Low temperature (77K) solid state emission, in glass matrix, recorded for all heterodinuclear and mononuclear complexes as seen in Figure 2.15-2.17 and summarised in Table 2.3. The mononuclear Ru(II) complexes (**JA1-3.Ru**) blue shift relative to when in solution, this is a phenomena called rigidochromism and is typical for Ru(II) diimine complexes.[62] Luminescent rigidochromism affects the longer lived ^{3}MLCT states when the complex is "rigid", where solvent molecules are hindered to rearrange the dipole-dipole interactions. As the solvent molecules are frozen in a glass matrix, the solvent molecules are considered to be closer to the excited-state complex increasing the dipole interactions.[165] As there are no available solvent molecules to facilitate vibrational induced relaxations, the vibronic structure appears. The mononuclear Ir(III) complexes (**JA1-3.Ir** and **JA1-3.IrF**) exhibit highly structure and vibronic emission bands which display the ^{3}ILCT/^{3}MLCT character commonly seen in analogous complexes.[85, 86, 90, 163] These complexes do not significantly blue shift relative to when in solution unlike the mononuclear Ru(II) complexes.

The heterodinuclear complexes **JA1-3** display a significantly different emission profile than at room temperature. Similar to the mononuclear complexes the Ru(II) emission blue shifts whilst the Ir(III) emission does not significantly shift. The emission profile is dominated by the Ru(II) emission, which intensifies considerably compared to the much weaker Ir(III) emission. The Ru(II) dominated emission indicates that the partial energy transfer is far more efficient at low temperatures in a glass matrix than at room temperature. When comparing between the isomers of **JA1-3** at low temperature there is further evidence that there is distance dependent Förster energy transfer as the *para*- complexes show more Ir(III) emission intensity than the *meta*- and *ortho*- complexes.

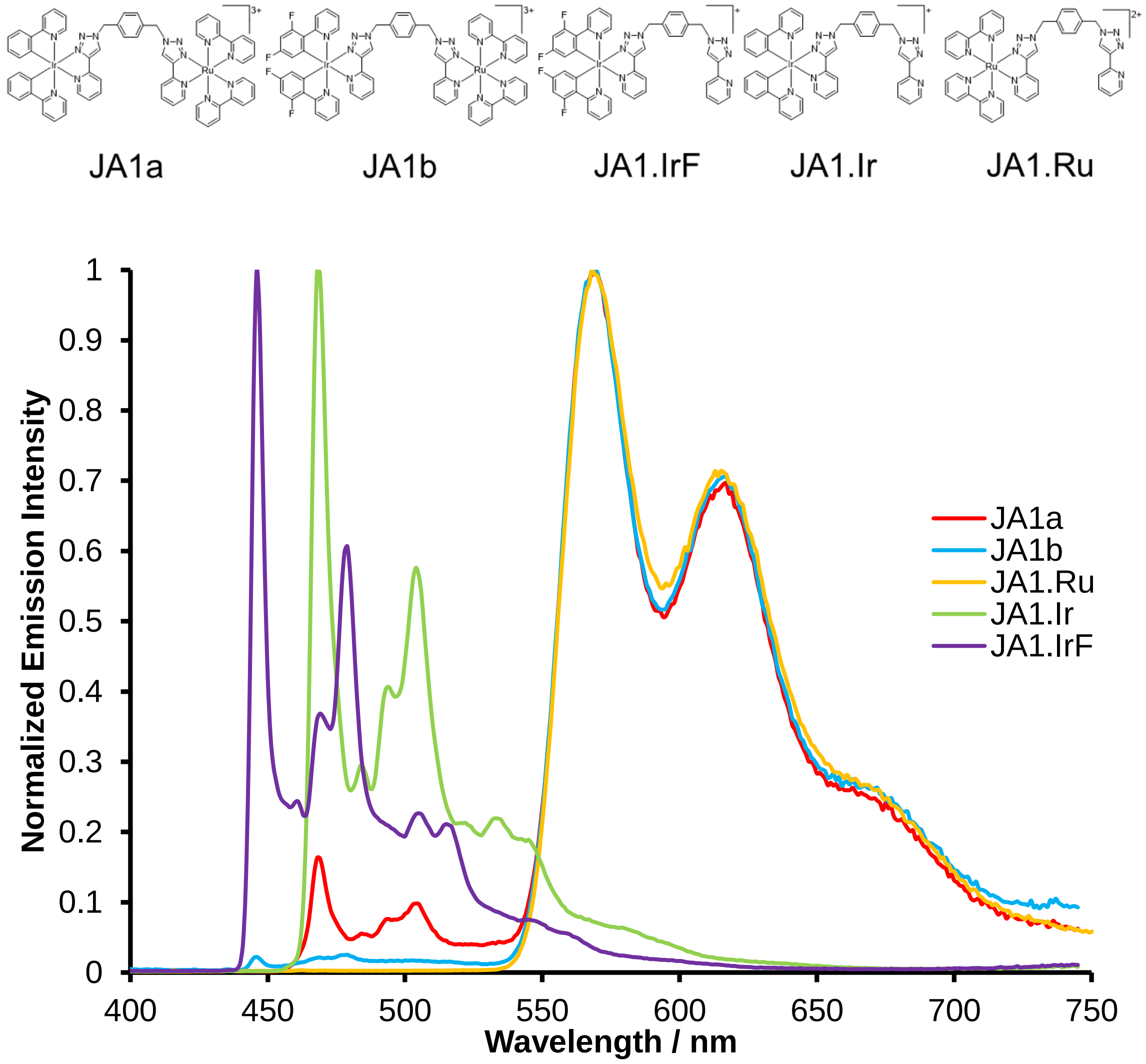

*Figure 2. 15 Low temperature emission spectra of **JA1** (para) heterodinuclear and mononuclear complexes. Recorded in EtOH:MeOH (4:1) glass at 77K. Excitation wavelength for emission spectroscopy was 380 nm for JA1a+b, JA1.Ir and JA1.IrF. The excitation wavelength for JA1.Ru was 445 nm.*

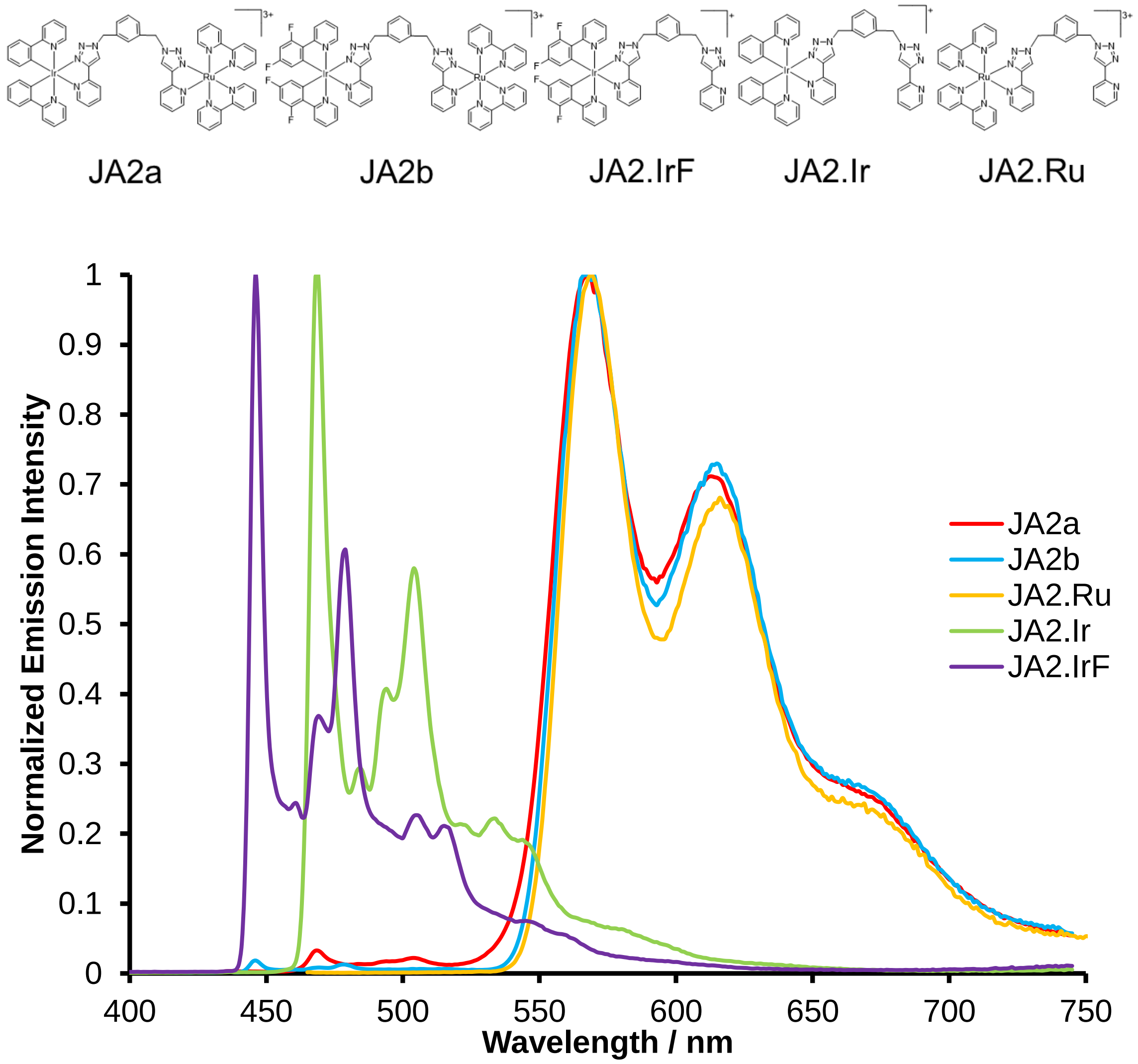

Figure 2. 16 Low temperature emission spectra of ***JA2*** *(meta) heterodinuclear and mononuclear complexes. Recorded in EtOH:MeOH (4:1) glass at 77K. Excitation wavelength for emission spectroscopy was 380 nm for JA2a+b, JA2.Ir and JA2.IrF. The excitation wavelength for JA2.Ru was 445 nm.*

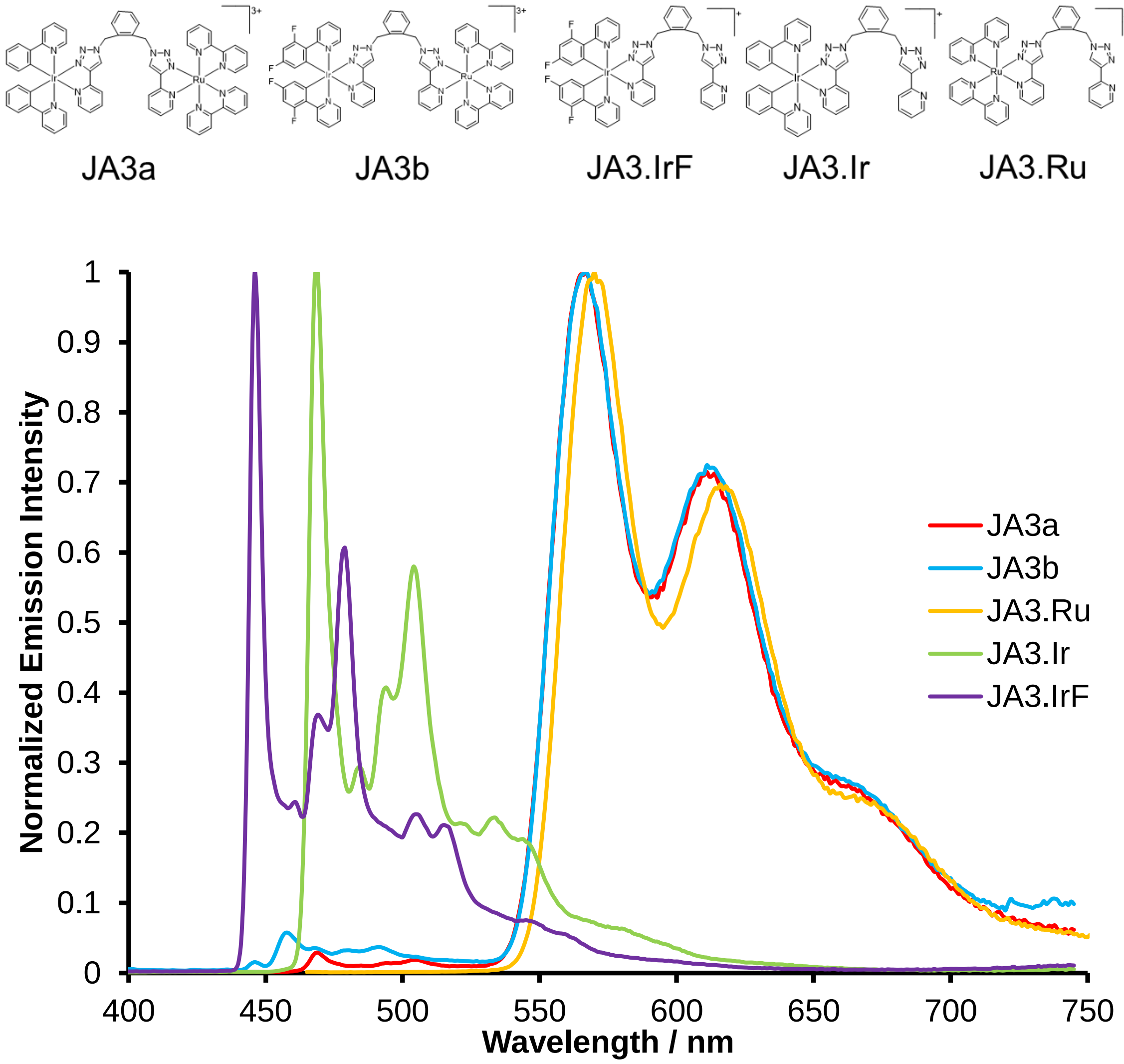

*Figure 2. 17 Low temperature emission spectra of **JA3** (ortho) heterodinuclear and mononuclear complexes. Recorded in EtOH:MeOH (4:1) glass at 77K. Excitation wavelength for emission spectroscopy was 380 nm for JA3a+b, JA3.Ir and JA3.IrF. The excitation wavelength for JA3.Ru was 445 nm.*

2. 4. 2. 1. Excitation Dependent Emission

Emission spectra, in MeCN at 298 K, were taken for complexes **JA1-3** whilst varying the wavelength of excitation to explore the effects on the emission profile (Figure 2.18.). As the excitation wavelength was increased the Ir(III) centre's emission decreases for all complexes until 450nm where no Ir(III) based emission is observed and Ru(II) centre was being excited into exclusively. This is in line with absorption spectra for the mononuclear reference complexes where the Ir(III) complexes absorption spectra tail off by 430 nm.[85, 86, 163] Therefore, beyond this point excitation is exclusively Ru(II) ^{1}MLCT based and no Ir(III) based emission is expected.

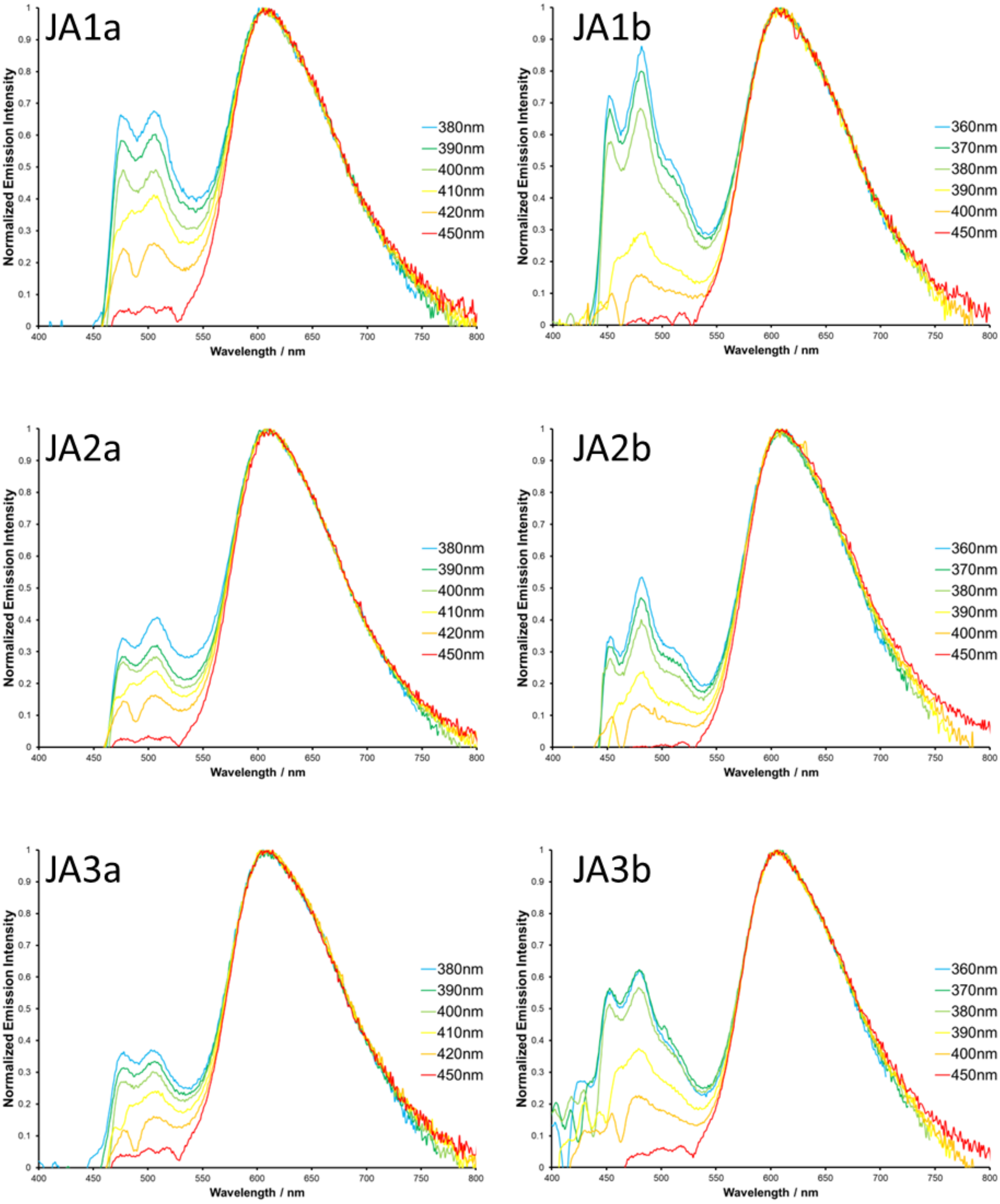

*Figure 2. 18 Emission spectra of complexes **JA1-3** whilst being excited at different wavelengths between the Ir absorption band. Recorded in aerated MeCN at room temperature.*

2. 4. 2. 2. Oxygen Dependant Emission

The triplet-based emission of these complexes leads to the excited state being sensitive to $^3O_2$ as it may quench the luminescent excited state by triplet-triplet annihilation. In certain biological circumstances this phenomenon can utilised to produce $^1O_2$ that can be used in a variety of biological applications such as the induction of apoptosis or necrosis,[30, 116] photoactive antiviral drugs and photodynamic tumour ablation.[117-119] For potential use in light emitting devices the photophysical properties of target complexes **JA1-3** and the mononuclear analogues were investigated in an aerated solution, oxygen saturated, and deaerated solution. (Figure 2.19 and Table 2.3).

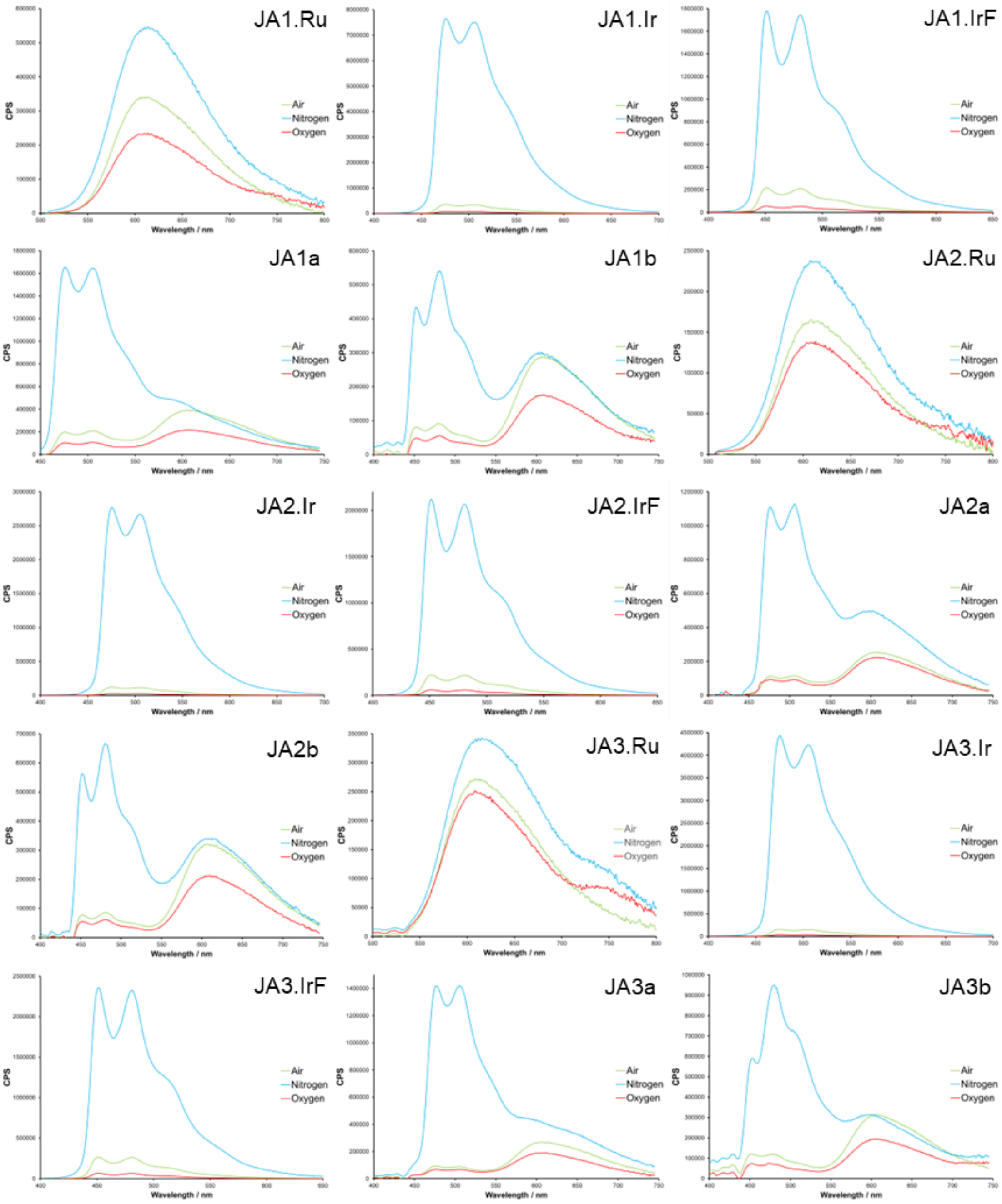

Figure 2. 19 Emission spectra of heteronuclear and mononuclear complexes ***JA1-3*** *in MeCN solutions with varying levels of oxygen presence. Excitation wavelength for emission spectroscopy was 380 nm for JA1-3a, JA1-3b, JA1-3.Ir and JA1-3.IrF. The excitation wavelength for JA1-3.Ru was 445 nm. Air is for aerated solution, Nitrogen is a deaerated solution that has been freeze pump thawed and filled with nitrogen, Oxygen is for an 100% oxygen saturated solution. Recorded at room temperature.*

The **JA1-3.Ru** complexes showed some sensitivity to the presence of O_2, this can be seen by the variation in emission intensities from very low in the air and oxygen atmosphere, <0.1 %, to about ~0.10 %, however as the complex is only weakly emissive the effect is less pronounced. The mononuclear Ir(III) complexes, **JA1-3.Ir** and **JA1-3.IrF**, showed more extreme O_2 sensitivity through their quantum efficiency. For the non-fluorinated complexes, **JA1-3.Ir**, the relative quantum yields dramatically increased from 0.24-0.30 %, in oxygen saturated solution, to 23.7-35.0 % when de-aerated. The fluorinated complexes, **JA1-3.IrF**, quantum yield increased from 0.44-0.57 % (O_2) to 15.8-17.8 % deaerated. The Ir(III) complexes are highly sensitive to the presence of oxygen, having an extreme effect on the luminescent quantum efficiency of the complexes. The mononuclear Ir(III) complexes are quenched significantly more than the Ru(II) mononuclear complexes, this is consistent with the longer lifetimes of the Ir(III) complexes and thus far greater chance for of an encounter with $^3O_2$ in solution during the excited state lifetime.

Similar oxygen dependant phosphorescence has been reported in the literature. For complexes $[Ir(R\text{-}ppy)_2(pytz\text{-}ada)]^+$, reported by De Cola and co-workers,[90] observed similar effects in the presence of O_2. $[Ir(ppy)_2(pytz\text{-}ada)]PF_6$ had an increase from 1.3 % to 35 % in quantum efficiency. Similar properties were observed for $[Ir(dfppy)_2(pytz\text{-}ada)]Cl$, where the quantum yield dramatically increased when the aerated solution was deaerated, from 7.1 % to 16 %.

Heterodinuclear complexes **JA1-3** show sensitivity to O_2 like their mononuclear counterparts, as they effectively work as a combination of the mononuclear counterparts this is to be expected. The Ir(III) emission is more sensitive than Ru(II) therefore is quenched more, as seen in the mononuclear complexes, leading to more intense Ru(II) emission than Ir(III) emission. Complexes **JA1a-3a** quantum efficiency increases from <0.1% (O_2 atmosphere) to 0.23-0.30 % when in an absence of O_2. The fluorinated complexes, **JA1b-3b**, similarly noticed an increase in quantum efficiency from <0.1 % to 0.12-0.18 %.

Table 2.3 Summarised Photophysical Data of JA1-3 at Low Temperature (77K) in EtOH:MeOH glass and in Aerated, Deaerated and Oxygenated MeCN Solutions Measured at r.t.

Complex	λ^{em}/nm^{a}	ϕ/%^{b,e}	ϕ/%^{c,e}	ϕ/%^{d,e}	τ/ns^{b}		τ/ns^{c}		τ/ns^{d}	
					Ir^{f}	Ru^{g}	Ir^{f}	Ru^{g}	Ir^{f}	Ru^{g}
JA1a	468, 504, 569, 617, 671	0.10	0.30	<0.1	55	247	895	856	13	6.4
JA1b	446, 479, 569, 616, 672	<0.1	0.13	<0.1	137	274	1628	1701	46	143
JA1.Ru	568, 615, 672	<0.1	0.10	<0.1	-	20	-	1545	-	32
JA1.Ir	468, 504, 533	1.06	24.2	0.24	59	-	813	-	13	-
JA1.IrF	446, 478, 507	2.12	17.8	0.57	145	-	973	-	35	-
JA2a	470, 505, 568, 617, 672	<0.1	0.23	<0.1	53	40	1996	1858	46	53
JA2b	447, 479, 568, 616, 671	<0.1	0.12	<0.1	142	42	1693	1392	79	56
JA2.Ru	569, 616, 671	<0.1	<0.1	<0.1	-	48	-	729	-	20
JA2.Ir	469, 504, 535	1.02	23.7	0.26	57	-	716	-	13	-
JA2.IrF	446, 478, 508	1.76	16.7	0.48	147	-	873	-	35	-
JA3a	471, 506, 568, 615, 668	<0.1	0.27	<0.1	50	28.4	1895	1837	15	16
JA3b	460, 568, 616, 668	<0.1	0.18	<0.1	109	163	1726	2096	88	68
JA3.Ru	571, 619, 672	<0.1	<0.1	<0.1	-	15	-	1382	-	12
JA3.Ir	469, 505, 535	1.20	35.0	0.30	58	-	1247	-	13	-
JA3.IrF	446, 479, 506	1.74	15.8	0.44	149	-	1087	-	34	-

a) EtOH:MeOH (4:1) glass, aerated at 77K b) MeCN, aerated at 298K c) MeCN deaerated at 298K d) MeCN, oxygenated at 298K e) PLQY, $[Ru(bpy)_3](PF_6)$ in MeCN was used as relative standard. f) Band pass filter applied to beam before detector for TCSPC between 450-500 nm. g) Bandpass filter between 600-650 nm applied to beam before detector for TCSPC.

2. 4. 2. 3. CIE Coordinate Plot

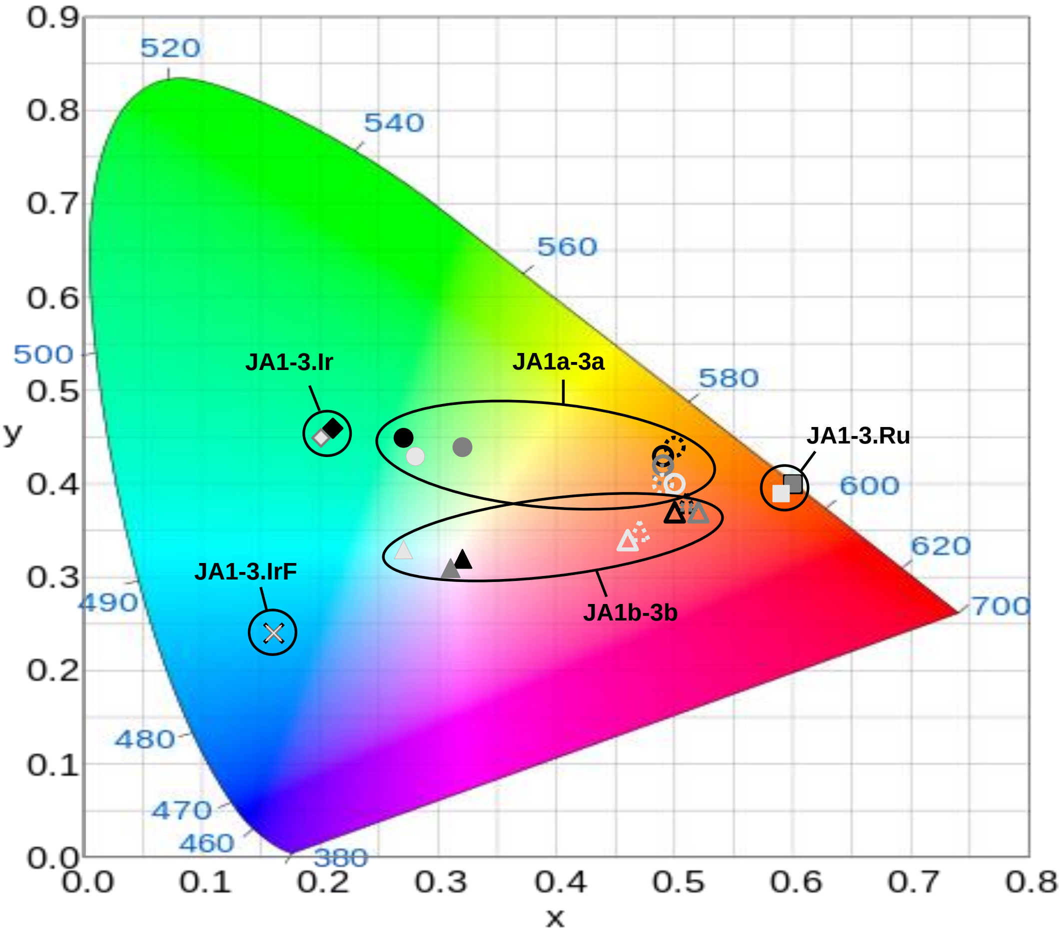

Figure 2. 20 CIE coordinate plot for heterodinuclear and mononuclear complexes JA1-3. Deaearted complexes are filled icons, aerated complexes are just the border, and oxygen saturated complexes are dashed border. JA1 (para) complexes are black, JA2 (meta) icons are grey and JA3 (ortho) icons are white. JA1-3.Ru = squares, JA1-3.Ir = diamonds, JA1-3.IrF = crosses, JA1a-3a = circles, and JA1b-3b = triangles.

Table 2.4 CIE Coordinates for MeCN Solutions of JA1-3 and their Mononuclear Counterparts Measured at r.t.

Complex	CIE Coordinates (x, y)		
	Aerated[a]	Deaerated[b]	Pure O_2[c]
JA1a	0.49, 0.43	0.27, 0.45	0.50, 0.44
JA1b	0.50, 0.37	0.32, 0.32	0.51, 0.38
JA1.Ru	0.61, 0.39	0.60, 0.40	0.61, 0.40
JA1.Ir	0.20, 0.45	0.21, 0.46	0.21, 0.45
JA1.IrF	0.16, 0.23	0.16, 0.24	0.17, 0.24
JA2a	0.49, 0.42	0.32, 0.44	0.49, 0.41
JA2b	0.52, 0.37	0.31, 0.31	0.51, 0.38
JA2.Ru	0.61, 0.40	0.60, 0.40	0.60, 0.40
JA2.Ir	0.20, 0.45	0.20, 0.45	0.21, 0.42
JA2.IrF	0.16, 0.24	0.16, 0.24	0.17, 0.24
JA3a	0.50, 0.40	0.28, 0.43	0.49, 0.40
JA3b	0.46, 0.34	0.27, 0.33	0.47, 0.35
JA3.Ru	0.60, 0.39	0.59, 0.39	0.59, 0.40
JA3.Ir	0.20, 0.45	0.20, 0.45	0.20, 0.43
JA3.IrF	0.16, 0.24	0.16, 0.24	0.17, 0.24

a) Deaerated MeCN solution at 298K *b*) Aerated MeCN solution at 298K *c*) 100% oxygen saturated MeCN solution at 298K

The emission spectra of complexes **JA1-3** and their mononuclear analogues were converted to CIE chromaticity coordinates to determine their emission colour (Figure 2.20). Mononuclear Ru complexes, **JA1-3.Ru**, emitted in the orange/red region of the spectrum. Ir mononuclear complexes **JA1-3.Ir** emit in the cyan/green colour whereas complexes JA1-3.IrF are significantly blue shifted to the sky blue colour. There was little to no difference between the isomers of the mononuclear complexes, there was also no difference in the emission colour in the presence of oxygen.

Heterodinuclear complexes, **JA1-3**, are highly oxygen dependent where the Ir(III) emission intensity is more greatly reduced than the Ru(II) emission intensity, this resulted in a change in emission colour dependent on the presence of oxygen. Complexes in aerated and oxygenated solutions emit in the orange/red region, non-fluorinated complexes **JA1a-3a** have more orange coloured emission, whereas the fluorinated complexes, **JA1b-3b**, have more red emission. In deaerated solutions the Ir(III) emission intensity increases dramatically causing a significant change in the colour of emission. For the non-fluorinated complexes, the emission colour shifts into the green/yellow region. Most significantly, the fluorinated complexes, in deaerated solutions, emit in the white light region. Complexes **JA1b** and

JA2b are white light emitters that have near pure white light emission with coordinates x = 0.32, y = 0.32 and x = 0.31, y = 0.31 respectively, which are very close to the target pure white light coordinates x = 0.33, y = 0.33.

2. 5. Photostability of Complexes

For use in white light emitting devices the photostability of the complexes had to be studied for complexes **JA1-3**. Similar Ru(II) triazole complexes have exhibited photolysis as reported by Elliott and co-workers, with tz based complexes.[83] The addition of triazole moieties into Ru(II) complexes has been reported to destabilise the ^{3}MLCT to a closer energetic proximity of ^{3}MC states.[61, 62, 78, 83] The heterodinuclear complexes accessed the ^{3}MC state, through the Ru(II) fragment, which caused a population of the dσ* antibonding orbital resulting in photoejection and photoproducts being produced (Scheme 2.2). It is therefore important to assess the photostability of the phosphorescent dinuclear complexes in this study.

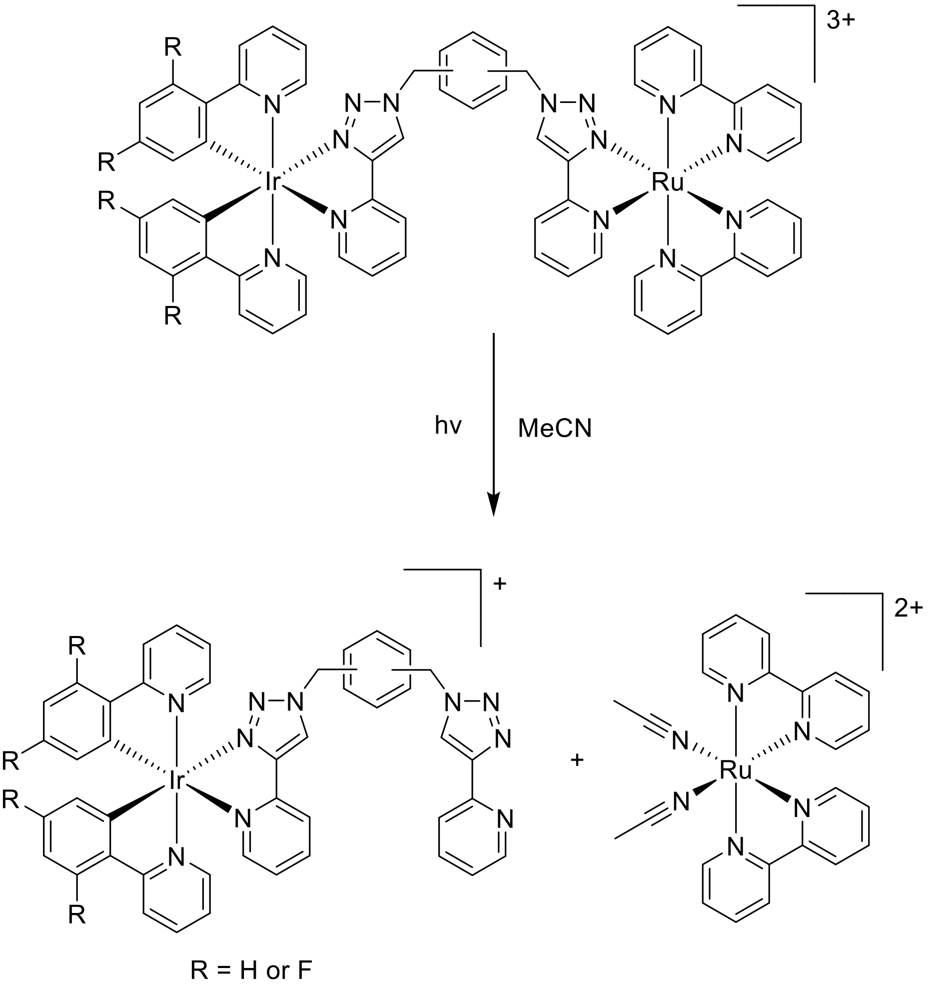

*Scheme 2. 2 Photolysis of heterodinuclear complexes **JA1-3** in a solution of MeCN, resulting in mononuclear Ir complexes (**JA1-3.Ir/F**) and [Ru(bpy)$_2$(NCMe)$_2$]$^{2+}$ as the photoproducts.*

2. 5. 1. ^{1}H NMR Spectroscopic Monitoring of Photolysis

When exposed to light source (mercury emission lines from a 23 W fluorescent light bulb), in MeCN at room temperature, heterodinuclear complexes **JA1-3** underwent photolysis, where the Ru(bpy)$_2$ fragment was photoejected forming [Ru(bpy)$_2$(NCMe)$_2$]$^{2+}$ and [Ir(R-ppy)$_2$(pytz-*o/m/p*-xyl-pytz)]$^+$ (**JA1-3.Ir** and **JA1-3.IrF**). Photolysis process was monitored by ^{1}H NMR spectroscopy (Appendix 8.1), as can be seen for complex **JA1b** in Figure 2.21. As photolysis proceeds resonances for the heterodinuclear complexes are observed to decrease in intensity whilst those for the corresponding mononuclear Ir(III) complex are observed to grow in along with resonances consistent with those for [Ru(bpy)$_2$(NCMe)$_2$]$^{2+}$. The photolysis observed the transition of the chelated CH$_2$ (stars) to the non-chelated CH$_2$ (triangles), in addition the triazole peaks shift (squares) and the formation of the [Ru(bpy)$_2$(NCMe)$_2$]$^{2+}$ can be observed (circles).

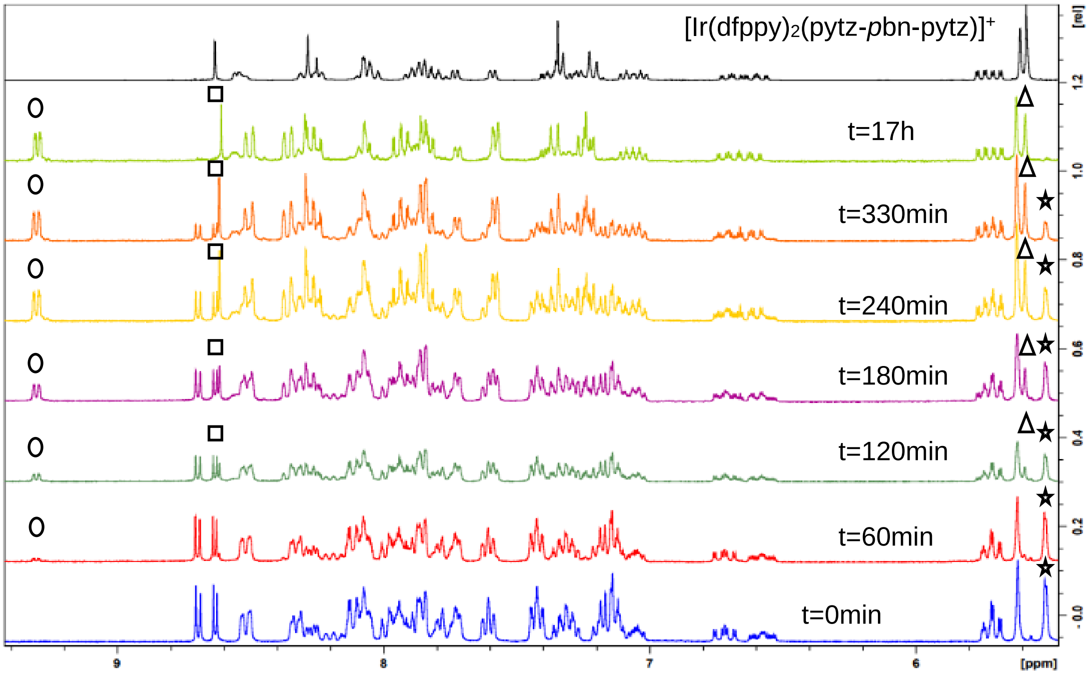

*Figure 2. 21 ^{1}H NMR Spectra taken of the Complex **JA1b** in MeCN at 298K at different times of exposure to white light. Stars = Chelated CH$_2$, Triangle = Non-chelated CH$_2$, Square = Triazole, Circle = [Ru(bpy)$_2$(NCMe)$_2$]$^{2+}$.*

2. 5. 2. UV-Vis Spectroscopic Monitoring of Photolysis

Complexes **JA1-3** were monitored by electronic UV-vis absorption spectroscopy as they underwent the photolysis in MeCN at 298 K, the irradiation source for this was the same as used for the ^{1}H NMR spectroscopic measurements, the mercury emission lines from a 23 W fluorescent light bulb (Figure 2.22). The spectra for each complex appear to be an isobestic point showing a clean conversion in one step to photoproducts. There is also a notable decrease and blue shift in the ^{1}MLCT state absorption for Ru(bpy)$_2$ fragment, at 450 nm, which was observed for all dinuclear complexes as the Ru(II) centre was being ejected. A decrease in absorption intensity is also seen over the ^{1}MLCT absorption of the Ir(III) fragment, as the mononuclear counterparts showed they have lower absorption intensity than the heterodinuclear complexes.

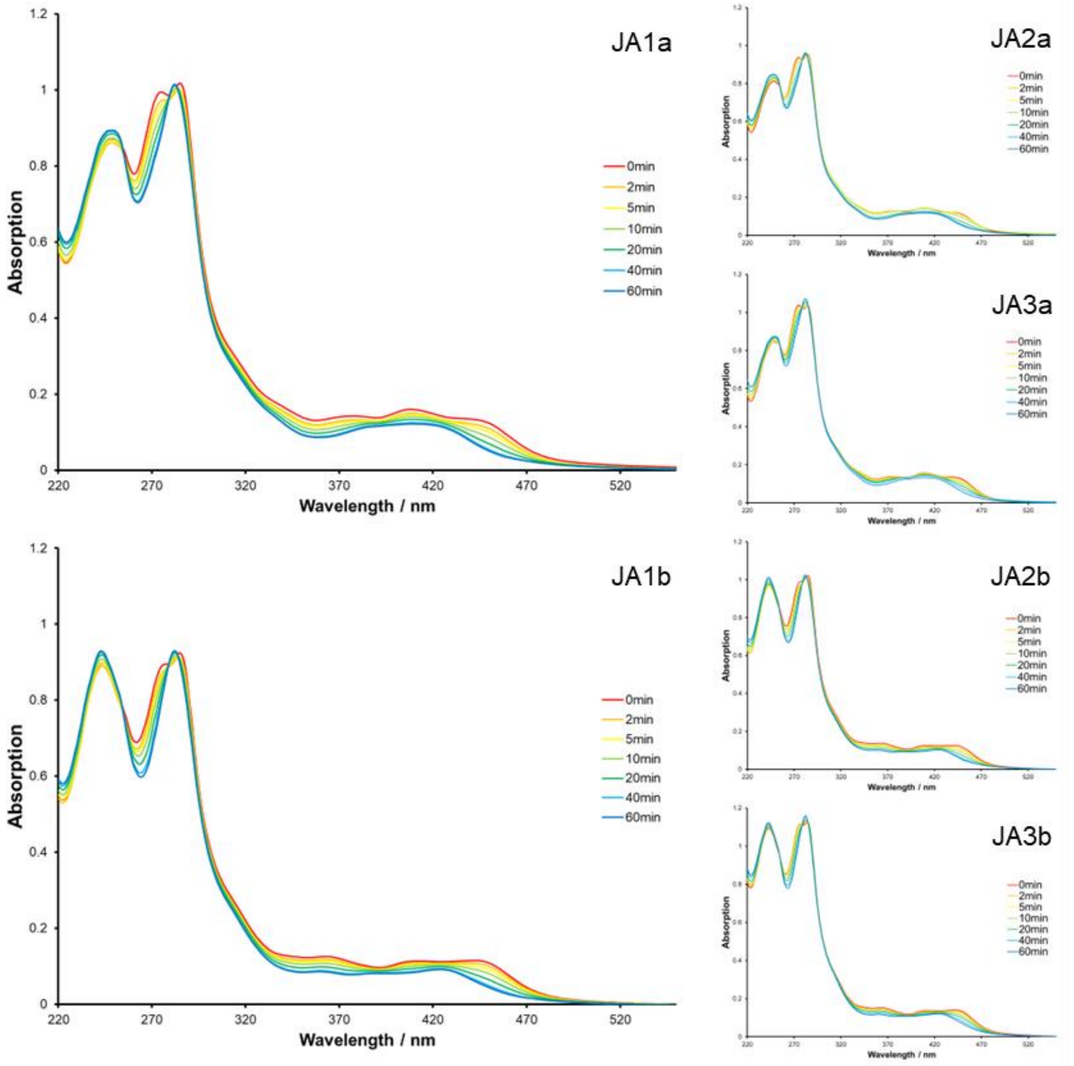

Figure 2. 22 Photolysis process monitored by UV-vis for heterodinuclear complexes ***JA1-3*** *in MeCN. The light source is mercury emission lines from a 23 W fluorescent light bulb.*

Mononuclear Ru(II) complexes, **JA1-3.Ru**, were also recorded to observe their photolysis when exposed to the same light source in a MeCN solution (Figure 2.22). These complexes also showed a blue shift in absorption at 450 nm confirming that the heterodinuclear complexes photoejected the Ru(II) fragment to produce the $[Ru(bpy)_2(NCMe)_2]^{2+}$ complexes.

Table 2.5 Quantum Yields for Photochemical Release of $[Ir(R\text{-}ppy)_2(pytz\text{-}o/m/p\text{-}xyl\text{-}pytz)]^+$ from $[Ir(R\text{-}ppy)_2(pytz\text{-}o/m/p\text{-}xyl\text{-}pytz)Ru(bpy)_2]^{3+}$ in MeCN

Complex	$\phi/\%^{a,b}$
JA1a	0.23
JA1b	0.24
JA2a	0.28
JA2b	0.34
JA3a	0.27
JA3b	0.28

a) Photochemical Quantum Yield *b)* Irradiated by blue-light emitting diode with emission maxima at 446nm.

For the photochemical quantum yields, the photolysis was monitored by UV-visible absorption spectra when the complexes were irradiated by a blue light-emitting diode with an emission maxima at 446nm. Photochemical quantum yields were calculated from the evolution of the UV-visible absorption spectra using the spectrometric approach reported by Slep and co-workers.[166] The blue LED was used at a specific wavelength (446 nm) as the photon flux had been measured, which is necessary to be able to calculate the photochemical quantum yield. Due to the observed isobestic points it was modelled as a single-step photochemical reaction (Table 2.5). Complexes **JA1-3** all had comparable quantum yields between 0.23 % and 0.34 %. For comparison, Elliott and co-workers reported the photochemical quantum yield for release of benzyl-substituted pytz from analogous $[Ru(bpy)_2(pytz)]^+$ as 0.3%.[62] It is possible that excitation at the Ir(III) centre will sensitise photorelease from the Ru(II) metal centre, however for determination of photochemical quantum yields a 446 nm light emitting source is used so only pure Ru(II) ^{1}MLCT excitation for the quantum yield is calculated. To sensitise the Ru(II) photochemistry via the Ir(III) metal centre a shorter wavelength energy light source would be required, unfortunately we did not have access to this so cannot assess the sensitisation by the Ir(III) metal centre. However, the reduced photoluminescent quantum yields for the heterodinuclear complexes suggest that there is a possible sensitisation.

2. 5. 3. Emission Spectroscopic Monitoring of Photolysis

Photoluminescence spectra were recorded throughout the photolysis process and overlaid on plots shown in Figure 2.23 (Appendix 8.2) for complexes **JA1-3**. The spectra were recorded at the same point in the process as was recorded in the monitoring by electronic UV-visible absorption spectra.

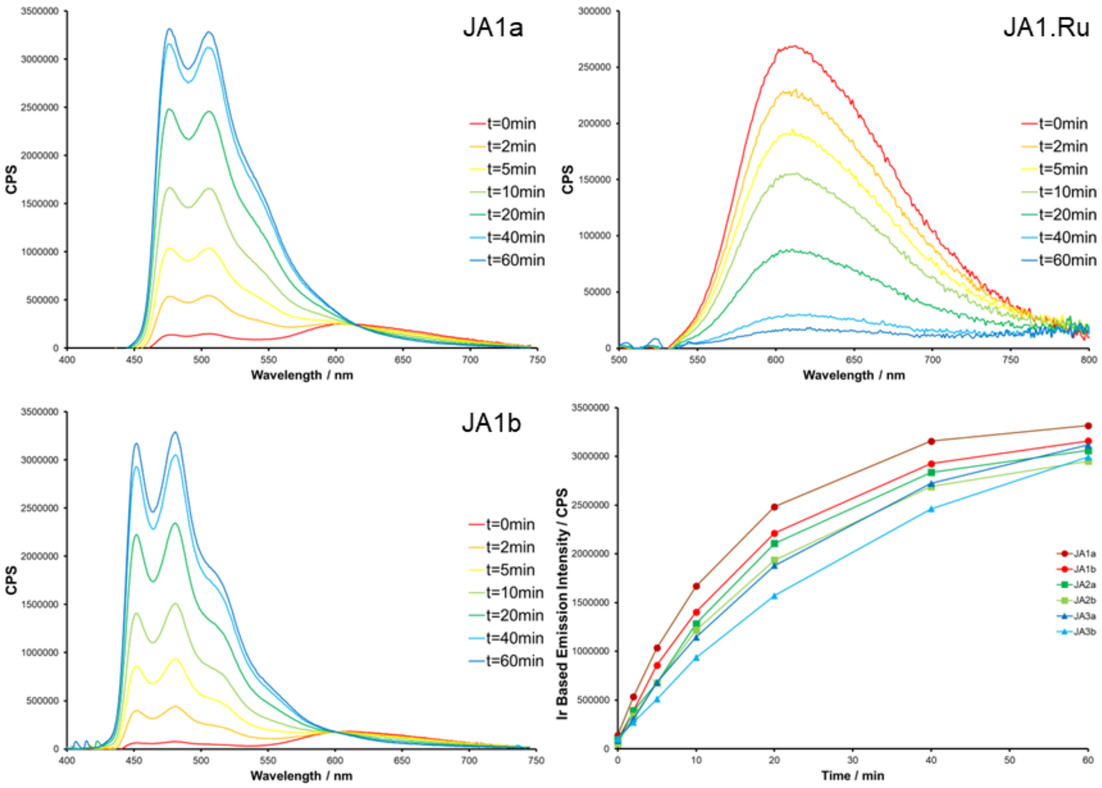

Figure 2. 23 Emission spectra recorded whilst monitoring the photolysis process for heterodinuclear complexes JA1-3. Excitation wavelength for emission spectroscopy was 380 nm for JA1-3a, JA1-3b, JA1-3.Ir and JA1-3.IrF. The excitation wavelength for JA1-3.Ru was 445 nm. Complex JA1a emission profile over 60mins (top left), complex JA1b emission profile over 60 mins (bottom left) and JA1.Ru emission profile recorded undergoing photolysis over 60mins (top right). The Ir(III) emission intensity for each of the complexes was plotted over time to observe it across the series (bottom right).

The Ir(III) fragment ^{3}LC/^{3}MLCT emission intensity increases 30 fold from t = 0 min to t = 60 mins, λ = 430-550 nm, and the Ru(II) based emission decreases, λ = 600-700 nm. The quantum yields increased 10-fold from 0.05 % at t = 0 mins to 0.36-0.53 % and 0.39-0.48 % for **JA1a-3a** and **JA1b-3b** respectively at t = 60 mins (Table 2.6). The photolysis of the Ru(II) mononuclear complexes, **JA1-3.Ru**, were also monitored by emission spectrometry. The decrease in emission intensity matches that of the Ru(II) fragment of the heterodinculear complexes further confirming ejection of the Ru(II) fragments from the complexes. The photoejection of the Ru(bpy)$_2$ fragment meant there was no more energy transfer from the Ir(III) fragment, leading to reduction in non-radiative decay pathways and an increase in PLQY. These dramatic changes in photophysical properties confirmed that the Ru(II) fragment was quenching the Ir(III) emission by partial energy transfer. The PLQY increased as the mononuclear Ir(III) fragment had a higher PLQY compared to the Ru(II) fragment which could be seen when comparing **JA1-3.Ir/F** and **JA1-3.Ru**. The PLQY's for **JA1a-3a** and **JA1b-3b** which were still significantly lower than the emission for **JA1-3.Ir** and **JA1-3.IrF** counterparts, 1.02-1.20 % and 1.74-2.14 %. The complexes do appear less efficient than those in Table 2.2 as the PLQY calculations here do not account for two absorbing species (i.e both **JA1-3.Ir/F** and [Ru(bpy)$_2$(NCMe)$_2$]$^{2+}$).

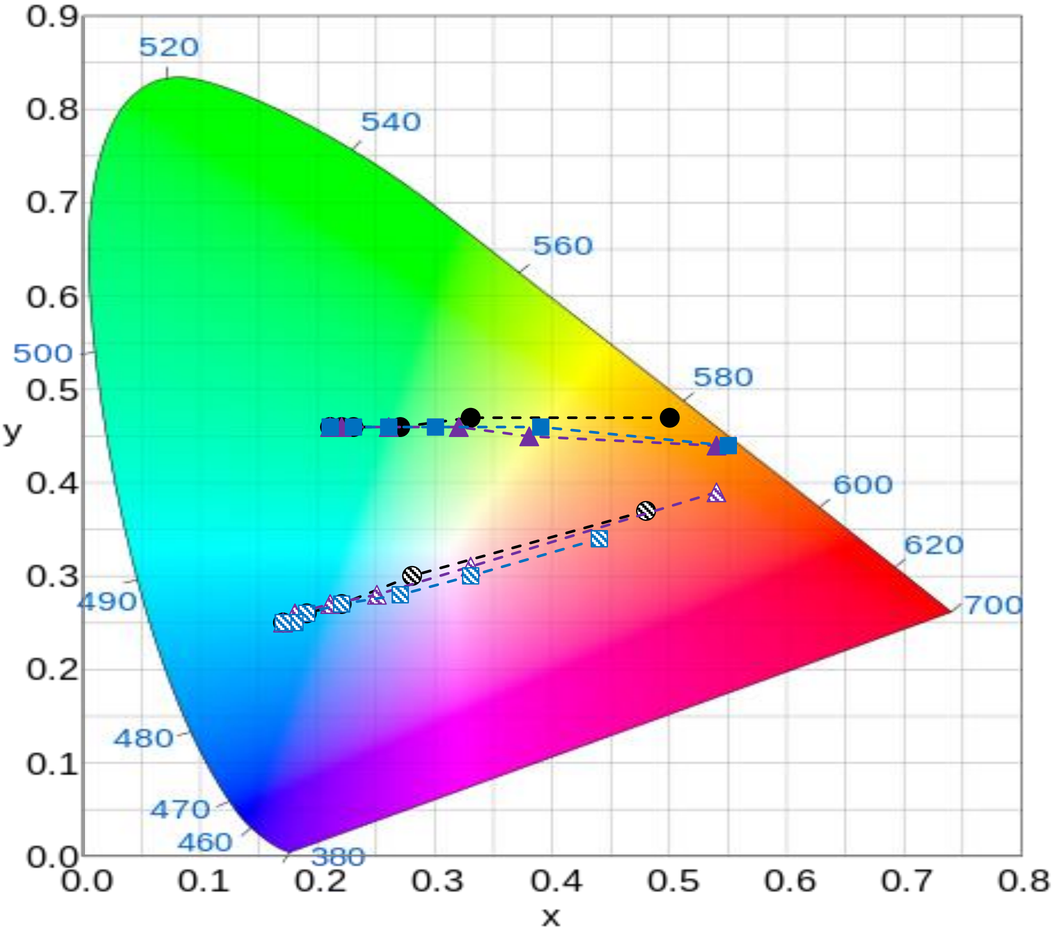

*Figure 2. 24 CIE Coordinate plot of heterodinuclear complexes **JA1-3** throughout the photolysis process. JA1 = black, JA2 = purple and JA3 = blue. Non-fluorinated = block colour and fluorinated = stripes.*

The spectra for each timeframe of the photolysis process were calculated as CIE coordinates (Table 2.6) and plotted on Figure 2.24 for complexes **JA1-3**. The increase of Ir(III) emission intensity, as they were exposed in light, showed a shift from orange/red towards the green/blue for **JA1a-3a** and **JA1b-3b** respectively.

Table 2.6 CIE Chromaticity Coordinates and Quantum Yields of Photoluminescence as Complexes JA1-3 are Monitored by Emission Spectroscopy^{a}

Time (min)	JA1a		JA1b		JA2a		JA2b		JA3a		JA3b	
	CIE (x, y)	ϕ/%^{b}	CIE (x, y)	ϕ/%^{b}	CIE (x, y)	ϕ/%^{b}	CIE (x, y)	ϕ/%^{b}	CIE (x, y)	ϕ/%^{b}	CIE (x, y)	ϕ/%^{b}
0	0.50, 0.47	0.05	0.48, 0.37	0.05	0.54, 0.44	0.06	0.54, 0.39	0.06	0.55, 0.44	0.05	0.44, 0.34	0.05
2	0.33, 0.47	0.11	0.28, 0.30	0.07	0.38, 0.45	0.08	0.33, 0.31	0.08	0.39, 0.46	0.06	0.33, 0.31	0.06
5	0.27, 0.46	0.17	0.22, 0.27	0.13	0.32, 0.46	0.11	0.25, 0.28	0.12	0.30, 0.46	0.10	0.27, 0.28	0.09
10	0.23, 0.46	0.25	0.19, 0.26	0.20	0.26, 0.46	0.17	0.21, 0.27	0.19	0.26, 0.46	0.14	0.22, 0.27	0.13
20	0.22, 0.46	0.38	0.17, 0.25	0.31	0.22, 0.46	0.28	0.18, 0.26	0.29	0.23, 0.46	0.21	0.19, 0.26	0.21
40	0.21, 0.46	0.50	0.17, 0.25	0.43	0.21, 0.46	0.38	0.17, 0.25	0.41	0.21, 0.46	0.30	0.18, 0.25	0.32
60	0.21, 0.46	0.53	0.17, 0.25	0.48	0.21, 0.46	0.42	0.17, 0.25	0.43	0.21, 0.46	0.36	0.17, 0.25	0.39

a) Irradiated by mercury emission lines from a 23 W fluorescent light bulb *b*) [Ru(bpy)3](PF_6)$_2$ was used as relative standard.

2. 6. Conclusion

Target complexes **JA1-3** were prepared and have interesting photophysical and photochemical properties. The complexes are not necessarily good for light emitting devices due to their low PLQY's and photoinstability. The heterodinuclear complexes showed that there was partial energy transfer between the Ir(III) fragment and the Ru(II) fragment (Scheme 2.3), that could be observed by difference in PLQY of the heterodinuclear complexes compared to the Ir(III) mononuclear counterparts as well as the low temperature emission. This partial energy transfer was most likely Förster's energy transfer due to the difference in distances between metal centres in the *para*, *meta* and *ortho* isomers. The partial energy transfer resulted in white light emitting complexes **JA1b** and **JA2b**, which achieved white light emission. This shows that there is a good proof of principle and that with some redesign of the bridging ligands it may be possible to increase the PLQY and have a photostable white light emitter.

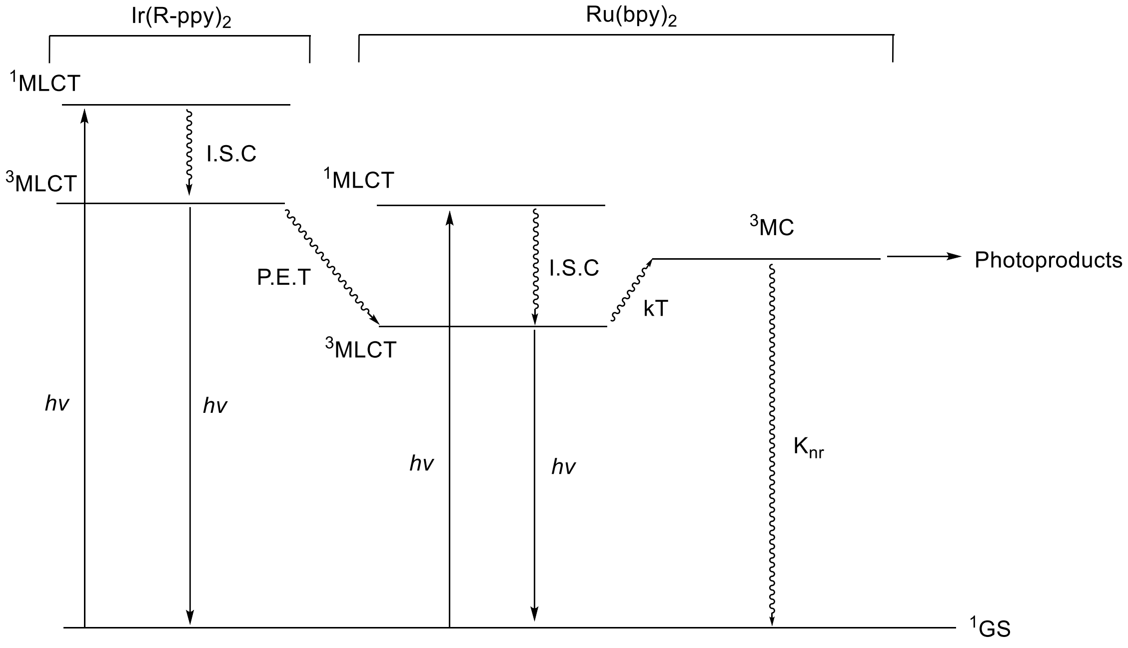

*Scheme 2. 3 Jablonski diagram showing the photophysical processes and partial energy transfer in the excited states for heterodinuclear complexes **JA1-3**.*

Complexes **JA1-3** and mononuclear Ir(III) complexes are highly sensitive to the presence of oxygen. As the heterodinculear complexes change colour and intensity of emission they could be potentially used as colourimetric oxygen sensing. Mononuclear Ir(III) complexes, **JA1-3.Ir** and **JA1-3.IrF**, also have dramatic changes in emission intensity when in the presence of oxygen, these complexes could be further explored for alternative uses as they have an open chelation site that could be used as an on/off switch for when other metals coordinated to the complexes, this would make them viable candidate for biological imaging probes. As the mononuclear complexes **JA1-3.Ir/F** have relatively long excited state lifetimes they also have potential used as PDT agents for type-II sensitisation. The photochemical properties of **JA1-3** do open their potential applications, specifically they could be used as photoactivated chemotherapy agents (PACT). Ru(II) fragment could be developed to be cytotoxic, then once administered to cancer cells the complex could be excited and photoeject the Ru(II) fragment. Before photoejection the complexes would emit in the orange/red however upon more prolonged excitation and when the cytotoxic payload had been delivered the colour of the luminescence would change to green/blue emission confirming the activation.

3. Development of Ir(III) Complexes to Investigate the High Energy T_1 States

3. 1. Introduction

Ir(III) cyclometalated complexes have a wide range of applications and are most prominently known for their excellent photophysical properties, as mentioned in Chapter 1. These complexes have high phosphorescence quantum efficiency, long excited state lifetimes and a significant scope for tunability. This makes this class of complexes excellent candidates for light emitting device such as OLEDs and LEECs.

Neutral cyclometalated Ir(III) complexes have been used in OLEDs due to their fantastic electroluminescent properties. First reported by Thompson and co-workers,[75] $Ir(ppy)_3$ is commonly used as a green light emitter due to its high quantum efficiency, with a PLQY of 97 % in toluene,[92] a long-lived excited state lifetime of 2 μs and with λ_{em}= 510 nm.[167] Red light emitting Ir(III) complexes have lower quantum yields compared to their green and blue light emitting counterparts,[168] this is due to the energy gap between the excited state and the ground state being reduced and therefore k_{nr} is greater due to an increase in vibrational overlap between ground and excited states.[169] $Ir(piq)_3$ and $Ir(piq)_2(acac)$ (Figure 3.1) reported by Tsuboyama and co-workers and Liu and co-workers respectively,[73,170] are often used in OLEDs due to their pure red emission, good quantum yields (PLQY[ii] = 26 % and PLQY = 20 %) and moderately long-lived lifetimes (0.74 μs and 1.67 μs), the lifetimes are not too long as triplet-triplet annihilation occurs in the triplet excited state and quenches the emission.[171] Hence, complexes with longer live excited state lifetimes can result in lower emission intensity. Devices with $Ir(piq)_3$ and $Ir(piq)_2(acac)$ have pure red emission CIE coordinates (0.68, 0.32) which are almost identical to the target coordinates for pure red emission (0.67, 0.33), recommended by the National Television System Committee (NTSC).

[ii] Based on an old value for $Ir(ppy)_3$ as a reference, where PLQY = 40 %.

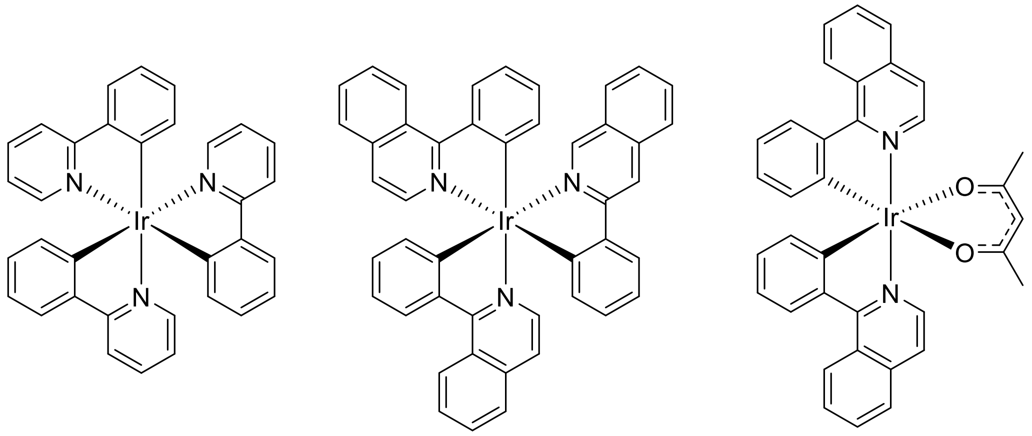

Ir(ppy)$_3$ Ir(piq)$_3$ Ir(piq)$_2$(acac)

Thompson et al. *Tsuboyama et al.* *Liu et al.*

Figure 3. 1 Highly efficient neutral Ir(III) emitting complexes, Thompson and co-workers (green emitter), [75] *Tsuboyama and co-workers (red emitter),*[73] *and Liu and co-workers (red emitter).*[170]

In comparison to the red and green emitting Ir(III) complexes, blue light emitting complexes are less frequently used in light emitting devices as the deep pure blue colour and long-term operational stability are hard to obtain. One of the reasons cyclometalated Ir(III) complexes might be expected to be good blue light emitters is that the non-radiative ^{3}MC states are very high in energy, therefore most complexes cannot populate these deactivating states as opposed to other heavy metal complexes such as Ru(II).[172,63] However, to obtain the deep pure blue colour recommended by the NTSC (0.14, 0.08), the HOMO-LUMO energy gap will need to be immense. Even with the strong Ir-C bond, population of ^{3}MC states is an issue as the energy gap is so great that the ^{3}MC can be thermal populated from the ^{3}MLCT/^{3}LLCT states.

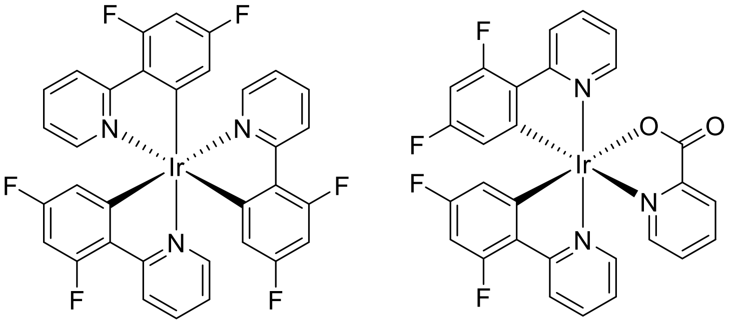

Ir(dfppy)$_3$ Ir(dfppy)$_2$(pic)

Wang et al. *Yersin et al.*

Figure 3. 2 Highly efficient sky-blue emitters reported by Wang and co-workers,[174] *and Yersin and co-workers.* [175]

The majority of blue light emitting Ir(III) complexes that have been reported are efficient sky-blue complexes, whereas there have been very few deep-blue phosphorescent complexes. A ubiquitous method of blue shifting cyclometalated complexes is by fluorination of the cyclometalated phenyl ring and thusly stabilising the HOMO. Ir(dfppy)$_3$ has a significant hypsochromic shift compared to its non-fluorinated counterpart, Ir(ppy)$_3$, the λ_{em} goes from 510 nm to 468 nm, transforming from a green to sky-blue emission.[176,174] The most noteworthy sky-blue emitting complex is Ir(dfppy)$_2$(pic) (Figure 3.2) it has an emission maximum of 468 nm, high quantum yield PLQY = >80 % and a relatively long excited state lifetime of 1.9 μs.[175,126] Fernandez-Hernandez and co-workers,[89] reported a series of neutral 1,4-disubsitituted-1*H*-1,2,3-triazole Ir(III) complexes, that were all blue light emitters (Figure 3.3). The homoleptic Ir(dfptz)$_3$ complex was non-emissive at room temperature, potentially due to the population of the ^{3}MC states, but at 77 K showed deep blue emission. Heteroleptic complexes Ir(dfptz)$_2$(pfptz) and Ir(dfptz)$_2$(dfppy) had λ_{em} of 440 and 465 nm respectively, Ir(dfptz)$_2$(pfptz) had significantly lower quantum yield (ϕ = 5 %) and a shorter lifetime (τ = 0.56 μs) than Ir(dfptz)$_2$(dfppy) respectable quantum yield (ϕ = 50 %) and relatively long lifetime (τ = 1.15 μs). When prepared in a device Ir(dfptz)$_2$(dfppy) had a deeper-blue coordinates (0.17, 0.34) than Ir(dfppy)$_2$(pic) (0.19, 0.40), the emission was still in the sky-blue range.

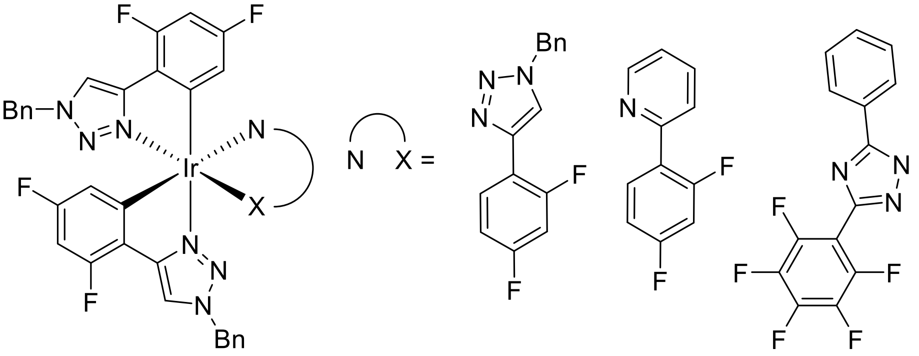

Fernandez-Hernandez et al.

Figure 3. 3 Neutral cyclometalated Ir(III) triazole complexes reported by Fernandez-Hernandez and co-workers. [89]

It has been reported that the polarised C-F bonds on the cyclometalated device can degrade either during OLED fabrication or during the operating process.[177] This can lead to low colour purity and efficiency. Due to these findings new strategies were developed to producer deep-blue emitters. N-heterocyclic carbenes (NHC) have been investigated due to their strong σ-donor and weak π-accepting properties, therefore increasing the energy of the LUMO and increasing stability due to a stronger Ir-carbene bond than the Ir-N bond.[178] Holmes and co-workers reported homoleptic facial (*fac*) and meridional (*mer*) isomer complexes, *fac*-Ir(pmb)$_3$ and *mer*-Ir(pmb)$_3$ (Figure 3.4).[179] Where both isomers produced deep-blue emission, with the *mer* isomer displaying a high energy emission maximum, moderate quantum yield and lifetime (λ_{em} = 395 nm, ϕ = 5 %, τ = 0.62 μs) and was doped in a device, where a pure-deep blue colour was produced with CIE coordinates (0.17, 0.06) close to the NTSC recommendations for pure blue colour (0.14, 0.08). Whilst the carbene complexes showed promising results they had relatively low quantum yields.

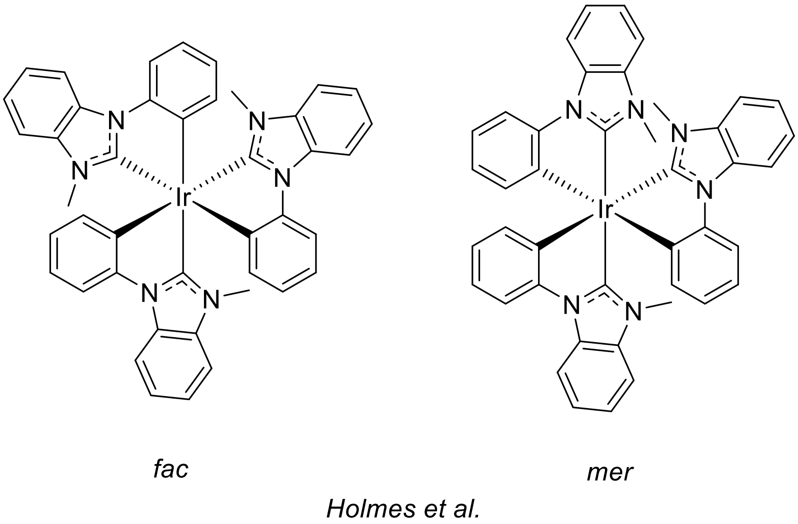

Figure 3. 4 Deep blue emitting carbene Ir(III) complexes developed by Holmes and co-workers. [179]

Cyclometalated cationic Ir(III) complexes have extremely promising use in LEECs due to their highly efficient phosphorescence, long lived lifetimes and high stability. One of the main advantages of using cationic Ir(III) complexes in LEECs is that they can be solution processed, such as spin coated or printed.[125, 129, 133, 134] Neutral Ir(III) complexes typically require more complex preparations such as vapour deposited by sublimination via a high vacuum.[139] The archetypal cationic Ir(III) complexes, $[Ir(ppy)_2(bpy)]^+$ and its derivatives, were initially reported by Güdel and co-workers,[180] the majority of heteroleptic bidentate Ir(III) complexes come from a structural modification of this complex. The substitutions occur at three specific sites; the ancillary ligands N^N heterocycles, the aryl ring on the C^N ligand and the pyridyl or other heterocycle on the C^N ligand. Complexes $[Ir(ppy)_2(bpy)]^+$ and $[Ir(ppy)_2(t\text{Bu-bpy})]^+$ reported by Güdel (Figure 3.5) are yellow/orange phosphorescent with moderate quantum yields, λ_{em} = 602 nm ϕ = 6% and λ_{em} = 588 nm ϕ = 23 %, respectively. This is an excellent example of modification of the ancillary ligand, electron donating *tert*-butyl moieties were added to the bpy ligand causing the LUMO to be destabilised and a blue shift in the emission. As mention previously adding electron withdrawing fluorine substituents to the phenyl ring will stabilise the HOMO and increase the energy gap and further causing hypsochromic shift as can be seen for $[Ir(dfppy)_2(t\text{Bu-bpy})]^+$ reported by Zysman-Colman and co-workers.[181] There was a significant blue shift of emission maxima, compared to $[Ir(ppy)_2(t\text{Bu-bpy})]^+$, from 588 nm to 515 nm and a significant increase in quantum yield as it went from 23 % to 72 %. The fluorinated complex, is one of the most efficient emitters in an LEEC device.[182]

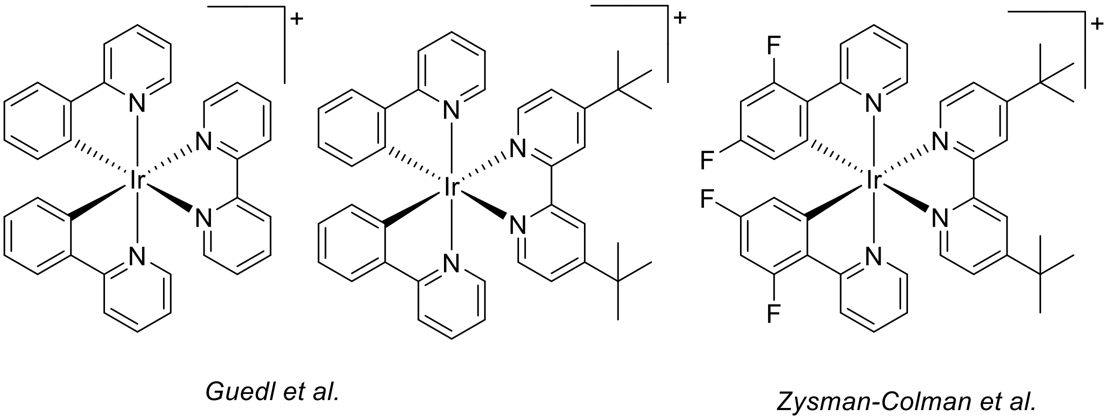

Figure 3. 5 Archetypal cationic Ir(III) complexes reported by Guedl and co-workers, [180] and Zysman-Colman co-workers complex that has been thoroughly investigated. [181]

As the strongly polarised C-F bonds can lead to instability in light emitting devices other methods must be investigated to blue-shift the emission.[177,183,184] Substituting the heterocycle on the cyclometalated ligand is an efficient way to modulate the electronic properties of these set of complexes. One method is via 1-phenyl-1*H*-pyrazole (ppz) substitution of the cyclometalated ligands. The five membered heterocycle blue-shifts the emission of a complex due to stabilisation of the HOMO by the second nitrogen atom, this is due to the electron withdrawing effects of the N(1) atom of the pyrazole ring that is connected to the aryl ring.[71,185,186] A complex reported by Su and co-workers,[187] [Ir(dfppz)$_2$(*t*Bu-bpy)]$^+$ (Figure 3.6) where it is evident the HOMO is stabilised as the complex exhibits a blue shifted emission maxima compared to the [Ir(dfppy)$_2$(*t*Bu-bpy)]$^+$ complex from 515 nm to 492 nm. The complex also has an excellent quantum yield, ϕ = 100 %. An alternate heterocycle to substitute on the C^N ligand would be the 1,2,3-triazole moiety, rather than stabilising the HOMO the LUMO is destabilised, even though the LUMO is largely located over the ancillary N^N ligand.[188] This is thought to be due to the reduced π-acceptor properties of the triazole moiety which would then increase the electron density at the metal centre and thusly increasing π back bonding to the ancillary N^N ligand. This demonstrates that changes to the complex designed to primarily modulate the energy of one orbital, e.g the HOMO, can also affect the energy of other orbitals, e.g. the LUMO. Zysman-Colman and co-workers,[129] reported the sky-blue emitting complex [Ir(dfptz)$_2$(*t*Bu-bpy)]$^+$ (Figure 3.6) with an emission maximum of 498 nm which is higher in energy compared to [Ir(dfppy)$_2$(*t*Bu-bpy)]$^+$ (λ_{em} = 515 nm) but lower compared to [Ir(dfppz)$_2$(*t*Bu-bpy)]$^+$ (λ_{em} = 492 nm). The HOMO stabilising capabilities of the ppz moiety provides the largest HOMO-LUMO energy gap and hence the largest blueshift in emission.

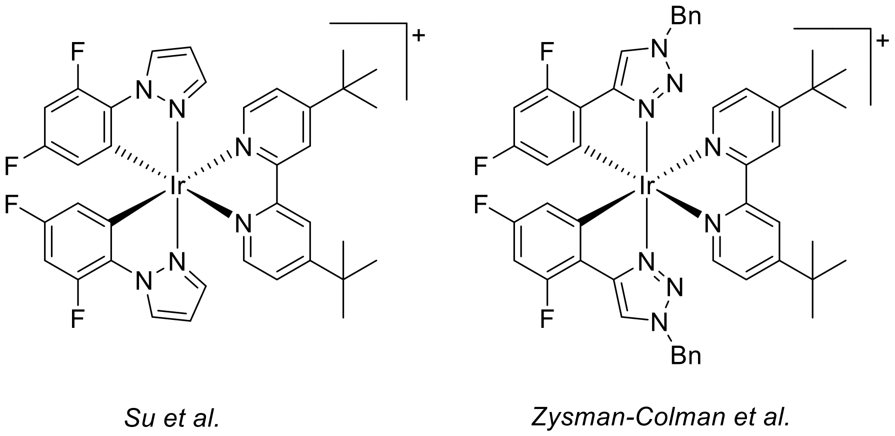

Figure 3. 6 Sky-blue emitting complexes reported by Su and co-workers, [187] and Zysman-Colman and co-workers.

Modulating the N^N ancillary ligand on these complexes primarily has a direct effect on the LUMO. De Cola and co-workers reported complexes in which triazole rings are incorporated into the ancillary ligand, $[Ir(dfppy)_2(pytz)]^+$ (Figure 3.7).[85, 86] This complex had higher energy emission with respectable phosphorescent quantum yields (λ_{em} = 452, 483 nm ϕ = 22 %), and this complex showed structure emission bands indicative of ^{3}MLCT/^{3}ILCT character. This effect of the ancillary ligand on the LUMO is prominent, which can be seen when comparing the emission maximum of $[Ir(dfppy)_2(t\text{Bu-bpy})]^+$ (λ_{em} = 515 nm), the pytz complex has a dramatic increase in emission energy due to the destabilisation of the LUMO. Whilst the LUMO is still localised on the ancillary pytz ligand the destabilisation of the ligand causes the unpaired electron to be relocalised, in the T_1 excited state, to the pyridine moiety on the cyclometalated dfppy ligands. Elliott and co-workers,[78] reported the same ^{3}MLCT/ILCT from the btz based complex, $[Ir(dfppy)_2(btz)]^+$ (Figure 3.7), as the LUMO had been destabilised to the point where the localisation of the emissive states switched to the cyclometalated ligands. The $[Ir(dfppy)_2(btz)]^+$ complex had significantly blue-shifted emission, λ_{em} = 454 nm, compared to the *t*Bu-bpy complex and very similar the pytz complex. The btz complex has a significantly lower quantum yield, ϕ = 0.28%, compared to the 22% of the pytz complex. This could be due to a greater accessibility to thermally populate the higher lying non-radiative states, specifically the ^{3}MC states, which is more commonly seen in the Ru(II) analogues which are weakly/non-emissive.[78] Sarkar and co-workers reported the btz ligand to be a weaker σ-donor and poorer π-acceptor than pyridyl based ligands, the combination of these effects dramatically increase the accessibility of the ^{3}MC states from T_1.[189] For both triazole based ancillary ligands the effective HOMO and LUMO take place on the cyclometalated ligand and thusly the tuning of these complexes photophysical properties is based on these ligands.

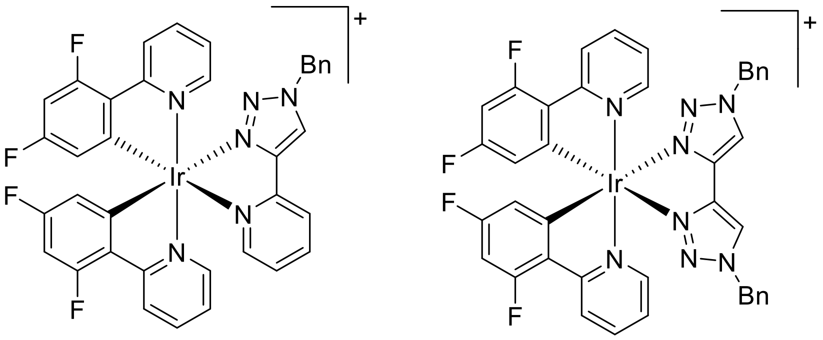

De Cola et al.   *Elliott et al.*

Figure 3. 7 Blue emitting triazole based Ir(III) complexes reported by De Cola and co-workers, [85, 86] and Elliott and co-workers. [78]

3.1.1 Aims and Objectives

As mentioned above there are only very limited deep blue emitting Ir(III) complexes due to their lack of their stability when trying to populate high energy states and induce blue emission. Due to this problem, we are aiming to explore the lowest triplet potential energy of Ir(III) complexes with respect to population of the ^{3}MC states from their T_1 states. This will be achieved following these objectives:

- Cyclometalated cationic Ir(III) complexes have been designed as it provides relative ease to modulate the frontier orbitals and destabilise the LUMO to higher energy where thermal population of the ^{3}MC states is possible.
- Ligand architecture has been carefully developed based on the reported complexes above. We have designed the complexes to include dimethyl pyrazole donor in the cyclometalated C^N ligand, as this will destabilise the ^{3}ILCT/^{3}LC states and stabilise the ^{3}MC states via steric congestion about the metal centre.
- The N^N ancillary ligand is then systematically varied in order to reduce its π-acceptor properties, raising the energy of the LUMO and thus destabilising the energy of the ^{3}LLCT states in the order bpy < pytz < btz (**JA4-6**, Figure 3.8).
- Additionally, **JA7** (Figure 3.8) is designed incorporating an extra methyl substituent on the N^N ligand in order to ensure a moderately destabilised ^{3}LLCT state but further stabilised ^{3}MC state.

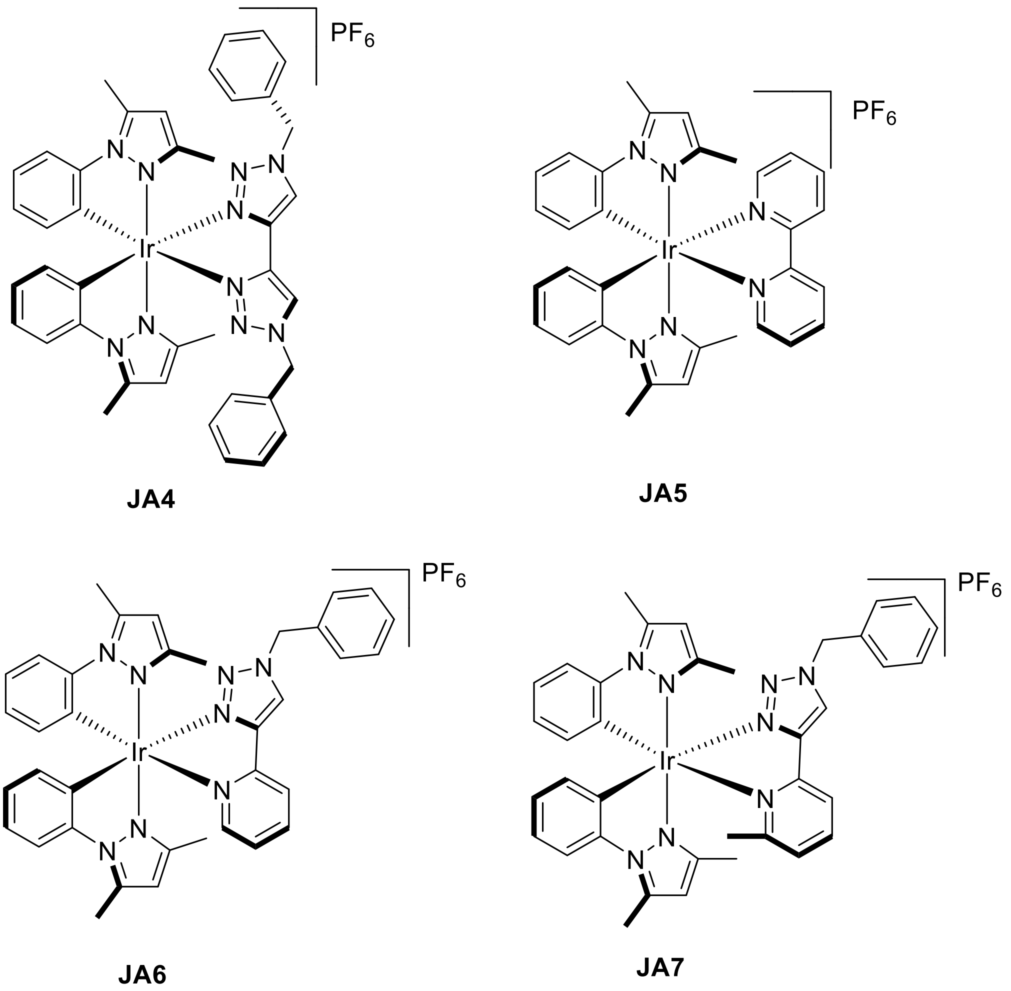

JA4 **JA5**

JA6 **JA7**

Figure 3. 8 Target Ir(III) complexes to explore the high energy triplet excited states.

3. 2. Synthesis of Ligands

The dmppz ligand was synthesised from a one-step cyclocondensation, adapting a previously reported method.[190] Commercially available acetylacetone and phenylhydrazine were added to ethanol in equivalence, conc. HCl was then added to act as a catalyst in the process, and the mixture refluxed overnight (Scheme 3.1a). Dilute sodium bicarbonate solution was added to the reaction mixture and dmppz was extracted and purified by column chromatography.

The ^{1}H NMR spectrum (Figure 3.9) showed four unique proton environments. As can be seen in the figure, **a** referred to the methyl groups on the pyrazole, **b** is the single remaining proton on the pyrazine and **c** refers to the environments on the aromatic ring. The slightly more shielded environment is in the *para* position to the pyrazole. It is also important to note the methyl groups at **a** are inequivalent and the resonances are just coincident appearing as singlet with an integration for 6 protons. The proton environments corroborate reported results.[191]

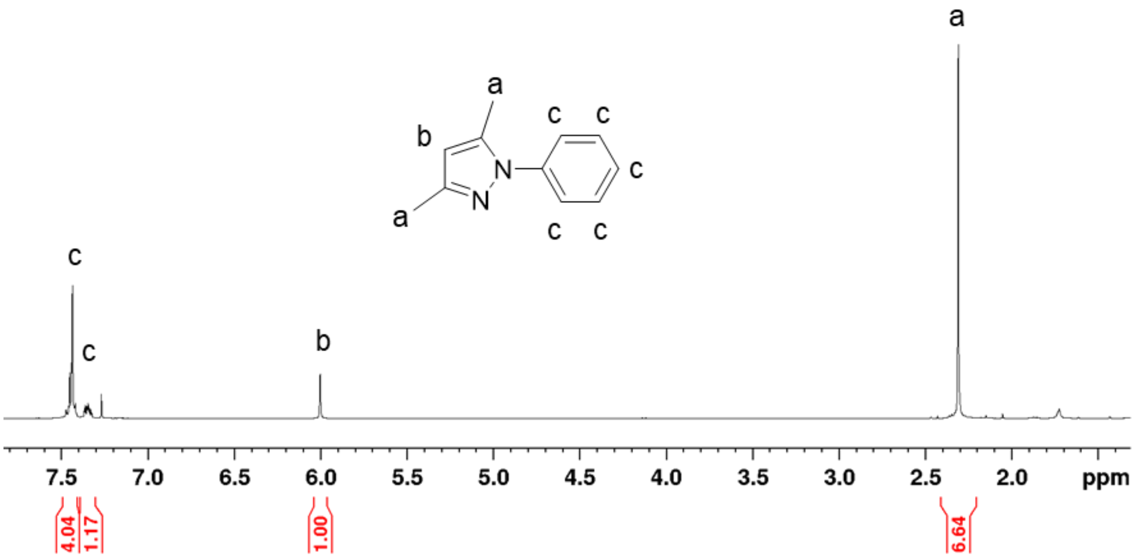

Figure 3. 9 ^{1}H NMR spectrum of the dmppz ligand in $CDCl_3$.

3. 2. 2. General procedure for synthesis of triazole based ligands

Triazole based ligands (btz, pytz and m-pytz) were prepared via a copper(I)-catalysed alkyne-azide cycloaddition. Starting materials (TMS$_2$-butadieyene, 2-ethynylpyrdine, and 2-ethynyl-6-methylpyridine) were combined with benzyl azide, copper sulphate, potassium carbonate, sodium ascorbate and a solvent mixture containing water, *tert*-butanol and pyridine (and tetrahydrofuran for pytz and m-pytz). Mixture left to stir at room temperature for 16 h. After the work up the products were afforded with good yields of 69-75 %. The ligands were characterised by ^{1}H NMR spectroscopy, ^{13}C NMR spectroscopy, and electrospray ionization mass spectrometry (ESI-MS).

3. 3. Synthesis and Characterisation of Iridium Complexes

3. 3. 1. General procedure for synthesis of complexes **JA4-7**

The μ-dichloro bridged Ir dimer, [Ir(dmppz)$_2$(μ-Cl)]$_2$, was prepared following reported procedures (Scheme 3.1b).[162] Complexes **JA4-7** were prepared from [Ir(dmppz)$_2$(μ-Cl)]$_2$ and N^N diimine ligand, in excess (Scheme 3.1c). The mixture was brought to reflux for 20 h, allowed to cool and then ammonia hexafluorophosphate was added to the solution and product precipitated out. Complexes were than purified via silica chromatography, affording **JA4-7**. The yields afforded were varied, with some excellent results, 31-89 %, complexes were confirmed by ^{1}H NMR spectroscopy, ^{13}C NMR spectroscopy and ESI-MS.

The ^{1}H NMR spectrum of **JA4** is shown in Figure 3.10 displaying the resonances and how it relates to the complex. The methyl groups, a, on the dmppz ligand are not one proton environment the resonances are coincident. When observing **JA6** (Figure 3.11), the asymmetric pytz complex, there is a visible separation of the methyl groups. When compared against the free dmppz ligand (Figure 3.9) there is one less proton in the complex due to the cyclometallation at that site.

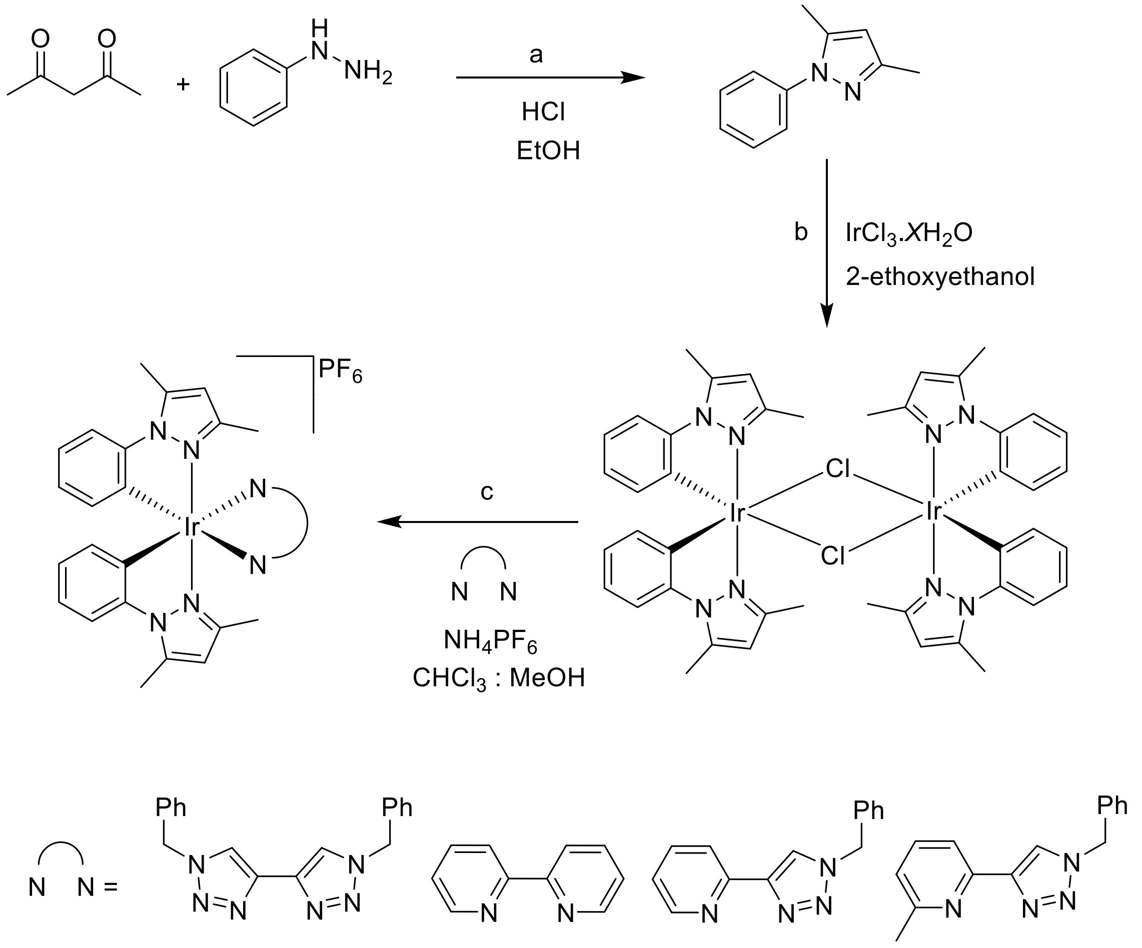

*Scheme 3. 1 a) Preparation of cyclometalated ligand dmppz. b) Preparation of [Ir(dmppz)$_2$(μ-Cl)]$_2$, c) Preparation of target complexes **JA4-7**. N^N diimine ligands for each complex (bottom).*

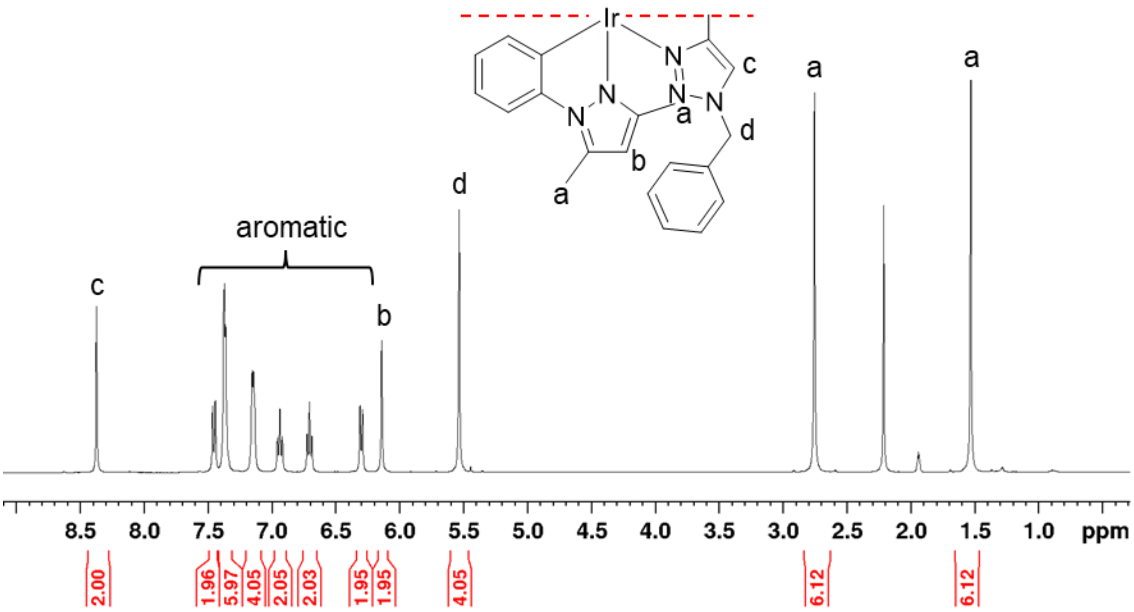

Figure 3. 10 ^{1}H NMR spectrum of complex JA4, in CD_3CN, showing the different resonances.

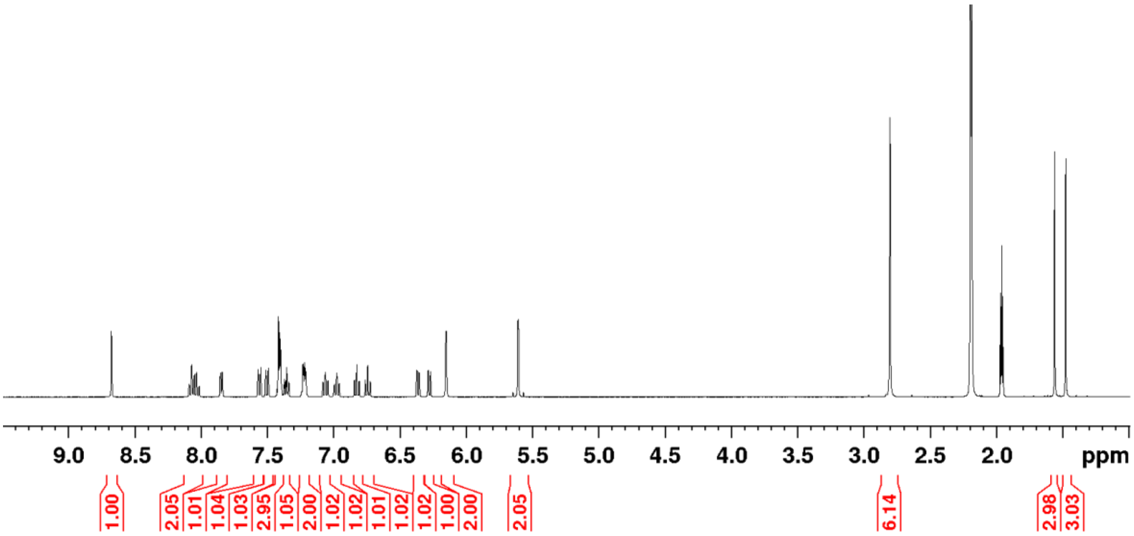

Figure 3. 11 ^{1}H NMR spectrum of JA6, in CD_3CN, showing the difference in the asymmetric pytz complex.

3. 4. Electrochemistry

Cyclic voltammograms for complexes **JA4-7** are shown in Figure 3.12 with the electrochemical data presented in Table 3.1. The series of complexes, **JA4-7**, show one reversible oxidation in the region of +0.86 V, as reported by analogous Ir(III) ppz complexes,[71] and the oxidation values are unaffected by the modulation of the ancillary ligands. This characteristic has been observed in similar Ir(III) cyclometalated complexes,[139, 150, 163, 188, 192] this has been accredited to the removal of an electron from the HOMO, which is localised over the Ir(III) metal centre and the cyclometalated phenyl rings. Due to the electron removal from the HOMO the Ir(III) metal centre is oxidised from Ir(III) to Ir(IV).

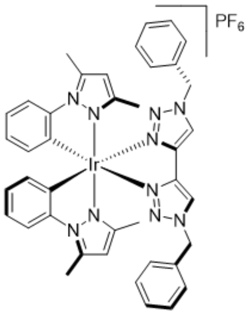

JA4

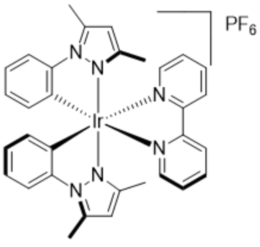

JA5

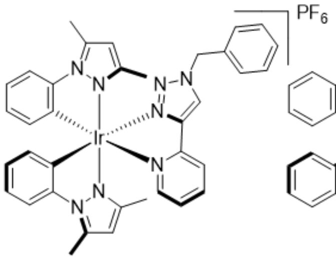

JA6

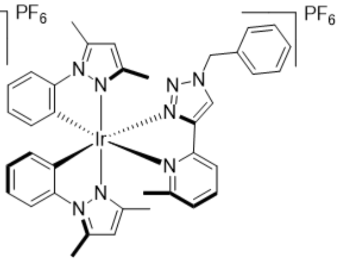

JA7

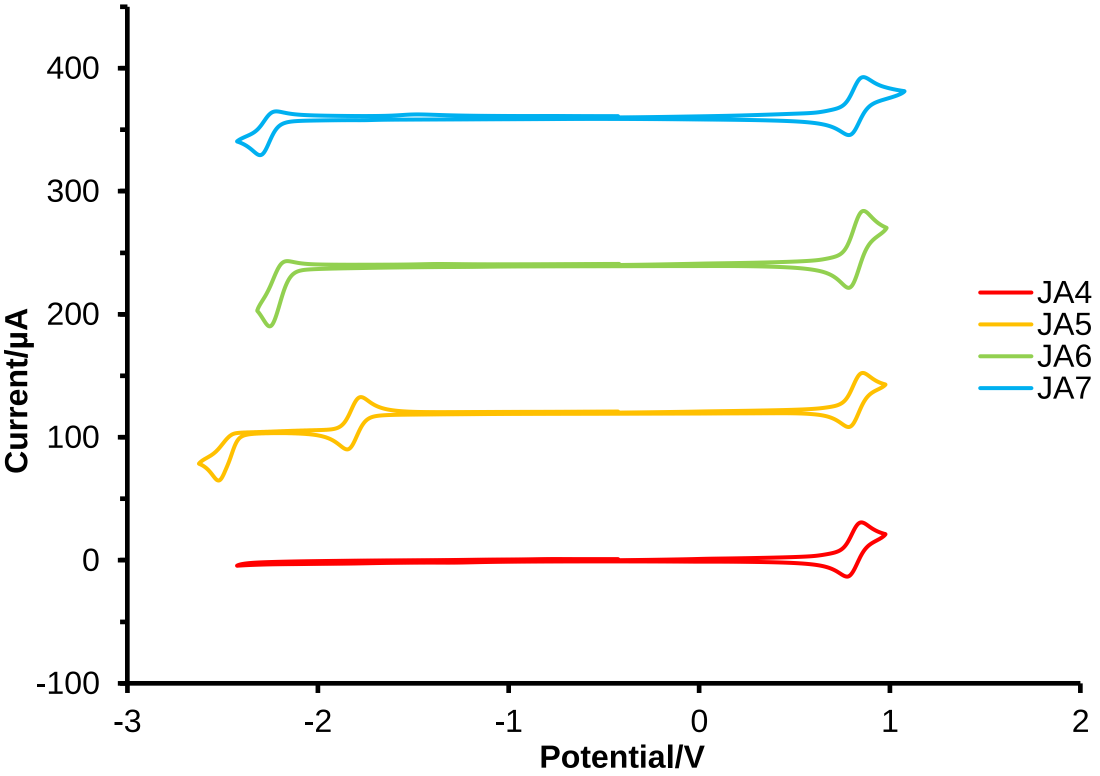

*Figure 3. 12 Cyclic Voltammograms of complexes **JA4-7**. Recorded in MeCN using Fc+/Fc as an internal standard, NBu_4PF_6 was used as the supporting electrolyte with a solution concentration of 0.2 $moldm^{-3}$. Measurements were performed under an atmosphere of N_2 at a scan rate of 100mV s^{-1}.*

The btz complex **JA4** shows no reduction process, due to the high energy of the btz centred LUMO, and thus the reduction process is no longer in the cyclic voltammetry window. Complexes **JA5-7** have visible reduction processes which are attributed to the gain of an electron at the LUMO localised on the N^N ligand. **JA5** has two reduction process, a fully reversible process at -1.85 V and an irreversible process at -2.52 V assigned to the reduction of the pyridine moieties on the bpy ligand. Complexes **JA6** and **7** have a quasi-reversible reduction at -2.25 V and -2.30 V respectively, these can be assigned to the pyridine and 2-methylpyridine moieties.

Table 3.1 Summarised Electrochemical Data for 1.5mmol dm^{-3} MeCN Solutions of JA 4-7 Measured at r.t.at 100mV s^{-1}.^{a,b}

Complex	E_{ox}(V)	E_{red} (V)	E_{ox}-E_{red} Gap (V)
JA4	+0.85	-	-
JA5	+0.86	-1.85 (80), -2.52	2.71
JA6	+0.86	-2.25	3.11
JA7	+0.86	-2.30	3.16

a) Potentials are shown in V vs Fc+/Fc. Reversible couples E1/2 is quoted with anodic-cathodic peak separation shown in mV in brackets. b) NBu_4PF_6 was used as the supporting electrolyte with a solution concentration of 0.2 moldm^{-3}.

This series of complexes has a lower oxidation potential compared to $[Ir(ppy)_2(L)]^+$, this is due to the stabilisation effect the dimethylpyrazole moieties have on the HOMO which is directly related to the oxidation potential.[173] Thompson and co-workers reported $[Ir(ppz)_2(bpy)]^+$ to have an oxidation of +0.96 V which is a greater potential than observed in **JA4-7**, dmppz complexes have lower oxidation potential due to, presumably, the electron donating effect of the methyl groups.[71]

Regarding complex **JA4**, The LUMO could potentially be assigned as being on localised on the pyrazole moieties on the dmppz ligand or the btz ligand. However, the Elliott and Zysman-Colman groups reported the LUMO was localised on the btz ligand for $[Ir(ppy)_2(btz)]^+$.[188, 192] As the pyrazole moiety's LUMO is probably higher in energy than the pyridyl moiety's LUMO on the reported complex, it is more than likely that complex **JA4**'s LUMO is similarly centred on the btz ligand. The pyrazole moiety is less readily reduced compared to pyridine, the homoleptic $Ir(ppz)_3$ complex is thought to have reductions at -3.0 V.[176] Whilst the btz ligand has significantly less electron accepting properties than the typical pyridine-based ligands, due to the weak π accepting properties, resulting in the reduction being unobservable in the available solvent window.

Complex **JA5** is observed in Figure 3.10 and a reduction potential of -1.85 V can be seen, which is comparable to that of -1.80 V of reported complex $[Ir(ppz)_2(bpy)]^+$.[71] Complexes **JA6** and **7** have similar pyridine reduction potentials that have been observed with the reported $[Ir(ppy)_2(pytz)]^+$ complex.[91, 163, 193] The difference in reduction potentials between **JA6-7** is down to the electron donating effect of the methyl group on the pyridine ring.

The E_{ox}-E_{red} energy gap of **JA5** is lower, 2.71 V, compared to the ppz analogue, 2.75 V, due to the destabilisation effect of the methyl groups on the HOMO and therefore on the oxidation potential. Complexes **JA6-7** observed energy gaps of 3.11 V and 3.16 V respectively, these were akin to the reported complex $[Ir(ppy)_2(pytz)]^+$ which had an energy gap of 3.14 V. [91, 163, 193]

3. 5. Photophysical Properties

Table 3.2 Summarised Photophysical Data for MeCN Solutions of JA4-7 at 298 K.

Complex	λ^{abs}/nm^{a}	λ^{em}/nm^{b}	$\phi/\%^{b,c}$	τ/ns^{b}	$10^{6}\ kr/s^{-1\ b}$	$10^{6}\ k_{nr}/s^{-1\ b}$
JA4	230sh, 280sh, 310	394	<0.1	-	-	-
JA5	246, 272sh, 306, 340sh 380sh, 448	611	3.11	179	17	12
JA6	244, 312, 399	530	3.26	68	48	33
JA7	230, 247, 280sh, 312, 399	529	<0.1	-	-	-

a) MeCN, aerated at 298K b) MeCN deaerated at 298K c) PLQY, $[Ru(bpy)_3](PF_6)_2$ in MeCN was used as a relative standard.

3. 5. 1. Electronic UV-Vis Absorption Spectroscopy

The series of complexes **JA4-7** all display electronic UV-visible absorption spectra, in acetonitrile, typical of biscyclometalated Ir(III) complexes, and are shown in Figure 3.13 and summarised in Table 3.2. Intense higher energy bands that are <300 nm that primarily come from ligand centred $\pi \rightarrow \pi^*$ transitions. The lower energy absorption bands >300 nm are defined by excitations to the ^{1}MLCT states (300-380 nm), the longer tail, lower energy, transitions arise from direct, spin-forbidden, transitions to the ^{3}MLCT states (400-500 nm).

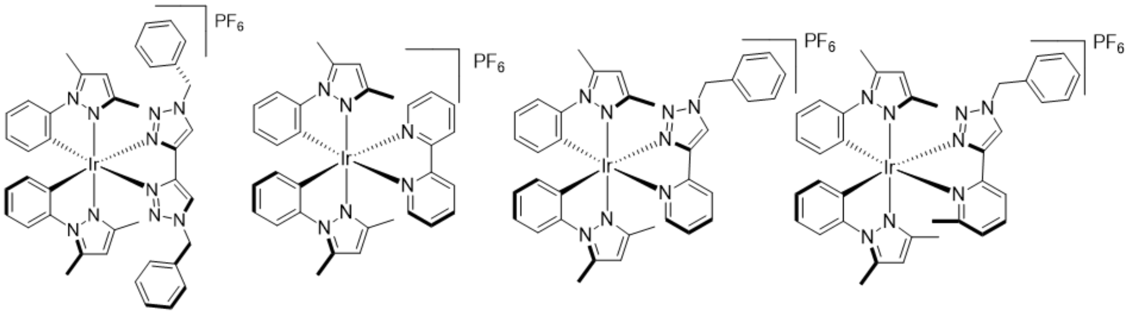

JA4 JA5 JA6 JA7

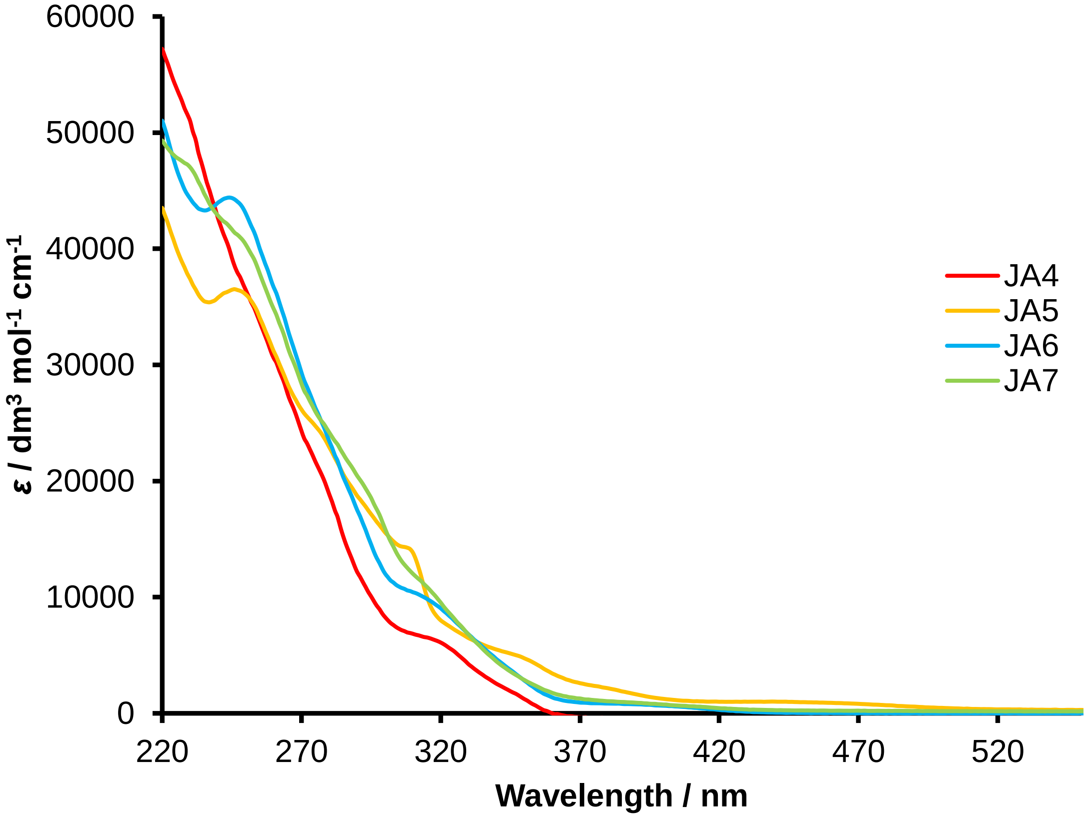

*Figure 3. 13 UV-visible absorption spectra recorded for **JA4-7** complexes. Recorded in MeCN at 298K.*

Complex **JA5** has a lower energy ^{1}MLCT absorption than the rest of the series, as the ancillary bpy ligand stabilised the LUMO due to its π back bonding nature, this is in agreement with the electrochemistry as the E_{ox}-E_{red} gap for the complex was the lowest value of the series. Thomspon and co-workers,[71] reported heteroleptic phenylpyrazole Ir(III) complexes which produced similar absorption bands to **JA4-7** complex **JA5** has an almost identical spectrum compared to their $[Ir(ppz)_2(bpy)]^+$ however **JA5** is marginally higher in energy with about a 2-5 nm blue shift. The ancillary ligands for the remainder of the series contain triazole moieties, which destabilise the LUMO, mean there ^{1}MLCT absorption bands are higher in energy, again this complements the electrochemistry.

This series of complexes have significantly higher absorption energies than compared to $[Ir(ppy)_2(L)]^+$ complexes this is due to the dimethylpyrazole moiety, their π* antibonding orbitals are higher in energy than pyridine. Similar hypsochromic shifts have been observed in Pt and Rh phenylpyrazole complexes,[194,195,196] as well as in Ir(III) complexes as reported by Thompson and co-workers when they developed the homoleptic $Ir(ppz)_3$ complexes.[176] Elliott and co-workers,[192] reported heteroleptic complex $[Ir(ppy)_2(btz)]^+$ absorption band to ^{1}MLCT as 382 nm which is lower in energy than corresponding complex **JA4**, 310 nm, further confirming the electronic differences between the two moieties. Both Zysman-Colman and Elliott groups have developed $[Ir(ptz)_2(L)]^+$ complexes, both showed similar effects where the triazole moieties have replaced the typical pyridyl moiety, causing the π* antibonding orbitals to be higher in energy.[188,163] Zysman-Colman and co-workers, produced $[Ir(ptz)_2(bpy)]^+$ which had a high energy ^{1}MLCT absorption of 330 nm, which is slightly higher in energy compared to 340 nm for **JA5**. Elliott and co-workers, reported $[Ir(ptz)_2(pytz)]^+$ had a ^{1}MLCT absorption of 304 nm, which again was blue shifted compared to equivalent complexes **JA6-7** which both have an absorption of 312 nm. From this we can conclude that the π* antibonding orbitals are greater in energy for triazole moieties compared to the pyrazole/dimethylpyrazole moieties.

3. 5. 2. Emission Spectroscopy

Complexes **JA4-7** were all emissive and spectra were at room temperature in acetonitrile solutions, are provided in Figure 3.14 with data summarised in Table 3.2. The photoluminescent quantum yields were calculated from the relative standard (ϕ_{rel}), $[Ru(bpy)_3][PF_6]_2$ which has an absolute quantum yield of 1.8%. The calculations used the emission spectra that were excited at the following wavelengths of excitation; λ_{ex} = 310 nm for **JA4**, λ_{ex} = 340 nm for **JA6** and **JA7**, and λ_{ex} = 350 nm for **JA5**. Broad featureless emission bands were recorded for all complexes indicative of ^{3}MLCT/LLCT character in the emissive excited states.[172, 175] Complex **JA4** emitted in the high energy blue/UV-vis region (λ_{em} = 394 nm), the complex was only very weakly emissive with a low quantum efficiency (ϕ_{rel} = <0.1 %) and precluding accurate measurement of the lifetime. In contrast, **JA5** observed significantly redshifted emission, in the orange/red region (λ_{em} = 611 nm) with reasonable quantum yields (ϕ_{rel} = 3.11 %) and excited state lifetime of 179 ns. Complexes **JA6-7** exhibit very similar emission spectra, with bands in the green region with very similar emission maxima at λ_{em} = 530 and 529 nm, respectively. The phosphorescent quantum efficiency varied greatly between the complexes, **JA6** had reasonable quantum yields (ϕ_{rel} = 3.26 %), whereas **JA7** was only weakly emissive with a low quantum yield (ϕ_{rel} = <0.1 %). Complex **JA6** had a relatively short excited lifetime (τ = 68 ns) whilst an accurate measurement for the excited state lifetime of **JA7** was not possible.

Complexes **JA6** and **JA7** have very similar emission bands, this is due to their almost identical structure. The triazole moiety of the pytz and m-pytz ligand destabilises the LUMO and therefore increases the energy gap and thus blue shifts the emission compared to **JA5**. These complexes have broad unstructured emission bands which correspond to ^{3}MLCT/^{3}LLCT character. De Cola and co-workers complex,[91, 193] $[Ir(ppy)_2(pytz)]^+$, showed structured emission of ^{3}MLCT/^{3}ILCT character. The reason for this difference is the unoccupied orbitals on the cyclometalated ligand have been destabilised by the dimethylpyrazole moiety so the excited electron can no longer switch to the cyclometalated ligand and is localised on the pyridine of the pytz ligand. As a result of this **JA6** and **JA7** are red shifted compared to $[Ir(ppy)_2(pytz)]^+$ (λ_{em} = 477, 507 nm). Complex **JA6** had a moderate quantum efficiency but was considerably lower than the ppy complex (ϕ = 21 %). The methylated version of the complex, **JA7**, had very low quantum efficiency, this is expected to be due to the steric hinderance caused by the methyl group meaning that the ^{3}MC states are more readily populated.

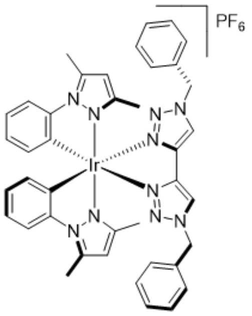

JA4

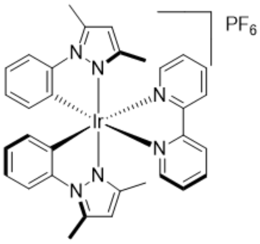

JA5

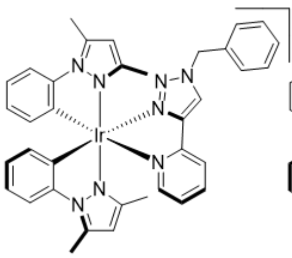

JA6

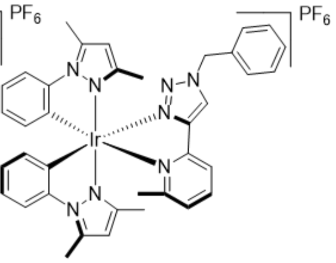

JA7

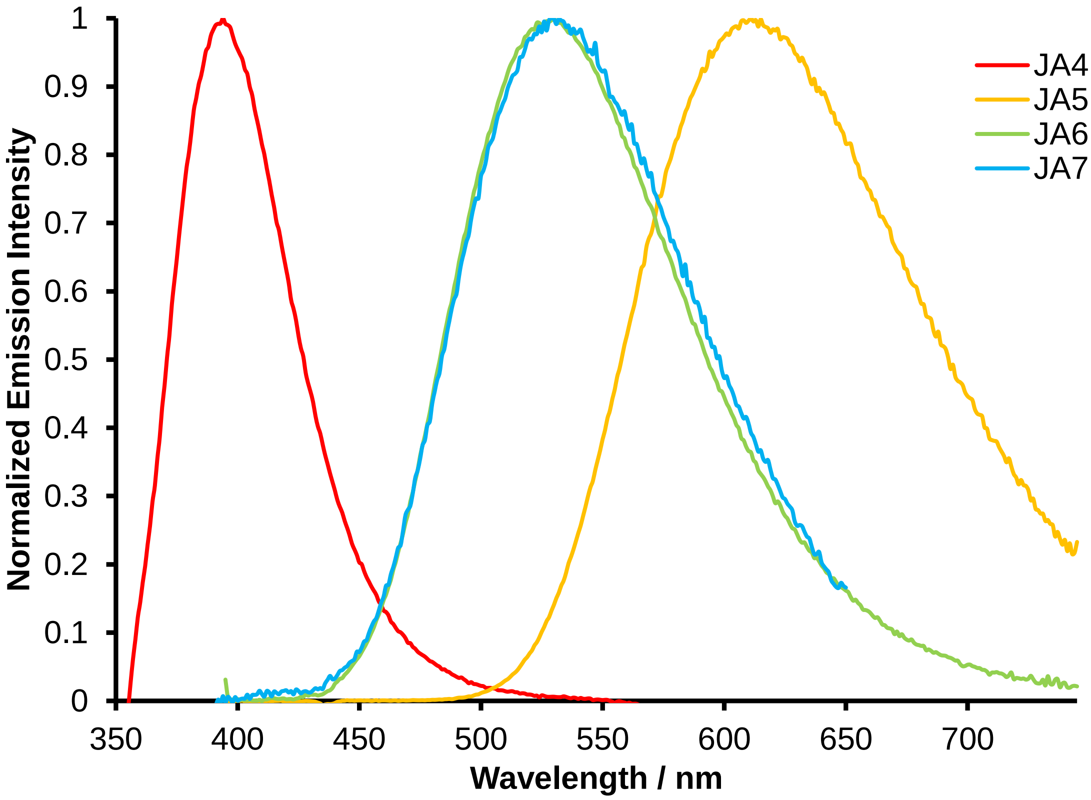

*Figure 3. 14 Emission recorded for **JA4-7** complexes. Recorded in de-aerated MeCN at 298K. Wavelength of excitation for JA4= 310 nm, JA6 and JA7 = 340 nm, and for JA5 = 350 nm.*

As anticipated complex, **JA4** was only very weakly emissive with a very short excited state lifetime that it was not observable through TCSPC, as it was designed with the goal of populating the non-radiative ^{3}MC states. Thermal population of the high energy non-radiative states explains the low quantum yield, a similar effect has been reported with Ru(II) complexes containing btz ligands when the ^{3}MC states are thermally accessible.[62, 63] Interestingly the emission band that is observed corresponds to ^{3}MLCT/LLCT character from the emissive states, initially indicating that the LUMO is on the btz ligand rather than the cyclometalated dmppz ligand. Elliott and co-workers reported complex $[Ir(ppy)_2(btz)]^+$ to have structured emission bands that correspond to ^{3}MLCT/ILCT character,[192] on the cyclometalated ligand. The switching does not occur in this instance as the dimethylpyrazole moiety, on the cyclometalated ligand, is higher in energy than the pyridine on the ppy ligand and higher in energy than the LUMO on the btz ligand. Due to the ligand design high energy emission is induced, with emission hypsochromically shifted by 82 nm compared to its ppy analogue (λ_{em} = 476, 508 nm), and to the rest of the series.

Complex **JA5** exhibits lower energy transitions, and more red shifted emission, as the bpy ligand localised LUMO is stabilised compared to triazole based ligands, as has been reported in the literature.[129] Complex **JA5** is significantly redshifted against the analogous ppz complex (λ_{em} = 563 nm), it is reasonable to presume this is related to the methyl groups however cannot determine if this an electronic or steric effect of these methyl groups. In fact, **JA5** is redshifted compared to the ppy analogous complex (λ_{em} = 605 nm), **JA5** has a reduced quantum efficiency compared to both the ppz and ppy complexes (ϕ = 17 % and 9 %, respectively). The lower quantum yields could be due to an alternative deactivation pathway through the methyl groups or could be due to more vibrational overlap with the non-radiative states due to the lower energy emission.

3. 5. 2. 1. Oxygen Dependent Emission

The unique properties of these heavy metal complexes which allows for triplet-based emission does also lead to the excited state being quenched by O_2 via excited state via triplet-triplet annihilation.[30]

All the target complexes, **JA4-7** show sensitivity to the presence of O_2, as can be seen in Figure 3.15. The complexes were in solution that had were wither aerated, deaerated or oxygenated, the deaerated solution was done via freeze pump thawing and applying a vacuum, the oxygenated solution was done by purging the solution with pure O_2. This can be seen in the change of quantum efficiencies and the lifetimes of complexes **JA5** and **JA6**, Table 3.3. The quantum efficiencies were too low, and the lifetimes were unobservable for **JA4** and **JA7**. Complex **JA5** quantum yields increased from 0.32 % in the oxygenated solution, to 1.00 % in the aerated solution and increased all the way to 3.11 % in the deaerated solution. The lifetimes also varied, in the oxygenated solution it was 18 ns, the aerated solution 52 ns, and in the deaerated solution it was 179 ns. For complex **JA6** the quantum yields and lifetimes increased with the less O_2 present, quantum yield of the complex in an oxygenated solution was 0.40%, in the aerated solution increased to 1.34% and finally to 3.4% in a deaerated solution. The lifetimes also changed, in an oxygenated solution 7.6 ns, to 24 ns in the aerated solution and finally to 68ns in the deaerated solution.

The oxygen dependent photophysical properties show this emission has come from the triplet state as phosphorescence. Triplet-triplet annihilation with $^3O_2$ causes the quenching of the emission and the effect on the decrease of the lifetimes, as this an alternative pathway for deactivation. The result of which produces $^1O_2$ which has many potential uses in biological scenarios as it is highly toxics, heavy metal complexes such as these have the potential to be used in photodynamic therapy.

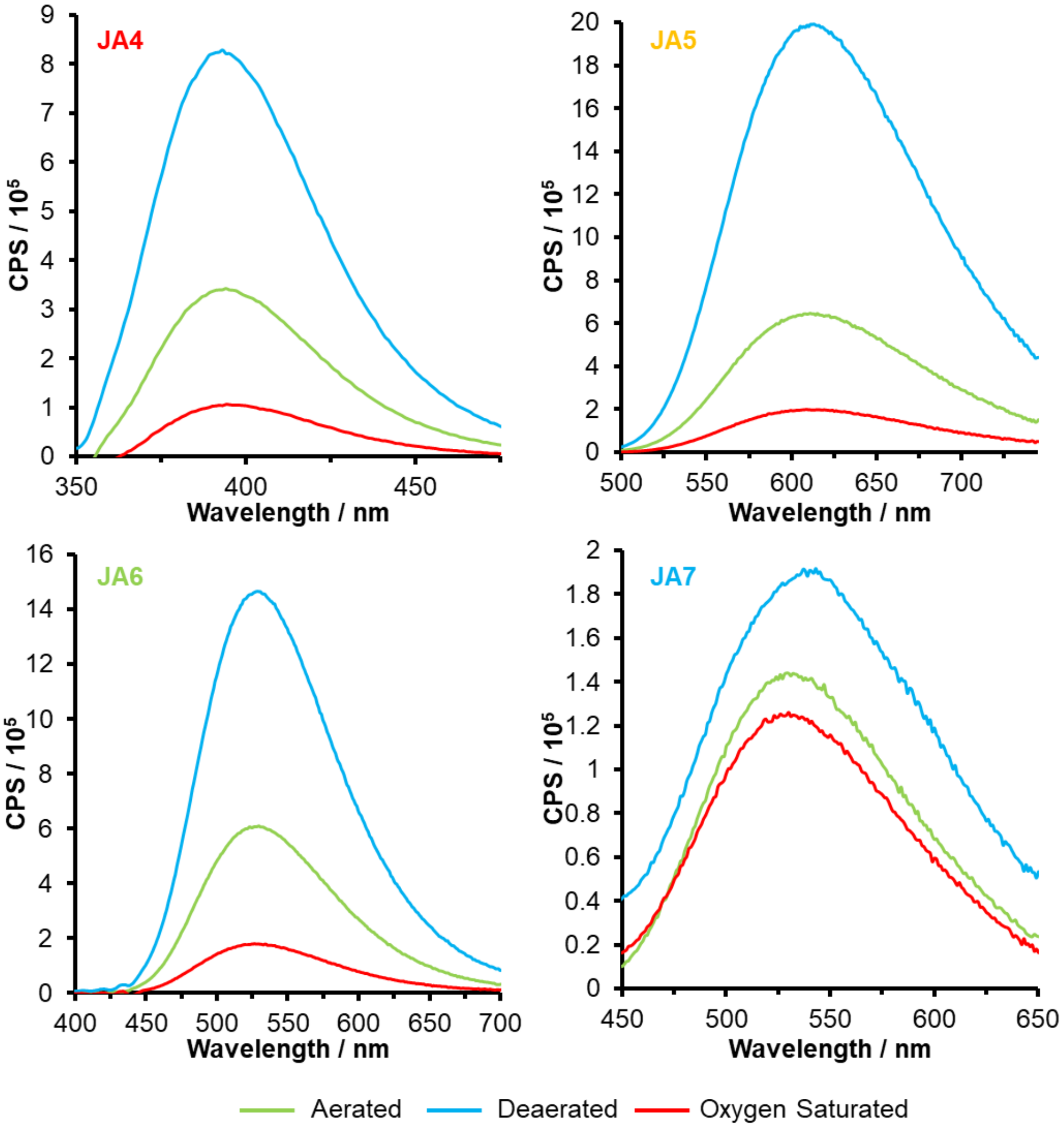

*Figure 3. 15 Emission spectra of complexes **JA4-7** in MeCN solutions with varying levels of oxygen presence Aerated (green), deaerated solution (blue) was free-pump thawed with all gases removed, solution was saturated with O_2 (red). Recorded at 298K. Wavelength of excitation for JA4= 310 nm, JA6 and JA7 = 340 nm, and for JA5 = 350 nm.*

Table 3.3 Summarised Photophysical Data of JA4-7 at Low Temperature (77K) in EtOH:MeOH glass and in Aerated, Deaerated and Oxygen Saturated MeCN Solutions Measured at r.t.

Complex	λ^{em}/nm[a]	ϕ/%[b,e]	ϕ/%[c,e]	ϕ/%[d,e]	τ/ns[b]	τ/ns[c]	τ/ns[d]
JA1	404, 430, 459, 481sh	<0.1	<0.1	<0.1	-	-	-
JA2	526	1.00	3.11	0.32	52	179	18
JA3	463	1.34	3.26	0.40	24	68	7.6
JA4	464	<0.1	<0.1	<0.1	-	-	-

a) EtOH:MeOH (4:1) glass, aerated at 77K b) MeCN, aerated at 298K c) MeCN deaerated at 298K d) MeCN, oxygenated at 298K e) PLQY, $[Ru(bpy)_3]2(PF_6)$ in MeCN was used as relative standard.

3. 5. 2. 2. Low Temperature Emission

The emission spectra of the complexes **JA4-7** had their emission spectra recorded at 77K in an EtOH:MeOH glass to investigate their photophysical properties, as specific vibronic structures can be observed. Complex **JA4** has the most noticeable change in band shape, at low temperature it has a highly structured band compared to the narrow band seen at room temperature. Complex **JA5-7** remain showing the broad band shown at room temperature, the emission bands had increased dramatically in energy. The emission maxima for **JA5** has blue shifted from 611 nm to 526 nm, similar effects have taken place for **JA6** and **JA7**, blue shifted from 530 nm and 529 nm to 463 nm and 464 nm respectively.

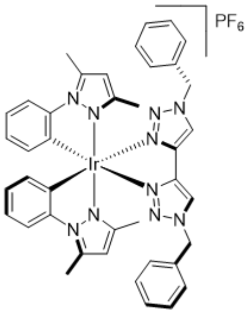

JA4

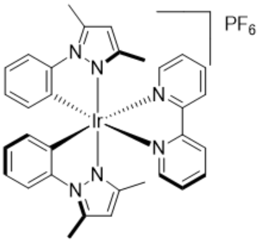

JA5

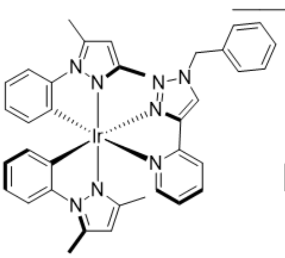

JA6

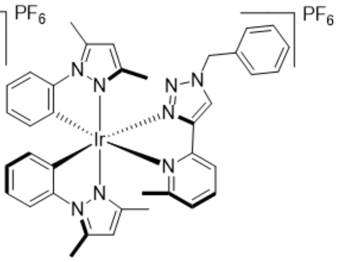

JA7

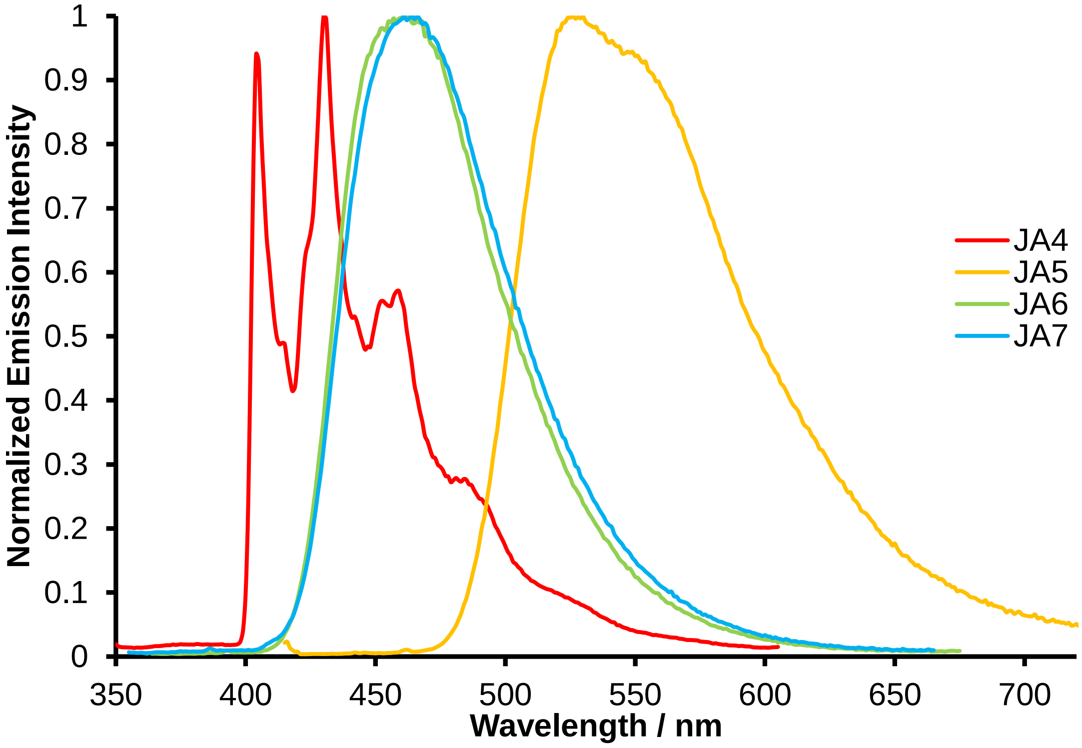

Figure 3. 16 Low temperature emission spectra of ***JA4-7*** *complexes. Recorded in EtOH:MeOH (4:1) glass at 77K. Wavelength of excitation for JA4= 310 nm, JA6 and JA7 = 340 nm, and for JA5 = 350 nm.*

This increase in energy of emission when in a rigid glass at low temperature is known as rigidochromism,[197] in charge transfer excited states the change in dipole due to charge transfer is stabilised by rearrangement of the solvent which is not possible when in the glass matrix so emission appears at a higher energy. Vibronic structures are also clearer due to this, which can be seen for **JA4** which has the vibronic structure commonly associated with ^{3}MLCT/^{3}ILCT character. Interestingly this is different to the room temperature emission, and the emission is slight red shifted in the solid state which is not expected. Complexes **JA5-7** do not show any vibronic structures indicating they are ^{3}MLCT/^{3}LLCT in character.

The specific reasoning behind the change in **JA4** emission properties is hard to define, it could be that the energy level for the unpaired electron to switch to the dimethylpyrazole is very close resulting in ^{3}MLCT/^{3}ILCT character under certain conditions where in room temperature conditions ^{3}MLCT/LLCT is more energetically favourable, similar reported occurrences in other Ir(III) complexes. However, that does not account for the red shift in emission at low temperature in the solid state when a blue shift is expected to happen. Tentatively it could be suggested that the emission at room temperature is ligand centred fluorescence which is being thermally activated from a ^{3}LC state. To fully understand the processes occurring for **JA4** some temperature dependent data would be required.

3. 5. 3. Transient Absorption Spectroscopy

As the aim was to investigate the population of the high energy excited states for Ir(III) complexes fs-ps transient absorption spectroscopic experiments were carried out for complexes **JA4-7**. With the intention to capture the exited state lifetimes and the time evolution of the predicted energy transfer process from the ^{3}MLCT states to the higher energy ^{3}MC states.

Table 3.4 Summary of Excited State Lifetimes for JA4-7

Complex	τ/ns^c
JA1^a	0.0077
JA2^b	52
JA3^b	24
JA4^a	2.3

a) Calculated from kinetic fits from global analysis to the UV-visible transient absorption spectra. *b)* Calculated from time-correlated single photon counting. *c)* Aerated MeCN solution at 298K

The transient absorption spectrum for btz complex **JA4** is displayed in Figure 3.17, from the emissive properties it appeared as if complex was populating high energy non-radiative states, like the ^{3}MC states as had been reported for Ru(II) btz containing complexes.[62, 78] Complex **JA4** exhibits a rapid decay to the ground state. Initially there are two bands, at 380 nm and 460 nm, that then broaden, this could potentially be vibrational cooling, and then the excited state absorption decays. Global analysis was fitted and can be seen in the Figure 3.18, from this the excited state lifetime was calculated to be 7.7 ps. This was a very short-lived excited state compared to **JA5-7** (Table 3.4) which agrees that the excited states are very high energy, ^{3}MLCT/^{3}LLCT that is very close to the ^{3}MC states so are readily thermally populating them.

The transient absorption spectra that were displayed for **JA5** and **JA6** in Figure 3.19 and 3.20, showed very slight decay but the transients were still present at the end of the time window. This was to be expected as it agrees with the time-correlated single photon counting lifetimes recorded (Table 3.4).

For complex **JA7** the transient absorption spectrum was displayed in Figure 3.21, an absorption band was observed at 350 nm that decayed quickly. Interestingly the transient absorption spectrum had a different profile to **JA6**'s profile, when the only difference on the complex is the methyl group on the pytz N^N ligand. The global analysis was fitted (Figure 3.22) and the excited state lifetime was calculated to be 2.3 ns, which is considerably faster than analogous complex **JA6**'s τ = 24 ns. The fast-decaying excited state lifetime corresponds to the weak emission intensity at room temperature and low quantum efficiency as it indicates that the non-radiative ^{3}MC are being thermally populated readily. It can be conceived that the steric hinderance of the methyl group on the N^N pytz ligand has reduced the energy of the ^{3}MC states and brought it much closer in energy to that of the ^{3}MLCT/LLCT states. Elliott and co-workers reported this exact effect with [Ru(bpy)$_2$(m-pytz)]$^{2+}$ where the elongation of the Ru-N bond by the steric hinderance of the methyl group resulted in a lowering of the ^{3}MC states that are more readily thermally populated.[62]

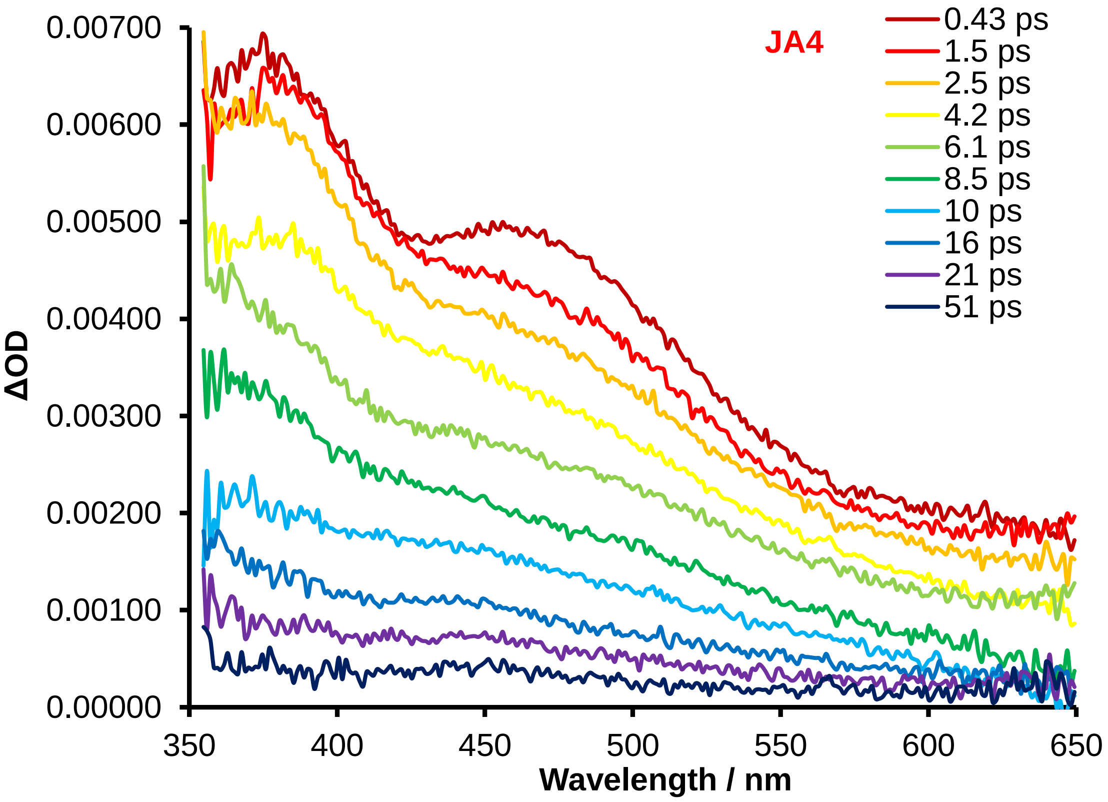

*Figure 3. 17 UV-visible transient absorption spectra for complex **JA4** in MeCN at 298K (λ_{ex} = 285 nm). Two excited state absorption maxima at 380 nm and 460 nm that broaden rapidly followed by excited state absorption decay.*

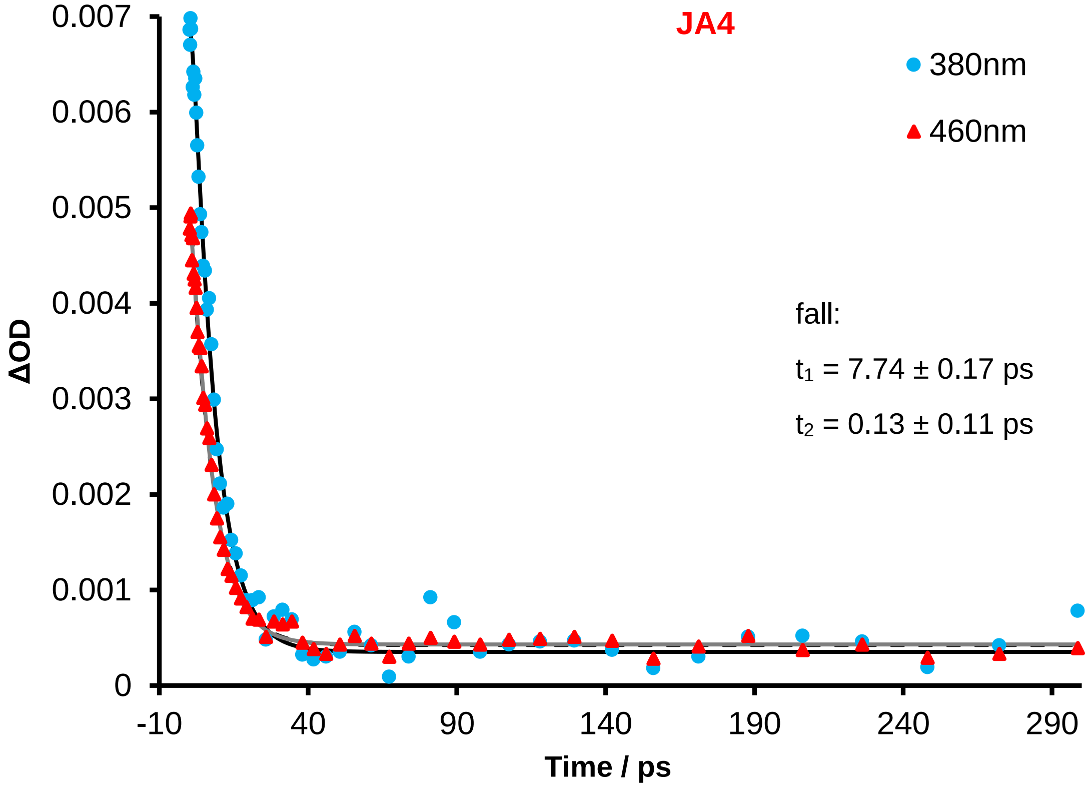

*Figure 3. 18 Time profile and kinetic fit from global analysis for associated transient absorption spectra for complex **JA4**.*

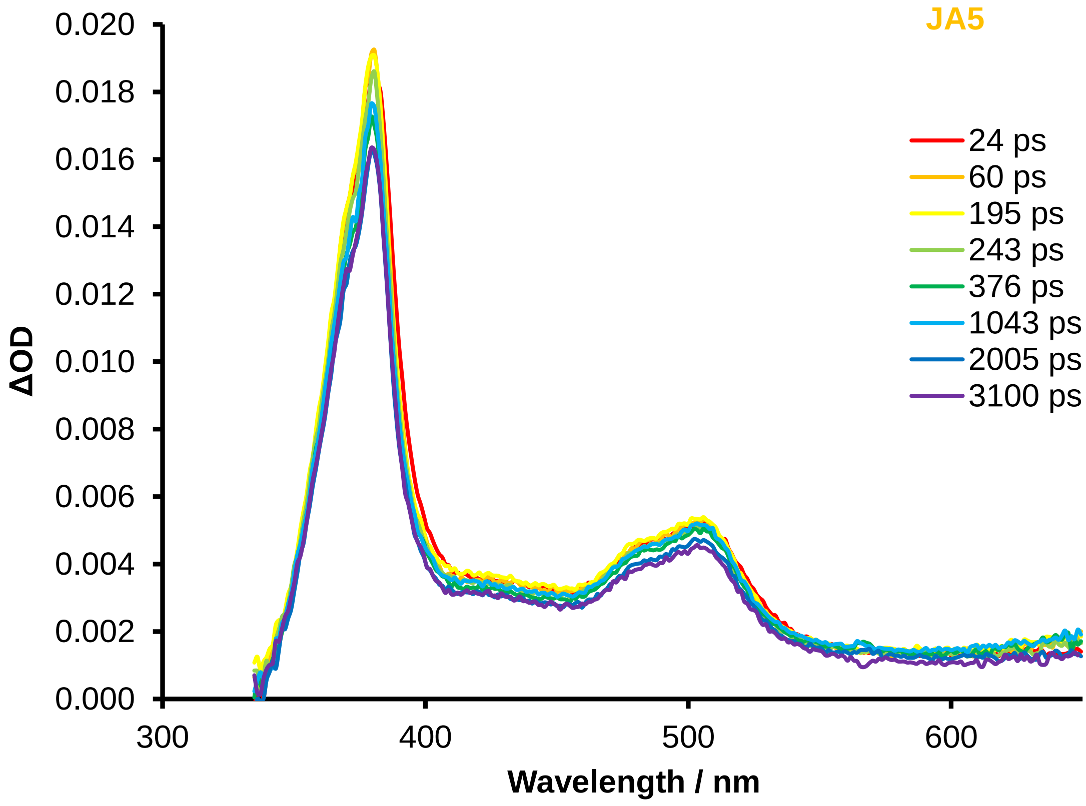

*Figure 3. 19 UV-visible transient absorption spectra for complex **JA5** in MeCN at 298K (λ_{ex} = 285 nm). Two excited state absorption maxima at 380 nm and 505 nm that are still present at the end of time window.*

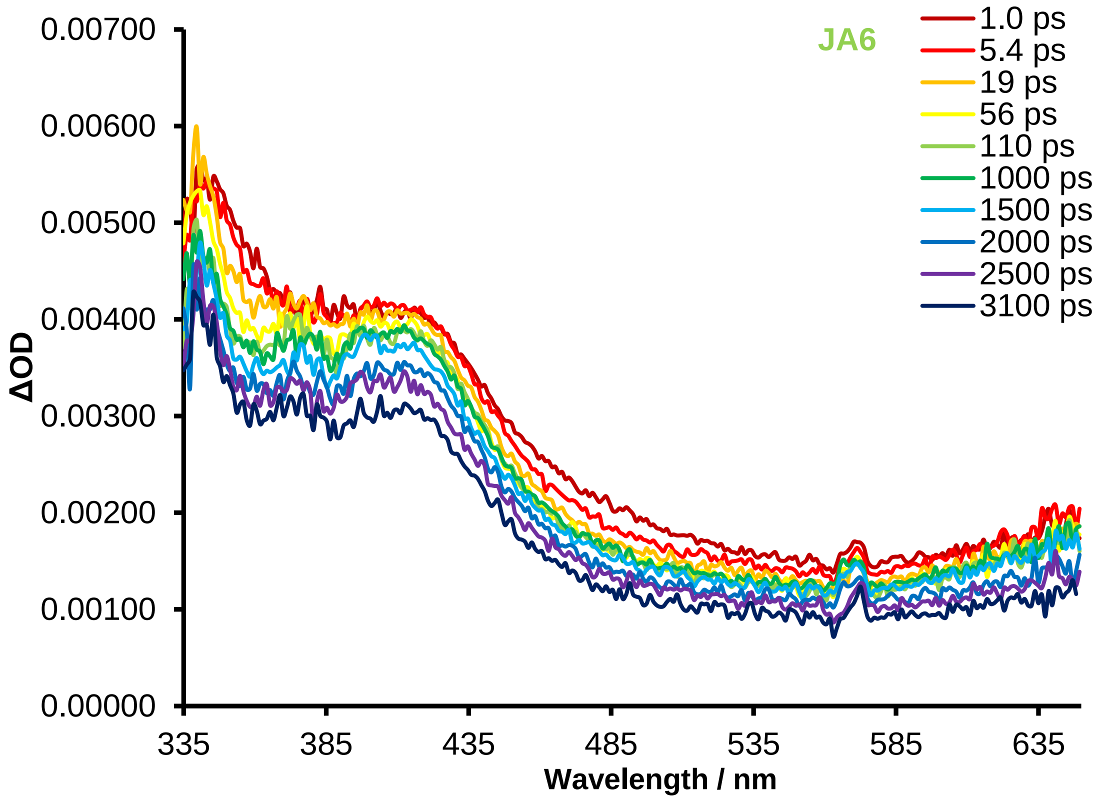

Figure 3. 20 UV-visible transient absorption spectra for complex ***JA6*** *in MeCN at 298K (λ_{ex} = 285 nm). Two excited state absorption maxima at 340 nm and 410 nm that are still present at the end of time window.*

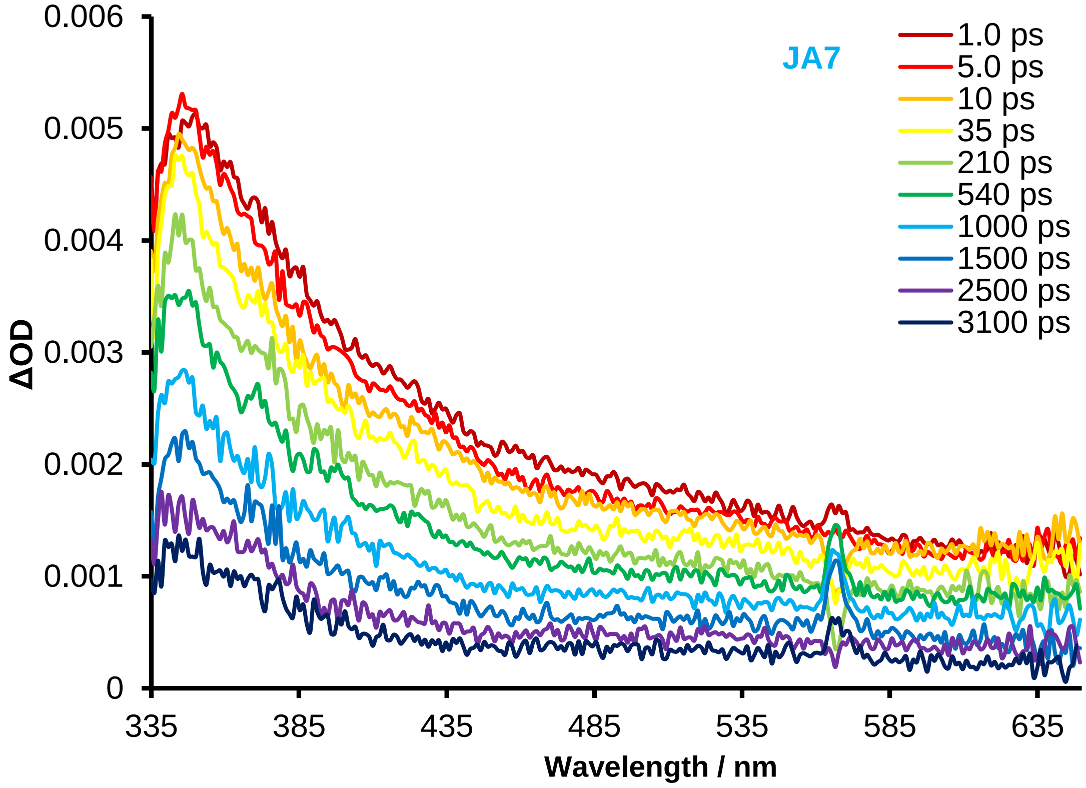

*Figure 3. 21 UV-visible transient absorption spectra for complex **JA7** in MeCN at 298K (λ_{ex} = 285 nm). Excited state absorption maximum at 345 nm which decays within the time window.*

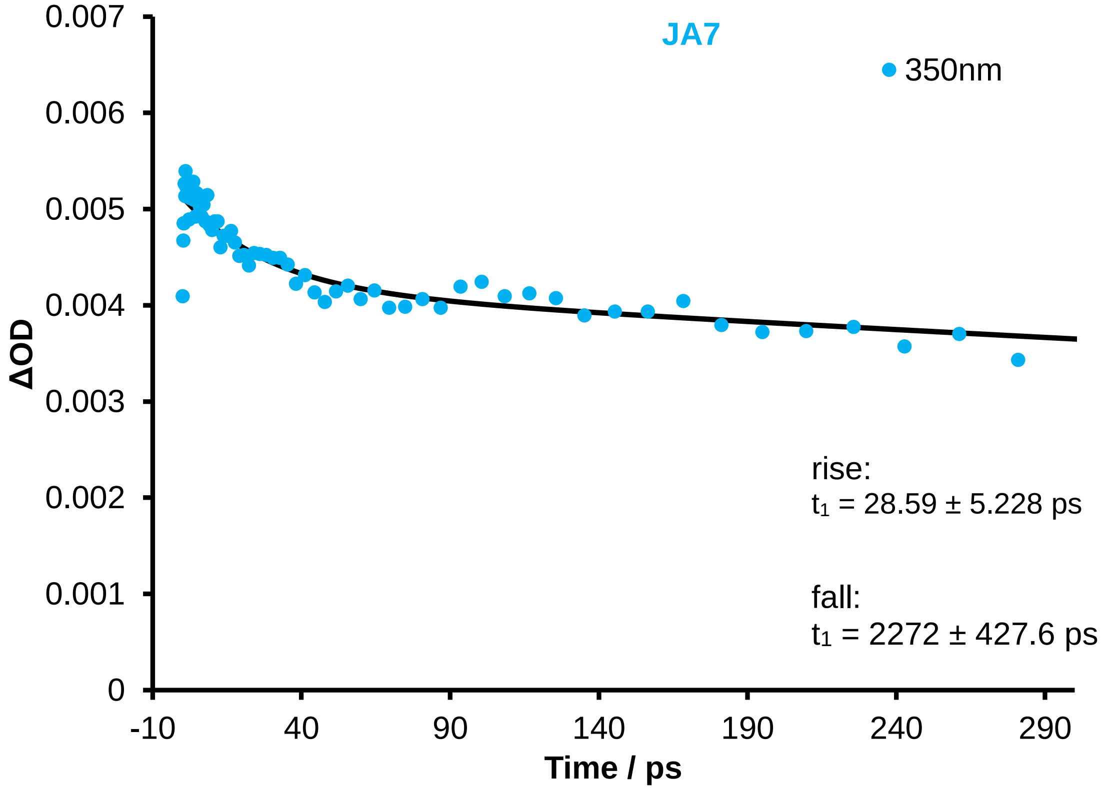

*Figure 3. 22 Time profile and kinetic fit from global analysis for associated transient absorption spectra for complex **JA7**.*

3. 5. DFT and TD-DFT Characterisation

To gain a better understanding of the electronic structure and photophysical properties of complexes **JA4-7** we conducted density function theory modelling, with a focus on geometry optimisation and frontier orbital patterns. Time-dependent DFT calculations were also carried out for UV-visible absorption spectra simulation. The DFT and TD-DFT calculations were carried out by my supervisor, Prof. Paul Elliott. The ground-state geometries of all the triazole containing complexes were optimised whilst substituting the benzyl groups with a methyl substituent, as the benzyl substituent is thought to have no/minimal impact on the photophysical properties, and the simplification allows for reduced computational cost.

Figure 3.23 and 3.24 displays the calculated energies for the frontier orbitals for all the complexes, figure 3.23 shows a depiction of the corresponding isosurfaces for these calculated orbitals. In this depiction the ground state HOMO and LUMO are shown, the HOMO for all the complexes is localised on the metal centre and cyclometalated dmppz ligand. Whilst the LUMO is localised on the N^N ancillary ligands for every complex. This further corroborates with the experimental data as all complexes showed broad emission that is a characteristic of ^{3}MLCT/LLCT.

In Figure 3.24 the calculated energies of the frontier orbitals are displayed as a molecular orbital diagram and the calculated energies for the HOMO, LUMO and dσ* antibonding orbital have been summarised in Table 3.5. The calculated HOMO energy levels remain roughly the same across this series, this was evidenced in the experimental findings as the HOMO is localised over the metal centre and the cyclometalated ppz ligand. The calculated LUMO energy level varies across the series as it is dependent on the ancillary N^N ligand, the btz complex **JA4** has the highest energy LUMO whereas the bpy complex **JA5** has the lowest energy LUMO. This is in agreement with the experimental data as the weaker σ-donor and poorer π-acceptor, triazole moiety, destabilises the LUMO relative to the pyridine moiety. This can be seen across the series as the number of pyridine moieties increases the further the LUMO is destabilised.

The calculated HOMO-LUMO energy gap (Table 3.5) agrees with the recorded electrochemical data, btz complex **JA4** reduction process was not within the observable window therefore would have the largest energy gap. Complexes **JA5-7** calculated data are in accordance with the E_{ox}-E_{red} energy gaps experimental data.

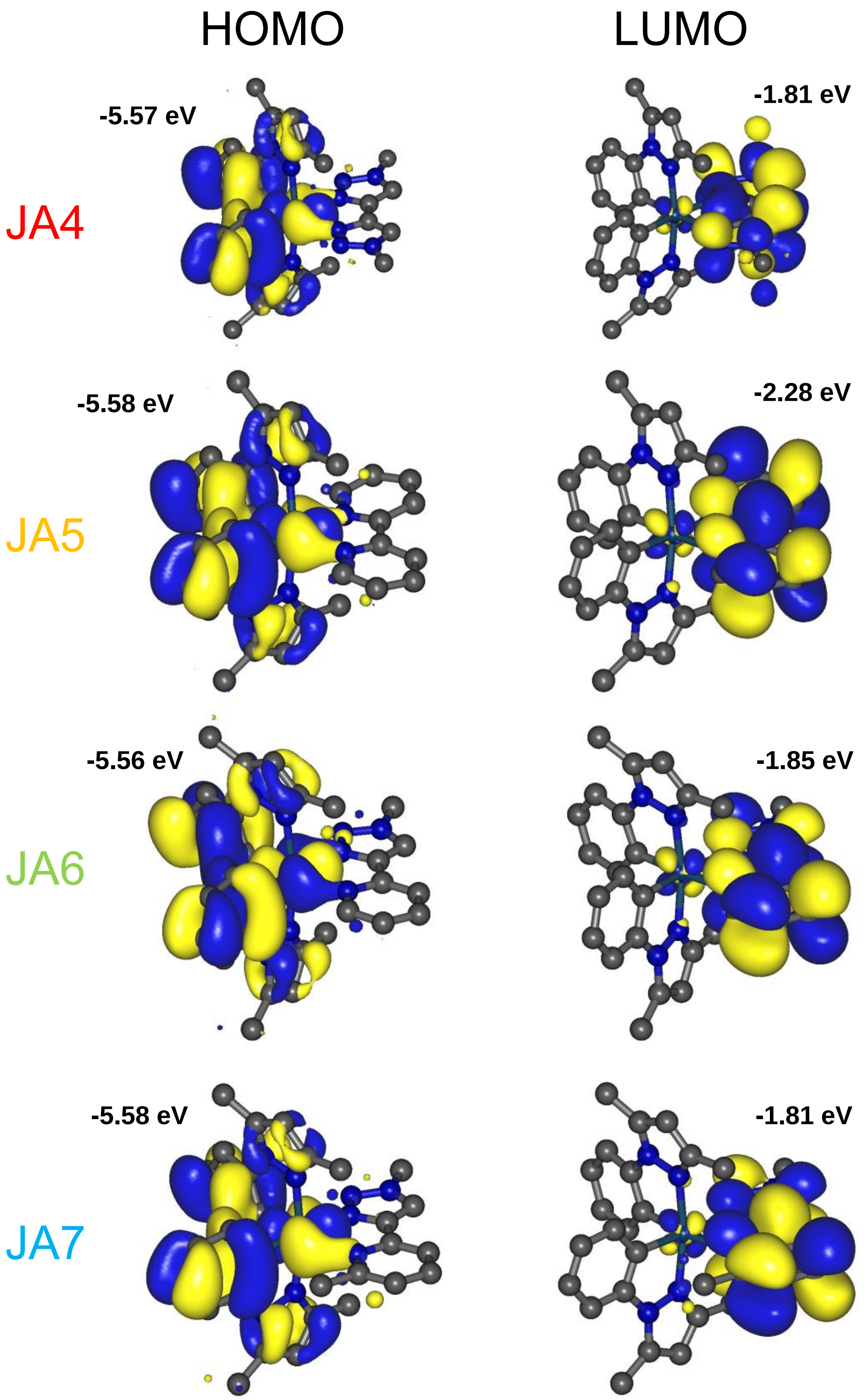

*Figure 3. 23 Ground state molecular orbital energy level diagram for complexes **JA4-7**, displaying the frontier orbitals on the isosurfaces.*

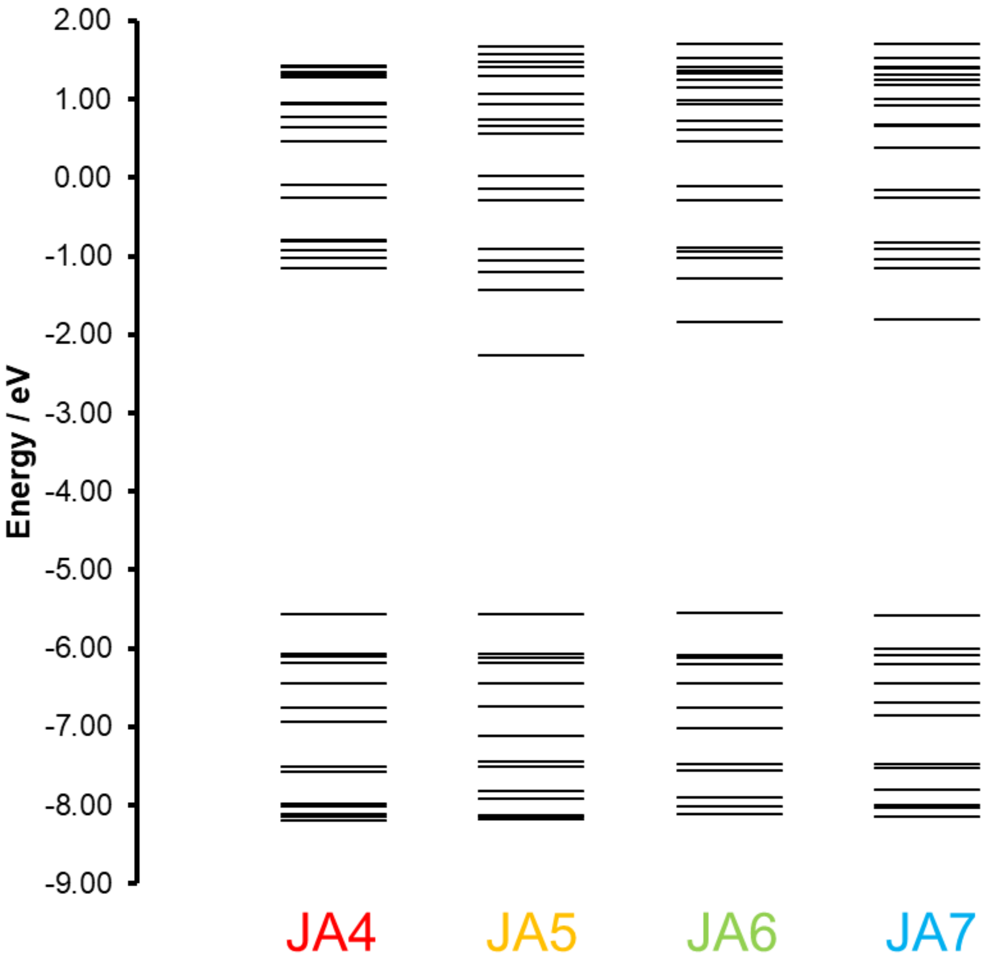

*Figure 3. 24 Molecular orbital energy level diagram for complexes **JA4-7**.*

The dσ* antibonding orbitals were calculated within the frontier orbitals and can be used as good indication of the effects of the MC states. When comparing analogous complexes **JA4** and **JA5** the dσ* antibonding orbital is lower in energy, and thus the MC states, for **JA4** than **JA5** as the triazole moieties have weaker σ-donation and are poorer π-acceptors than pyridyl moieties. The LUMO- dσ* energy gap is much lower for **JA4** then **JA5**, this further rationalises that the ^{3}MC states are thermally accessible from the LUMO of **JA4** as has been observed in the transient absorption and low quantum yields.

Complex **JA7**'s calculated dσ* antibonding orbital is the lowest in energy across the series as the methyl group's steric hindrance on the mpytz ligand significantly reduces energy for the MC states. This resulted in low quantum yields fast deactivation of the excited states as the ^{3}MC states are thermally populated.

Table 3.5 Summarised HOMO and LUMO Energy Values from DFT Calculations for Complexes JA4-7

Complex	HOMO (eV)	LUMO (eV)	dσ* (eV)	HOMO-LUMO Energy Gap (eV)	LUMO-dσ* Energy Gap (eV)
JA4	-5.57	-1.17	0.45	4.40	1.62
JA5	-5.58	-2.28	0.55	3.30	2.83
JA6	-5.56	-1.85	0.45	3.71	2.30
JA7	-5.58	-1.81	0.38	3.77	2.19

Time-dependent DFT (TD-DFT) calculations were performed on the optimised geometries of each individual complex to ascertain the vertical excitation energies (Figure 3.25). Simulated absorption spectra is overlaid against the predicted transitions, the simulated spectra are in agreement with the experimentally recorded data. In the calculations conducted, it has been observed that the excitations leading to the S_1 state in all the complexes predominantly exhibit HOMO→LUMO characteristics. Nonetheless, their oscillator strength remains relatively low, thereby resulting in minimal contributions to the absorption spectra. In accordance with Table 3.6 the S_1 absorption wavelength decreases with the number of triazole moieties present as is expected when looking at the experimental data and the DFT calculations. The primary transitions, within 300-400 nm, observed across all complexes are ^{1}MLCT in character.

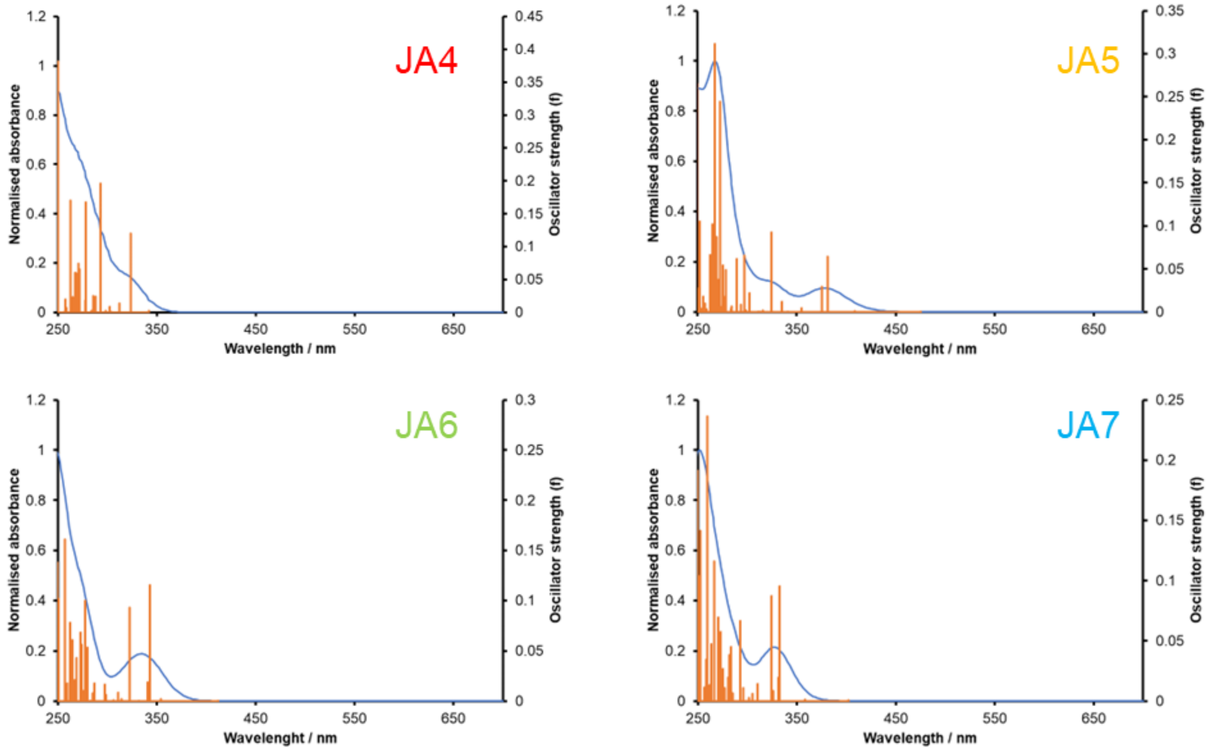

Figure 3. 25 TDDFT calculated absorption spectra for complexes ***JA4-7*** *with transition intensities.*

Table 3.6 Selected Energies (eV), Oscillator Strength (*f*), Wavelength (nm) and Compositions of Vertical Excitations from TDDFT Calculations.

Complex	Transition	Energy	λ	*f*	Composition	Character
JA4	S_1	3.63	342	0.0010	HOMO→LUMO 97%	MLCT/LLCT
	S_2	3.83	324	0.055	HOMO→LUMO+1 91%	MLCT/LC
	S_7	4.23	293	0.091	HOMO-2→LUMO 73%	MLCT/LLCT
JA5	S_1	2.61	475	0.00027	HOMO→LUMO 99%	MLCT/LLCT
	S_3	3.25	381	0.038	HOMO-3→LUMO 74%	MLCT/LLCT
					HOMO-2→LUMO 19%	MLCT/LLCT
	S_4	3.30	375	0.017	HOMO-3→LUMO 23%	MLCT/LLCT
					HOMO-2→LUMO 63%	MLCT/LLCT
	S_8	3.82	325	0.056	HOMO→LUMO+3 92%	MLCT/LC
JA6	S_1	3.01	412	0.00037	HOMO→LUMO 98%	MLCT/LLCT
	S_3	3.62	343	0.70	HOMO-2→LUMO 84%	MLCT/LLCT
	S_6	3.85	322	0.056	HOMO→LUMO+2 90%	MLCT/LC
JA7	S_1	3.08	402	0.00038	HOMO→LUMO 98%	MLCT/LLCT
	S_3	3.73	333	0.055	HOMO-3→LUMO 91%	MLCT/LLCT
	S_6	3.82	324	0.050	HOMO→LUMO+2 91%	MLCT/LC

3. 6. Conclusion

Complexes **JA4-7** exhibited some interesting photophysical properties. When the btz complex (**JA4**) is in the excited state it has thermal accessibility to the ^{3}MC states. The low quantum efficiency and rapid excited state lifetime, compared to analogous bpy complex (**JA5**), allude to this being the case. This is backed up by the DFT calculations that clearly showed the LUMO is destabilised considerably and is within much closer proximity of the ^{3}MC states than **JA5-7**. Interestingly, complex **JA7** also appears to potentially be thermally populating the ^{3}MC states, it has a considerably lower quantum yield and shorter lifetime than its analogous complex **JA6**. Even though **JA7** has very similar properties to **JA6** in terms of E_{ox}-E_{red} energy gap, absorption and emission bands, **JA7** thermally populates the ^{3}MC states and **JA6** does not. This is down the steric hinderance of the methyl group which stabilises the ^{3}MC states making them thermally accessible, this could be observed in the DFT calculations as the metal antibonding orbital, associated with the ^{3}MC states, had the lowest energy across the series of complexes.

This study has shown two potential pathways to populate ^{3}MC states for Ir(III) complexes which has helped us gain a better understanding of how to design ligand architectures for iridium complexes. It is important for the design of blue light emitting complexes to try and destabilise the Ir(III) ^{3}MC states and to not destabilise the LUMO excessively.

4. Development of Novel Ir(III) 3+2+1 Cyclometalated Complexes, [Ir(N^N^N)(C^N)Cl)]$^{+}$

4. 1. Introduction

As mentioned previously in Chapter 1, Ir(III) cyclometalated complexes have a wide range of potential applications from biomedical applications,[25] photocatalysis and developing light emitting devices such as OLEDs and LEECs.[68, 72, 140] The properties of these complexes are what allow for such a variety of applications; long excited-state times, high phosphorescence quantum efficiency, tunability and ability to be synthesised with a wide range of ligands.[139] These properties all stem from the phosphorescence nature of the complexes, the ISC from strong spin-orbit coupling.

Cyclometalted Ir(III) complexes have a large field splitting which makes thermal population of deactivating metal states (^{3}MC) unlikely.[133] In comparison Ru(II) complexes are limited by an energy ceiling as they have lower lying ^{3}MC states which can be thermally populated readily,[63, 78] limiting their functionality. The heteroleptic structure, $[Ir(ppy)_2(bpy)]^+$, and its derivatives are the most popular species as they are excellent luminophores, photosensitizers and photocatalysts.[142] Due to the spatial separation of the HOMO and LUMO, the energies of each orbital can be individually modulated via ligand modifications. A drawback for these heteroleptic species is when the charge transfer populates the π^* orbitals of the diimine ligand it becomes a source of photodegradation.[198]

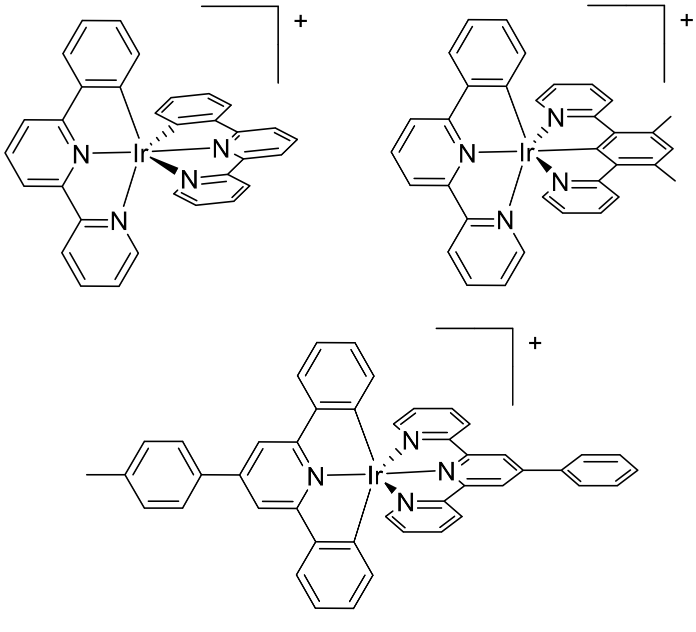

Bernhard et al.

Figure 4. 1 Ir terdentate complexes reported by Bernhard and co-workers.[199]

Bernhard and co-workers,[199] looked to develop a species of tridentate Ir(III) cyclometalted complexes to avoid the aforementioned problem by situating the LUMO on more stable tridentate ligands.[200] A series of complexes were developed (Figure 4.1), and this improved the photostability leading to long excited state lifetimes and spatial separation of the frontier orbitals similar to that of the $[Ir(ppy)_2(bpy)]^+$ complexes. However, these complexes required more complex preparation routes due to multiple binding sites and are less tuneable than complexes with bidentate ligands. The tridentate ligands have more widespread π-systems making it more challenging to modify them and in addition straightforward, synthetically accessible, changes have less of an effect.[201] Bernhard and co-workers, explored the structure of $[Ir(N^{\wedge}N^{\wedge}N)(C^{\wedge}N)L]^+$ complexes as it was a relatively unexplored chemical space which could combine the stability of tridentate ligands for the LUMO and tunability of the bidentate coordinated ligands where the HOMO would be situated.[67, 75] Sato and co-workers initially looked at $[Ir(tpy)(ppy)Cl]^+$ as a photocatalyst but had not fully characterised its photophysical and electrochemical properties,[202] therefore Bernhard and co-workers looked to expand on this and design derivatives which led to the series shown in Figure 4.2.[203] This series exhibited excellent photophysical properties, PLQY up to 28.6 % and lifetimes of 3 μs, also showing the tunability of the complexes via ligand modification. The complexes also showed great potential for use as a photosensitiser as they are more robust than their $[Ir(ppy)_2(bpy)]^+$ counterparts due to the tridentate ligand.[198, 200, 201]

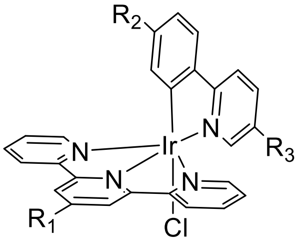

R_1:	R_2:	R_3:
H	H	H
H	F	Me
H	MeO	Me
Ph	F	Me
Ph	MeO	Me

Bernhard et al.

Figure 4. 2 Ir 3+2+1 complexes designed by Bernhard and co-workers. [203]

Sadler and co-workers,[204] developed a photocatalytic Ir(III) complex, which has the same structure as $[Ir(N^{\wedge}N^{\wedge}N)(C^{\wedge}N)L]^+$, for use as in photodynamic therapy (PDT). Platinum compounds are the most commonly used anticancer drugs used at the moment however new metal-based anticancer agents are needed to reduce side effects and to beat drug resistance,[205] hypoxia is one of the main causes of resistance as most types of PDT relies on oxygen for its mechanism of action. Sadler and co-workers,[204] photocatalyst was photostable and had long phosphorescence lifetimes. It was reported to perform in-cell photocatalytic oxidation of NADH with a very high turnover frequency (TOF). The complex not only generated $NAD^{\bullet}$ free radicals but also reduced Fe^{3+}-cytochrome c, which disturbed electron transfer pathways in mitochondria, a combination of both effects caused a redox imbalance in the cancer cells.[114] The Ir(III) complex worked equally well in normoxic and hypoxic cancer cells by disrupting the mitochondrial membrane potential leading to immunogenic apoptic cell death. In addition to the excellent PDT characteristics the complex showed low toxicity to normal cells that were in the dark, which suggest it would have a reduced amount of side effects. Sadler and co-workers, work showed that the species of [Ir(N^N^N)(C^N)L]$^+$ complexes has great potential as PDT agents.

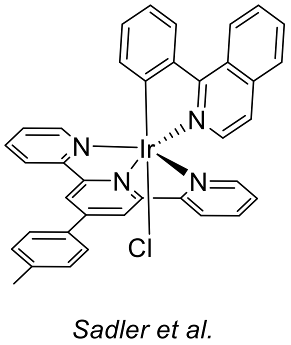

Figure 4. 3 Ir complex reported by Sadler and co-workers for utilisation as a PDT agent. [204]

Bernhard and co-workers,[206] reported a series of [Ir(N^N^N)(C^N)L]$^+$ complexes (Figure 4.3) that were used to investigate the selectivity of C-F/C-H activation and develop novel photocatalytic luminophores. The complexes were designed to have electron rich tri-*tert*-butyl terpyridine ligand as the LUMO and then alternate the number of F moieties on the phenylpyridine ligand, where the HOMO was, to observe the effects on the orbital and photophysical properties. This series of complexes exhibited excellent photophysical properties with PLQY ranging from 69.3-41.4 % with excellent lifetimes >3 μs, as well as showing a reasonable range of tunability with λ_{em} = 470-537 nm. These complexes were also reported to have good photosensitiser capabilities for decarboxylation fluorination of carboxylic acids as two of the complexes achieved remarkably better yields than the leading photosensitiser for the reaction.

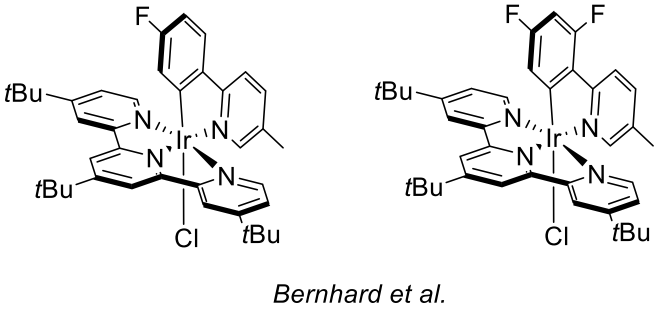

Figure 4. 4 Ir 3+2+1 complexes developed by Bernhard and co-workers. [206]

4. 1. 1. Aim and Objectives

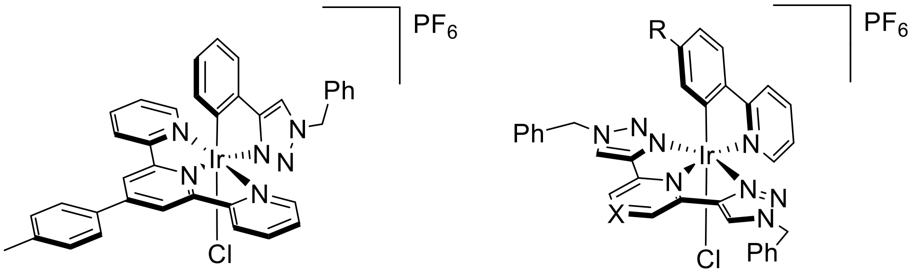

JA8

JA9 R=H X=H
JA10 R=H X=N
JA11 R=F X=H
JA12 R=F X=N

*Figure 4. 5 Ir complexes designed to investigate novel chemical spaces with triazoles, **JA8-12**.*

This piece of work will be to further investigating the [Ir(N^N^N)(C^N)L]$^+$, where L is a monodentate anionic ligand, complex structure as it is still a relatively unexplored chemical space with great potential. Whilst the anionic ligand (L) has been investigated as Cl or CN, this study will focus on Cl based complexes. It will be following these objectives:

- Will look to further expand on the work of Bernhard and co-workers as they illustrated the excellent photophysical properties these complexes can achieve through tuning of the ligands and modifying the frontier orbitals, and that they have potential to be used as photosensitisers.
- Explore the used of triazole moieties within this field as it is completely novel unexplored chemical space. Utilise the moieties on the cyclometalated ligand and the ancillary N^N^N ligand. Triazoles are readily available, synthetically, therefore could potentially facilitate a wide range of modification to these complexes. Complexes **JA8-12** (Figure 4.5) have been designed to incorporated triazoles throughout the chemical space.

4. 2. Synthesis of Ligands

4. 2. 1 Synthesis of ptz-bn

Ptz-bn was prepared via a copper(I)-catalysed alkyne-azide cycloaddition. Starting materials phenylacetylene, benzyl azide, copper sulphate, potassium carbonate, sodium ascorbate and a solvent mixture containing water, *tert*-butanol, tetrahydrofuran and pyridine were combined. The mixture was left to stir at room temperature for 16 h. After the work up the product were afforded with good yields of 78 %. The compound was characterised by ^{1}H NMR spectroscopy, ^{13}C NMR spectroscopy, and electrospray ionization mass spectrometry (ESI-MS).

4. 2. 2. Synthesis of tz-py-tz and tz-pyz-tz

The tz-py-tz and tz-pyz-tz ligand were prepared through a two-step process (Scheme 4.1). The first step (a) is a Sonogashira coupling to attach the acetylene moieties to the pyridine, this allows for the "click" CuAAC reaction to take place, which is step b, and affords the target ligands.

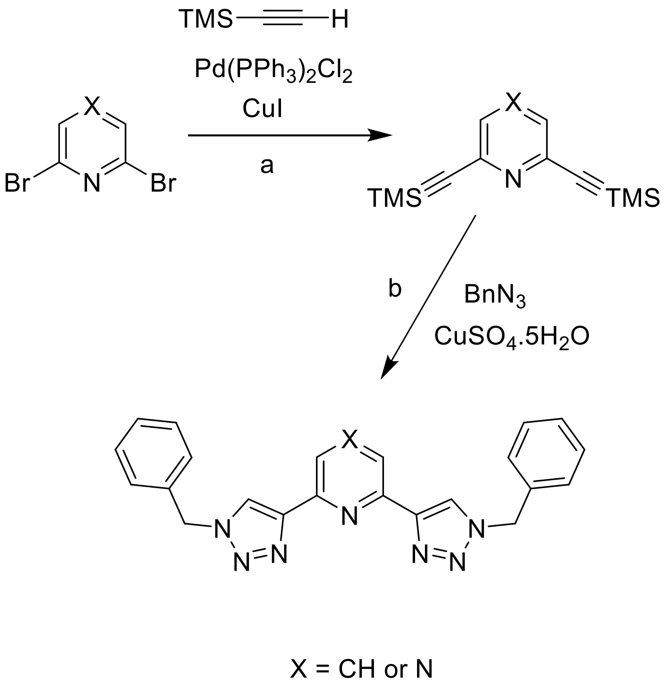

Scheme 4. 1 Synthetic procedure for tz-py/z-tz ligands, a) Sonogashira coupling that afford the pyridine/pyrazine compound with protected acetylenes. b) A "click" CuAAC reaction using the acetylenes and the benzyl azide to produce the target ligand.

4. 3. Synthesis and Characterisation of Iridium Complexes

For the complexes to be prepared (Scheme 4.2), an intermediate trichloride complex had to be made for all the N^N^N ligand. The ligand was heated to reflux with $IrCl_3.XH_2O$ in ethylene glycol to afford the $Ir(N^\wedge N^\wedge N)Cl_3$. Following on from that the cyclometalating, C^N, ligand and the $Ir(N^\wedge N^\wedge N)Cl_3$ were combined and brought to reflux for 20 h, after the work up this afforded the desired products. The products were purified by silica chromatography, complexes were confirmed by ^{1}H NMR spectroscopy and ESI-MS.

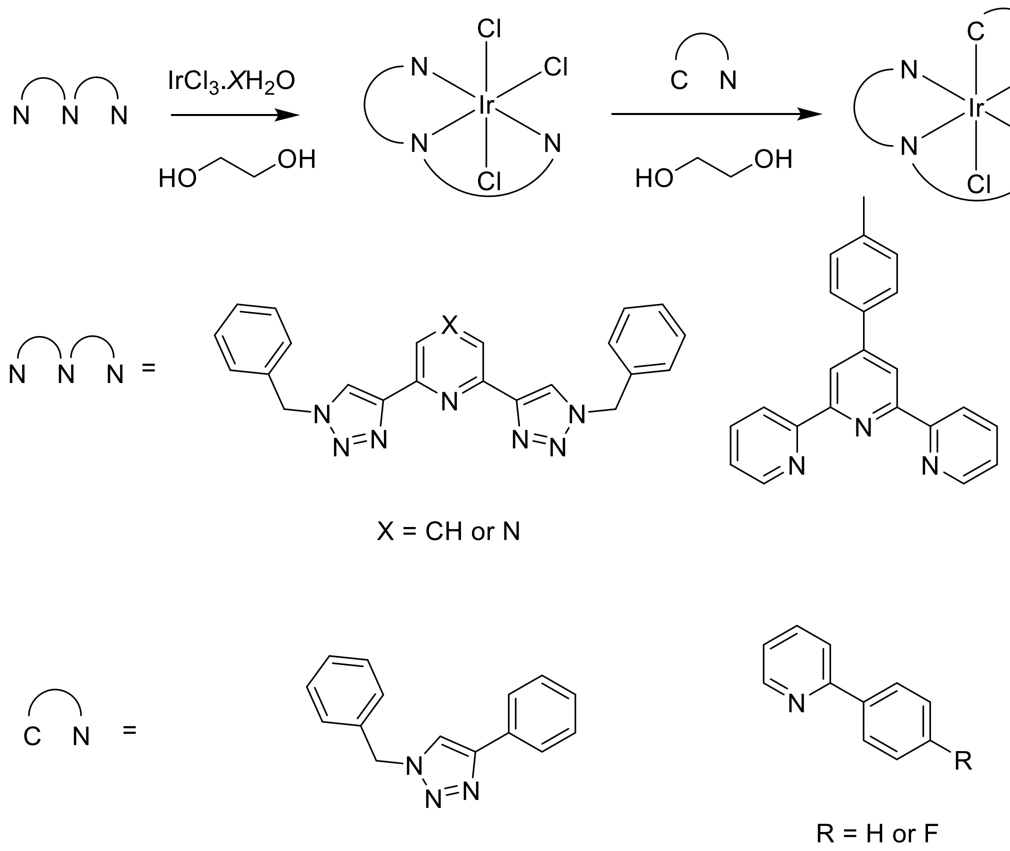

Scheme 4. 2 Synthetic process for these [Ir(N^N^N)(C^N)Cl]$^+$ complexes, initial trichlorides are prepared, then the desired complexes are afforded.

The complex design [Ir(N^N^N)(C^N)Cl]$^+$ has two possible stereoisomers, where the cyclometalated carbon on ppy is trans to the Cl or trans to the N^N^N ligand. As reported by Haga and co-workers,[207] heating the reaction to high temperatures promotes selectivity for the cyclometalated carbon to be trans to the Cl. As the complexes were refluxed in ethylene glycol it is expected that complexes will be this stereoisomer. The ^{1}H NMR spectra for this series further confirm that the Ir-C on ppy is trans to the Cl. The neighbouring proton to the nitrogen on the ppy ligand, for complexes **JA9-12**, is de-shielded and the chemical shift is much further downfield δ 9.89-9.94. This is a result of the deshielding effect of the Ir-Cl bond, this would only occur in this stereoisomer. This is due to the Ir-Cl bond neighbouring the proton on the pyridine moiety of the cyclometalated ppy ligand. Similar complex structures have been reported by Bernhard and co-workers where they confirmed the structure through x-ray crystallography.[203]

Interestingly when trying to synthesise the fluorinated complexes dfppy was used as the cyclometalating ligand but would only produce the monofluorinated ligand. This is due to C-F bond activation, which has become a synthetic route of interest for fluorinated organic compounds and for transition metal complexes that are fluorinated.[206] C-H bond activation has been shown to be typically the favoured activation process over C-F for second and third row transition metals.[208] This is expected to be due to the higher kinetic barrier for C-F bond even though C-F activation is energetically favourable,[209] although some Rh and Ir complexes have been reported to have C-F activation over C-H activation. The selectivity between C-F and C-H activation is affected by factors such as the oxidation state of the metal centre and the kinetic versus thermodynamic preference of the products.

4. 4. Electrochemistry

Cyclic voltammograms were recorded for complexes **JA8-12** (Figure 4.6, Table 4.1), in MeCN, to investigate their electrochemical properties. All complexes show one irreversible oxidation between +1.28-1.47 V and multiple reduction processes.

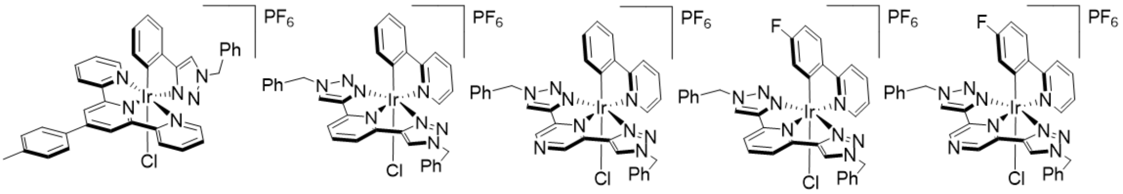

JA8 JA9 JA10 JA11 JA12

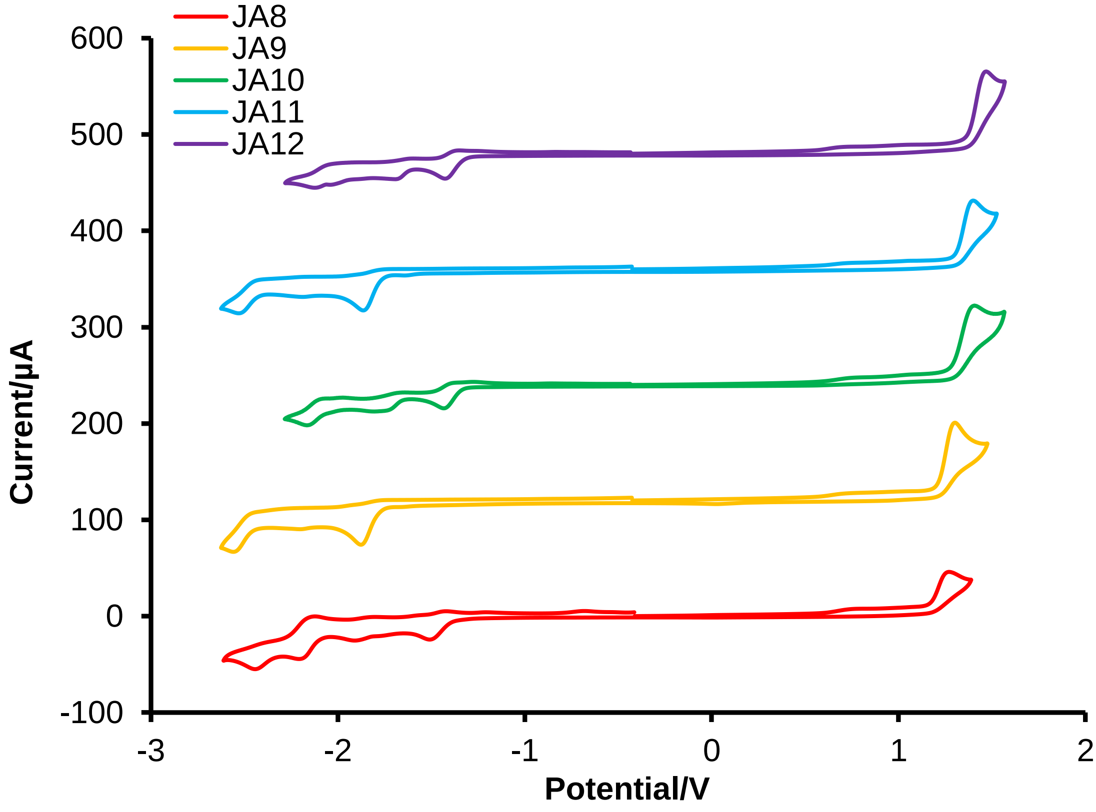

*Figure 4. 6 Cyclic Voltammograms of complexes **JA8-12**. Recorded in MeCN using Fc+/Fc as an internal standard, NBu_4PF_6 was used as the supporting electrolyte with a solution concentration of 0.2 $moldm^{-3}$. Measurements were performed under an atmosphere of N_2 at a scan rate of 100mV s^{-1}.*

The oxidation potential observed of these complexes can be assigned to the removal of an electron from the HOMO, resulting in the irreversible oxidation of Ir(III)→Ir(IV).[85, 186, 200] The HOMO was thought to be centred on a combination of the metal and the cyclometalated ligands as seen in other octahedral cyclometalated Ir(III) complexes.[72, 139] The effect on the HOMO is negligibly affected using ptz instead of the more ever-present ppy cyclometalated ligand as seen when comparing **JA8** and **JA9**. The N-coordinated moiety of the cyclometalating ligand does not or only marginally effects the HOMO on the cyclometalated ligand. The mono-fluorination of the cyclometalating phenyl ligand resulted in an anodic shift of the oxidation potential, this can be seen between **JA9** and **JA11** (+1.30 V to +1.40 V), and between **JA10** and **JA12** (+1.41 V to +1.47 V). The anodic shift upon fluorination of the phenyl moiety further confirms the localisation of the HOMO on the cyclometalated ligand and the metal centre. The anodic shift occurs due to the stabilisation of the HOMO by the electron withdrawing effect of the fluorine group. It is important to note the anodic shift of the oxidation peaks between the pyridyl complexes (**JA9+11**) and their analogous pyrazine complexes (**JA10+12**), the increase in potential was assumed to be a result of the electron withdrawing effect on the pyrazine leading to an electron deficient metal centre.

All complexes undergo multiple reduction processes, the reduction assumes a gain of an electron therefore the first reduction often corresponds to the LUMO. Complex **JA8** has an initial irreversible reduction process at -1.55 V that can be assigned to the polypyridyl tol-terpy ligand. The following reductions are also all assigned to be on the tol-terpy ligand as the two more of the pyrdine moieties and the tolyl moiety. The triazole cyclometalated N-donor ligand is shifted too low to appear within the solvent window. Complexes **JA9** and **JA11** have nearly identical reduction potentials, the first reduction at -1.88 V and -1.86 V are assigned to the reduction of the pyridyl moiety in the tz-py-tz ligand, with the second reductions at -2.56 V and -2.53 V respectively being the N-donor pyridine moiety on their respective cyclometalated ligands. Correspondingly the analogous pyrazine complexes **JA10** and **JA12** also have comparable reduction potentials, the first reduction potentials at -1.43 V, for both, is assigned as the pyrazine moiety on the tz-pyz-tz ligand. The second and third reductions are not defined, the third reduction suspected to be the pyridyl moiety on the ppy cyclometalating ligand.

When comparing the initial reductions of **JA8** and **JA9,** there is a significant cathodic shift for **JA9** of about 370 mV. The substitution of pyridine moieties, on the ancillary terdentate ligand, with triazoles destabilises the LUMO due to their poor π-accepting abilities this effect has been reported by a number of groups.[62, 189] Assessing the effect on the reduction potentials between the alternate pyridine (**JA9+11**) and pyrazine (**JA10+12**) moieties, on the terdentate ligand, show a considerable anodic shift for the pyrazine complexes. The pyrazine complexes initial reduction showed and increase in potential by 430-450 mV, this substantial shift is due to the electron withdrawing nature of the pyrazine resulting in a more stabilised LUMO. Similar effects have been reported when comparing pyridine and pyrazine $[Ir(C\string^N)_2(N\string^N)]^+$ complexes.[210]

Table 4.1 Summarised Electrochemical Data for 1.5mmol dm^{-3} MeCN Solutions of JA8-12 Measured at r.t.at 100mV s^{-1}.^{a,b}

Complex	Oxidation (V)	Reduction (V)	E_{ox}-E_{red} Energy Gap (V)
JA8	+1.28	-1.51, -1.91, -2.21, -2.41	2.79
JA9	+1.30	-1.88, -2.56	3.18
JA10	+1.41	-1.43, -1.73, -2.17	2.84
JA11	+1.40	-1.86, -2.53	3.26
JA12	+1.47	-1.43, -1.69, -2.12	2.90

a) Potentials are shown in V vs Fc+/Fc. Reversible couples E1/2 is quoted with anodic-cathodic peak separation shown in mV in brackets. b) NBu_4PF_6 was used as the supporting electrolyte with a solution concentration of 0.2 moldm^{-3}.

The energy gap between the oxidation and the reduction can be associated with the HOMO-LUMO energy gap. This allowed for predictions of how complexes **JA8-12** will behave photophysically. The lowest energy gap, **JA8**, was predicted to have the greatest red shifted emission band. The pyrazine-based complexes **JA10** and **JA12** have the are the next lowest energy band gaps and will correspondingly have the next furthest red shifted emission, this is anticipated as the electron withdrawing effects of the pyrazine have monumental effect on the stability of the LUMO. The tz-py-tz complexes **JA9** and **JA11** have the largest energy gap, as the LUMO is destabilised by the triazole moieties. The fluorinated complex **JA11** has an even greater energy gap, and thusly is the furthest blue shifted, due to the electron withdrawing effect on the HOMO causing further stabilisation.

4. 5. Photophysical Properties

Table 4.2 Summarised Photophysical Data for MeCN Solutions of JA8-12 at 298 K

Complex	λ^{abs}/nm^{a}	λ^{em}/nm^{a}	λ^{77K}/nm^{b}	ϕ/%^{c,d}	τ/ns^{c}	10^4 kr/s^{-1} ^{c}	10^5 k_{nr}/s^{-1} ^{c}
JA8	233, 284, 310, 370sh, 398, 508	563	537, 578, 632sh	9.1	1671	54	5.4
JA9	230, 282sh, 350	510	452, 485, 512sh, 525sh	0.3	701	0.43	14
JA10	230, 266sh, 342, 466	612	511sh, 534	1.8	3960	0.45	2.5
JA11	227, 264sh, 339	505	445, 478sh, 505sh, 516sh	<0.1	-	-	-
JA12	230, 264sh, 327sh, 340, 458	570	497sh, 523	1.3	3564	0.36	2.8

a) MeCN, aerated at 298K b) EtOH:MeOH (4:1) glass at 77K c) MeCN deaerated at 298K d) PLQY, [Ru(bpy)$_3$]2(PF$_6$) in MeCN was used as relative standard.

4. 3. 1. Electronic UV-Vis Absorption Spectroscopy

All complexes **JA8-12** exhibit UV-visible absorption spectra in MeCN solutions at room temperature (Figure 4.7). The photophysical data is summarised in Table 4.2. Absorption bands that were observed <300 nm were assigned as ligand centred (π→π*) transitions for all the complexes. Aside from complex **JA1**, which has a significantly different absorption profile, all the complexes displayed lower energy absorption bands between 320-400 nm which were ascribed as a combination of ^{1}MLCT/^{1}LLCT transitions, these bands are $S_0 \rightarrow S_1$ which primarily come from the Ir(III) d orbitals. These complexes also have a long tail that extends more into the visible region. These bands are direct population of the triplet excited states, $S_0 \rightarrow T_1$.

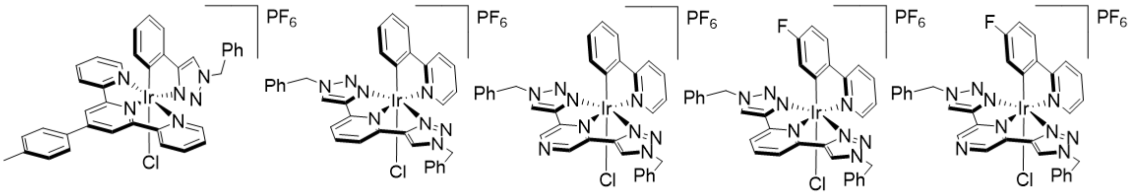

JA8 JA9 JA10 JA11 JA12

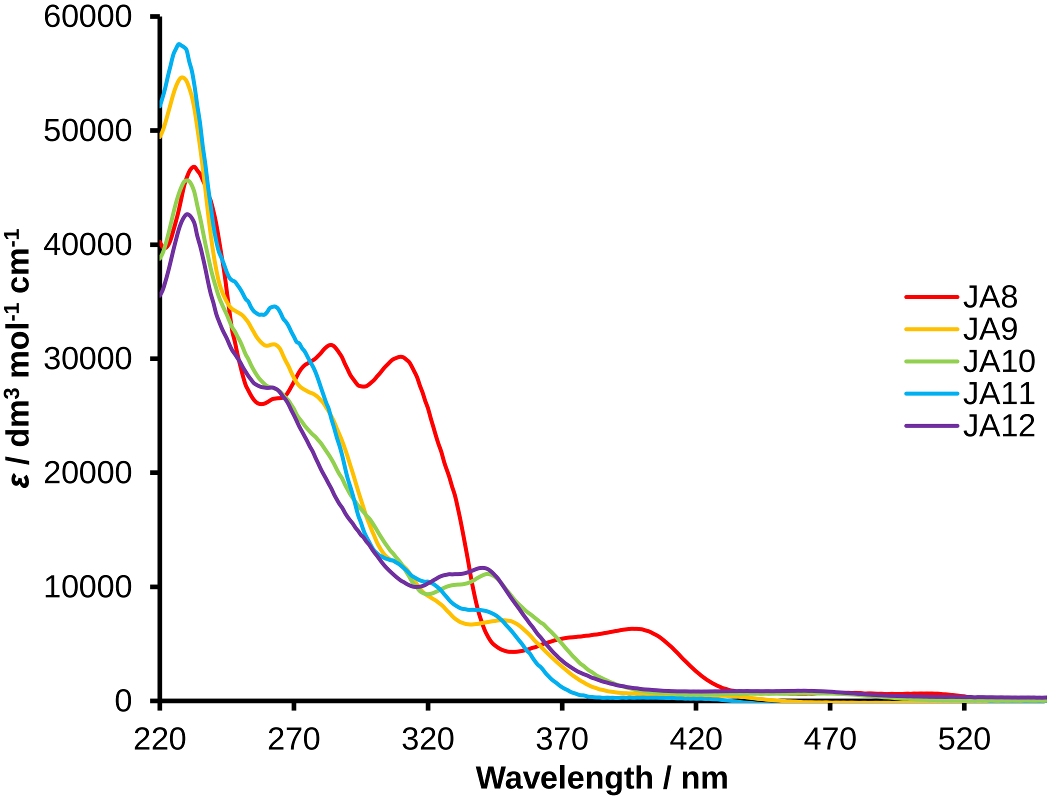

*Figure 4. 7 UV-visible absorption spectra recorded for **JA8-12** complexes. Recorded in MeCN at 298K*

Complex **JA8** has two very strong and well resolved high energy bands, UV, at 284 nm and 310 nm, these are assigned as ligand centred transitions, $\pi\rightarrow\pi^*$. In the lower energy, visible region, the complex shows a strong absorption band at 398 nm and a shoulder peak at 370 nm. These transitions, similar to the triazole complexes, are predominately ^{1}MLCT transitions ($S_0\rightarrow S_1$). There is also an extended tail band that has maxima at 508 nm, these are ^{3}MLCT transitions ($S_0\rightarrow T_1$). Terdentate [Ir(tol-dppy)(tol-terpy)]$^+$ complex reported by Scandola and co-workers showed a very similar absorption profile to **JA8**,[211] with two strong ligand centred bands in the UV at 280 nm and 320 nm and with metal centred transitions between 435 and 515 nm. **JA8** has significantly red shifted absorption bands compare to the triazole terdentate complexes. This was to be anticipated to an extent as the electrochemical data showed it had the smallest E_{ox}-E_{red} energy gap, insinuating it has the smallest HOMO-LUMO energy gap.

Complexes **JA9-12** correspond to similar reported Ir triazole complexes where the ^{1}MLCT absorption band are observed between 300-400 nm.[84, 95] The transitions higher in energy <300 nm correspond to the ^{1}LC absorptions, these absorption profiles are similar to analogous $[Ir(tpy)(ppy)Cl]^+$ reported by Bernhard and co-workers.[203] Altering the π system on the terdentate ligand has a substantial effect on absorption profile whereas modifying the N-donor on the cyclometalated ligand has no substantial effect. This explains why the two strong LC bands in the UV are not present in **JA2-5** as the non-aromatic triazoles reduce the intensity of $\pi \rightarrow \pi^*$ transitions.

4. 3. 2. Emission Spectroscopy

Room temperature emission spectra were recorded for complexes **JA8-12** in MeCN. The normalised emission profiles of the complexes in aerated solution were compared in Figure 4.8 and the photophysical properties were listed in Table 4.2. The relative photoluminescent quantum yields and lifetimes were recorded in deaerated solution of MeCN. The photoluminescent quantum yields were calculated from the relative standard (ϕ_{rel}), $[Ru(bpy)_3][PF_6]_2$ which has an absolute quantum yield of 1.8 %. The calculations used the emission spectra that were excited at the following wavelengths of excitation; λ_{ex} = 350 nm for **JA9** and **JA10**, λ_{ex} = 355 nm for **JA11** and **JA12**, and λ_{ex} = 400 nm for **JA8**.

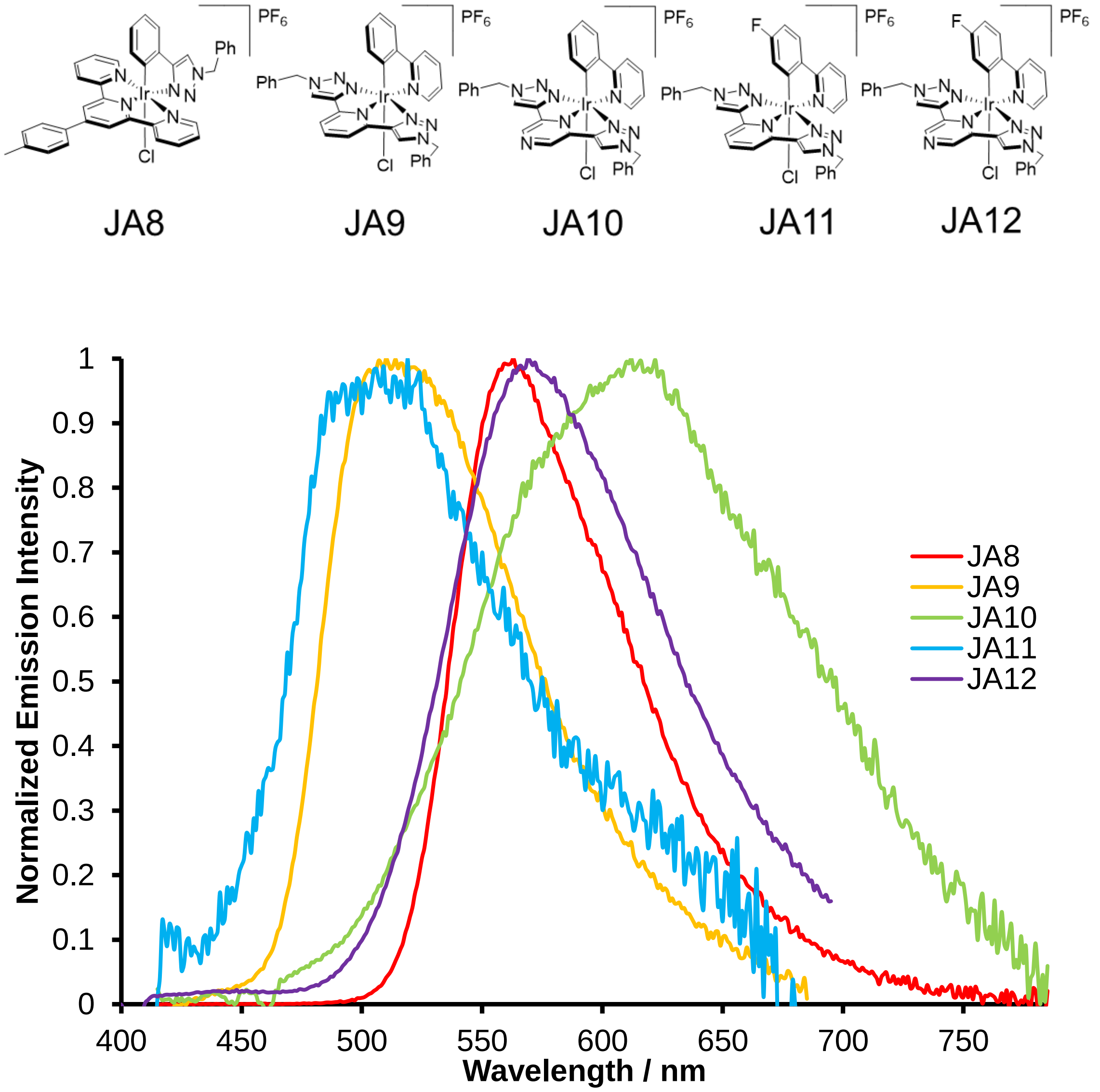

*Figure 4. 8 Emission recorded for **JA8-12** complexes. Recorded in aerated MeCN at 298K. Wavelengths of excitation; λ_{ex} = 350 nm for **JA9** and **JA10**, λ_{ex} = 355 nm for **JA11** and **JA12**, and λ_{ex} = 400 nm for **JA8.***

All complexes have broad band emission profiles which are indicative of ^{3}MLCT/^{3}LLCT character in aerated solutions, similar to reported [Ir(ppy)$_2$(bpy)]$^+$ and [Ir(dppy)(terpy)]$^+$.[66, 201, 211] Complex **JA8** observed a broad yellow/orange emission band, λ_{max} = 563 nm, with respectable quantum efficiency of ϕ_{rel} = 9.1% and a relatively long excited state lifetime τ = 1.7 μs, recorded in a deaerated solution. These photophysical properties are admirable and allow for potential applications in light emitting devices. Complex **JA8** is comparable to the ppy based analogue reported by Bernhard and co-workers,[212] [Ir(tpy)(ppy)Cl]$^+$. Bernhard's complex had λ_{max} = 541 nm, excellent quantum efficiency ϕ = 15.0% and a relatively long excited state lifetime τ = 1.7 μs. Complex **JA8** is slightly red shifted compared to [Ir(tpy)(ppy)Cl]$^+$ this is down to the tol-terpy N^N^N ligand as there is further conjugation on the ancillary ligand which has shown to stabilise the LUMO and red shift emission in multiple Ir(III) based complexes.[211] Interestingly **JA8**'s emission band is not the lowest in energy as had been expected from the E_{ox}-E_{red} energy gap in the electrochemical data.

The tz-py-tz complexes **JA9** and **JA11** have the highest energy emission bands, λ_{max} = 510 nm and 505 nm respectively, emitting in the blue/green region. Both complexes were only weakly emissive with low quantum efficiencies, **JA10** ϕ_{rel} = 0.3% and **JA11** ϕ_{rel} = <0.1%, the excited state lifetime recorded for complex **JA9** was a moderate τ = 701 ns. The excited state lifetime was not observed for **JA11** due to its weak emissive properties. The high energy emission bands correspond to the electrochemical data reported as these complexes has the highest energy gaps, furthermore the fluorination and thus stabilisation of the HOMO further blue shifted the emission in **JA11** compared to **JA9**.

The tz-pyz-tz complexes **JA10** and **JA12** observed lower energy emission bands in the orange/red region of the visible spectrum, λ_{max} = 612 nm and 570 nm respectively. These complexes were moderately efficient emitters with quantum yields of ϕ_{rel} = 1.8% and 1.3% and relatively long lived excites state lifetimes, τ = 4 μs and 3.6 μs respectively. The pyrazine complexes were expected to show lower energy emission bands than their pyridine counterparts as had been shown in the electrochemical data. Similar to the pyridine counterparts the fluorinated complex is blue shifted due to the stabilisation of the HOMO.

Williams and co-workers developed a series of Ir(III) 1,2,4-triazole terdentate analogous complexes, $[Ir(N^{\wedge}C^{\wedge}N)(R\text{-}Tz\text{-}Py\text{-}Tz\text{-}R)]^{+}$.[213] This series of complexes was only weakly emissive as the non-radiative processes were more efficient. This was theorised to be due to the weak ligand field offered by the triazoles resulting in intensifying non-radiative decay through the d-d states. The same reasoning likely applies here to explain why complexes **JA9-12** are relatively weak emitters, this is further confirmed as the lower energy emitters **JA10** and **JA12** have a higher quantum efficiency. This is due to the LUMO being lower in energy, so the metal centred states are less readily populated.

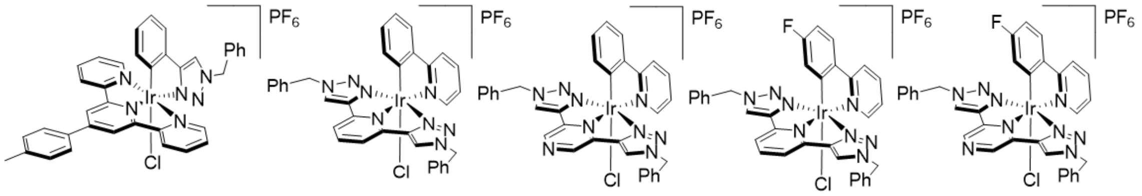

JA8 **JA9** **JA10** **JA11** **JA12**

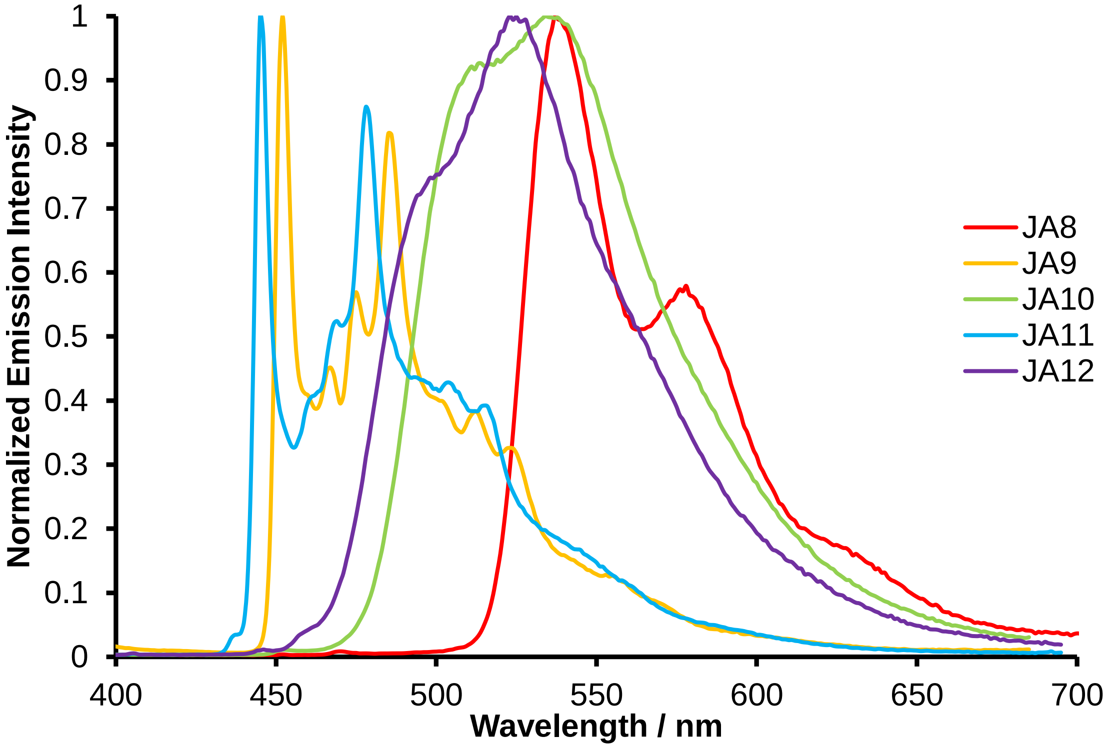

*Figure 4. 9 Low temperature emission spectra of **JA8-12** complexes. Recorded in EtOH:MeOH (4:1) glass at 77K. Wavelengths of excitation; λ_{ex} = 350 nm for **JA9** and **JA10**, λ_{ex} = 355 nm for **JA11** and **JA12**, and λ_{ex} = 400 nm for **JA8.***

The complexes were all observed to be emissive at low temperature (77 K) in an EtOH:MeOH glass matrix (Figure 4.9), all the bands underwent rigidochromic blue-shift compared to the room temperature spectra. Complex **JA8** has a broad band emission characterised by ^{3}MLCT/LLCT emitting states, at low temperatures there are visible vibronic progressions that occur within broad band emission, these are not observable at room temperature due to the large number of vibrational relaxations occurring. The low temperature band for **JA8** is additional evidence that the emission is generated from ^{3}MLCT/^{3}LLCT character and that the LUMO is located on the tol-terpy ligand.

The tz-py-tz complexes, **JA9** and **JA11**, exhibit bands that have vibronic progressions that are a characteristic of ^{3}MLCT/^{3}ILCT emitting states. This indicates at low temperature in a glass matrix there is a destabilisation of the N^N^N ligand causing the unpaired electron to be relocalised, in the T_1 excited state, to the pyridine moiety on the cyclometalated ppy ligands, although this occurs in the excited state the LUMO is still defined on the ancillary tz-py-tz.

The pyrazine, tz-pyz-tz, complexes **JA10** and **JA12** emission bands indicate broad structureless emission that is commonly associated with ^{3}MLCT/^{3}LLCT emitting state character. However, there is a shoulder peak for both complexes which could be assigned as the 0-0 band, followed by the other vibrational progressions being mixed in with the broad band. The emission bands at low temperatures are more in accordance with what was foreseen with the electrochemical data, complexes **JA10** and **JA12** are blue shifted compared to **JA8**. It can be presumed that the triazole N^N^N ligand complexes (**JA9-12**) are more significantly affected by alternative vibrational pathways than **JA8**. As can be seen **JA9-12** emission maxima shift ~50-80 nm when in a solid state, where as **JA8** only shifts 26 nm.

4. 5. DFT Characterisation

In order to enhance our comprehension of the electronic structure and photophysical characteristics exhibited by complexes **JA8-12**, comprehensive density functional theory (DFT) modelling was carried out. The DFT calculations were carried out in collaboration with my supervisor, Prof. Paul Elliott. The focus of the calculations were on geometry optimisation and the analysis of frontier orbital patterns. Considering computational efficiency, the ground-state geometries of the triazole-containing complexes were optimised by replacing the benzyl groups with a methyl substituent. It is worth noting that the benzyl substituent was deemed to have negligible or minimal influence on the photophysical properties, thereby allowing for a simplified computational approach with reduced computational costs.

Figure 4.10, exhibits the calculated energies for the frontier orbitals as a depiction on the isosurfaces of the complexes **JA8-12**. The ground state HOMO and LUMO are being portrayed, the HOMO for all complexes is localised over the metal centre and the cyclometalated bidentate C^N ligand, and the LUMO is localised on the ancillary N^N^N ligand for all ligands. The calculation of these is in accordance with the experimental results that were observed that showed emission from ^{3}MLCT/LLCT broad band characteristics. It appears that the monodentate chlorine ligand mainly plays a role in the HOMO, therefore any modifications there could affect the HOMO properties.

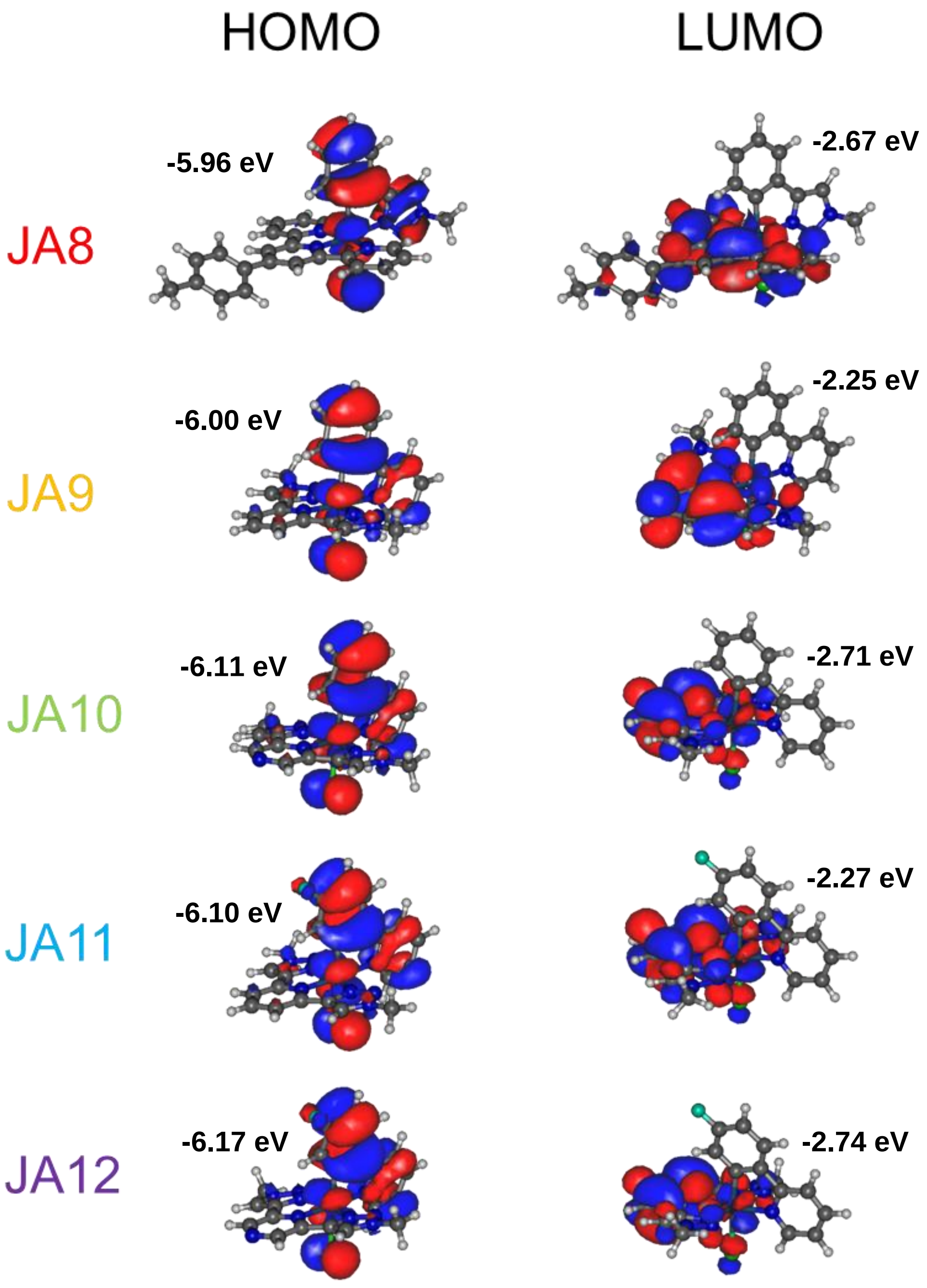

*Figure 4. 10 Ground state molecular orbital energy level diagram for complexes **JA8-12**, displaying the frontier orbitals on the isosurfaces.*

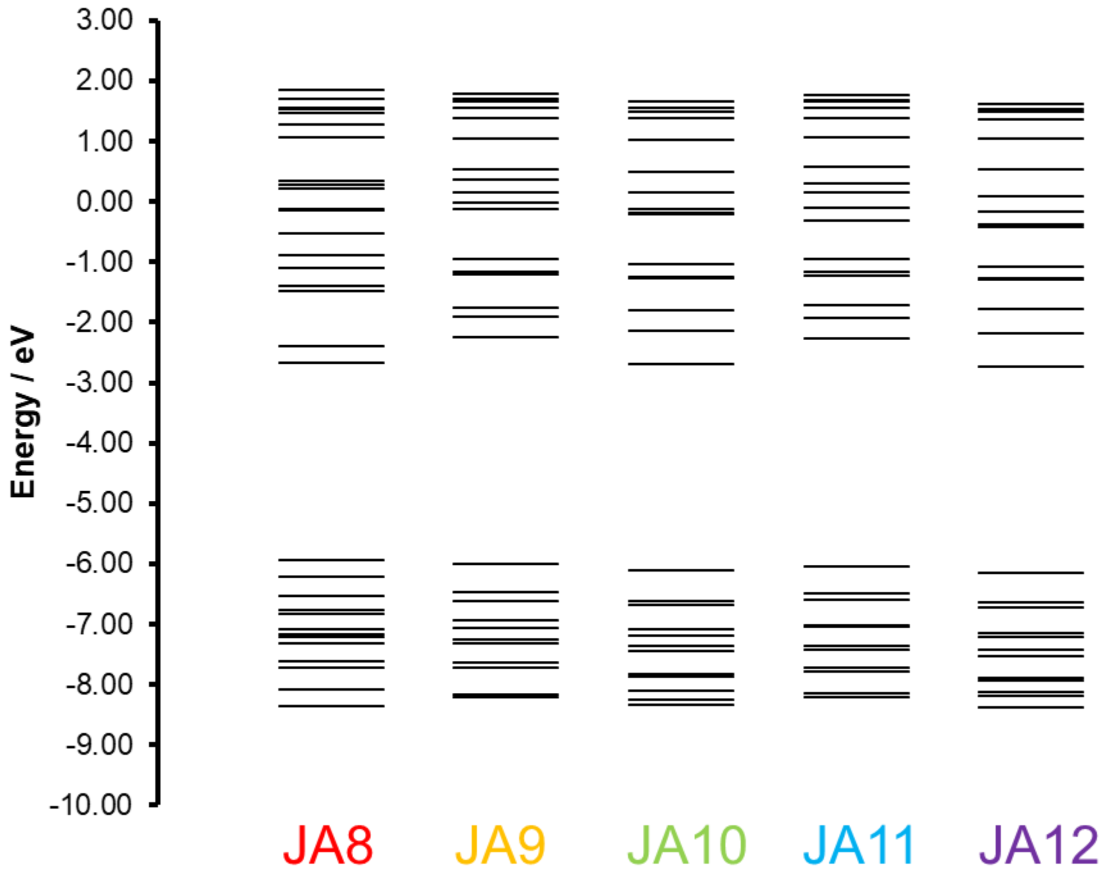

Figure 4. 11 Molecular orbital energy level diagram for complexes ***JA8-12***

Figure 4.11 illustrates a comprehensive molecular orbital diagram showcasing the calculated energies of the frontier orbitals. Additionally, Table 4.3 presents a succinct summary of the computed energies pertaining to the HOMO and LUMO. Across the series the HOMO remains at relatively the same energy level with a slight decrease for the pyrazine-based complexes **JA10** and **JA12**. This corroborates with the effect seen in the electrochemical data as **JA9** and **JA11** required a higher oxidation potential than their pyridyl counterparts **JA9** and **JA11.** This is due to the electron withdrawing effects of the pyrazine resulting in electron deficiency at the metal centre and stabilising the HOMO. The fluorination of cyclometalated ligand also showed decrease in HOMO energy as it was stabilised by the electron withdrawing effects. The LUMO energy level alters throughout the series due to the modification of the N^N^N ligand. The tol-terpy complex **JA8** has a lower energy LUMO compared to **JA9** and **JA11**, the pyridyl moieties are much stronger π-acceptors than the triazole moieties meaning increased stabilisation of the LUMO. Complex **JA8** had the lowest calculated HOMO-LUMO gap, which is in agreement with the electrochemical data, and the photophysical data as the UV-visible absorbance and low temperature emission displayed the lowest energy bands.

The difference between the pyridine and pyrazine containing N^N^N complexes is starkly clear regarding their LUMO energies. The electron withdrawing effect of the pyrazine causes a stabilisation of the LUMO and lowering its energy to the lowest across the series, this results in a smaller HOMO-LUMO energy gap for complexes **JA10** and **JA12** compared to **JA9** and **JA11**. This was also reflected in the experimental data as the pyrazine complexes emission and absorption bands were red shifted compared to the pyridine base complexes.

Table 4.3 Summarised HOMO and LUMO Energy Values from DFT Calculations for Complexes JA8-12

Complex	HOMO (eV)	LUMO (eV)	HOMO-LUMO Energy Gap (eV)
JA8	-5.96	-2.67	3.29
JA9	-6.00	-2.25	3.75
JA10	-6.11	-2.71	3.40
JA11	-6.10	-2.27	3.83
JA12	-6.17	-2.74	3.43

4. 6. Conclusion

Novel complexes were developed to explore new chemical space through the $[Ir(N^\wedge N^\wedge N)(C^\wedge N)Cl]^+$ structure using triazoles. The complex that used ptz ligand in the C^N position (**JA8**), had promising set of photophysical properties with good quantum efficiency (ϕ_{rel} = 9.1 %) and a relatively long excited state lifetime. The complexes containing triazoles in the N^N^N ligand (**JA9-12**) were less effective for applications in light emitting devices due to relatively low quantum yields. Especially the pyridine-based complexes, **JA9** and **JA11**, had very low quantum yields, it was thought that the reason for this could be due to population of the ^{3}MC states. The pyrazine-complexes (**JA10** and **JA12**), however, had moderate quantum efficiencies and long excited state lifetimes.

Moving forward modification of the C^N cyclometalated ligand looks an area that needs to be further explored especially with the versatility of the triazole moieties. Even though complexes **JA9** and **JA11** were not efficient emitters it has provided insight into designing ligand architecture for this structure and the structures fundamental photophysical properties. I think potentially **JA10** and **JA12** have potential applications, or at least a fundamental basis to investigate, as PDT agent. The complexes have long excited state lifetimes which increases the chance of them being effective PDT agents.

5. General Conclusions and Future Work

5.1 General Conclusions

The thesis presented has undertaken a comprehensive investigation encompassing a diverse range of Ir(III) photophysics relevant to light-emitting devices. Through extensive research, various aspects crucial to the understanding and advancement of such devices have been investigated. By delving into a wide range of different aspects of Ir(III) photophysics, this study contributes to the broader comprehension and optimization of light-emitting devices, paving the way for future advancements in the field.

The investigation in Chapter 2 looking at the heterodinculear Ir(III)-Ru(II) complexes has provided two white light emitting complexes, **JA1b** and **JA2b**. Even though the complexes themselves are not particularly emissive or photostable, it begins to pave the way for future complex and ligand design. Even though it was not the primary goal of the chapter some potential applications have been reported for some of the novel complexes. The mononuclear Ir(III) complexes (**JA1-3.Ir/F**) are reasonable efficient and highly sensitive to oxygen with long excited state lifetimes, this opens them up to the potential as PDT agents. Another potential application for the mononuclear Ir(III) complexes is a biological imaging probe, the complex has high quantum efficiency and has a free coordination site that could be used to coordinate to metal complexes in the biological world, this would behave with potentially a turn-on/off ability depending on what it is coordinated to. The heterodinuclear complexes (**JA1-3**) could potentially be used as colourimetric oxygen sensors, due to their sensitivity to oxygen and that their emission colour varies from orange/red to blue/green dependent on the oxygen concentration.

In Chapter 2 when the complexes were found to not be photostable they would no longer be suitable for light emitting devices, their PLQY were relatively poor anyway. However, that lead us down an unexpected path and looking at the photochemical properties of the heterodinuclear complexes. Complexes **JA1-3** have unique photochemical properties as the Ir(III) emission is being quenched by the partial energy transfer to the Ru metal centre. Therefore, when the Ru(II) fragment is photoejected from the complex the Ir(III) emission switches on with a 30-fold increase. This makes them a viable candidate as a PACT agent, whereby the complexes enter the cancerous cell and is irradiated with light causing the Ru(II) (with cytotoxic payload) to be ejected and then the Ir(III) fragment switches the emission on confirming delivery of the cytotoxic payload.

As summarised above the mononuclear Ir(III) complexes are good blue light emitters, the Ir(III) blue light emitters tend to not be stable enough for application in light emitting devices. Hence in Chapter 3 a series of complexes were developed to probe the ^{3}MC states of Ir(III) complexes. Two complexes **JA4** and **JA7** were able to populate the Ir(III) ^{3}MC states via two alternate pathways providing great insight into how to develop and design new complexes moving forward. Complex **JA4** had been designed to manipulate the electronic effects whereas complex **JA7** had been crafted to modulate the ^{3}MC states via the steric effects.

As well as probing fundamental photophysics, we have explored new chemical space through the development of novel triazole based Ir(III) 3+2+1 complexes ([Ir(N^N^N)(C^N)Cl]$^+$) in Chapter 4. The complex (**JA8**) with the triazole moiety substituted for the pyridine on the cyclometalated C^N, provided promising photophysical properties. The complexes that were designed with triazole moieties on the N^N^N ligand did not have quite as admirable photophysical properties. The higher energy emitting complexes, **JA9** and **JA11**, were barely emissive at all. However, the pyrazine-based complexes **JA10** and **JA11** had reasonable quantum yield but had long excited state lifetimes, with that property they could potentially be effective PDT agents.

As has just been summarized, throughout this thesis a number of complexes have been reported that contribute and help progress the field of light emitting devices, moving forward the results we have reported will help to produce more efficient light emitting devices through complex design and ligand architecture.

5.2 Future Work

A running theme throughout is the versatility of cyclometalated Ir(III) complexes and the multitude of applications they can be used for. This is also reflected when the target aim of a project did not go to plan theirs is always another avenue with exciting potential.

As mentioned in the 5.1 in Chapter 2 we produced two white light emitting complexes that can be improved in regard to their quantum efficiencies. Some potential ideas to move forward would be to potential add CH_2 spacers between the triazole and the xylene. This should reduce the Förster energy transfer and therefore the Ir(III) emission will not be as quenched and thus increasing the efficiency. Alternatively, or in combination with the Ru(II) metal centre could substituted with a different orange/red emitter that is more efficient. The problem that could occur here is if the partial energy transfer is too efficient the Ir(III) energy will just go to the orange/red emitter. I have shown a couple of examples that could potentially be used in Figure 5.1.

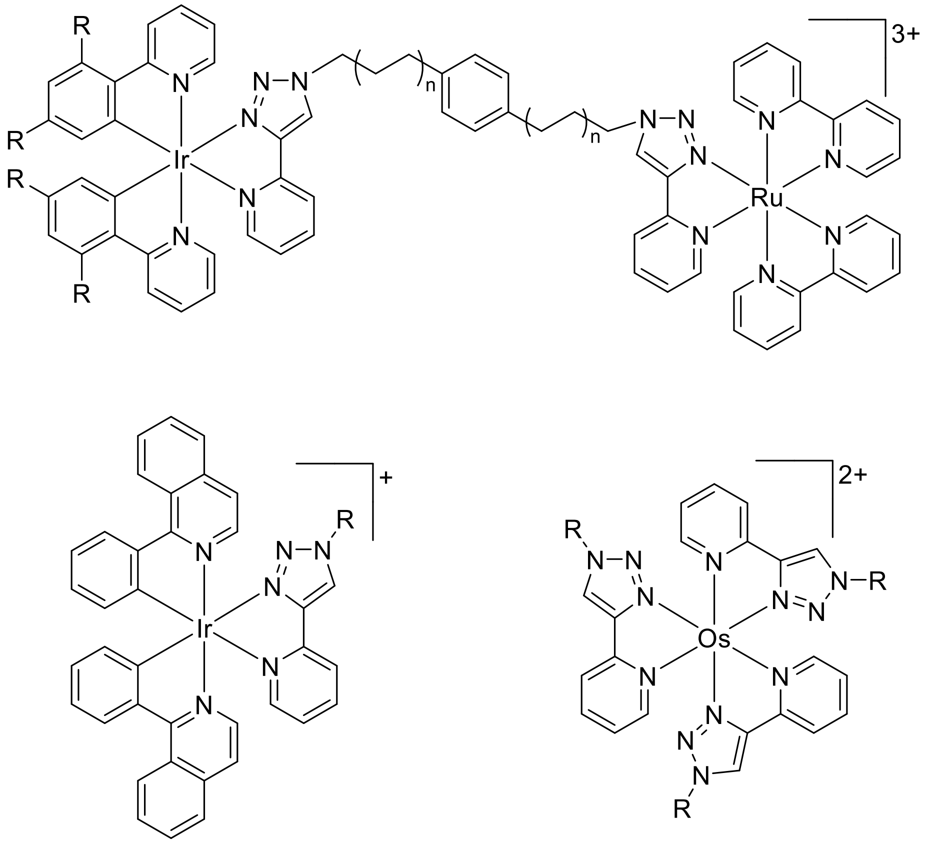

Figure 5. 1 Concepts for developing an efficient white light emitter, developing on JA1b and JA2b.

Continuing on with the heterodinuclear complexes **JA1-3** in Chapter 2, due to their uniquie photochemical properties they should be investigated as potential PACT agents. The ligands on the Ru(II) fragment could be modified into DNA intercalaters ensuring the fragment is cytotoxic and causing cell death. Potentially heterodinuclear complex [Ir(R-ppy)(pytz-*o/m/p*-xyl-pytz)Ru(phen)]$^{3+}$ could be developed as, 1,10-phenanthroline has be been reported to be a DNA intercalater.[214]

For Chapter 3, it would be ideal if temperature-dependent emission could be recorded so there could be a better understanding of the excited state process, in particualr for **JA4**. What we have reported so far has given a clearer ability to manipulate the ^{3}MC states. Novel blue light emitting complexes need to be desigened trying to destabilise the ^{3}MC states and stabilise the HOMO. Whislt not destabilising the HOMO to energy levels where it may be possible to thermally populate the ^{3}MC states.

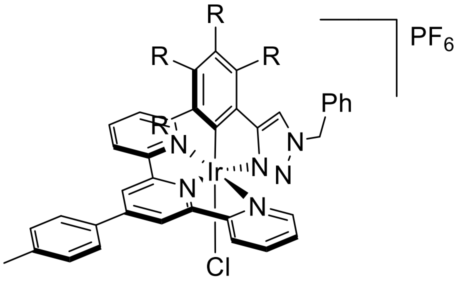

Figure 5. 2 Modified Ir(III) 3+2+1 complex JA8 with a series of R groups.

The ptz C^N complex **JA8** showed reasonable photophysical properties so it would be of interest to modulate the phenyl ring with EWG and EDG groups to observe the effect they have on the photophysical properties. Modulating the LUMO to induce blue emission did not work, therefore it would be interesting to see if any combination triazole could potentially blue shift the emission with good quantum efficency.

6. Experimental

6.1 General Characterisation Methods

The $Ru(bpy)_2Cl_2$[215] and the Ir(III) dimers $[Ir(ppy)_2(\mu\text{-}Cl)]_2$[162] and $[Ir(dfppy)_2(\mu\text{-}Cl)]_2$[216] were all prepared according to previously reported procedures. All reagents were purchased from Alfa Aesar, Acros Organics, Sigma Aldrich, and Fluorochem they were used as received. NMR spectra were recorded on a Bruker Ascend 400 MHz spectrometer, all chemical shifts reported in ppm and was calibrated relative to the residual solvent signal ($CHCl_3$, ^1H δ 7.26, ^{13}C δ 7.16 and MeCN, ^1H δ 1.94, ^{13}C δ 1.32, 118.26). High resolution mass spectrometry (HRMS) was performed on an Agilent 6210 time-of-flight instrument with a dual electrospray ionisation source. UV-Visible electronic absorption spectra were recorded on an Agilent Cary-60 spectrophotometer utilising quartz cells of 1 cm pathlength. Emission spectra were recorded on a Fluoromax-4 spectrophotometer utilising 1 cm pathlength quartz cells. Photoluminescence quantum yields (ϕ) are quoted relative to $[Ru(bpy)_3][PF_6]_2$ in aerated MeCN, with all complexes being excited at a single wavelength with common optical density. Quantum yields are therefore determined from the ratio of integrated areas under the relevant emission profiles, with an assumed experimental uncertainty of ±10%. Luminescence lifetimes were determined using an Edinburgh Instruments Mini-τ equipped with a picosecond diode laser (404 nm, 56 ps) excitation source.

6.2 Electrochemistry

Cyclic voltammograms were measured using a PalmSens EmStat3 potentio stat with PSTrace electrochemical software (version 4.8). Analyte solutions (typical concentration 1.5 mmoldm^{-3}) were prepared using N_2 saturated MeCN, freshly distilled from CaH_2. All measurements were performed under an atmosphere of N_2 at scan rates ranging from 50 to 500 mV s^{-1}. NBu_4PF_6 was employed as supporting electrolyte, being recrystallised from EtOH and oven dried prior to use, with a typical solution concentration of 0.2 moldm^{-3}. The working electrode was glassy carbon, the counter electrode Pt wire and the reference Ag/AgCl, the latter being chemically isolated from the analyte solution by an electrolyte containing bridge tube tipped with a porous frit. Ferrocene was employed as an internal reference, with all potentials being reported relative to the Fc^+ /Fc couple.

6.3 Transient Absorption Spectroscopy

Spectra were recorded using a broadband ultrafast pump-probe transient absorption spectrometer “Helios” (Ultrafast Systems LLC), collecting data over a 3 ns time window with a time resolution of approximately 250 fs. A Ti:Sapphire amplifier system (Newport Spectra-Physics, Solstice Ace) producing 800 nm pulses at 1 kHz with 100 fs pulse duration was used to generate the probe beam and to also pump a TOPAS Prime OPA with associated near-infrared (NIR)−UV−vis unit to generate the excitation beam. The probe beam consisted of a white light continuum generated in a CaF2 crystal. Absorbance changes were monitored between 330 and 650 nm. Samples were excited with 0.5 µJ pulses at 285 nm, contained within a 0.2 cm pathlength quartz cuvette that was magnetically stirred during the measurements. Before data analysis, pre-excitation data was subtracted, and spectral chirp was corrected for. Kinetics were analysed at the wavelengths of the highest intensity transient and bleach features. These traces were fitted with multiexponential functions with shared lifetime parameters.

6.4 Density Functional Theory Calculations

All calculations have been performed with ORCA Quantum Chemistry software.[217,218] The structures of all complexes, in their respective ground and lowest excited triplet states, have been fully optimized at the DFT/(U)DFT levels with hybrid functional B3LYP,[219,220] including Grimme's dispersion correction (D3- BJ),[221,222] with a triple-ζ Ahlrichs basis set, namely def2-TZVP(-f), with a p polarization function for the H atoms, two d polarization functions for the second row elements, and for the iridium the triple-ζ basis set def2-TZVPP with two f and one g polarization functions and its associated relativistic effective core potential.[223] Following geometry optimizations, vibrational frequency analyses were performed at the same level of theory to verify the nature of the stationary points. The absorption spectra have been calculated by means of TD-DFT/B3LYP applied to the lowest 40 states. In these TD-DFT calculations the resolution-ofidentity (RI) approximation for hybrid functionals (as implemented in ORCA) was employed to calculate the Coulomb energy term using the Ahlrichs/Weigand Def2-TZV basis as the auxiliary basis set and the exchange term by the so-called 'chain-of-spheres exchange' (COSX) algorithm. In order to analyse the nature of the electronic transitions in the TD-DFT spectra, the Natural Transition Orbitals (NTO) were computed. Previous studies have shown that B3LYP accurately reproduces structural and energetics of Ir(III) complexes.[224,225] Solvent effects were simulated using the Solvation Model (SMD) that has been proposed by Cramer and Truhlar.[226]

6.5 Ligand Release Photochemistry

Photolysis experiments were carried out by irradiating the appropriate solutions contained within either NMR tubes with a compact 23 W fluorescent light bulb (Hg) or within 10 mm pathlength quartz cuvettes with light from a blue LED (Thorlabs, LED450LW, $\lambda = 446$ nm) at a forward current of 50 mA (2.7 V) provided by a direct current power supply (RSComponents, RS-3005D). Light from the blue LED was delivered to the sample through a liquid light guide (17 ± 1 mW at the exit of the light guide). Samples were maintained at room temperature (25 °C) throughout the measurements with the aid of a Peltier temperature-controlled cuvette holder or an electronic fan (NMR samples). The determination of photochemical quantum yields was performed for MeCN solutions of known concentration (2.5 mL volume, 10 mm pathlength cuvette) under irradiation with the aforementioned blue LED excitation source, the photon flux density of which was determined to be 2.01×10^{-5} einstein s^{-1} dm^{-3} through use of a $K_3Fe(C_2O_4)_3{\cdot}3H_2O$ chemical actinometer. Photorelease quantum yield calculations were performed using GNU Octave software (version 6.2.0), freely available at https://www.gnu.org/software/octave/, using the method of Slep and co-workers.[166]

6.6 General Synthesis of pytz-*o/m/p*-xyl-pytz[160]

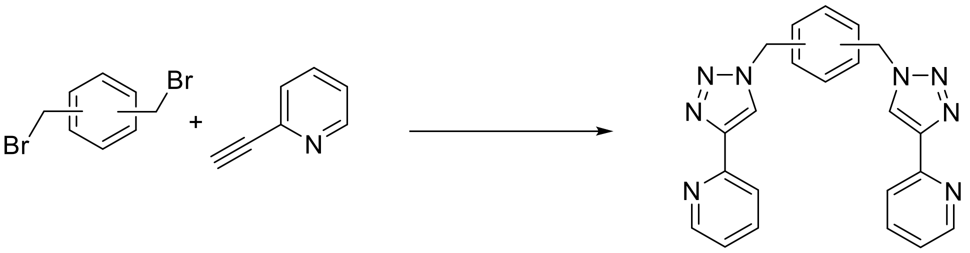

The following was charged to an RBF DMF:H_2O (1:1, 15-30 ml), *o/m/p*-xylene dibromide (1.58 g, 6.00 mmol), sodium azide (819 mg, 12.6 mmol), K_2CO_3 (829 mg, 6.00 mmol), $CuSO_4.5H_2O$ (599 mg, 2.40 mmol) and sodium ascorbate (951 mg, 4.80 mmol) 2-ethynylpyridinie (1.24 ml, 12.3 mmol) was then added to the solution and then mixture was stirred at room temperature for 16 h. H_2O (100 ml), $CHCl_3$ (100 ml) and conc. NH_3 (15 ml) were added to the mixture and then left to stir for 30 mins. The mixture was then separated and aq. layers extracted with $CHCl_3$ (2 x 100 ml). Org. layers were combined and washed with dil. NH_4OH (3 x 100 ml), H_2O (100 ml) and brine (100 ml). Org. layers combine and dried over $MgSO_4$ followed by gravity filtration. Solvent removed under reduced pressure. Recrystallised from $CHCl_3$:Hexane, a white product precipitates and is collected by vacuum filtration, washed with hexane.

6.5.1 1,4-bis((4-(pyridin-2-yl)-1*H*-1,2,3-triazol-1-yl)methyl)benzene

Yield: 1.68 g (71 %). ^{1}H NMR ($CDCl_3$, 400MHz): δ 8.66 (s, 1H), 8.57 (d, $^3J_{HH}$ = 4.42 Hz, 2H), 8.01 (d, $^3J_{HH}$ = 7.90 Hz, 2H), 7.87 (td, $^3J_{HH}$ = 7.65 Hz, $^4J_{HH}$ = 1.65 Hz, 2H), 7.39 (s, 4H), 7.32 (tdd, $^3J_{HH}$ = 7.47 Hz, $^3J_{HH}$ = 6.63 Hz, $^4J_{HH}$ = 1.15, 2H), 5.66 (s, 4H) ^{13}C NMR ($CDCl_3$, 101MHz): δ 150.31, 150.07, 147.94, 137.66, 136.41, 128.93, 123.91, 123.48, 119.87, 53.08, 26.80. HRMS (ESI). Calcd for $C_{22}H_{18}N_8$: *m/z* 394.11. Found: *m/z* 395.17.

6.5.2 1,3-bis((4-(pyridin-2-yl)-1*H*-1,2,3-triazol-1-yl)methyl)benzene

Yield: 1.84 g (78 %). ^{1}H NMR (MeCN-*d*$_3$, 400MHz): δ 8.53(s, 2H), 8.16 (d, $^3J_{HH}$ = 7.87 Hz, 2H), 8.06 (s, 2H), 7.76 (t, $^3J_{HH}$ = 7.79 Hz, 2H), 7.33 (m, 4H), 7.21(td, $^3J_{HH}$ = 6.97 Hz, $^3J_{HH}$ = 6.02 Hz, 2H), 5.56 (s, 4H). ^{13}C NMR ($CDCl_3$, 101MHz): δ 150.15, 149.42, 149.01, 137.01, 135.67, 130.20, 128.69, 123.06, 122.08, 120.37, 54.00. HRMS (ESI). Calcd for $C_{22}H_{18}N_8$: *m/z* 394.11. Found: *m/z* 395.17.

6.5.3 1,2-bis((4-(pyridin-2-yl)-1*H*-1,2,3-triazol-1-yl)methyl)benzene

Yield: 1.73 g (73 %). ^{1}H NMR ($CDCl_3$, 400MHz): δ 8.51 (s, 2H), 8.13 (d, $^3J_{HH}$ = 7.75 Hz, 2H), 8.00 (s, 2H), 7.74 (t, $^3J_{HH}$ = 7.51 Hz, 2H), 7.36 (dt, $^3J_{HH}$ = 30.80 Hz, $^3J_{HH}$ = 5.65 Hz, 4H), 7.20 (td, $^3J_{HH}$ = 6.97 Hz, $^3J_{HH}$ = 6.01 Hz), 5.72 (s, 2H). ^{13}C NMR ($CDCl_3$, 101MHz): δ 150.00, 149.34, 148.93, 136.90, 133.18, 130.74, 130.06, 123.00, 122.04, 120.3, 51.49. HRMS (ESI). Calcd for $C_{22}H_{18}N_8$: *m/z* 394.11. Found: *m/z* 395.17.

6.7 Synthesis of 2-(1-benzyl-1*H*-1,2,3-triazol-4-yl)pyridine (pytz)[227]

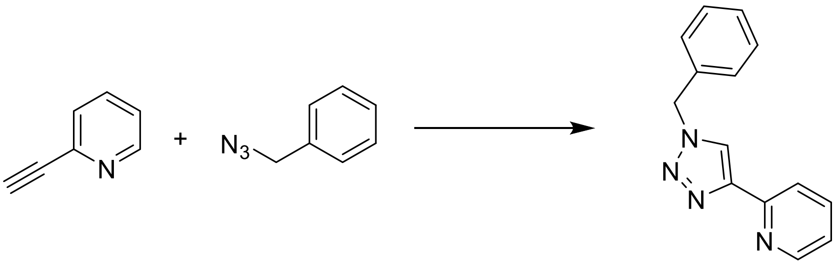

2-ethynylpyridine (1.32 g, 12.8 mmol) was added to BnN_3 (1.87 g, 14.1mmol) in an RBF followed by H_2O (125 ml), THF (125 ml), *tert*-BuOH (25 ml), K_2CO_3 (2.65 g, 19.2 mmol), $CuSO_4.5H_2O$ (799 mg, 3.20 mmol), sodium ascorbate (1.27 g, 6.40 mmol) and pyridine (25 ml). Mixture stirred at room temperature for 16 h. Organic solvents were removed under vacuum leaving an aqueous solution. $CHCl_3$ (100 ml), H_2O (20 ml) and conc. NH_3 (20 ml) were added and stirred at room temperature for 1 h. Mixture separated, aq. layer extracted with $CHCl_3$ (2 x 100 ml), org. layers collected and washed with dil. NH_4OH (2 x 100 ml), H_2O (100 ml) and brine (100 ml). Org. layers collected and dried over Na_2SO_4 and gravity filtered. Solvents reduced under vacuum affording white product. Purified by recrystallisation from DCM:Et_2O. Yield: 2.27 g (75 %). ^1H NMR ($CDCl_3$, 400MHz): 8.57 (s, 1H), 8.20 (d, $^3J_{HH}$ = 7.98 Hz, 1H), 8.07 (s, 1H), 7.76 (t, , $^3J_{HH}$ = 7.64 Hz, 1H), 7.35 (m, 5H), 7.21 (t, , $^3J_{HH}$ = 6.86 Hz, $^3J_{HH}$ = 6.05 Hz, 1H), 5.61 (s, 2H). HRMS (ESI). Calcd for $C_{14}H_{12}N_4$: *m/z* 236.11. Found: *m/z* 237.11.

6.8 Synthesis of 2-methyl-6-((trimethyl-silylidyne)methyl)pyridine[228]

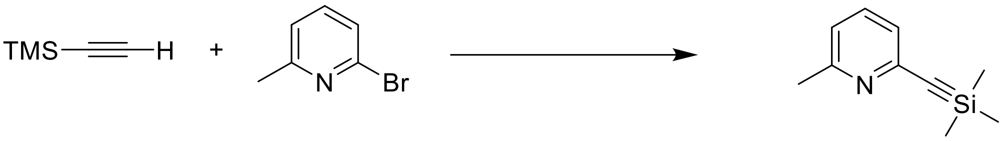

The reaction was done under N_2, $Pd(PPh_3)_2Cl_2$ (306 mg, 0.44 mmol) and CuI (166 mg, 0.87 mmol) were charged to a RBF. Deaerated THF/Et_3N (2:1, 60 ml) was added to the RBF, followed by 2-bromo-6-methylpyridine (0.99 ml, 8.72 mmol). The mixture was then heated at 50ºC and stirred for 15 min. TMS-acetylene (1.86 ml, 13.1 mmol) was then added via syringe and the solution went from orange to black. Mixture stirred and heated at 50ºC under N_2 for 16 h. Cooled to r.t. and filtered through a silica pad and washed with DCM. The filtrate was collected and reduced under pressure to afford the product as a yellow oil. Purified by SiO_2 DCM:MeOH (99:1) column. Yield: 974 mg (59 %). ^1H NMR ($CDCl_3$, 400MHz): δ 7.52 (t, $^3J_{HH}$ = 7.74 Hz, 1H), 7.27 (d, $^3J_{HH}$ = 7.46 Hz, 1H), 7.08 (d, J = 7.78 Hz, 1H), 2.55 (s, 3H), 0.25 (s, 9H).

6.9 Synthesis of 2-(1-benzyl-1*H*-1,2,3-triazol-4-yl)-6-methylpyridine (m-pytz)[227]

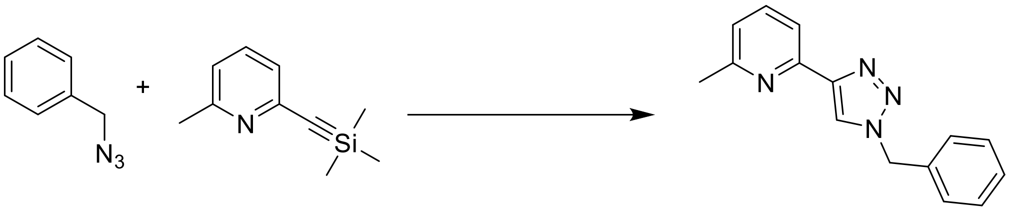

2-TMS-ethynyl-6-methylpyridine (859 mg, 4.54 mmol) was added to BnN_3 (683 mg, 5.13 mmol) in an RBF followed by H_2O (50 ml), THF (50 ml), *tert*-BuOH (100 ml), K_2CO_3 (979 g, 1.56 mmol), $CuSO_4.5H_2O$ (285 mg, 1.14 mmol), sodium ascorbate (472 mg, 2.38 mmol) and pyridine (10 ml). Mixture stirred at room temperature for 16 h. Organic solvents were removed under vacuum leaving an aqueous solution. $CHCl_3$ (70 ml), H_2O (30 ml) and conc. NH_3 (5 ml) were added and stirred at room temperature for 1 h. Mixture separated, aq. layer extracted with $CHCl_3$ (30 ml), org. layers collected and washed with dil. NH_4OH (2 x 100 ml), H_2O (100 ml) and brine (100 ml). Org. layers collected and dried over $MgSO_4$ and gravity filtered. Solvents reduced under vacuum affording white product. Purified via recrystalisation with DCM:Hexane. Yield: 886 mg (78 %). ^1H NMR ($CDCl_3$, 400MHz): δ 8.10 (s, 1H), 7.97 (d, $^3J_{HH}$ = 7.81 Hz, 1H), 7.64 (t, $^3J_{HH}$ = 7.74 Hz, 1H) 7.34 (m, 5H), 7.07 (d, $^3J_{HH}$ = 7.65 Hz, 1H). 5.57 (s, 2H), 2.53 (s, 3H).[1] HRMS (ESI). Calcd for $C_{15}H_{14}N_4$: *m/z* 250.12. Found: *m/z* 251.12.

6.10 Synthesis of 1-benzyl-4-phenyl-1*H*-1,2,3-triazole (ptz)[227]

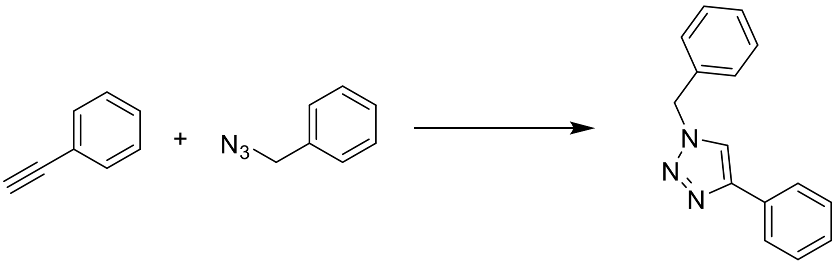

Phenylacetylene (1.05 ml, 9.56 mmol) was added to BnN_3 (1.40 g, 10.5 mmol) in an RBF followed by H_2O (100 ml), THF (100 ml), *tert*-BuOH (20 ml), K_2CO_3 (1.98 g, 14.3 mmol), $CuSO_4.5H_2O$ (597 mg, 2.39 mmol), sodium ascorbate (947 g, 4.78 mmol) and pyridine (20 ml). Mixture stirred at room temperature for 16 h. Organic solvents were removed under vacuum leaving an aqueous solution. $CHCl_3$ (100 ml), H_2O (20 ml) and conc. NH_3 (20 ml) were added and stirred at room temperature for 1 h. Mixture separated, aq. layer extracted with $CHCl_3$ (2 x 100 ml), org. layers collected and washed with dil. NH_4OH (2 x 100 ml), H_2O (100 ml) and brine (100 ml). Org. layers collected and dried over Na_2SO_4 and gravity filtered. Solvents reduced under vacuum affording white product. Purified by recrystallisation from DCM:Et_2O. Yield: 1.76 g (78 %). ^1H NMR ($CDCl_3$, 400MHz): δ 7.80, (d, $^3J_{HH}$ = 7.11 Hz, 2H), 7.67 (s, 1H), 7.39 (m, 5H), 7.32 (m, 3H), 5.57 (s, 2H). HRMS (ESI). Calcd for $C_{15}H_{13}N_3$: *m/z* 235.11. Found: *m/z* 236.12.

6.11 Synthesis of 1,1'-dibenzyl-1*H*,1'*H*-4,4'-bi(1,2,3-triazole) (btz)[227]

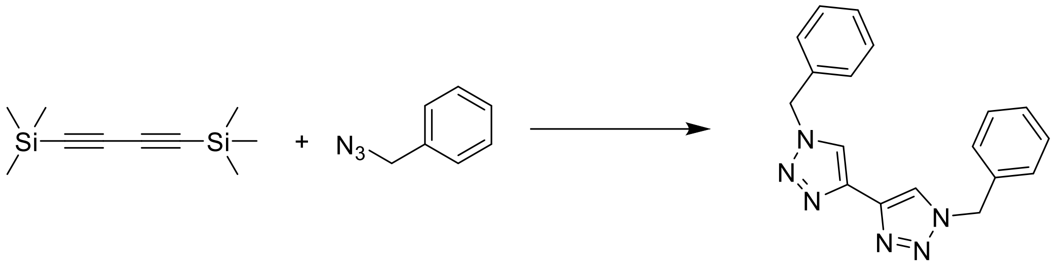

1,4-bis(trimethylsilyl)buta-1,3-diyne (1.41 g, 7.23 mmol) was added to BnN_3 (2.01 g, 15.1 mmol) in an RBF followed by H_2O (30 ml), *tert*-BuOH (20 ml), K_2CO_3 (2.99 g, 21.6 mmol), $CuSO_4.5H_2O$ (597 mg, 2.39 mmol), sodium ascorbate (1.48 g, 7.47 mmol) and pyridine (5 ml). Mixture stirred at room temperature for 16 h. Organic solvents were removed under vacuum leaving an aqueous solution. $CHCl_3$ (100 ml), H_2O (100 ml) and conc. NH_3 (15 ml) were added and stirred at room temperature for 1 h. Mixture separated, org. layers collected and washed with dil. NH_4OH (2 x 100 ml), H_2O (100 ml) and brine (100 ml). Org. layers collected and dried over $MgSO_4$ and gravity filtered. Solvents reduced under vacuum, recrystallised from DCM:Hexane to afford desired white product. Yield: 1.57 g (69 %). ^1H NMR ($CDCl_3$, 400MHz): δ 7.94 (s, 1H), 7.37 (m, 3H), 7.31 (m, 2H) 5.56 (s, 2H). Calcd for $C_{18}H_{16}N_6$: *m/z* 316.14. Found: *m/z* 317.13.

6.12 Synthesis of 3,5-dimethyl-1-phenyl-1*H*-pyrazole (dmppz)

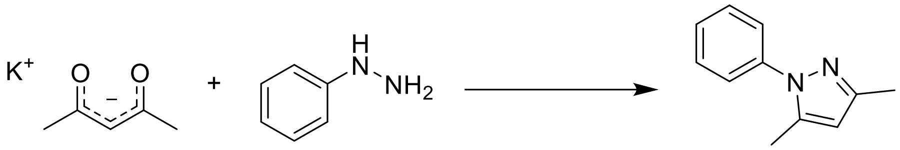

This is a cyclocondensation reaction. To an RBF, with EtOH (100 ml) in, was charged with potassium acetylacetone (2.35 g, 16.0 mmol) and phenylhydrazine (1.6 ml, 16.0 mmol), followed by conc. HCl (0.8 ml). Mixture stirred and heated to reflux for 20 h. Cooled to r.t. and then 1M $NaHCO_3$ (100 ml) and DCM (150 ml) were added, mixture was then separated. Aq. layers were collected and extracted with DCM (100 ml), org layers combined and washed with H_2O (100 ml), then dried of $MgSO_4$ and gravity filtered. The org. solvents were then removed under reduced pressure to afford a red oil residue. Purified by SiO_2 dry loaded column chromatography, solvent EtOAc:Hexane (15:85). Affording the pure product as a yellow oil. Yield: 1.27 g (46 %). ^{1}H NMR ($CDCl_3$, 400MHz): δ 7.43 (m, 3H), 7.34 (tdd, $^3J_{HH}$ = 7.48 Hz, $^3J_{HH}$ = 6.32 Hz, $^4J_{HH}$ = 2.38 Hz, 1H), 5.99 (s, 1H), 2.30 (s, 6H). ^{13}C NMR ($CDCl_3$, 101MHz): δ 148.97, 139.94, 139.38, 128.99, 127.23, 124.76, 106.90, 13.53, 12.40. HRMS (ESI). Calcd for $C_{11}H_{12}N_2$: *m/z* 172.10. Found: *m/z* 173.11.

6.13 Synthesis of 2,6-bis((trimethyl-silylidyne)methyl)pyridine[228]

The reaction was done under N_2, $Pd(PPh_3)_2Cl_2$ (148 mg, 0.21 mmol), CuI (80 mg, 0.42 mmol) and 2,6-dibromopyridine (1.00 g, 4.2 mmol) were charged to a RBF. Deaerated THF/Et_3N (2:1, 40 ml) was added to the RBF. The mixture was then heated at 50ºC and stirred for 15 min. TMS-acetylene (1.75 ml, 12.66 mmol) was then added via syringe and the solution went from orange to black. Mixture stirred and heated at 50ºC under N_2 for 16 h. Cooled to r.t. and filtered through a silica pad and washed with DCM. The filtrate was collected and reduced under pressure to afford the product as an oil. Purified by SiO_2 Hexane:DCM (2:1) column. Yield: 757 mg (66 %). ^1H NMR ($CDCl_3$, 400MHz): δ 7.58 (t, $^3J_{HH}$ = 7.76, 1H), 7.38 (d, $^3J_{HH}$ = 7.81, 2H), 0.25 (s,18H).

6.14 Synthesis of 2,6-bis((trimethyl-silylidyne)methyl)pyrazine[228]

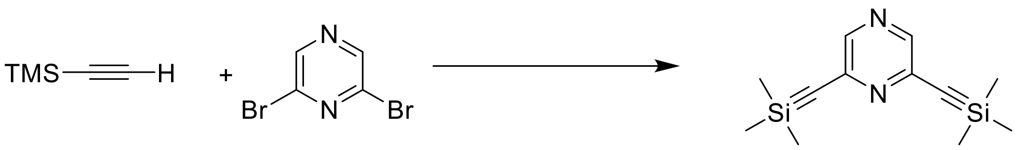

The reaction was done under N_2, $Pd(PPh_3)_2Cl_2$ (219 mg, 0.31 mmol), CuI (120 mg, 0.63 mmol) and 2,6-dibromopyrazine (1.50 g, 6.3 mmol) were charged to a RBF. Deaerated THF/Et_3N (2:1, 40 ml) was added to the RBF. The mixture was then heated at 50ºC and stirred for 15 min. TMS-acetylene (2.6 ml, 18.4 mmol) was then added via syringe and the solution went from orange to black. Mixture stirred and heated at 50ºC under N_2 for 17 h. Cooled to r.t. and filtered through a silica pad and washed with DCM. The filtrate was collected and reduced under pressure to afford the product as an oil. Purified by SiO_2 Hexane:DCM (1:1) column. Yield: 999 mg (58 %). ^1H NMR ($CDCl_3$, 400MHz): δ 8.53 (s, 2H), 0.26 (s,18H).

6.15 Synthesis of 2,6-bis(1-benzyl-1*H*-1,2,3-triazol-4-yl)pyridine (tz-py-tz)[227]

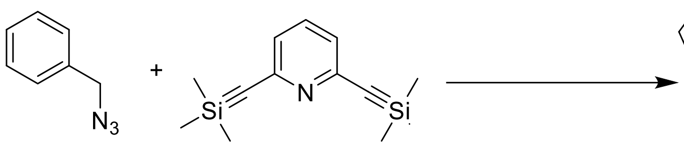

2,6-bis((trimethyl-silylidyne)methyl)pyridine (800 mg, 2.95 mmol) was added to BnN_3 (982 mg, 7.4 mmol) in an RBF followed by H_2O (100 ml), THF (100 ml), *tert*-BuOH (20 ml), K_2CO_3 (2.65 g, 19.2 mmol), $CuSO_4.5H_2O$ (552 mg, 2.21 mmol), sodium ascorbate (878 mg, 4.43 mmol) and pyridine (3.5 ml). Mixture stirred at room temperature for 16 h. Organic solvents were removed under vacuum leaving an aqueous solution. $CHCl_3$ (150 ml), H_2O (60 ml) and conc. NH_3 (15 ml) were added and stirred at room temperature for 1 h. Mixture separated, aq. layer extracted with $CHCl_3$ (2 x 100 ml), org. layers collected and washed with dil. NH_4OH (2 x 100 ml), H_2O (100 ml) and brine (100 ml). Org. layers collected and dried over $MgSO_4$ and gravity filtered. Solvents reduced under vacuum until 20% left and then added hexane, resulted in precipitation of white product. Yield: 847 mg (73 %). ^{1}H NMR ($CDCl_3$, 400MHz): δ 8.07 (d, $^3J_{HH}$ = 7.79 Hz, 2H), 8.04 (s, 2H), 7.84 (t, $^3J_{HH}$ = 7.76 Hz, 1H), 7.34 (m, 6H), 7.28 (m, 4H), 5.56 (s, 1H) ^{13}C NMR ($CDCl_3$, 101MHz): δ 149.90, 148.73, 137.76, 134.54, 129.15, 128.80, 128.06, 122.01, 119.42, 54.32.

6.16 Synthesis of 2,6-bis(1-benzyl-1*H*-1,2,3-triazol-4-yl)pyrazine (tz-pyz-tz)

2,6-bis((trimethyl-silylidyne)methyl)pyrazine (900 mg, 3.3 mmol) was added to BnN_3 (1.09 g, 8.2 mmol) in an RBF followed by H_2O (50 ml), THF (50 ml), *tert*-BuOH (20 ml), K_2CO_3 (2.96 g, 21.4 mmol), $CuSO_4.5H_2O$ (617 mg, 2.47 mmol), sodium ascorbate (983 g, 4.96 mmol) and pyridine (3.5 ml). Mixture stirred at room temperature for 16 h. Organic solvents were removed under vacuum leaving an aqueous solution. $CHCl_3$ (150 ml), H_2O (60 ml) and conc. NH_3 (15 ml) were added and stirred at room temperature for 1 h. Mixture separated, aq. layer extracted with $CHCl_3$ (2 x 100 ml), org. layers collected and washed with dil. NH_4OH (2 x 100 ml), H_2O (100 ml) and brine (100 ml). Org. layers collected and dried over $MgSO_4$ and gravity filtered. Solvents reduced under vacuum until 20% left and then added hexane, resulted in precipitation of off-white product. Yield: 957 mg (73 %). ^1H NMR ($CDCl_3$, 400MHz): δ 9.30 (s, 2H), 8.06 (s, 2H), 7.37 (m, 6H), 7.30 (m, 4H), 5.60 (s, 1H).

6.17 General synthesis of [Ru(bpy)$_2$(pytz-*o/m/p*-xyl-pytz)]2PF$_6$, JA1-3.Ru

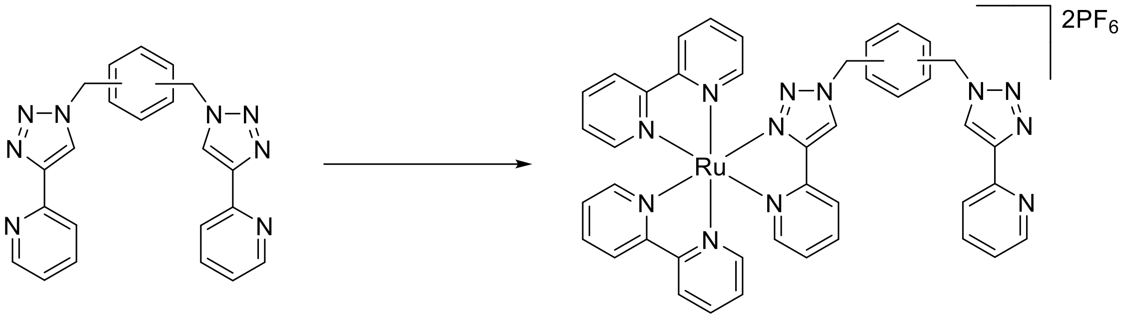

Pytz-*o/m/p-xyl*-pytz (686 mg, 1.74 mmol), Ru(bpy)$_2$Cl$_2$ (400 mg, 0.83 mmol) and a stirrer bar were charged to a round bottom flask (RBF), then placed under N$_2$. Deaerated EtOH (30ml) was added via syringe and solution refluxed, in the absence of light and under N$_2$, for 16h. Solution was cooled to RT and NH$_4$PF$_6$ (676 mg, 4.2 mmol) was added, bright orange precipitate crashed out instantly. Collected by vacuum filtration and washed with H$_2$O (~5ml) and Et$_2$O (~5ml) and left to dry for 1h. Crude product was purified by column chromatography; SiO$_2$, MeCN:H$_2$O:KNO$_3$ (10:1:1). Column vials were combined, and solvent removed under reduced pressure, re-dissolved in min. MeOH and NH$_4$PF$_6$ (676 mg, 4.2 mmol) was added to change the counter ion from NO$_3$ to PF$_6$. Orange precipitate collected by vacuum filtration to afford the pure desired product.

6.17.1 [Ru(2,2'-bipyridine)$_2$(1,4-bis((4-(pyridin-2-yl)-1*H*-1,2,3-triazol-1-yl)methyl)benzene)]2PF$_6$

Yield: 750 mg (21 %). ^{1}H NMR (MeCN-*d$_3$*, 400MHz): δ 8.62 (s, 1H), 8.56 (d, $^3J_{HH}$ = 4.7 Hz, 1H), 8.49 (t, $^3J_{HH}$ = 7.0 Hz, 2H), 8.37 (d, $^3J_{HH}$ = 8.2 Hz, 2H), 8.29 (s, 1H), 7.91-8.12 (m, 7H), 7.79-7.88 (m, 3H), 7.76 (d, $^3J_{HH}$ = 5.6 Hz, 1H), 7.70 (d, $^3J_{HH}$ = 5.6 Hz, 1H), 7.57 (d, $^3J_{HH}$ = 5.6 Hz, 1H), 7.23-7.43 (m, 8H), 7.12 (d, $^3J_{HH}$ = 8.2 Hz, 2H), 5.62 (s, 2H), 5.50 (s, 2H). ^{13}C NMR (MeCN-*d$_3$*, 101MHz): δ 157.63, 157.27, 157.19, 156.96, 152.19, 152.13, 152.04, 151.77, 151.65, 150.76, 149.65 147.82, 138.21, 137.72, 137.69, 137.59, 137.11, 136.63, 134.08, 128.70, 128.69, 127.51, 127.41, 126.38, 126.72, 126.00, 125.77, 125.26, 124.26, 124.17, 124.05, 123.74, 123.41, 122.71, 55.04, 53.16. HRMS (ESI). Calcd for [C$_{42}$H$_{34}$N$_{12}$Ru]$^{2+}$ (M^{2+}): *m/z* 404.10. Found: *m/z* 404.1033.

6.17.2 [Ru(2,2'-bipyridine)$_2$(1,3-bis((4-(pyridin-2-yl)-1*H*-1,2,3-triazol-1-yl)methyl)benzene)]2PF$_6$

Yield: 699 mg (19 %). ^{1}H NMR (MeCN-d_3, 400MHz): δ 8.55-8.70 (m, 4H), 8.51 (dd, $^{3}J_{HH}$ = 8.2 Hz, $^{4}J_{HH}$ = 3.7 Hz, 2H), 8.44 (t, $^{3}J_{HH}$ = 7.8 Hz, 2H), 8.25 (d, $^{3}J_{HH}$ = 8.2 Hz, 1H), 7.89-8.10 (m, 7H), 7.79-7.87 (m, 3H), 7.75 (d, $^{3}J_{HH}$ = 5.7 Hz, 1H), 7.59 (d, $^{3}J_{HH}$ = 5.6 Hz, 1H), 7.24-7.47 (m, 8H), 7.12 (m, 1H), 5.66 (s, 2H), 5.53 (s, 2H). ^{13}C NMR (MeCN-d_3, 101MHz): δ 157.62, 157.30, 157.21, 156.99, 152.20, 152.10, 152.01, 151.84, 151.70, 150.75, 147.89, 141.32, 138.24, 137.82, 137.80, 137.72, 137.64, 135.63, 134.65, 129.90, 128.85, 128.46, 128.35, 127.61, 127.48, 126.79, 126.51, 126.05, 125.88, 125.81, 124.28, 124.19, 124.05, 123.84, 123.54, 122.73, 55.06, 53.94. HRMS (ESI). Calcd for $[C_{42}H_{34}N_{12}Ru]^{2+}$ (M^{2+}): *m/z* 404.10. Found: *m/z* 404.1040.

6.17.3 [Ru(2,2'-bipyridine)$_2$(1,2-bis((4-(pyridin-2-yl)-1*H*-1,2,3-triazol-1-yl)methyl)benzene)]2PF$_6$

Yield: 837 mg (23 %). ^{1}H NMR (MeCN-d_3, 400MHz): δ 8.59 (d, $^{3}J_{HH}$ = 5.5 Hz, 1H), 8.52 (d, $^{3}J_{HH}$ = 8.2 Hz, 2H), 8.36-8.45 (m, 4H), 8.29 (t, $^{3}J_{HH}$ = 7.9 Hz, 1H), 7.95-8.12 (m, 6H), 7.79-7.94 (m, 4H), 7.67-7.76 (m, 2H), 7.59 (d, $^{3}J_{HH}$ = 5.6 Hz, 1H), 7.36-7.54 (m, 6H), 7.32 (t, $^{3}J_{HH}$ = 6.4 Hz, 1H), 7.25 (t, $^{3}J_{HH}$ = 6.4 Hz, 1H), 7.14 (d, $^{3}J_{HH}$ = 7.5 Hz, 1H), 5.70 (dd, $^{5}J_{HH}$ = 15.2 Hz, $^{2}J_{HH}$ = 14.9, 2H), 5.55 (dd, $^{2}J_{HH}$ = 37.0 Hz, $^{5}J_{HH}$ = 15.2 Hz, 2H) . ^{13}C NMR (MeCN-d_3, 101MHz): δ 157.62, 157.27, 157.19, 156.97, 152.23, 152.02, 152.04, 151.87, 151.68, 150.83, 147.79, 141.29, 138.34, 137.83, 137.75, 137.68, 135.61, 134.65, 129.90, 128.85, 128.46, 128.35, 127.61, 127.48, 126.79, 126.48, 126.15, 125.78, 124.32, 124.14, 124.06, 123.82, 123.53, 122.73, 55.03, 53.20. HRMS (ESI). Calcd for $[C_{42}H_{34}N_{12}Ru]^{2+}$ (M^{2+}): *m/z* 404.10. Found: *m/z* 404.1038.

6.18 General synthesis of [Ir(ppy)$_2$(pytz-*o/m/p*-xyl-pytz)]PF$_6$, JA1-3.Ir

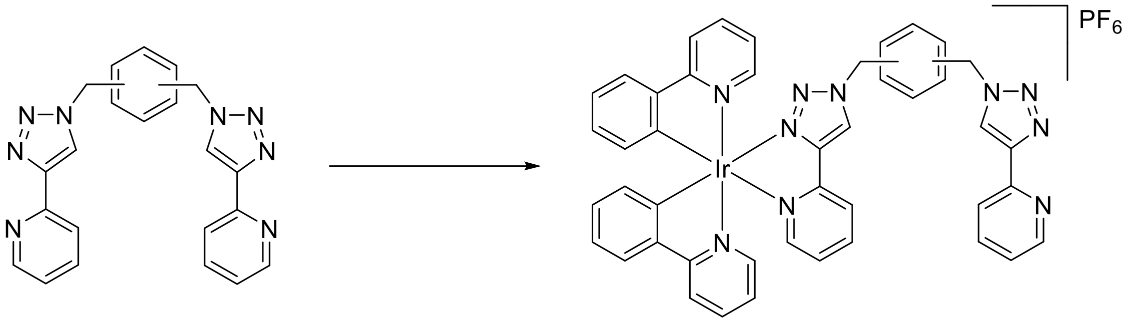

[Ir(ppy)$_2$(μ-Cl)]$_2$ (1.0 eq.), pytz-o/m/p-xyl-pytz (2.1 eq.) and a stirrer bar were charged to an RBF, then placed under N_2. Deaerated DCM/MeOH (2:1, 30mL) was added via syringe, and solution refluxed, in absence of light and under N_2, for 16h. Solution allowed to cool to RT and then NH_4PF_6 (5 eq.) was added to precipitate a bright yellow solid. Collected by vacuum filtration and washed with H_2O (~5ml) and Et_2O (~5ml). Crude product was purified by column chromatography; SiO_2, DCM/MeOH (98.5:1.5). Column vials were combined, and solvent removed under reduced pressure. Residue was recrystallised from DCM/Et_2O to yield the pure desired yellow product.

6.18.1 [Ir(2-phenylpyridine)$_2$(1,4-bis((4-(pyridin-2-yl)-1*H*-1,2,3-triazol-1-yl)methyl)benzene)]PF$_6$

[Ir(ppy)$_2$(μ-Cl)]$_2$ (272 mg, 0.25 mmol), pytz-*p*-xyl-pytz (216 mg, 0.55 mmol), NH_4PF_6 (207 mg, 1.27 mmol). Yield: 43 mg (16 %). ^{1}H NMR (MeCN-*d*$_3$, 400MHz): δ 8.62 (s, 1H), 8.56 (d, $^3J_{HH}$ = 4.5 Hz, 1H), 8.28 (s, 1H), 7.96-8.10 (m, 5H), 7.75-7.86 (m, 5H), 7.70 (m, 2H), 7.57 (d, $^3J_{HH}$ = 5.7 Hz, 1H), 7.34 (m, 3H), 7.29 (t, $^3J_{HH}$ = 6.2 Hz, 1H), 7.19 (d, $^3J_{HH}$ = 8.1 Hz, 2H), 7.03 (t, $^3J_{HH}$ = 6.8 Hz, 2H), 6.99 (t, $^3J_{HH}$ = 6.8 Hz, 1H), 6.91 (m, 2H), 6.80 (t, $^3J_{HH}$ = 7.4 Hz, 1H), 6.26 (d, $^3J_{HH}$ J = 7.4, 1H), 6.22 (d, $^3J_{HH}$ = 7.4 Hz, 1H), 5.61 (s, 2H), 5.58 (d, $^2J_{HH}$ = 1.5 Hz, 2H). ^{13}C NMR (MeCN-*d*$_3$, 101MHz): δ 167.5844, 167.171, 150.3301, 149.6849, 149.4463, 149.3008, 149.2128, 148.8838, 144.3536, 144.2089, 139.6637, 138.5563, 138.4615, 137.1506, 136.7383, 133.9606, 131.8456, 131.4552, 130.3213, 129.644, 128.7665, 128.7395, 126.8079, 126.2715, 124.839, 124.3638, 123.5142, 123.2688, 123.0363, 122.9219, 122.8158, 122.673, 122.2039, 119.8261, 119.6586, 119.5823, 54.9511, 53.1268. HRMS (ESI). Calcd for $[C_{44}H_{34}IrN_{10}]^+$ (M^+): *m/z* 895.26. Found: *m/z* 895.2591.

6.18.2 [Ir(2-phenylpyridine)$_2$(1,3-bis((4-(pyridin-2-yl)-1*H*-1,2,3-triazol-1-yl)methyl)benzene)]PF$_6$

[Ir(ppy)$_2$(μ-Cl)]$_2$ (388 mg, 0.36 mmol), pytz-*m*-xyl-pytz (300 mg, 0.76 mmol), NH$_4$PF$_6$ (293 mg, 1.8 mmol). Yield: 35 mg (13 %). ^{1}H NMR (MeCN-*d*$_3$, 400MHz): δ 8.60 (s, 1H), 8.50 (m, 1H), 8.24 (s, 1H), 8.03 (m, 5H), 7.68-7.87 (m, 7H), 7.59 (d, $^3J_{HH}$ = 5.7 Hz, 1H), 7.39-7.42 (m, 2H), 7.34 (td, $^3J_{HH =}$ 6.4 Hz, $^3J_{HH}$ = 1.6 Hz, 1H), 7.27 (t, $^3J_{HH}$ = 6.0 Hz, 1H), 7.22 (m, 2H), 6.99-7.11 (m, 3H), 6.92 (d, $^3J_{HH}$ = 11.1 Hz, 1H), 6.92 (dtd, $^3J_{HH}$ = 7.44 Hz, $^3J_{HH}$ = 7.28 Hz, $^4J_{HH}$ = 1.37 Hz 1H), 6.80 (td, $^3J_{HH}$ = 7.4 Hz, $^4J_{HH}$ = 1.4 Hz, 1H), 6.24 (dd, $^3J_{HH}$ = 7.6 Hz, $^3J_{HH}$ = 7.4 Hz, 2H), 5.58 (s, 4H). ^{13}C NMR (MeCN-*d*$_3$, 101MHz): δ 167.5649, 167.0805, 150.3916, 150.1876, 149.8631, 149.5798, 149.4931, 149.3492, 149.1262, 148.3913, 148.3281, 146.4807, 144.4051, 144.2879, 139.3418, 138.5482, 138.4424, 136.859, 134.7373, 131.885, 131.431, 131.3521, 131.0707, 131.0453, 130.5194, 130.2636, 129.933, 129.647, 126.5077, 125.4647, 124.797, 124.3584, 123.75, 123.3513, 123.0233, 122.7442, 122.651, 122.5761. HRMS (ESI). Calcd for [$C_{44}H_{34}IrN_{10}$]$^+$ (M$^+$): *m/z* 895.26. Found: *m/z* 895.2591.

6.18.3 [Ir(2-phenylpyridine)$_2$(1,2-bis((4-(pyridin-2-yl)-1*H*-1,2,3-triazol-1-yl)methyl)benzene)]PF$_6$

[Ir(ppy)$_2$(μ-Cl)]$_2$ (190 mg, 0.18 mmol), pytz-*o*-xyl-pytz (210 mg, 0.53 mmol), NH$_4$PF$_6$ (147 mg, 0.9 mmol). Yield: 41 mg (21 %). ^{1}H NMR (MeCN-*d*$_3$, 400MHz): δ 8.47 (d, $^3J_{HH}$ = 4.5Hz, 1H), 8.14 (s, 1H), 7.98-8.09 (m, 4H), 7.88 (t, $^3J_{HH}$ = 7.8 Hz, 1H), 7.84 (t, $^3J_{HH}$ = 7.8 Hz, 1H), 7.67-7.81 (m, 6H), 7.49-7.63 (m, 4H), 7.45 (td, $^3J_{HH}$ = 7.3 Hz, $^3J_{HH}$ = 1.9 Hz, 1H), 7.16-7.27 (m, 4H), 7.03 (m, 2H), 6.95 (td, $^3J_{HH}$ = 7.6 Hz, $^3J_{HH}$ = 1.1 Hz, 1H), 6.90 (td, $^3J_{HH}$ = 7.6 Hz, $^3J_{HH}$ = 1.1 Hz, 1H), 6.83 (td, $^3J_{HH}$ = 7.6 Hz, $^3J_{HH}$ = 1.1 Hz, 1H), 6.27 (t, $^3J_{HH}$ = 8.0 Hz, 2H), 5.68 (dd, $^2J_{HH}$ = 16.3 Hz, $^5J_{HH}$ = 10.3 Hz, 2H), 5.67 (dd, $^2J_{HH}$ = 124.7 Hz, $^5J_{HH}$ = 15.4 Hz, 2H). ^{13}C NMR (MeCN-*d*$_3$, 101MHz): δ 149.58, 149.49, 149.35, 149.13, 148.39, 148.33, 146.48, 144.40, 144.29, 139.34, 138.55, 138.44, 136.86, 134.74, 131.88, 131.43, 131.35, 131.07, 131.04, 130.51, 130.26, 129.93, 129.65, 126.51, 125.46, 124.80, 124.36, 123.75, 123.35, 123.02, 122.74, 122.65, 122.57, 122.22, 119.72, 119.57, 119.47, 52.88, 51.00. HRMS (ESI). Calcd for [$C_{44}H_{34}IrN_{10}$]$^+$ (M$^+$): *m/z* 895.26. Found: *m/z* 895.2593.

6.19 General synthesis of [Ir(dfppy)$_2$(pytz-*o/m/p*-xyl-pytz)]PF$_6$, JA1-3.IrF

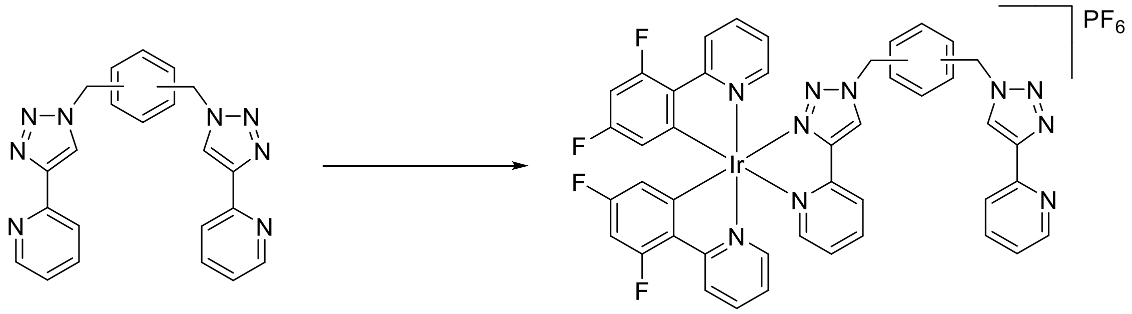

[Ir(dfppy)$_2$(μ-Cl)]$_2$ (1.0 eq.), pytz-*o/m/p*-xyl-pytz (2.1 eq.) and a stirrer bar were charged to an RBF, then placed under N_2. Deaerated DCM/MeOH (2:1, 30 mL) was added via syringe, and solution refluxed, in absence of light and under N_2, for 16 h. Solution allowed to cool to RT and then NH_4PF_6 (5 eq.) was added to precipitate a bright yellow solid. Collected by vacuum filtration and washed with H_2O (~5 ml) and Et_2O (~5 ml). Crude product was purified by column chromatography; SiO_2, DCM/MeOH (98:2). Column vials were combined, and solvent removed under reduced pressure. Residue was recrystallised from DCM/Et_2O to yield the pure desired yellow product.

6.19.1 [Ir(2-(4,6-difluorophenyl)pyridine)$_2$(1,4-bis((4-(pyridin-2-yl)-1*H*-1,2,3-triazol-1-yl)methyl)benzene)]PF$_6$

[Ir(dfppy)$_2$(μ-Cl)]$_2$ (505 mg, 0.42 mmol), pytz-*p*-xyl-pytz (500 mg, 1.27 mmol), NH_4PF_6 (342 mg, 2.1 mmol). Yield: 115 mg (25 %). ^{1}H NMR (MeCN-d_3, 400MHz): δ 8.63 (s, 1H), 8.55 (d, $^3J_{HH}$ = 4.9 Hz, 1H), 8.22-8.33 (m, 3H), 8.00-8.10 (m, 3H), 7.85-7.93 (m, 4H), 7.73 (d, $^3J_{HH}$ = 5.6 Hz, 1H), 7.59 (d, $^3J_{HH}$ = 5.6 Hz, 1H), 7.18-7.41 (m, 6H), 7.09 (td, $^3J_{HH}$ = 6.7 Hz, $^3J_{HH}$ = 1.2 Hz, 1H), 7.04 (td, $^3J_{HH}$ = 6.7 Hz, $^3J_{HH}$ = 1.2 Hz, 1H), 6.69 (td, $^3J_{HH}$ = 11.0 Hz, $^3J_{HH}$ = 2.5 Hz, 1H), 6.60 (td, $^3J_{HH}$ = 11.0 Hz, $^3J_{HH}$ = 2.5 Hz, 1H), 5.73 (tdd, $^3J_{HH}$ = 23.7 Hz, $^3J_{HH}$ = 8.6 Hz, $^4J_{HH}$ = 2.4 Hz, 1H), 5.61 (s, 2H), 5.59 (s, 2H). ^{13}C NMR (MeCN-d_3, 101MHz): δ 163.739, 163.5114, 153.5523, 150.737, 150.2824, 150.0241, 149.6765, 149.6276, 148.9501, 148.7452, 148.3579, 140.2458, 139.5639, 139.5109, 137.0507, 136.8196, 133.7168, 128.9034, 128.732, 128.5762, 127.1376, 126.4713, 123.9841, 123.7729, 123.6006, 123.5232, 123.3226, 123.2033, 123.0137, 122.8033, 119.6203, 114.036, 113.7506, 99.1477, 98.8791, 98.713, 98.4451, 55.1215. HRMS (ESI). Calcd for $[C_{44}H_{30}F_4IrN_{10}]^+$ (M^+): *m/z* 967.22. Found: *m/z* 967.2214.

6.19.2 [Ir(2-(4,6-difluorophenyl)pyridine)$_2$(1,3-bis((4-(pyridin-2-yl)-1*H*-1,2,3-triazol-1-yl)methyl)benzene)]PF$_6$

[Ir(dfppy)$_2$(μ-Cl)]$_2$ (440 mg, 0.36 mmol), pytz-*m*-xyl-pytz (300 mg, 0.76 mmol), NH_4PF_6 (293 mg, 1.8 mmol). Yield: 125 mg (27 %). ^{1}H NMR (MeCN-d_3, 400MHz): δ 8.59 (s, 1H), 8.50 (m, 1H), 8.24-8.34 (m, 3H), 7.99-8.11 (m, 3H), 7.78-7.95 (m, 4H), 7.73 (d, $^3J_{HH}$ = 5.6 Hz, 1H), 7.61 (d, $^3J_{HH}$ = 5.6 Hz, 1H), 7.35-7.45 (m, 3H), 7.18-7.32 (m, 3H), 7.14 (t, $^3J_{HH}$ = 6.7 Hz, 1H), 7.08 (t, $^3J_{HH}$ = 6.7 Hz, 1H), 6.73 (td, $^3J_{HH}$ = 12.0 Hz, $^3J_{HH}$ = 2.5 Hz, 1H), 6.65 (td, $^3J_{HH}$ = 12.0 Hz, $^4J_{HH}$ = 2.5 Hz, 1H), 5.73 (tdd, $^3J_{HH}$ = 11.5 Hz, $^3J_{HH}$ = 8.7 Hz, $^4J_{HH}$ = 2.4, 2H), 5.59 (s, 4H). ^{13}C NMR (MeCN-d_3, 101MHz): δ 150.7391, 149.9966, 149.6447, 149.4397, 148.9332, 148.6968, 140.2538, 139.5491, 137.2802, 136.8439, 134.1944, 129.8183, 128.7887, 128.3854, 127.9425, 127.1476, 126.4394, 124.0904, 123.8341, 123.5813, 123.1036, 122.8734, 113.8605, 98.4604, 55.2468, 53.2453, 123.3226, 123.2033, 123.0137, 122.8033, 119.6203, 114.036, 113.7506, 99.1477, 98.8791, 98.713, 98.4451, 55.1215. HRMS (ESI). Calcd for $[C_{44}H_{30}F_4IrN_{10}]^+$ (M^+): *m/z* 967.22. Found: *m/z* 967.2217.

6.19.3 [Ir(2-(4,6-difluorophenyl)pyridine)$_2$(1,2-bis((4-(pyridin-2-yl)-1*H*-1,2,3-triazol-1-yl)methyl)benzene)]PF$_6$

[Ir(dfppy)$_2$(μ-Cl)]$_2$ (440 mg, 0.36 mmol), pytz-*o*-xyl-pytz (300 mg, 0.76 mmol), NH_4PF_6 (293 mg, 1.8 mmol). Yield: 108 mg (23 %). ^{1}H NMR (MeCN-d_3, 400MHz): δ 8.46 (d, $^3J_{HH}$ = 3.9 Hz, 1H), 8.33 (d, = 8.4 Hz, 1H), 8.28 (d, $^3J_{HH}$ = 8.4 Hz, 1H), 8.15 (s, 1H), 8.00-8.07 (m, 2H), 7.95 (t, $^3J_{HH}$ = 8.1 Hz, 1H) 7.90 (t, $^3J_{HH}$ = 8.1 Hz, 1H), 7.80 (m, 2H), 7.72 (d, $^3J_{HH}$ = 8.1 Hz, 1H), 7.67 (d, $^3J_{HH}$ = 8.1 Hz, 1H), 7.60 (m, 2H), 7.53 (m, 2H), 7.46 (m, 1H), 7.27 (m, 3H), 7.20 (t, $^3J_{HH}$ = 6.0 Hz, 1H), 7.09 (t, $^3J_{HH}$ = 6.6 Hz, 1H), 6.70 (td, $^3J_{HH}$ = 31.2 Hz, $^3J_{HH}$ = 11.0, 1H), 6.62 (td, $^3J_{HH}$ = 31.2 Hz, $^3J_{HH}$ = 11.0 Hz, 1H) 5.71 (m, 4H), 5.69 (dd, $^2J_{HH}$ = 132.5 Hz, $^5J_{HH}$ = 15.1Hz). ^{13}C NMR (MeCN-d_3, 101MHz): δ 153.61, 153.54, 150.70, 150.61, 149.78, 149.56, 148.76, 148.22, 139.92, 139.55, 139.48, 136.89, 131.59, 131.17, 130.85, 130.62, 129.98, 126.84, 125.66, 124.23, 123.88, 122.81, 122.73, 119.47, 114.05, 113.85, 113.66, 99.12, 98.85, 98.73, 98.58, 98.46, 98.19, 53.07, 51.03. HRMS (ESI). Calcd for $[C_{44}H_{30}F_4IrN_{10}]^+$ (M^+): *m/z* 967.22. Found: *m/z* 967.2213.

6.20 General synthesis of [Ru(bpy)$_2$(pytz-*o/m/p*-xyl-pytz)Ir(ppy)$_2$]3PF$_6$, JA1a-JA3a

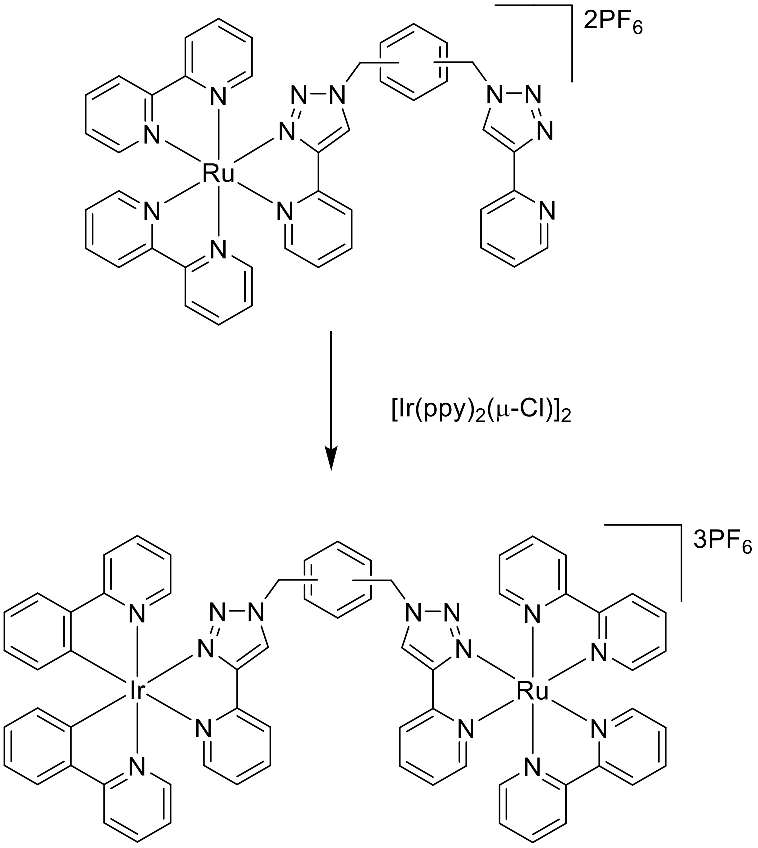

[Ir(ppy)$_2$(μ-Cl)]$_2$ (1.0 eq.), [Ru(bpy)$_2$(pytz-o/m/p-xyl-pytz)][PF$_6$]$_2$ (2.0 eq.) and a stirrer bar were charged to an RBF, then placed under N_2. Deaerated DCM/MeOH (2:1, 30mL) was added via syringe, and solution refluxed, in absence of light and under N_2, for 16h. Solution allowed to cool to RT and then NH_4PF_6 (5 eq.) was added to precipitate an orange solid. Precipitate was then collected by vacuum filtration and washed with H_2O (~5ml) and Et_2O (~5ml). Crude product was purified by column chromatography; SiO_2, DCM/MeOH (99:1). Column vials were combined, and solvent removed under reduced pressure. Residue was recrystallised from DCM/Et_2O to yield the pure desired red product.

6.20.1 [Ru(2,2'-bipyridine)$_2$(1,4-bis((4-(pyridin-2-yl)-1*H*-1,2,3-triazol-1-yl)methyl)benzene)Ir(2-phenylpyridine)$_2$]3PF$_6$

[Ir(ppy)$_2$(μ-Cl)]$_2$ (97.6 mg, 0.091 mmol), [Ru(bpy)$_2$(pytz-*p*-xyl-pytz)][PF$_6$]$_2$ (220 mg, 0.20 mmol), NH_4PF_6 (74 mg, 0.46 mmol). Yield: 110 mg (70 %). Calcd for $[C_{69}H_{62}IrN_{14}Ru]^{3+}$ (M^{3+}): *m/z* 460.47. Found: *m/z* 460.4762.

6.20.2 [Ru(2,2'-bipyridine)$_2$(1,3-bis((4-(pyridin-2-yl)-1*H*-1,2,3-triazol-1-yl)methyl)benzene)Ir(2-phenylpyridine)$_2$]3PF$_6$

[Ir(ppy)$_2$(μ-Cl)]$_2$ (49 mg, 0.046 mmol), [Ru(bpy)$_2$(pytz-*m*-xyl-pytz)][PF$_6$]$_2$ (100 mg, 0.091 mmol), NH$_4$PF$_6$ (37 mg, 0.23 mmol). Yield: 43 mg (53 %). Calcd for [$C_{69}H_{62}IrN_{14}Ru$]$^{3+}$ (M^{3+}): *m/z* 460.47. Found: *m/z* 460.4694.

6.20.3 [Ru(2,2'-bipyridine)$_2$(1,2-bis((4-(pyridin-2-yl)-1*H*-1,2,3-triazol-1-yl)methyl)benzene)Ir(2-phenylpyridine)$_2$]3PF$_6$

[Ir(ppy)$_2$(μ-Cl)]$_2$ (49 mg, 0.046 mmol), [Ru(bpy)$_2$(pytz-*o*-xyl-pytz)][PF$_6$]$_2$ (100 mg, 0.091 mmol), NH$_4$PF$_6$ (37 mg, 0.23 mmol). Yield: 49 mg (61 %). Calcd for [$C_{69}H_{62}IrN_{14}Ru$]$^{3+}$ (M^{3+}): *m/z* 460.47. Found: *m/z* 460.4729.

6.21 General synthesis of [Ru(bpy)$_2$(pytz-o/m/p-xyl-pytz)Ir(dfppy)$_2$]3PF$_6$, JA1b-JA3b

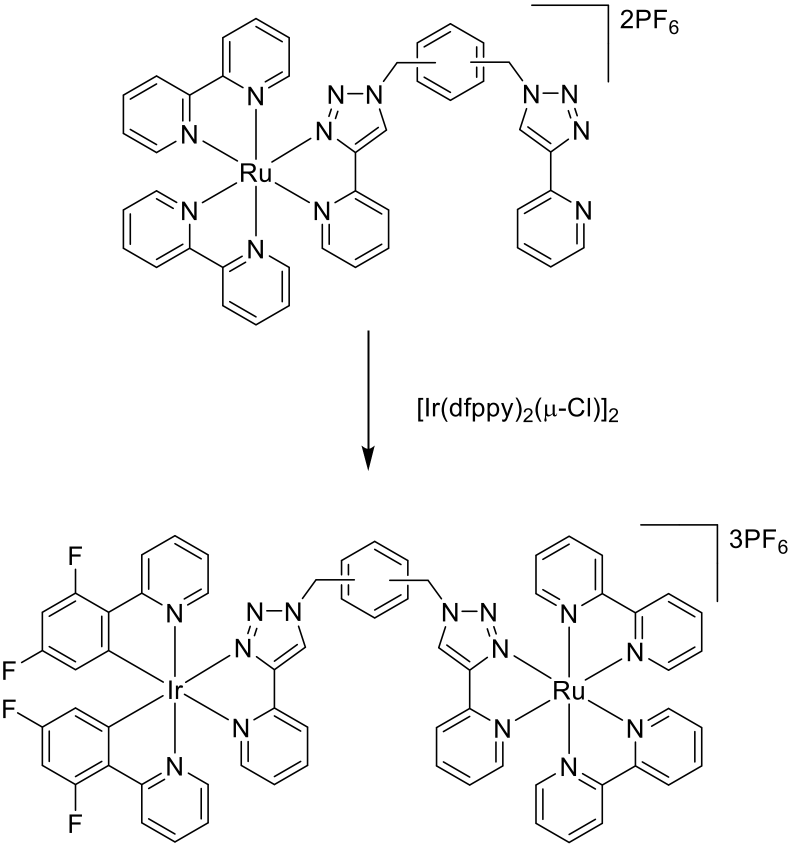

[Ir(dfppy)$_2$(μ-Cl)]$_2$ (1.0 eq.), [Ru(bpy)$_2$(pytz-o/m/p-xyl-pytz)][PF$_6$]$_2$ (2.0 eq.) and a stirrer bar were charged to an RBF, then placed under N$_2$. Deaerated DCM/MeOH (2:1, 30mL) was added via syringe, and solution refluxed, in absence of light and under N$_2$, for 16h. Solution allowed to cool to RT and then NH$_4$PF$_6$ (5 eq.) was added to precipitate an orange solid. Precipitate was then collected by vacuum filtration and washed with H$_2$O (~5ml) and Et$_2$O (~5ml). Crude product was purified by column chromatography; SiO$_2$, DCM/MeOH (98.5:1.5). Column vials were combined, and solvent removed under reduced pressure. Residue was recrystallised from DCM/Et$_2$O to yield the pure desired red product.

6.21.1 [Ru(2,2'-bipyridine)$_2$(1,4-bis((4-(pyridin-2-yl)-1*H*-1,2,3-triazol-1-yl)methyl)benzene)Ir(2-(4,6-difluorophenyl)pyridine)$_2$]3PF$_6$

[Ir(dfppy)$_2$(μ-Cl)]$_2$ (111 mg, 0.091 mmol), [Ru(bpy)$_2$(pytz-*p*-xyl-pytz)][PF$_6$]$_2$ (200 mg, 0.18 mmol), NH$_4$PF$_6$ (75 mg, 0.46 mmol). Yield: 46 mg (28 %). Calcd for [$C_{69}H_{58}F_4IrN_{14}Ru$]$^{3+}$ (M^{3+}): *m/z* 484.45. Found: *m/z* 484.4532.

6.21.2 [Ru(2,2'-bipyridine)$_2$(1,3-bis((4-(pyridin-2-yl)-1*H*-1,2,3-triazol-1-yl)methyl)benzene)Ir(2-(4,6-difluorophenyl)pyridine)$_2$]3PF$_6$

[Ir(dfppy)$_2$(μ-Cl)]$_2$ (55 mg, 0.046 mmol), [Ru(bpy)$_2$(pytz-*m*-xyl-pytz)][PF$_6$]$_2$ (100 mg, 0.091 mmol), NH$_4$PF$_6$ (37 mg, 0.23 mmol). Yield: 28 mg (33 %). Calcd for [C$_{69}$H$_{58}$F$_4$IrN$_{14}$Ru]$^{3+}$ (M^{3+}): *m/z* 484.45. Found: *m/z* 484.4485.

6.21.3 [Ru(2,2'-bipyridine)$_2$(1,2-bis((4-(pyridin-2-yl)-1*H*-1,2,3-triazol-1-yl)methyl)benzene)Ir(2-(4,6-difluorophenyl)pyridine)$_2$]3PF$_6$

[Ir(dfppy)$_2$(μ-Cl)]$_2$ (75 mg, 0.07 mmol), [Ru(bpy)$_2$(pytz-*o*-xyl-pytz)][PF$_6$]$_2$ (154 mg, 0.14 mmol), NH$_4$PF$_6$ (57 mg, 0.35 mmol). Yield: 32 mg (38 %). Calcd for [C$_{69}$H$_{58}$F$_4$IrN$_{14}$Ru]$^{3+}$ (M^{3+}): *m/z* 484.45. Found: *m/z* 484.4513.

6.22 Synthesis of [Ir(3,5-dimethyl-1-phenyl-1*H*-pyrazole)$_2$(1,1'-dibenzyl-1*H*,1'*H*-4,4'-bi(1,2,3-triazole)]PF$_6$, JA4

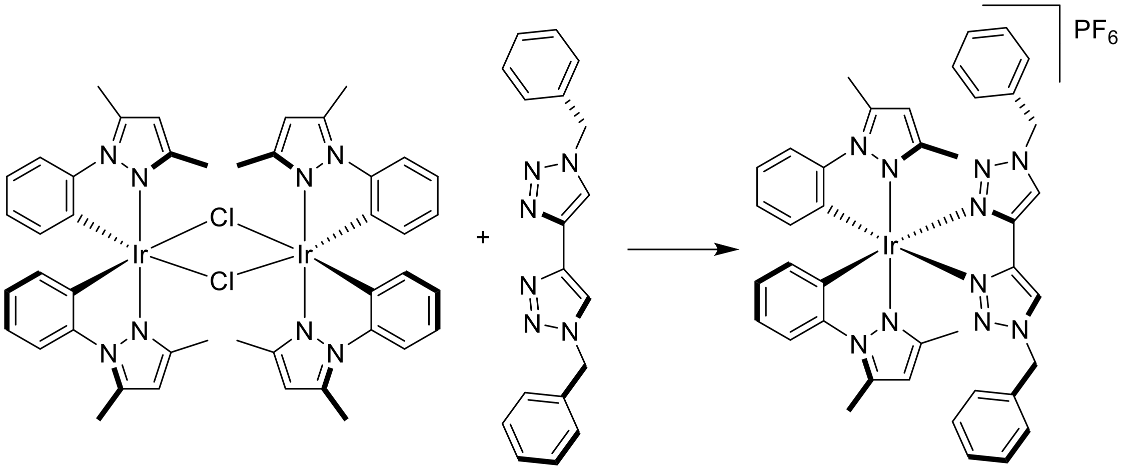

[Ir(dmppz)$_2$(μ-Cl)]$_2$ was prepared as per the literature.[162] This reaction took place under N_2 in the absence of light. An RBF was charged with [Ir(dmppz)$_2$(μ-Cl)]$_2$ (200 mg, 0.18 mmol), btz (166 mg, 0.53 mmol), deaerated $CHCl_3$:MeOH (3:1, 30 ml) was added and the mixture was stirred and heated at reflux for 17 h. Allow for the mixture to cool then add aqueous NH_4PF_6 (285 mg, 1.8 mmol) solution, leave solution to stir for 10 mins and then add Et_2O, product will precipitate. Then collect via vacuum filtration and wash with H_2O and EtOH. The product was purified via SiO_2 column with a DCM:MeOH (99:1) solvent system affording a white product. Yield: 54 mg (31 %). ^{1}H NMR (MeCN-*d$_3$*, 400MHz): δ 8.37 (s, 2H), 7.45 (d, $^3J_{HH}$ = 8.07 Hz, 2H), 7.37 (m, 6H), 7.14 (m, 4H), 6.94 (t, $^3J_{HH}$ = 7.12 Hz, 2H), 6.71 (t, $^3J_{HH}$ = 7.40 Hz, 2H), 6.30 (d, $^3J_{HH}$ = 7.20 Hz), 6.14 (s, 2H), 2.75 (s, 6H), 1.53 (s, 6H). HRMS (ESI). Calcd for $[C_{40}H_{38}IrN_{10}]^+$ (M^+): *m/z* 851.29. Found: *m/z* 851.2908.

6.23 Synthesis of [Ir(3,5-dimethyl-1-phenyl-1*H*-pyrazole)$_2$(2,2'-bipyridine)]PF$_6$, JA5

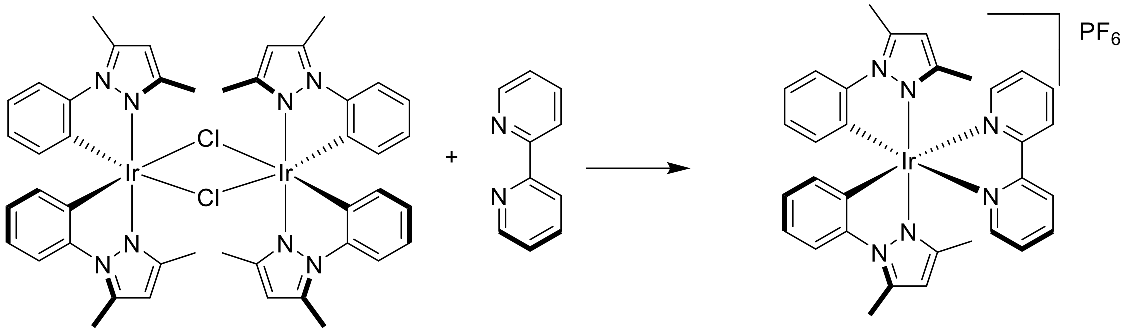

[Ir(dmppz)$_2$(μ-Cl)]$_2$ was prepared as per the literature.[162] This reaction took place under N_2 in the absence of light. An RBF was charged with [Ir(dmppz)$_2$(μ-Cl)]$_2$ (200 mg, 0.18 mmol), bpy (82 mg, 0.53 mmol), deaerated $CHCl_3$:MeOH (3:1, 30 ml) was added and the mixture was stirred and heated at reflux for 17 h. Allow for the mixture to cool then add aqueous NH_4PF_6 (285 mg, 1.8 mmol) solution, leave solution to stir for 10 mins and then add Et_2O, product will precipitate. Then collect via vacuum filtration and wash with H_2O and EtOH. The product was purified via SiO_2 column with a DCM:MeOH (99:1) solvent system affording a yellow product. Yield: 91 mg (62 %). ^{1}H NMR (MeCN-*d*$_3$, 400MHz): δ 8.52 (d, $^3J_{HH}$ = 8.18 Hz, 2H), 8.13 (td, $^3J_{HH}$ =8.28 Hz, $^3J_{HH}$ = 1.76 Hz, 2H), 8.03 (d, $^3J_{HH}$ =5.24 Hz, 2H), 7.60 (d, $^3J_{HH}$ = 8.12 Hz, 2H), 7.52 (td, $^3J_{HH}$ = 6.58 Hz, $^4J_{HH}$ = 1.27 Hz, 2H), 7.08 (td, $^3J_{HH}$ =8.48, $^4J_{HH}$ = 1.44 Hz, 2H), 6.84 (t, $^3J_{HH}$ = 7.59 Hz, 2H), 6.34 (d, $^3J_{HH}$ = 7.47 Hz, 2H), 6.14 (s, 2H), 2.81 (s, 3H), 1.48 (s, 3H). ^{13}C NMR (MeCN-*d*$_3$, 101MHz): δ 156.4338, 150.6578, 149.9594, 144.7851, 141.9525, 139.1914, 133.4256, 133.0176, 128.1517, 125.3879, 124.4017, 123.1363, 113.1322, 109.9616, 13.6371, 11.5019. HRMS (ESI). Calcd for $[C_{32}H_{30}IrN_6]^+$ (M^+): *m/z* 691.22. Found: *m/z* 691.2155.

6.24 Synthesis of [Ir(3,5-dimethyl-1-phenyl-1*H*-pyrazole)$_2$(2-(1-benzyl-1*H*-1,2,3-triazol-4-yl)pyridine)]PF$_6$, JA6

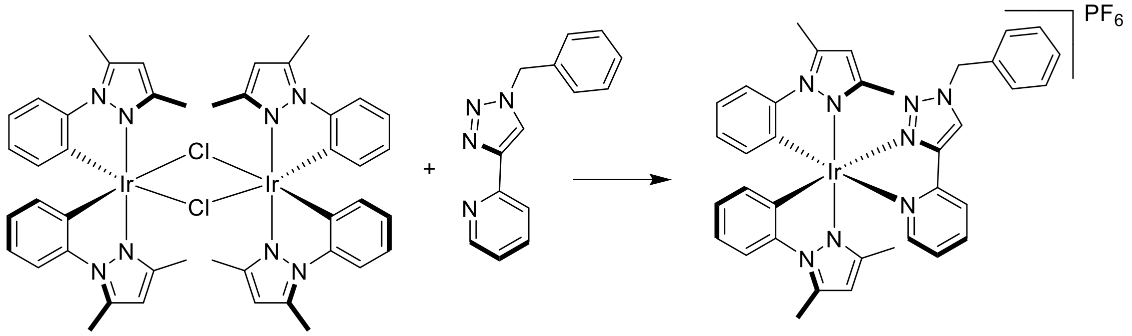

[Ir(dmppz)$_2$(μ-Cl)]$_2$ was prepared as per the literature.[162] This reaction took place under N_2 in the absence of light. An RBF was charged with [Ir(dmppz)$_2$(μ-Cl)]$_2$ (200 mg, 0.18 mmol), pytz (124 mg, 0.53 mmol), deaerated $CHCl_3$:MeOH (3:1, 30 ml) was added and the mixture was stirred and heated at reflux for 17 h. Allow for the mixture to cool then add aqueous NH_4PF_6 (285 mg, 1.8 mmol) solution, leave solution to stir for 10 mins and then add Et_2O, product will precipitate. Then collect via vacuum filtration and wash with H_2O and EtOH. The product was purified via SiO_2 column with a DCM:MeOH (99:1) solvent system affording a pale yellow product.Yield: 143 mg (89 %). ^{1}H NMR (MeCN-d_3, 400MHz): δ 8.67 (s, 1H), 8.06 (m, 2H), 7.85 (d, $^3J_{HH}$ = 5.40 Hz, 1H), 7.56 (d, $^3J_{HH}$ = 7.72 Hz, 1H), 7.50 (d, $^3J_{HH}$ = 8.11 Hz, 1H), 7.42 (m, 3H), 7.35 (t, $^3J_{HH}$ = 7.26 Hz, 1H), 7.22 (m, 2H), 7.07 (t, $^3J_{HH}$ = 7.04 Hz, 1H), 6.75 (t, $^3J_{HH}$ = 7.06 Hz, 1H), 6.83 (t, $^3J_{HH}$ = 7.42 Hz, 1H), 6.75 (t, $^3J_{HH}$ = 7.43 Hz, 1H), 6.36 (d, $^3J_{HH}$ = 7.07 Hz, 1H), 6.28 (d, $^3J_{HH}$ = 7.56 Hz, 1H), 6.15 (s, 2H), 5.61 (s, 2H), 2.80 (s, 6H), 1.56 (s, 3H), 1.47 (s, 3H). ^{13}C NMR (MeCN-d_3, 101MHz): δ 150.2521, 150.0393, 149.9441, 149.8086, 149.272, 145.185, 144.9035, 141.958, 141.5987, 139.5078, 134.0967, 133.656, 133.4309, 132.3961, 129.1156, 128.9857, 128.8695, 127.9505, 126.5464, 126.2147, 125.3137, 124.7842, 123.2721, 122.8931, 122.7915, 113.0711, 112.4526, 109.8199, 109.7965, 55.3414, 13.6558, 13.5811, 11.5231, 11.4021. HRMS (ESI). Calcd for $[C_{36}H_{34}IrN_8]^+$ (M^+): *m/z* 771.25. Found: *m/z* 771.2531.

6.25 Synthesis of [Ir(3,5-dimethyl-1-phenyl-1*H*-pyrazole)$_2$(2-(1-benzyl-1*H*-1,2,3-triazol-4-yl)-6-methylpyridine)]PF$_6$, JA7

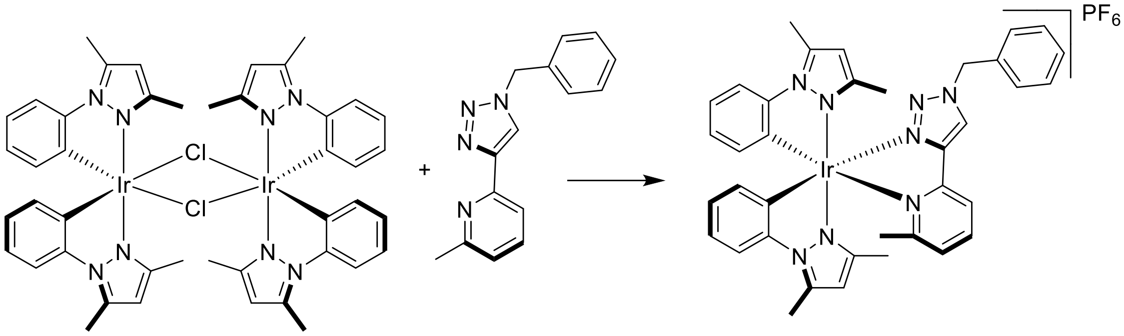

[Ir(dmppz)$_2$(μ-Cl)]$_2$ was prepared as per the literature.[162] This reaction took place under N_2 in the absence of light. An RBF was charged with [Ir(dmppz)$_2$(μ-Cl)]$_2$ (196 mg, 0.17 mmol), m-pytz (131 mg, 0.52 mmol), deaerated $CHCl_3$:MeOH (3:1, 30 ml) was added and the mixture was stirred and heated at reflux for 17 h. Allow for the mixture to cool then add aqueous NH_4PF_6 (285 mg, 1.72 mmol) solution, leave solution to stir for 10 mins and then add Et_2O, product will precipitate. Then collect via vacuum filtration and wash with H_2O and EtOH. The product was purified via SiO_2 column with a DCM:MeOH (99:1) solvent system afforded the pale yellow product. Yield: 86 mg (54 %). ^{1}H NMR (MeCN-d_3, 400MHz): δ 8.61 (s, 1H), 7.91 (m, 2H), 7.51 (d, $^3J_{HH}$ = 8.33 Hz, 1H), 7.40 (m, 4H), 7.29 (d, $^3J_{HH}$ = 7.48 Hz, 1H), 7.12 (m, 2H), 6.95 (t, $^3J_{HH}$ = 7.03 Hz, 2H), 6.71 (m, 2H), 6.30 (d, $^3J_{HH}$ = 8.01 Hz, 1H), 6.19 (d, $^3J_{HH}$ = 14.54 Hz, 2H), 6.01 (d, $^3J_{HH}$ = 7.70 Hz, 1H), 5.53 (s, 2H), 2.86 (s, 3H), 2.76 (s, 3H), 1.58 (s, 3H), 1.55 (s, 3H). ^{13}C NMR (MeCN-d_3, 101MHz): δ 163.7746, 150.4667, 150.1164, 149.7119, 144.6062, 142.0889, 141.5779, 139.7683, 134.1505, 133.5559, 132.7121, 129.0755, 128.9046, 127.695, 127.0485, 126.1565, 125.0924, 124.7126, 122.9195, 122.5127, 120.1477, 112.9234, 112.2516, 109.8604, 109.7046, 55.1549, 25.7671, 13.6472, 13.6043, 11.5499, 11.4972. HRMS (ESI). Calcd for $[C_{37}H_{36}IrN_8]^+$ (M^+): *m/z* 785.27. Found: *m/z* 785.2685.

6.26 Synthesis of [Ir(4'-(*p*-tolyl)-2,2':6',2''-terpyridine)(1-benzyl-4-phenyl-1*H*-1,2,3-triazole)Cl]PF$_6$, JA8

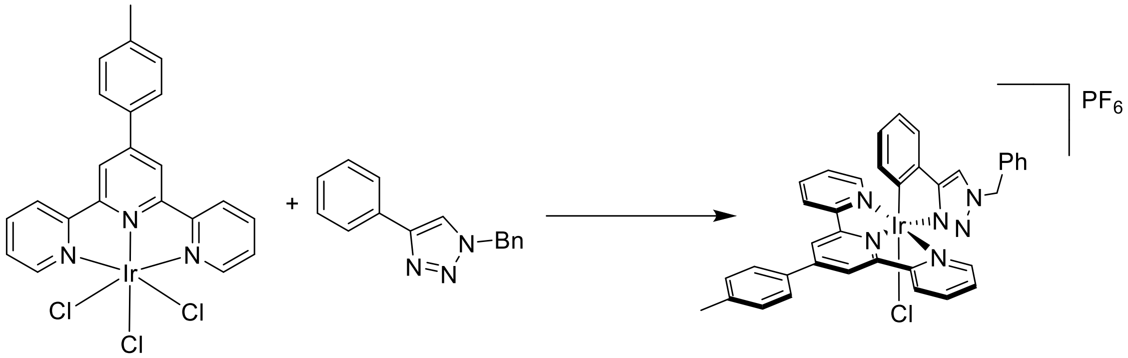

Ir(tol-terpy)Cl$_3$ was prepared via reported synthetic procedure.[229] The reaction was performed under N$_2$. An RBF was charged with Ir(tol-terpy)Cl$_3$ (200 mg, 0.32 mmol), ptz (265 mg, 1.13 mmol) and ethylene glycol (10 ml). The mixture was stirred and heated to reflux for 16 h. Allowed to cool to r. t., then NH$_4$PF$_6$ (420 mg, 2.58 mmol) dissolved in H$_2$O (20 ml) were added. Product precipitates and is collected via vacuum filtration and then washed with H$_2$O and Et$_2$O. rude product was purified by column chromatography; SiO$_2$, MeCN:H$_2$O:KNO$_3$ (10:1:1). Column vials were combined, and solvent removed under reduced pressure, re-dissolved in min. MeOH and NH$_4$PF$_6$ (420 mg, 2.58 mmol) was added to change the counter ion from NO$_3$ to PF$_6$. Another SiO$_2$ column, DCM:Acetone (99:1) and a recrystallisation from DCM:Et$_2$O resulted in orange precipitate collected by vacuum filtration to afford the pure desired product. Yield: 161 mg (54 %). ^{1}H NMR (MeCN-*d*$_3$, 400MHz): δ 8.84 (s, 1H), 8.74 (s, 1H), 8.61 (d, $^3J_{HH}$ = 9.12 Hz, 1H), 8.50 (d, $^3J_{HH}$ = 7.67 Hz, 1H), 8.43 (d, $^3J_{HH}$ = 17.72 Hz, 1H), 8.23 (td, $^3J_{HH}$ = 7.94 Hz, $^3J_{HH}$ = 1.46 Hz, 1H), 8.05 (m, 3H), 7.78 (d, $^3J_{HH}$ = 5.41 Hz, 2H), 7.65 (t, $^3J_{HH}$ = 9.01 Hz, 2H), 7.56 (m, 7H), 7.47 (t, $^3J_{HH}$ = 6.49 Hz, 1H), 6.92 (dt, $^3J_{HH}$ = 27.44 Hz, $^3J_{HH}$ = 7.31 Hz, 1H), 6.69 (dt, $^3J_{HH}$ = 22.32 Hz, $^3J_{HH}$ = 7.31 Hz), 1H), 5.97 (d, $^3J_{HH}$ = 41.80 Hz, 1H), 5.95 (d, $^3J_{HH}$ = 4.45 Hz, 2H), 2.54 (d, $^2J_{HH}$ = 10.42 Hz, 3H). HRMS (ESI). Calcd for [C$_{37}$H$_{29}$ClIrN$_6$]$^+$ (M$^+$): *m/z* 785.18. Found: *m/z* 785.1832.

6.27 Synthesis of [Ir(2,6-bis(1-benzyl-1*H*-1,2,3-triazol-4-yl)pyridine)(2-phenylpyridine)]PF$_6$, JA9

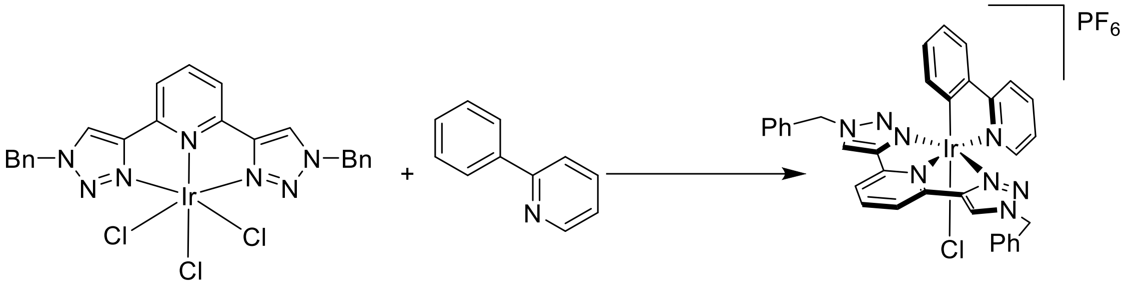

Ir(tz-py-tz)Cl$_3$ was prepared via reported synthetic procedure.[229] The reaction was performed under N_2. An RBF was charged with Ir(tz-py-tz)Cl$_3$ (200 mg, 0.29 mmol), ppy (157 mg, 1.01 mmol.) and ethylene glycol (10 ml). The mixture was stirred and heated to reflux for 16 h. Allowed to cool to r. t., then NH_4PF_6 (377 mg, 2.3 mmol) dissolved in H_2O (20 ml) were added. Product precipitates and is collected via vacuum filtration and then washed with H_2O and Et_2O. Crude product was purified by column chromatography; SiO_2, DCM:MeOH (96:4). Column vials were combined, and solvent removed under reduced pressure followed by recrystallisation from DCM:Et_2O resulting in yellow precipitate collected by vacuum filtration to afford the pure desired yellow product. Yield: 114 mg (43 %). ^{1}H NMR (MeCN-*d*$_3$, 400MHz): δ 9.94 (d, $^3J_{HH}$ = 5.78 Hz, 1H), 8.57 (s, 1H), 8.18 (m, 5H), 7.77 (d, $^3J_{HH}$ = 8.17 Hz, 1H), 7.56 (t, $^3J_{HH}$ = 5.92 Hz, 1H), 7.36 (m, 6H), 7.19 (m, 4H), 6.99 (t, $^3J_{HH}$ = 7.55 Hz, 1H), 6.79 (t, $^3J_{HH}$ = 7.47 Hz, 1H), 6.03 (d, $^3J_{HH}$ = 7.57 Hz, 1H), 5.50 (s, 4H). ^{13}C NMR (MeCN-*d*$_3$, 101MHz): δ 166.8488, 151.6193, 149.775, 149.3606, 144.3966, 141.1141, 139.9679, 138.7147, 133.0838, 130.754, 130.2886, 129.2882, 129.2254, 128.4656, 127.3922, 124.6582, 124.2512, 123.253, 120.9304, 119.7298, 55.988. HRMS (ESI). Calcd for $[C_{34}H_{27}ClIrN_8]^+$ (M^+): *m/z* 775.17. Found: *m/z* 775.1670.

6.28 Synthesis of [Ir(2,6-bis(1-benzyl-1*H*-1,2,3-triazol-4-yl)pyrazine)(2-phenylpyridine)]PF_6 ,JA10

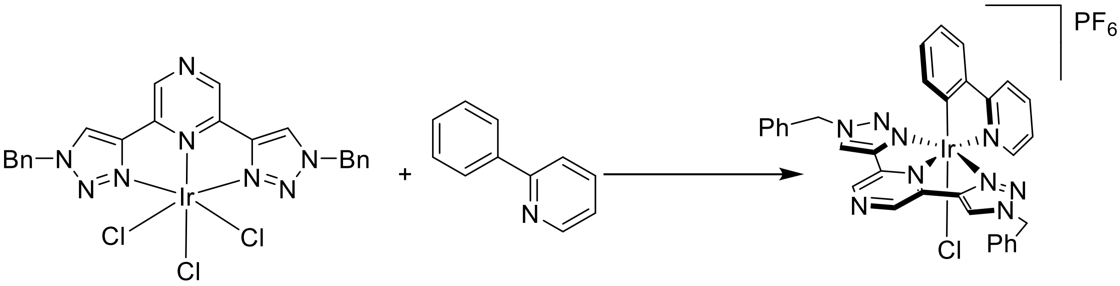

Ir(tz-pyz-tz)Cl_3 was prepared via reported synthetic procedure.[229] The reaction was performed under N_2. An RBF was charged with Ir(tz-pyz-tz)Cl_3 (200 mg, 0.29 mmol), ppy (157 mg, 1.01 mmol) and ethylene glycol (10 ml). The mixture was stirred and heated to reflux for 16 h. Allowed to cool to r. t., then NH_4PF_6 (377 mg, 2.31 mmol) dissolved in H_2O (20 ml) were added. Product precipitates and is collected via vacuum filtration and then washed with H_2O and Et_2O. Crude product was purified by column chromatography; SiO_2, DCM:MeOH (98:2). Column vials were combined, and solvent removed under reduced pressure followed by recrystallisation from DCM:Et_2O resulting in yellow precipitate collected by vacuum filtration to afford the pure desired yellow product. Yield: 29 mg (11 %). ^{1}H NMR (MeCN-d_3, 400MHz): δ 9.93 (d, $^3J_{HH}$ = 6.50 Hz, 1H), 9.27 (s, 2H), 8.69 (s, 2H), 8.22 (d, $^3J_{HH}$ = 7.84 Hz, 1H), 8.13 (t, $^3J_{HH}$ = 7.45 Hz, 1H), 7.79 (d, $^3J_{HH}$ = 7.83 Hz, 1H), 7.60 (t, $^3J_{HH}$ = 7.34 Hz, 1H), 7.37 (m, 6H), 7.20 (m, 4H), 7.00 (t, $^3J_{HH}$ = 7.56 Hz, 1H), 6.80 (t, $^3J_{HH}$ = 7.48 Hz, 1H), 6.03 (d, $^3J_{HH}$ = 7.75 Hz, 1H), 5.53 (s, 4H). HRMS (ESI). Calcd for $[C_{33}H_{26}ClIrN_9]^+$ (M^+): *m/z* 776.16. Found: *m/z* 776.1622.

6.29 Synthesis of [Ir(2,6-bis(1-benzyl-1*H*-1,2,3-triazol-4-yl)pyridine)(2-(4-fluorophenyl)pyridine)]PF_6, JA11

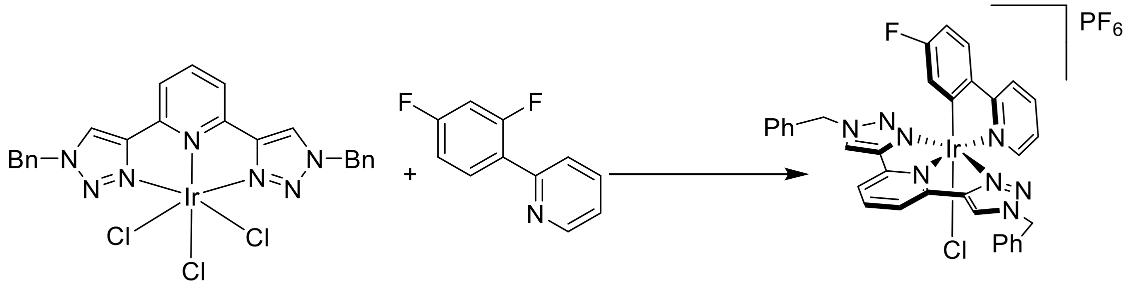

Ir(tz-py-tz)Cl_3 was prepared via reported synthetic procedure.[229] The reaction was performed under N_2. An RBF was charged with Ir(tz-py-tz)Cl_3 (200 mg, 0.29 mmol), dfppy (193 mg, 1.01 mmol) and ethylene glycol (10 ml). The mixture was stirred and heated to reflux for 16 h. Allowed to cool to r. t., then NH_4PF_6 (377 mg, 2.31 mmol) dissolved in H_2O (20 ml) were added. Product precipitates and is collected via vacuum filtration and then washed with H_2O and Et_2O. Crude product was purified by column chromatography; SiO_2, DCM:MeOH (98:2). Column vials were combined, and solvent removed under reduced pressure followed by recrystallisation from DCM:Et_2O resulting in yellow precipitate collected by vacuum filtration to afford the pure desired yellow product. Yield: 136 mg (49 %). ^1H NMR (MeCN-d_3, 400MHz): δ 9.91 (d, $^3J_{HH} = 5.84$ Hz, 1H), 8.57 (s, 2H), 8.26 (t, $^3J_{HH} = 8.03$ Hz, 1H), 8.14 (m, 3H), 8.09 (td, $^3J_{HH} = 7.40$ Hz, $^3J_{HH} = 1.57$ Hz, 1H) 7.82 (dd, $^3J_{HH} = 8.63$ Hz, $^3J_{HH} = 5.52$ Hz, 1H), 7.56 (td, $^3J_{HH} = 7.26$ Hz, $^3J_{HH} = 1.54$ Hz, 1H), 7.37 (m, 6H), 7.21 (m, 4H), 6.75 (td, $^3J_{HH} = 8.83$ Hz, $^3J_{HH} = 2.82$ Hz, 1H) 5.72 (dd, $^3J_{HH} = 9.00$ Hz, $^3J_{HH} = 2.55$ Hz, 1H) 5.51 (s, 4H). HRMS (ESI). Calcd for $[C_{34}H_{26}ClFIrN_8]^+$ (M^+): *m/z* 793.16. Found: *m/z* 793.1575.

6.30 Synthesis of [Ir(2,6-bis(1-benzyl-1*H*-1,2,3-triazol-4-yl)pyrazine)(2-(4-fluorophenyl)pyridine)]PF$_6$, JA12

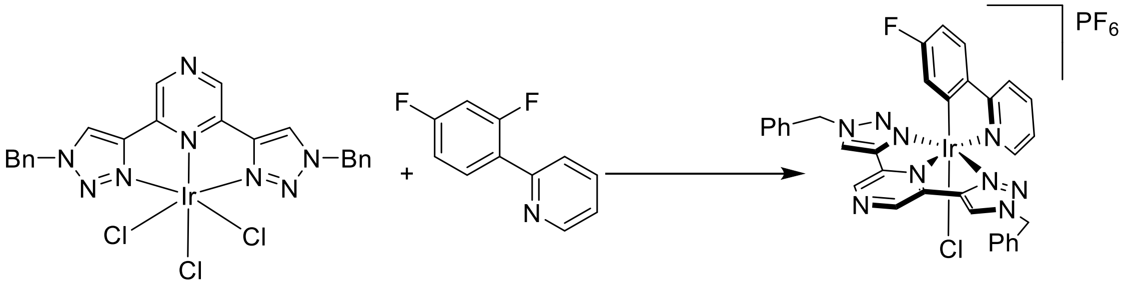

Ir(tz-pyz-tz)Cl$_3$ was prepared via reported synthetic procedure.[229] The reaction was performed under N_2. An RBF was charged with Ir(tz-pyz-tz)Cl$_3$ (200 mg, 0.29 mmol), dfppy (193 mg, 1.01 mmol) and ethylene glycol (10 ml). The mixture was stirred and heated to reflux for 16 h. Allowed to cool to r. t., then NH_4PF_6 (377 mg, 2.31 mmol) dissolved in H_2O (20 ml) were added. Product precipitates and is collected via vacuum filtration and then washed with H_2O and Et_2O. Crude product was purified by column chromatography; SiO_2, DCM:MeOH (99:1). Column vials were combined, and solvent removed under reduced pressure followed by recrystallisation from DCM:Et_2O resulting in yellow precipitate collected by vacuum filtration to afford the pure desired product. Yield: 83 mg (30 %). ^{1}H NMR (MeCN-*d*$_3$, 400MHz): δ 9.89 (d, $^3J_{HH}$ = 5.72 Hz, 1H), 9.27 (s, 2H), 8.68 (s, 2H), 8.14 (m, 2H), 7.83 (dd, $^3J_{HH}$ = 8.59 Hz, $^3J_{HH}$ = 5.55 Hz, 1H), 7.58 (td, $^3J_{HH}$ = 6.52 Hz, $^3J_{HH}$ = 1.82 Hz, 1H) , 7.37 (m, 6H), 7.22 (m, 4H), 6.77 (td, $^3J_{HH}$ = 8.85 Hz, $^3J_{HH}$ = 2.40 Hz, 1H), 5.79 (dd, $^3J_{HH}$ = 8.93 Hz, $^3J_{HH}$ = 2.55 Hz, 1H), 5.54 (s, 4H) HRMS (ESI). Calcd for $[C_{33}H_{25}ClFIrN_9]^+$ (M^+): *m/z* 794.15. Found: *m/z* 794.1528

7. References

1. M. Paul, *Annals of Botany*, 2013, **111**, ix-ix.
2. X. Ma and H. Tian, *Angewandte Chemie International Edition*, 2014, **53**, 8817-8817.
3. Q. Wang, R. W. Schoenlein, L. A. Peteanu, R. A. Mathies and C. V. Shank, *Science*, 1994, **266**, 422-424.
4. P. C. Hanawalt, *Photophysiology*, 1964, **4**, 203-251.
5. Y. Kamegaya, W. A. Farinelli, A. V. Vila Echague, H. Akita, J. Gallagher, T. J. Flotte, R. R. Anderson, R. W. Redmond and I. E. Kochevar, *Lasers in Surgery and Medicine*, 2005, **37**, 264-270.
6. A. M. Shaw, *Astrochemistry: From Astronomy to Astrobiology*, Wiley, 2006.
7. J. W. Hastings, C. J. Potrikusv, S. C. Gupta, M. Kurfürst and J. C. Makemson, in *Advances in Microbial Physiology*, eds. A. H. Rose and D. W. Tempest, Academic Press, 1985, vol. 26, pp. 235-291.
8. J. A. Prescher and C. H. Contag, *Current Opinion in Chemical Biology*, 2010, **14**, 80-89.
9. R. L. House, N. Y. M. Iha, R. L. Coppo, L. Alibabaei, B. D. Sherman, P. Kang, M. K. Brennaman, P. G. Hoertz and T. J. Meyer, *Journal of Photochemistry and Photobiology C: Photochemistry Reviews*, 2015, **25**, 32-45.
10. S. Berardi, S. Drouet, L. Francàs, C. Gimbert-Suriñach, M. Guttentag, C. Richmond, T. Stoll and A. Llobet, *Chemical Society Reviews*, 2014, **43**, 7501-7519.
11. B. Zhang and L. Sun, *Chemical Society Reviews*, 2019, **48**, 2216-2264.
12. H. Hennig, *Coordination Chemistry Reviews*, 1999, **182**, 101-123.
13. J. Twilton, C. Le, P. Zhang, M. H. Shaw, R. W. Evans and D. W. C. MacMillan, *Nature Reviews Chemistry*, 2017, **1**, 0052.
14. J. D. Bell and J. A. Murphy, *Chemical Society Reviews*, 2021, **50**, 9540-9685.
15. E. C. Harvey, B. L. Feringa, J. G. Vos, W. R. Browne and M. T. Pryce, *Coordination Chemistry Reviews*, 2015, **282-283**, 77-86.
16. J. W. Canary, S. Mortezaei and J. Liang, *Coordination Chemistry Reviews*, 2010, **254**, 2249-2266.
17. M. Natali and S. Giordani, *Chemical Society Reviews*, 2012, **41**, 4010-4029.
18. B. Parida, S. Iniyan and R. Goic, *Renewable and Sustainable Energy Reviews*, 2011, **15**, 1625-1636.
19. L. El Chaar, L. A. lamont and N. El Zein, *Renewable and Sustainable Energy Reviews*, 2011, **15**, 2165-2175.
20. L. L. Kazmerski, *Renewable and Sustainable Energy Reviews*, 1997, **1**, 71-170.
21. T. Fleetham, G. Li and J. Li, *Advanced Materials*, 2017, **29**, 1601861.
22. L. Xiao, Z. Chen, B. Qu, J. Luo, S. Kong, Q. Gong and J. Kido, *Advanced Materials*, 2011, **23**, 926-952.
23. E. Holder, B. M. W. Langeveld and U. S. Schubert, *Advanced Materials*, 2005, **17**, 1109-1121.
24. F. L. Thorp-Greenwood, R. G. Balasingham and M. P. Coogan, *Journal of Organometallic Chemistry*, 2012, **714**, 12-21.
25. D.-L. Ma, H.-Z. He, K.-H. Leung, D. S.-H. Chan and C.-H. Leung, *Angewandte Chemie International Edition*, 2013, **52**, 7666-7682.
26. C. Caporale and M. Massi, *Coordination Chemistry Reviews*, 2018, **363**, 71-91.
27. Z. Liu, W. He and Z. Guo, *Chemical Society Reviews*, 2013, **42**, 1568-1600.
28. D.-L. Ma, V. P.-Y. Ma, D. S.-H. Chan, K.-H. Leung, H.-Z. He and C.-H. Leung, *Coordination Chemistry Reviews*, 2012, **256**, 3087-3113.
29. S. E. Angell, C. W. Rogers, Y. Zhang, M. O. Wolf and W. E. Jones, *Coordination Chemistry Reviews*, 2006, **250**, 1829-1841.
30. L. K. McKenzie, H. E. Bryant and J. A. Weinstein, *Coordination Chemistry Reviews*, 2019, **379**, 2-29.
31. S. Monro, K. L. Colón, H. Yin, J. Roque, III, P. Konda, S. Gujar, R. P. Thummel, L. Lilge, C. G. Cameron and S. A. McFarland, *Chemical Reviews*, 2019, **119**, 797-828.

32. S. Y. Lee, C. Y. Kim and T.-G. Nam, *Drug Design, Development and Therapy*, 2020, **14**, 5375-5392.
33. L. Gourdon, K. Cariou and G. Gasser, *Chemical Society Reviews*, 2022, **51**, 1167-1195.
34. J. Frenkel, *Physical Review*, 1931, **37**, 1276-1294.
35. S. I. Pekar, *Journal of Physics and Chemistry of Solids*, 1958, **5**, 11-22.
36. B. W. Shore, *Journal*, 2020, DOI: 10.1093/oso/9780198862857.003.0003, 0.
37. P. a. W. Klan, J., *Photochemistry of Organic Compounds: From Concepts to Practice*, Wiley, Chichester, 2009.
38. R. Rennie and J. Law, *A Dictionary of Chemistry*, Oxford University Press, 2016.
39. D. F. Swinehart, *Journal of Chemical Education*, 1962, **39**, 333.
40. A. A. Svidzinsky, M. O. Scully and D. R. Herschbach, *Proceedings of the National Academy of Sciences*, 2005, **102**, 11985-11988.
41. J. M. Hollas, *Modern Spectroscopy*, Wiley, Chichester, 4th edn., 2004.
42. J. M. Brown, *Molecular Spectroscopy*, Oxford University Press, New York, 1998.
43. P. W. Langhoff, S. T. Epstein and M. Karplus, *Reviews of Modern Physics*, 1972, **44**, 602-644.
44. C. L. Hammer and T. A. Weber, *Journal of Mathematical Physics*, 2004, **6**, 1591-1606.
45. M. Born and R. Oppenheimer, *Annalen der Physik*, 1927, **389**, 457-484.
46. J. G. Duque, H. Chen, A. K. Swan, A. P. Shreve, S. Kilina, S. Tretiak, X. Tu, M. Zheng and S. K. Doorn, *ACS Nano*, 2011, **5**, 5233-5241.
47. E. Condon, *Physical Review*, 1926, **28**, 1182-1201.
48. J. Franck and E. G. Dymond, *Transactions of the Faraday Society*, 1926, **21**, 536-542.
49. T. Moitra, P. Karak, S. Chakraborty, K. Ruud and S. Chakrabarti, *Physical Chemistry Chemical Physics*, 2021, **23**, 59-81.
50. F. A. Cotton, *Chemical Applications of Group Theory*, Wiley, Chichester, 3rd edn., 1990.
51. C. M. Marian, *WIREs Computational Molecular Science*, 2012, **2**, 187-203.
52. J. Heine and K. Müller-Buschbaum, *Chemical Society Reviews*, 2013, **42**, 9232-9242.
53. A. Jablonski, *Nature*, 1933, **131**, 839-840.
54. S. Campagna, F. Puntoriero, F. Nastasi, G. Bergamini and V. Balzani, in *Photochemistry and Photophysics of Coordination Compounds I*, eds. V. Balzani and S. Campagna, Springer Berlin Heidelberg, Berlin, Heidelberg, 2007, DOI: 10.1007/128_2007_133, pp. 117-214.
55. D. J. Nesbitt and R. W. Field, *The Journal of Physical Chemistry*, 1996, **100**, 12735-12756.
56. M. Bixon and J. Jortner, *The Journal of Chemical Physics*, 2003, **48**, 715-726.
57. T. Itoh, *Chemical Reviews*, 2012, **112**, 4541-4568.
58. M. Kasha, *Discussions of the Faraday Society*, 1950, **9**, 14-19.
59. T. Förster, 1973, **34**, 225-234.
60. C. C. J. Roothaan, *Reviews of Modern Physics*, 1951, **23**, 69-89.
61. P. A. Scattergood and P. I. P. Elliott, *Dalton Transactions*, 2017, **46**, 16343-16356.
62. K. Eastham, P. A. Scattergood, D. Chu, R. Z. Boota, A. Soupart, F. Alary, I. M. Dixon, C. R. Rice, S. J. O. Hardman and P. I. P. Elliott, *Inorganic Chemistry*, 2022, **61**, 19907-19924.
63. C. E. Welby, S. Grkinic, A. Zahid, B. S. Uppal, E. A. Gibson, C. R. Rice and P. I. P. Elliott, *Dalton Transactions*, 2012, **41**, 7637-7646.
64. C. E. Housecroft and E. C. Constable, *Coordination Chemistry Reviews*, 2017, **350**, 155-177.
65. E. Baranoff, J.-H. Yum, M. Graetzel and M. K. Nazeeruddin, *Journal of Organometallic Chemistry*, 2009, **694**, 2661-2670.
66. S. Lamansky, P. Djurovich, D. Murphy, F. Abdel-Razzaq, H.-E. Lee, C. Adachi, P. E. Burrows, S. R. Forrest and M. E. Thompson, *Journal of the American Chemical Society*, 2001, **123**, 4304-4312.
67. P. Coppo, E. A. Plummer and L. De Cola, *Chemical Communications*, 2004, DOI: 10.1039/B406851C, 1774-1775.
68. M. S. Lowry and S. Bernhard, *Chemistry – A European Journal*, 2006, **12**, 7970-7977.
69. S.-H. Wu, J.-W. Ling, S.-H. Lai, M.-J. Huang, C. H. Cheng and I. C. Chen, *The Journal of Physical Chemistry A*, 2010, **114**, 10339-10344.
70. K. Dedeian, P. Djurovich, F. Garces, G. Carlson and R. Watts, *Inorganic Chemistry*, 1991, **30**, 1685-1687.

71. A. B. Tamayo, S. Garon, T. Sajoto, P. I. Djurovich, I. M. Tsyba, R. Bau and M. E. Thompson, *Inorganic Chemistry*, 2005, **44**, 8723-8732.
72. L. Flamigni, A. Barbieri, C. Sabatini, B. Ventura and F. Barigelletti, in *Photochemistry and Photophysics of Coordination Compounds II*, eds. V. Balzani and S. Campagna, Springer Berlin Heidelberg, Berlin, Heidelberg, 2007, DOI: 10.1007/128_2007_131, pp. 143-203.
73. A. Tsuboyama, H. Iwawaki, M. Furugori, T. Mukaide, J. Kamatani, S. Igawa, T. Moriyama, S. Miura, T. Takiguchi, S. Okada, M. Hoshino and K. Ueno, *Journal of the American Chemical Society*, 2003, **125**, 12971-12979.
74. A. Juris, V. Balzani, F. Barigelletti, S. Campagna, P. Belser and A. von Zelewsky, *Coordination Chemistry Reviews*, 1988, **84**, 85-277.
75. M. A. Baldo, S. Lamansky, P. E. Burrows, M. E. Thompson and S. R. Forrest, *Applied Physics Letters*, 1999, **75**, 4-6.
76. M. Meldal and C. W. Tornøe, *Chemical Reviews*, 2008, **108**, 2952-3015.
77. B. S. Uppal, R. K. Booth, N. Ali, C. Lockwood, C. R. Rice and P. I. Elliott, *Dalton Transactions*, 2011, **40**, 7610-7616.
78. C. E. Welby, S. Grkinic, A. Zahid, B. S. Uppal, E. A. Gibson, C. R. Rice and P. I. Elliott, *Dalton Transactions*, 2012, **41**, 7637-7646.
79. B. Happ, C. Friebe, A. Winter, M. D. Hager, R. Hoogenboom and U. S. Schubert, *Chemistry–An Asian Journal*, 2009, **4**, 154-163.
80. J. T. Fletcher, B. J. Bumgarner, N. D. Engels and D. A. Skoglund, *Organometallics*, 2008, **27**, 5430-5433.
81. S. A. Omar, P. A. Scattergood, L. K. McKenzie, H. E. Bryant, J. A. Weinstein and P. I. Elliott, *Molecules*, 2016, **21**, 1382.
82. D. A. Ross, P. A. Scattergood, A. Babaei, A. Pertegás, H. J. Bolink and P. I. Elliott, *Dalton Transactions*, 2016, **45**, 7748-7757.
83. C. E. Welby, L. Gilmartin, R. R. Marriott, A. Zahid, C. R. Rice, E. A. Gibson and P. I. Elliott, *Dalton Transactions*, 2013, **42**, 13527-13536.
84. L. Donato, P. Abel and E. Zysman-Colman, *Dalton Transactions*, 2013, **42**, 8402-8412.
85. S. Zanarini, M. Felici, G. Valenti, M. Marcaccio, L. Prodi, S. Bonacchi, P. Contreras-Carballada, R. M. Williams, M. C. Feiters and R. J. Nolte, *Chemistry–A European Journal*, 2011, **17**, 4640-4647.
86. M. Mydlak, C. Bizzarri, D. Hartmann, W. Sarfert, G. Schmid and L. De Cola, *Advanced Functional Materials*, 2010, **20**, 1812-1820.
87. B. Beyer, C. Ulbricht, D. Escudero, C. Friebe, A. Winter, L. González and U. S. Schubert, *Organometallics*, 2009, **28**, 5478-5488.
88. T. U. Connell, J. M. White, T. A. Smith and P. S. Donnelly, *Inorganic Chemistry*, 2016, **55**, 2776-2790.
89. J. M. Fernández-Hernández, J. I. Beltrán, V. Lemaur, M.-D. Gálvez-López, C.-H. Chien, F. Polo, E. Orselli, R. Fröhlich, J. Cornil and L. De Cola, *Inorganic Chemistry*, 2013, **52**, 1812-1824.
90. M. Felici, P. Contreras-Carballada, Y. Vida, J. M. M. Smits, R. J. M. Nolte, L. De Cola, R. M. Williams and M. C. Feiters, *Chemistry – A European Journal*, 2009, **15**, 13124-13134.
91. M. Mydlak, C. Bizzarri, D. Hartmann, W. Sarfert, G. Schmid and L. De Cola, *Advanced Functional Materials*, 2010, **20**, 1812-1820.
92. T. Sajoto, P. I. Djurovich, A. B. Tamayo, J. Oxgaard, W. A. Goddard, III and M. E. Thompson, *Journal of the American Chemical Society*, 2009, **131**, 9813-9822.
93. J. M. Fernandez-Hernandez, J. I. Beltran, V. Lemaur, M.-D. Galvez-Lopez, C.-H. Chien, F. Polo, E. Orselli, R. Fröhlich, J. Cornil and L. De Cola, *Inorganic Chemistry*, 2013, **52**, 1812-1824.
94. J. M. Fernández-Hernández, C.-H. Yang, J. I. Beltrán, V. Lemaur, F. Polo, R. Fröhlich, J. Cornil and L. De Cola, *Journal of the American Chemical Society*, 2011, **133**, 10543-10558.
95. S. Ladouceur, D. Fortin and E. Zysman-Colman, *Inorganic Chemistry*, 2011, **50**, 11514-11526.
96. T. Hirayama, K. Okuda and H. Nagasawa, *Chemical Science*, 2013, **4**, 1250-1256.
97. E. Baggaley, J. A. Weinstein and J. G. Williams, *Coordination Chemistry Reviews*, 2012, **256**, 1762-1785.

98. L. E. Wedlock and S. J. Berners-Price, *Australian Journal of Chemistry*, 2011, **64**, 692-704.
99. K. K.-W. Lo, A. W.-T. Choi and W. H.-T. Law, *Dalton Transactions*, 2012, **41**, 6021-6047.
100. K. Qiu, Y. Chen, T. W. Rees, L. Ji and H. Chao, *Coordination Chemistry Reviews*, 2019, **378**, 66-86.
101. D. Ma, S. Lin, W. Wang, C. Yang and C. Leung, *Journal*, 2017.
102. S. C. Dodani, S. C. Leary, P. A. Cobine, D. R. Winge and C. J. Chang, *Journal of the American Chemical Society*, 2011, **133**, 8606-8616.
103. D. Toomre and J. Bewersdorf, *Annual Review of Cell and Developmental Biology*, 2010, **26**, 285-314.
104. M. Yu, Q. Zhao, L. Shi, F. Li, Z. Zhou, H. Yang, T. Yi and C. Huang, *Chemical Communications*, 2008, DOI: 10.1039/B800939B, 2115-2117.
105. Q. Zhao, M. Yu, L. Shi, S. Liu, C. Li, M. Shi, Z. Zhou, C. Huang and F. Li, *Organometallics*, 2010, **29**, 1085-1091.
106. Q. Zhao, S. Liu, M. Shi, C. Wang, M. Yu, L. Li, F. Li, T. Yi and C. Huang, *Inorganic Chemistry*, 2006, **45**, 6152-6160.
107. G. Zhang, H. Zhang, Y. Gao, R. Tao, L. Xin, J. Yi, F. Li, W. Liu and J. Qiao, *Organometallics*, 2014, **33**, 61-68.
108. J. Liu, W. Bu, L. Pan and J. Shi, *Angewandte Chemie International Edition*, 2013, **52**, 4375-4379.
109. S. Gorski and T. Misteli, *Journal of cell science*, 2005, **118**, 4083-4092.
110. C. Li, M. Yu, Y. Sun, Y. Wu, C. Huang and F. Li, *Journal of the American Chemical Society*, 2011, **133**, 11231-11239.
111. J. R. Friedman and J. Nunnari, *Nature*, 2014, **505**, 335-343.
112. S. A. Detmer and D. C. Chan, *Nature Reviews Molecular Cell Biology*, 2007, **8**, 870-879.
113. J. Nunnari and A. Suomalainen, *Cell*, 2012, **148**, 1145-1159.
114. S. Vyas, E. Zaganjor and M. C. Haigis, *Cell*, 2016, **166**, 555-566.
115. Y. Liu, P. Zhang, X. Fang, G. Wu, S. Chen, Z. Zhang, H. Chao, W. Tan and L. Xu, *Dalton Transactions*, 2017, **46**, 4777-4785.
116. B. Kar, U. Das, N. Roy and P. Paira, *Coordination Chemistry Reviews*, 2023, **474**, 214860.
117. S.-Q. Zhang, T.-T. Meng, J. Li, F. Hong, J. Liu, Y. Wang, L.-H. Gao, H. Zhao and K.-Z. Wang, *Inorganic Chemistry*, 2019, **58**, 14244-14259.
118. U. Das, B. Kar, S. Pete and P. Paira, *Dalton Transactions*, 2021, **50**, 11259-11290.
119. X. Zhao, J. Liu, J. Fan, H. Chao and X. Peng, *Chemical Society Reviews*, 2021, **50**, 4185-4219.
120. H. Huang, S. Banerjee and P. J. Sadler, *ChemBioChem*, 2018, **19**, 1574-1589.
121. Z. Jin, S. Qi, X. Guo, N. Tian, Y. Hou, C. Li, X. Wang and Q. Zhou, *Chemical Communications*, 2020, **56**, 2845-2848.
122. L. Wang, S. Monro, P. Cui, H. Yin, B. Liu, C. G. Cameron, W. Xu, M. Hetu, A. Fuller, S. Kilina, S. A. McFarland and W. Sun, *ACS Applied Materials & Interfaces*, 2019, **11**, 3629-3644.
123. M. C. DeRosa and R. J. Crutchley, *Coordination Chemistry Reviews*, 2002, **233**, 351-371.
124. S. Reineke, F. Lindner, G. Schwartz, N. Seidler, K. Walzer, B. Lüssem and K. Leo, *Nature*, 2009, **459**, 234-238.
125. R. D. Costa, E. Ortí, H. J. Bolink, F. Monti, G. Accorsi and N. Armaroli, *Angewandte Chemie International Edition*, 2012, **51**, 8178-8211.
126. E. Baranoff and B. F. E. Curchod, *Dalton Transactions*, 2015, **44**, 8318-8329.
127. H.-C. Su, Y.-R. Chen and K.-T. Wong, *Advanced Functional Materials*, 2020, **30**, 1906898.
128. S. B. Meier, D. Tordera, A. Pertegás, C. Roldán-Carmona, E. Ortí and H. J. Bolink, *Materials Today*, 2014, **17**, 217-223.
129. A. F. Henwood and E. Zysman-Colman, in *Photoluminescent Materials and Electroluminescent Devices*, eds. N. Armaroli and H. J. Bolink, Springer International Publishing, Cham, 2017, DOI: 10.1007/978-3-319-59304-3_2, pp. 25-65.
130. H. C. Su, F. C. Fang, T. Y. Hwu, H. H. Hsieh, H. F. Chen, G. H. Lee, S. M. Peng, K. T. Wong and C. C. Wu, *Advanced Functional Materials*, 2007, **17**, 1019-1027.
131. C.-T. Liao, H.-F. Chen, H.-C. Su and K.-T. Wong, *Physical Chemistry Chemical Physics*, 2012, **14**, 9774-9784.

132. D. Tordera, J. Frey, D. Vonlanthen, E. Constable, A. Pertegás, E. Ortí, H. J. Bolink, E. Baranoff and M. K. Nazeeruddin, *Advanced Energy Materials*, 2013, **3**, 1338-1343.
133. J. Zhang, L. Zhou, H. A. Al-Attar, K. Shao, L. Wang, D. Zhu, Z. Su, M. R. Bryce and A. P. Monkman, *Advanced Functional Materials*, 2013, **23**, 4667-4677.
134. C.-T. Liao, H.-F. Chen, H.-C. Su and K.-T. Wong, *Physical Chemistry Chemical Physics*, 2012, **14**, 1262-1269.
135. G. Hong, X. Gan, C. Leonhardt, Z. Zhang, J. Seibert, J. M. Busch and S. Bräse, *Advanced Materials*, 2021, **33**, 2005630.
136. U. Mitschke and P. Bauerle, *J. Mater. Chem.*, 2000, **10**, 1471-1507.
137. B. W. D'Andrade and S. R. Forrest, *Adv. Mater. (Weinheim, Ger.)*, 2004, **16**, 1585-1595.
138. E. F. Schubert and J. K. Kim, *Science (Washington, DC, U. S.)*, 2005, **308**, 1274-1278.
139. E. Longhi and L. De Cola, *Iridium (III) in optoelectronic and photonics applications*, 2017, 205-274.
140. D. N. Tritton, F.-K. Tang, G. B. Bodedla, F.-W. Lee, C.-S. Kwan, K. C.-F. Leung, X. Zhu and W.-Y. Wong, *Coordination Chemistry Reviews*, 2022, **459**, 214390.
141. Z. Ning, Y. Fu and H. Tian, *Energy & Environmental Science*, 2010, **3**, 1170-1181.
142. K. A. King and R. J. Watts, *J. Am. Chem. Soc.*, 1987, **109**, 1589.
143. K. T. Kamtekar, A. P. Monkman and M. R. Bryce, *Adv. Mater. (Weinheim, Ger.)*, 2010, **22**, 572-582.
144. H. Wu, L. Ying, W. Yang and Y. Cao, *Chem. Soc. Rev.*, 2009, **38**, 3391-3400.
145. G. M. Farinola and R. Ragni, *Chemical Society Reviews*, 2011, **40**, 3467-3482.
146. F. Laquai, Y. S. Park, J. J. Kim and T. Basché, *Macromolecular rapid communications*, 2009, **30**, 1203-1231.
147. Q. Wang and D. Ma, *Chemical Society Reviews*, 2010, **39**, 2387-2398.
148. G. Schwartz, S. Reineke, T. C. Rosenow, K. Walzer and K. Leo, *Advanced Functional Materials*, 2009, **19**, 1319-1333.
149. F. Babudri, G. M. Farinola, F. Naso and R. Ragni, *Chemical Communications*, 2007, 1003-1022.
150. R. Ragni, E. A. Plummer, K. Brunner, J. W. Hofstraat, F. Babudri, G. M. Farinola, F. Naso and L. De Cola, *Journal of Materials Chemistry*, 2006, **16**, 1161-1170.
151. B. W. D’Andrade, M. E. Thompson and S. R. Forrest, *Advanced Materials*, 2002, **14**, 147-151.
152. B. W. D'Andrade and S. R. Forrest, *Advanced Materials*, 2004, **16**, 1585-1595.
153. S. Brovelli, F. Meinardi, G. Winroth, O. Fenwick, G. Sforazzini, M. J. Frampton, L. Zalewski, J. A. Levitt, F. Marinello and P. Schiavuta, *Advanced functional materials*, 2010, **20**, 272-280.
154. M. Mazzeo, V. Vitale, F. Della Sala, M. Anni, G. Barbarella, L. Favaretto, G. Sotgiu, R. Cingolani and G. Gigli, *Advanced Materials*, 2005, **17**, 34-39.
155. P. Coppo, M. Duati, V. N. Kozhevnikov, J. W. Hofstraat and L. De Cola, *Angewandte Chemie International Edition*, 2005, **44**, 1806-1810.
156. A. Baschieri, S. Muzzioli, E. Matteucci, S. Stagni, M. Massi and L. Sambri, *Dalton Transactions*, 2015, **44**, 37-40.
157. D. Sykes, I. S. Tidmarsh, A. Barbieri, I. V. Sazanovich, J. A. Weinstein and M. D. Ward, *Inorganic Chemistry*, 2011, **50**, 11323-11339.
158. Z. Chen, C. L. Ho, L. Wang and W. Y. Wong, *Advanced Materials*, 2020, **32**, 1903269.
159. B. Happ, C. Friebe, A. Winter, M. D. Hager, R. Hoogenboom and U. S. Schubert, *Chemistry – An Asian Journal*, 2009, **4**, 154-163.
160. J. D. Crowley and P. H. Bandeen, *Dalton Transactions*, 2010, **39**, 612-623.
161. R. A. Krause, *Inorganica Chimica Acta*, 1978, **31**, 241-242.
162. M. Nonoyama, *Bulletin of the Chemical Society of Japan*, 1974, **47**, 767-768.
163. P. A. Scattergood, A. M. Ranieri, L. Charalambou, A. Comia, D. A. W. Ross, C. R. Rice, S. J. O. Hardman, J.-L. Heully, I. M. Dixon, M. Massi, F. Alary and P. I. P. Elliott, *Inorganic Chemistry*, 2020, **59**, 1785-1803.
164. S. Tang, A. Sandström, P. Lundberg, T. Lanz, C. Larsen, S. van Reenen, M. Kemerink and L. Edman, *Nature Communications*, 2017, **8**, 1190.
165. A. J. Lees, *Comments on Inorganic Chemistry*, 1995, **17**, 319-346.

166. J. P. Marcolongo, J. Schmidt, N. Levin and L. D. Slep, *Physical Chemistry Chemical Physics*, 2017, **19**, 21373-21381.
167. K. A. King, P. J. Spellane and R. J. Watts, *Journal of the American Chemical Society*, 1985, **107**, 1431-1432.
168. D. Schneidenbach, S. Ammermann, M. Debeaux, A. Freund, M. Zöllner, C. Daniliuc, P. G. Jones, W. Kowalsky and H.-H. Johannes, *Inorganic Chemistry*, 2010, **49**, 397-406.
169. S. D. Cummings and R. Eisenberg, *Journal of the American Chemical Society*, 1996, **118**, 1949-1960.
170. Y. J. Su, H. L. Huang, C. L. Li, C. H. Chien, Y. T. Tao, P. T. Chou, S. Datta and R. S. Liu, *Advanced Materials*, 2003, **15**, 884-888.
171. S. J. Yeh, M. F. Wu, C. T. Chen, Y. H. Song, Y. Chi, M. H. Ho, S. F. Hsu and C. H. Chen, *Advanced Materials*, 2005, **17**, 285-289.
172. Y. You and S. Y. Park, *Dalton Transactions*, 2009, DOI: 10.1039/B812281D, 1267-1282.
173. S. Kang and T. K. Kim, *Dyes and Pigments*, 2022, **201**, 110191.
174. V. V. Grushin, N. Herron, D. D. LeCloux, W. J. Marshall, V. A. Petrov and Y. Wang, *Chemical Communications*, 2001, DOI: 10.1039/B103490C, 1494-1495.
175. A. F. Rausch, M. E. Thompson and H. Yersin, *The Journal of Physical Chemistry A*, 2009, **113**, 5927-5932.
176. A. B. Tamayo, B. D. Alleyne, P. I. Djurovich, S. Lamansky, I. Tsyba, N. N. Ho, R. Bau and M. E. Thompson, *Journal of the American Chemical Society*, 2003, **125**, 7377-7387.
177. V. Sivasubramaniam, F. Brodkorb, S. Hanning, H. P. Loebl, V. van Elsbergen, H. Boerner, U. Scherf and M. Kreyenschmidt, *Journal of Fluorine Chemistry*, 2009, **130**, 640-649.
178. C.-F. Chang, Y.-M. Cheng, Y. Chi, Y.-C. Chiu, C.-C. Lin, G.-H. Lee, P.-T. Chou, C.-C. Chen, C.-H. Chang and C.-C. Wu, *Angewandte Chemie International Edition*, 2008, **47**, 4542-4545.
179. R. J. Holmes, S. R. Forrest, T. Sajoto, A. Tamayo, P. I. Djurovich, M. E. Thompson, J. Brooks, Y. J. Tung, B. W. D'Andrade, M. S. Weaver, R. C. Kwong and J. J. Brown, *Applied Physics Letters*, 2005, **87**, 243507.
180. M. G. Colombo and H. U. Guedel, *Inorganic Chemistry*, 1993, **32**, 3081-3087.
181. A. F. Henwood, A. K. Bansal, D. B. Cordes, A. M. Z. Slawin, I. D. W. Samuel and E. Zysman-Colman, *Journal of Materials Chemistry C*, 2016, **4**, 3726-3737.
182. H. J. Bolink, E. Coronado, R. D. Costa, N. Lardiés and E. Ortí, *Inorganic Chemistry*, 2008, **47**, 9149-9151.
183. Y. Zheng, A. S. Batsanov, R. M. Edkins, A. Beeby and M. R. Bryce, *Inorganic Chemistry*, 2012, **51**, 290-297.
184. D. Tordera, J. J. Serrano-Pérez, A. Pertegás, E. Ortí, H. J. Bolink, E. Baranoff, M. K. Nazeeruddin and J. Frey, *Chemistry of Materials*, 2013, **25**, 3391-3397.
185. C. D. Ertl, J. Cerdá, J. M. Junquera-Hernández, A. Pertegás, H. J. Bolink, E. C. Constable, M. Neuburger, E. Ortí and C. E. Housecroft, *RSC Advances*, 2015, **5**, 42815-42827.
186. D. Tordera, A. M. Bünzli, A. Pertegás, J. M. Junquera-Hernández, E. C. Constable, J. A. Zampese, C. E. Housecroft, E. Ortí and H. J. Bolink, *Chemistry – A European Journal*, 2013, **19**, 8597-8609.
187. H.-C. Su, H.-F. Chen, Y.-C. Shen, C.-T. Liao and K.-T. Wong, *Journal of Materials Chemistry*, 2011, **21**, 9653-9660.
188. S. Ladouceur, D. Fortin and E. Zysman-Colman, *Inorganic Chemistry*, 2011, **50**, 11514-11526.
189. L. Suntrup, S. Klenk, J. Klein, S. Sobottka and B. Sarkar, *Inorganic Chemistry*, 2017, **56**, 5771-5783.
190. M. Damm, T. N. Glasnov and C. O. Kappe, *Organic Process Research & Development*, 2010, **14**, 215-224.
191. Z.-X. Wang and H.-L. Qin, *Green Chemistry*, 2004, **6**, 90-92.
192. C. E. Welby, L. Gilmartin, R. R. Marriott, A. Zahid, C. R. Rice, E. A. Gibson and P. I. P. Elliott, *Dalton Transactions*, 2013, **42**, 13527-13536.
193. S. Zanarini, M. Felici, G. Valenti, M. Marcaccio, L. Prodi, S. Bonacchi, P. Contreras-Carballada, R. M. Williams, M. C. Feiters, R. J. M. Nolte, L. De Cola and F. Paolucci, *Chemistry – A European Journal*, 2011, **17**, 4640-4647.
194. L. Chassot and A. Von Zelewsky, *Inorganic Chemistry*, 1987, **26**, 2814-2818.

195. U. Maeder, A. Von Zelewsky and H. Stoeckli-Evans, *Helvetica Chimica Acta*, 1992, **75**, 1320-1332.
196. D. Sandrini, M. Maestri, M. Ciano, U. Maeder and A. von Zelewsky, *Helvetica Chimica Acta*, 1990, **73**, 1306-1313.
197. A. J. Lees, *Comments Inorg. Chem.*, 1995, **17**, 319.
198. I. N. Mills, J. A. Porras and S. Bernhard, *Accounts of Chemical Research*, 2018, **51**, 352-364.
199. L. L. Tinker and S. Bernhard, *Inorganic Chemistry*, 2009, **48**, 10507-10511.
200. J. A. G. Williams, A. J. Wilkinson and V. L. Whittle, *Dalton Transactions*, 2008, DOI: 10.1039/B716743A, 2081-2099.
201. Y. Chi, T.-K. Chang, P. Ganesan and P. Rajakannu, *Coordination Chemistry Reviews*, 2017, **346**, 91-100.
202. S. Sato, T. Morikawa, T. Kajino and O. Ishitani, *Angewandte Chemie International Edition*, 2013, **52**, 988-992.
203. D. N. Chirdon, W. J. Transue, H. N. Kagalwala, A. Kaur, A. B. Maurer, T. Pintauer and S. Bernhard, *Inorganic Chemistry*, 2014, **53**, 1487-1499.
204. H. Huang, S. Banerjee, K. Qiu, P. Zhang, O. Blacque, T. Malcomson, M. J. Paterson, G. J. Clarkson, M. Staniforth, V. G. Stavros, G. Gasser, H. Chao and P. J. Sadler, *Nature Chemistry*, 2019, **11**, 1041-1048.
205. N. Eckstein, *Journal of Experimental & Clinical Cancer Research*, 2011, **30**, 91.
206. J. A. Porras, I. N. Mills, W. J. Transue and S. Bernhard, *Journal of the American Chemical Society*, 2016, **138**, 9460-9472.
207. S. Obara, M. Itabashi, F. Okuda, S. Tamaki, Y. Tanabe, Y. Ishii, K. Nozaki and M.-a. Haga, *Inorganic Chemistry*, 2006, **45**, 8907-8921.
208. H.-J. Ai, X. Ma, Q. Song and X.-F. Wu, *Science China Chemistry*, 2021, **64**, 1630-1659.
209. M. Aizenberg and D. Milstein, *Science*, 1994, **265**, 359-361.
210. G. Ge, J. He, H. Guo, F. Wang and D. Zou, *Journal of Organometallic Chemistry*, 2009, **694**, 3050-3057.
211. M. Polson, M. Ravaglia, S. Fracasso, M. Garavelli and F. Scandola, *Inorganic Chemistry*, 2005, **44**, 1282-1289.
212. M. J. Jurow, A. Bossi, P. I. Djurovich and M. E. Thompson, *Chemistry of Materials*, 2014, **26**, 6578-6584.
213. M. T. Walden, D. S. Yufit and J. A. G. Williams, *Inorganica Chimica Acta*, 2022, **532**, 120737.
214. A. Mihailovic, I. Vladescu, M. McCauley, E. Ly, M. C. Williams, E. M. Spain and M. E. Nuñez, *Langmuir*, 2006, **22**, 4699-4709.
215. B. S. Howerton, D. K. Heidary and E. C. Glazer, *Journal of the American Chemical Society*, 2012, **134**, 8324-8327.
216. E. Baranoff, B. F. E. Curchod, F. Monti, F. Steimer, G. Accorsi, I. Tavernelli, U. Rothlisberger, R. Scopelliti, M. Grätzel and M. K. Nazeeruddin, *Inorganic Chemistry*, 2012, **51**, 799-811.
217. F. Neese, *WIREs Computational Molecular Science*, 2012, **2**, 73-78.
218. F. Neese, *WIREs Computational Molecular Science*, 2018, **8**, e1327.
219. A. D. Becke, *The Journal of Chemical Physics*, 1993, **98**, 1372-1377.
220. C. Lee, W. Yang and R. G. Parr, *Physical Review B*, 1988, **37**, 785-789.
221. S. Grimme, J. Antony, S. Ehrlich and H. Krieg, *The Journal of Chemical Physics*, 2010, **132**, 154104.
222. S. Grimme, S. Ehrlich and L. Goerigk, *Journal of Computational Chemistry*, 2011, **32**, 1456-1465.
223. F. Weigend and R. Ahlrichs, *Physical Chemistry Chemical Physics*, 2005, **7**, 3297-3305.
224. X. Zhou, P. L. Burn and B. J. Powell, *Inorganic Chemistry*, 2016, **55**, 5266-5273.
225. X. Zhou and B. J. Powell, *Inorganic Chemistry*, 2018, **57**, 8881-8889.
226. A. V. Marenich, C. J. Cramer and D. G. Truhlar, *The Journal of Physical Chemistry B*, 2009, **113**, 6378-6396.
227. M. Obata, A. Kitamura, A. Mori, C. Kameyama, J. A. Czaplewska, R. Tanaka, I. Kinoshita, T. Kusumoto, H. Hashimoto, M. Harada, Y. Mikata, T. Funabiki and S. Yano, *Dalton Transactions*, 2008, DOI: 10.1039/B718538C, 3292-3300.
228. K. Sonogashira, *Journal of Organometallic Chemistry*, 2002, **653**, 46-49.

229. J.-P. Collin, I. M. Dixon, J.-P. Sauvage, J. A. G. Williams, F. Barigelletti and L. Flamigni, *Journal of the American Chemical Society*, 1999, **121**, 5009-5016.

8. Appendix

8. 1. ^{1}H NMR Spectroscopic Monitoring of Photolysis

Recorded in MeCN at 298 K using mercury emission lines from a 23 W fluorescent light bulb as light source.

8. 1. 1. [Ir(ppy$_2$)(pytz-*p*-xyl-pytz)Ru(bpy)]$^+$, **JA1a**

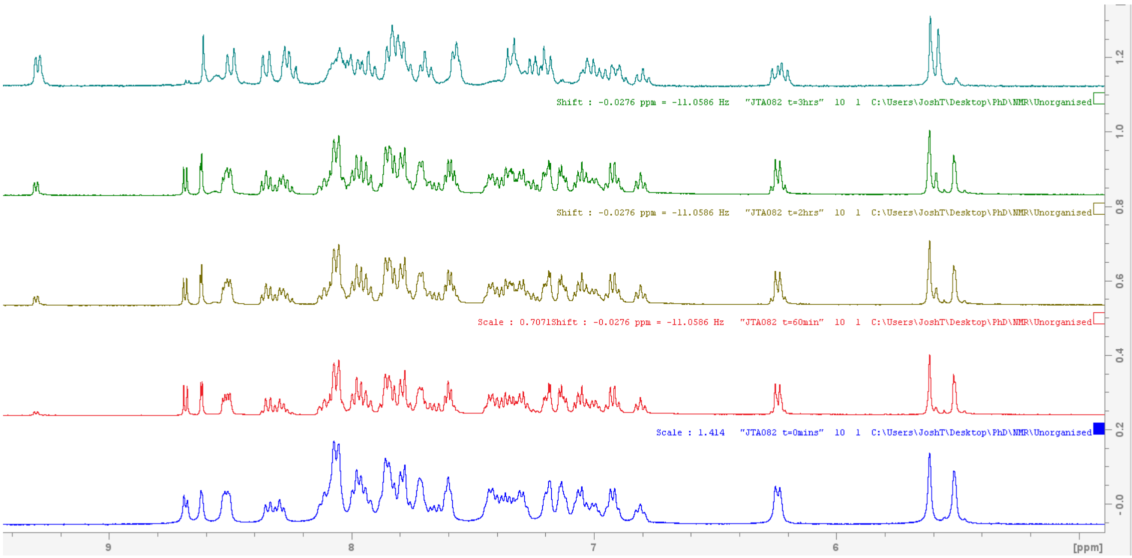

8. 1. 2. [Ir(ppy$_2$)(pytz-*m*-xyl-pytz)Ru(bpy)]$^+$, **JA2a**

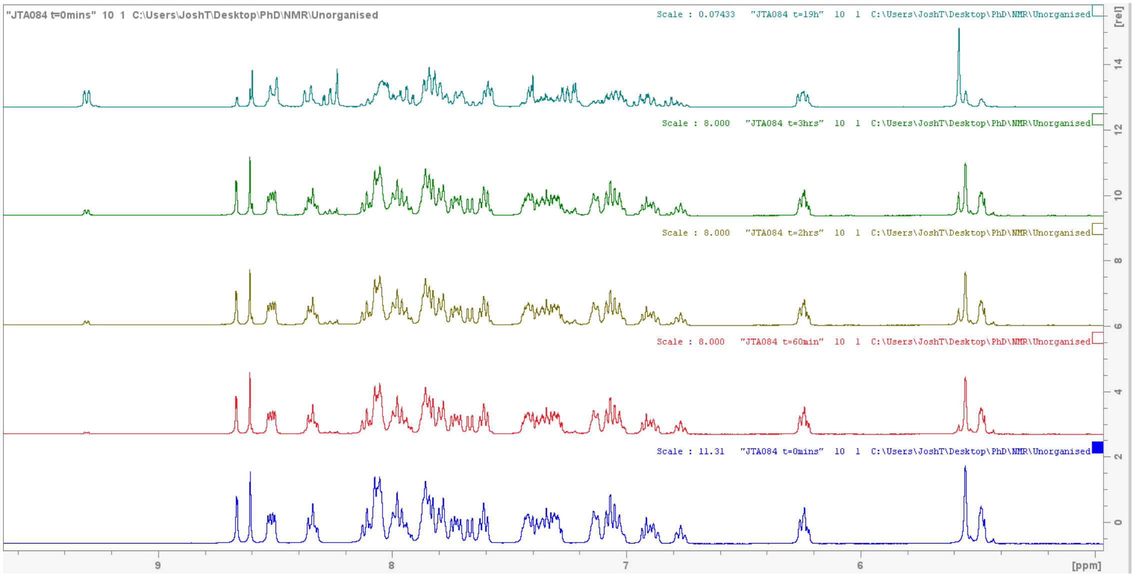

8. 1. 3. [Ir(dfppy$_2$)(pytz-*m*-xyl-pytz)Ru(bpy)]$^+$, **JA2b**

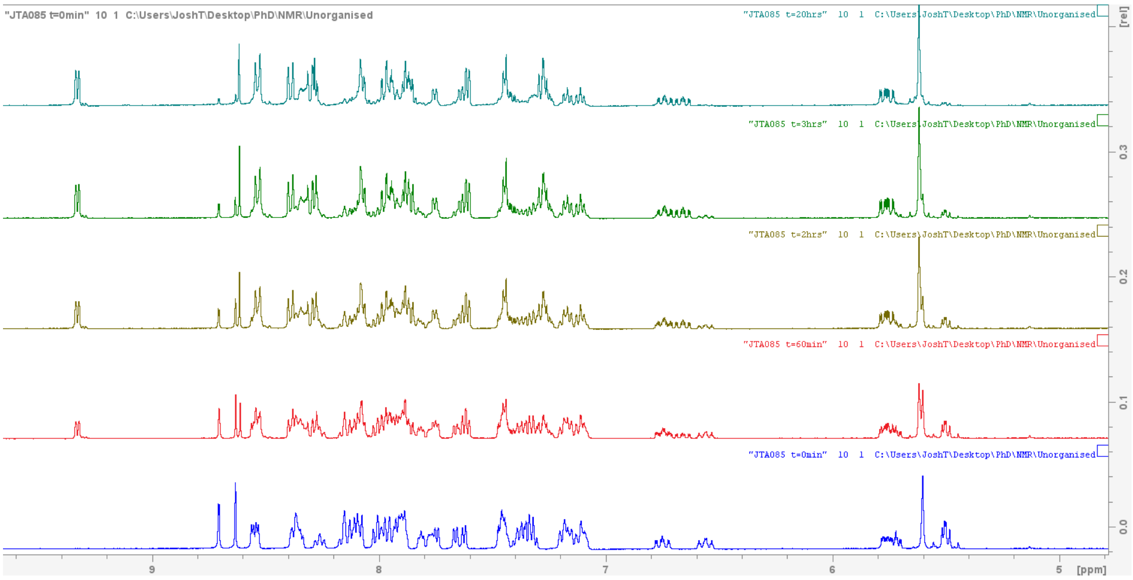

8. 1. 4. [Ir(ppy$_2$)(pytz-*o*-xyl-pytz)Ru(bpy)]$^+$, **JA3a**

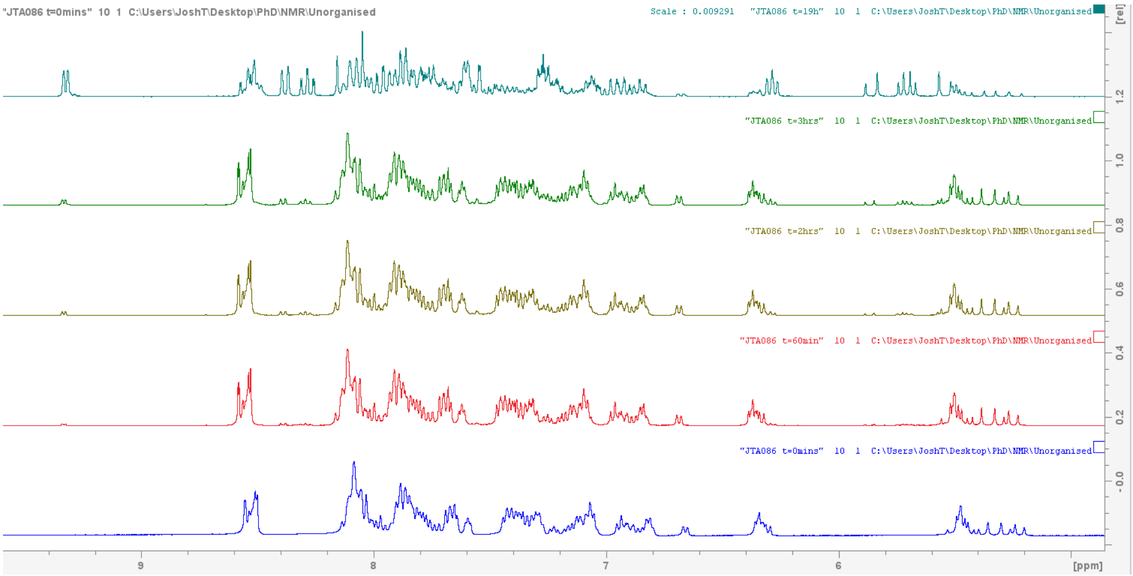

8. 1. 5. [Ir(dfppy$_2$)(pytz-*o*-xyl-pytz)Ru(bpy)]$^+$, **JA3b**

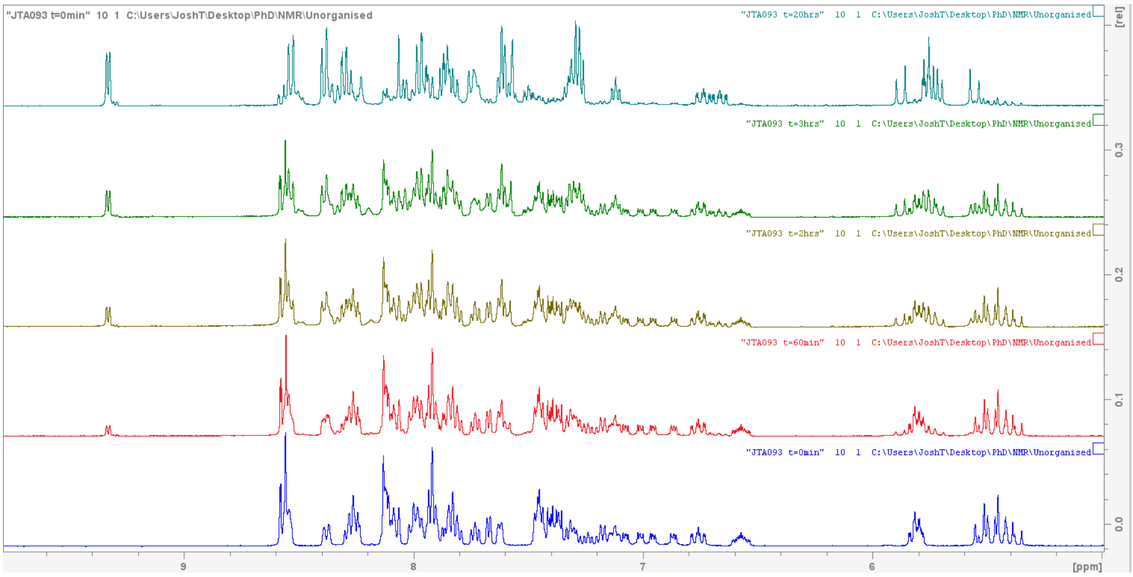

8. 2 Emission Spectroscopic Monitoring of Photolysis

8. 2. 1 [Ir(ppy$_2$)(pytz-*m*-xyl-pytz)Ru(bpy)]$^+$, **JA2a**

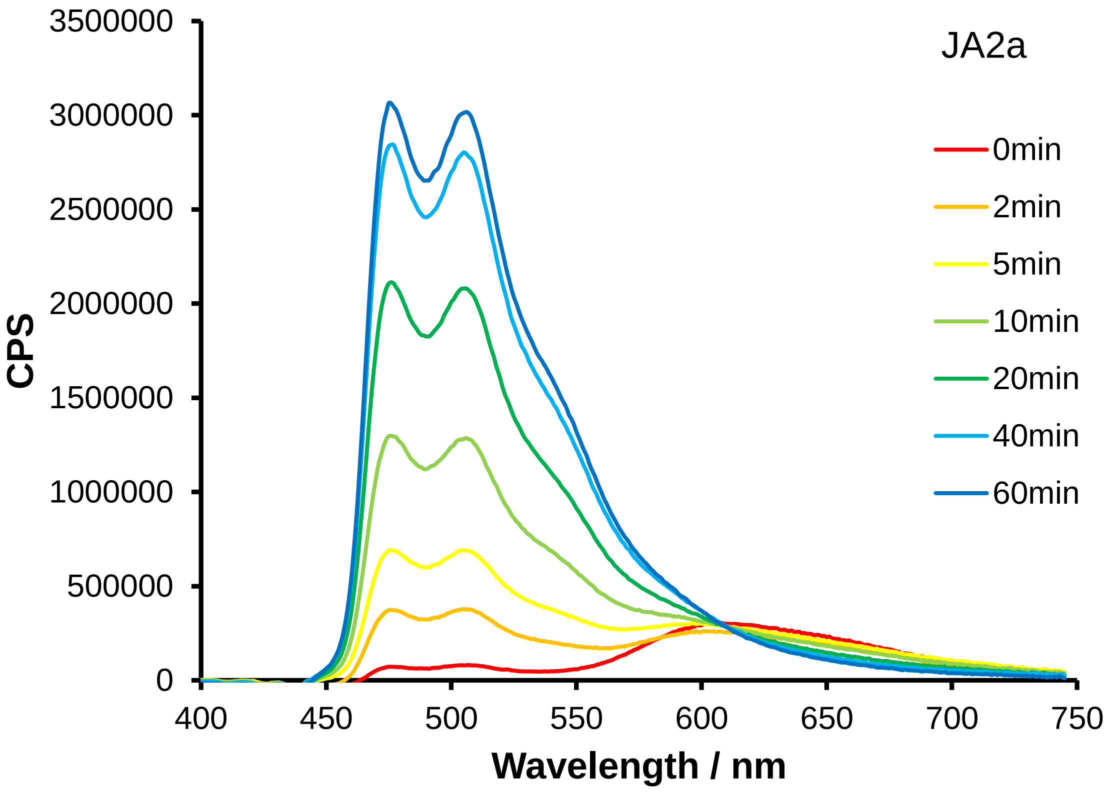

8. 2. 2 [Ir(dfppy$_2$)(pytz-*m*-xyl-pytz)Ru(bpy)]$^+$, **JA2b**

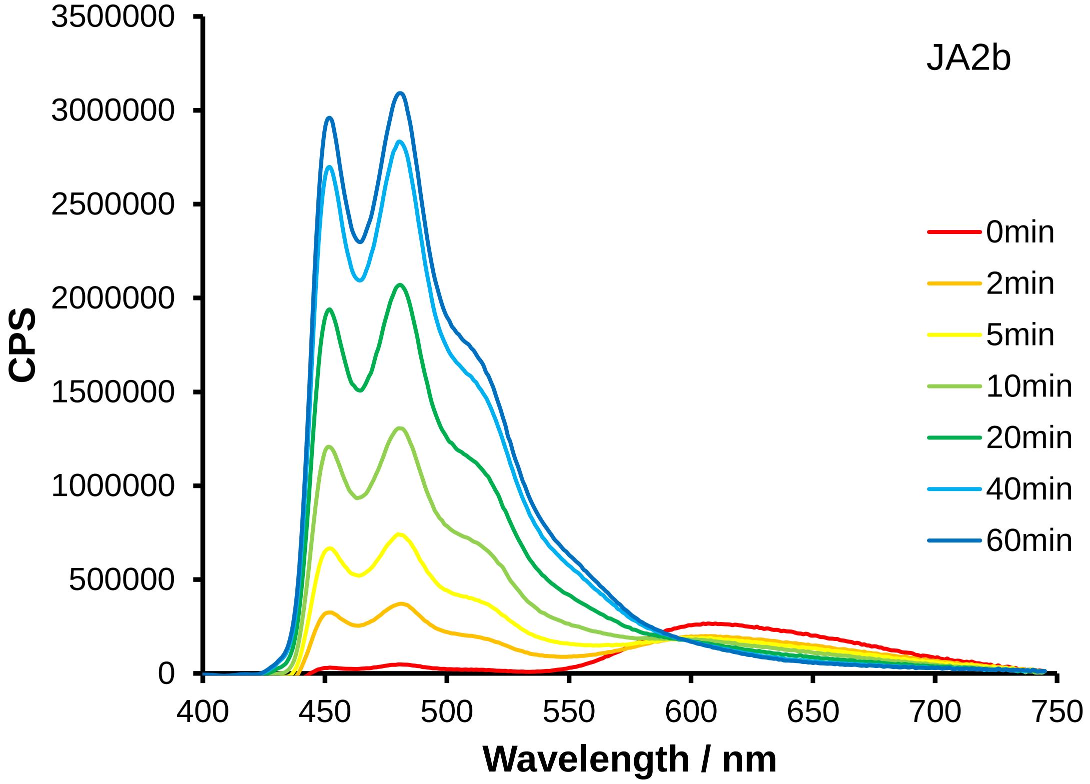

8. 2. 3 [Ir(ppy$_2$)(pytz-*o*-xyl-pytz)Ru(bpy)]$^+$, **JA3a**

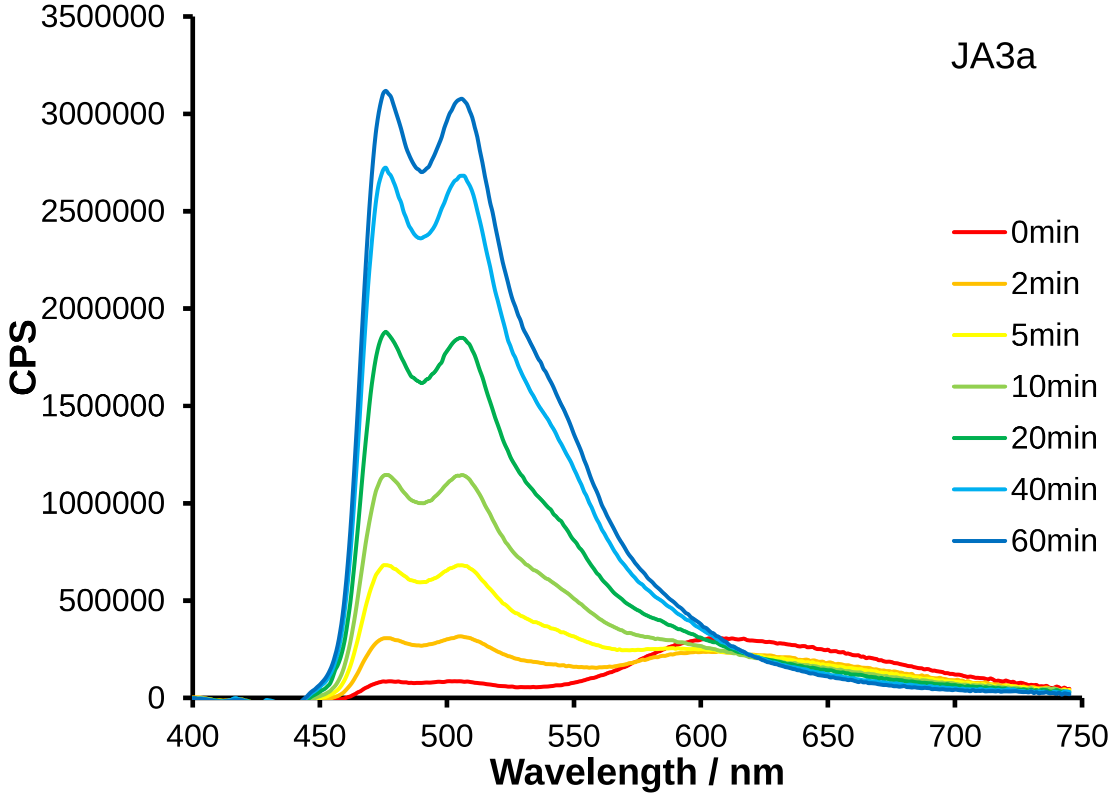

8. 2. 4 [Ir(dfppy$_2$)(pytz-*o*-xyl-pytz)Ru(bpy)]$^+$, **JA3b**